UNIVERSITY OF GAZİANTEP GRADUATE SCHOOL OF NATURAL & APPLIED SCIENCES

MODELING LOCAL SCOUR USING k-ε TURBULENCE MODEL AND SOFT COMPUTING TECHNIQUES

Ph.D THESIS
IN
CIVIL ENGINEERING

BY
AYTAÇ GÜVEN
MARCH 2008

Modeling Local Scour Using k-ε Turbulence Model and Soft Computing Techniques

PhD Thesis
in
Civil Engineering
University of Gaziantep

Supervisor
Assoc. Prof. Dr. Mustafa GÜNAL

by

Aytaç GÜVEN

March 2008

T.C.
UNIVERSITY OF GAZİANTEP
GRADUATE SCHOOL OF
NATURAL & APPLIED SCIENCES
(CIVIL ENGINEERING DEPARTMENT)

Name of the thesis: Modeling Local Scour Using k-ε Turbulence Model and Soft Computing Techniques
Name of the student: Aytaç GÜVEN
Exam date: 28/03/2008

Approval of the Graduate School of Natural and Applied Sciences

Prof. Dr. Sadettin ÖZYAZICI
Director

I certify that this thesis satisfies all the requirements as a thesis for the degree of Doctor of Philosophy.

Assoc. Prof. Dr. Mustafa GÜNAL
Head of Department

This is to certify that we have read this thesis and that in our opinion it is fully adequate, in scope and quality, as a thesis for the degree of Doctor of Philosophy.

Assoc. Prof. Dr. Mustafa GÜNAL
Supervisor

Examining Committee Members	Signature
Prof.Dr. Yalçın YÜKSEL	_____
Prof.Dr.Mustafa ÖZAKÇA	_____
Assoc.Prof.Dr. Mustafa GÜNAL	_____
Assoc.Prof.Dr. Yaşar GÜNDOĞDU	_____
Assist.Prof.Dr. Mazen KAVVAS	_____

To my wife and my son
Ebru and Arda Güven

ABSTRACT

Modeling Local Scour Using k-ε Turbulence Model
and Soft Computing Techniques
GÜVEN, Aytaç

Ph.D. Thesis in Civil Engineering

Supervisor: Assoc. Prof. Dr. Mustafa GÜNAL

March 2008, 204 pages

In this study, a hybrid numerical-analytical model is developed, which simulates the temporal evolution of local scour downstream of hydraulic structures, and simulates the flow patterns in the scoured zone. The hybrid model consists of an analytical model and a k-ε turbulence model. The analytical model analyzes the external forces acting on a bed grain and models the instantaneous shape of the scour hole solving an integro-parabolic equation. The numerical model derives the instantaneous shape of mobile bed and simulates the flow patterns in the corresponding scour hole.

The proposed model is verified by experimental data taken from the studies of others in the literature, predictions of commercial software and numerical studies in the literature. The proposed hybrid model predicted the temporal evolution of local scour downstream of hydraulic structures, and simulated the flow patterns in scoured hole with quite good agreements with the experimental ones. The proposed hybrid model proved to be efficiently used in complex hydraulic engineering problems. The use of a new approach to prediction of local scour, soft computing technique, is presented. Artificial Neural Networks and Genetic Programming based models are developed, which predict the local scour downstream of hydraulic structures. The results encourage the use of soft computing technique in very complex hydraulic engineering problems.

Keywords: Scour, turbulent jet, numerical model, soft computing, artificial neural networks, genetic programming

ÖZET

Yerel Oyulmanın k-ε Türbülans Modeli ve
Yapay Zeka Teknikleri Kullanarak Modellenmesi

GÜVEN, Aytaç

Doktora Tezi, İnşaat Mühendisliği

Tez Yöneticisi: Doç. Dr. Mustafa GÜNAL

Mart 2008, 204 sayfa

Bu çalışmada, hidrolik yapıların mansap kısmında meydana gelen yerel oyulmanın zamana bağlı değişimini ve oyulan bölgedeki akım şartlarını simule eden bir karma numerik-analitik model geliştirildi. Karma model, bir analitik model ve bir de k-ε türbülans modelden oluşmaktadadır. Analitik model taban parçacığı üzerinde etki eden dış kuvvetleri analiz eder ve bir integro-parabolik denklemi çözerek taban profilinin zamana bağlı değişimini modeller. Nümerik model elde edilen oyulma çukuru içerisinde meydana gelen akım şartlarını simule eder.

Önerilen model literatürdeki deneysel çalışmalar, ticari programlar ve nümerik çalışmaların tahminleri kullanılarak değerlendirildi. Önerilen karma model, hidrolik yapıların mansap kısmında meydana gelen yerel oyulmanın zamana bağlı değişimini ve oyulan çukur içerisindeki akım şartlarını, deneysel verilerle oldukça iyi uyum içinde modelledi. Önerilen karma model, karmaşık hidrolik mühendisliği problemlerinde verimli bir şekilde kullanılabileceğini kanıtladı. Yerel oylmanın tahminine yeni bir yaklaşım olan yapay zeka ile hesaplama tekniğinin kullanımı sunulmuştur. Yapay Sinir Ağları ve Genetik Programlama kullanılarak, hidrolik yapıların mansap kısmında oluşan yerel oyulmayı tahmin eden modeller gerçekleştirilmiştir. Sonuçlar, yapay zeka ile hesaplama tekniğinin çok karmaşık hidrolik mühendisliği problemlerinde kullanımını desteklemiştir.

Anahtar Kelimeler: Oyulma, türbülanslı jet, numerik model, yapay zeka ile hesaplama, yapay sinir ağları, genetik proglamlama

ACKNOWLEDGEMENTS

CONTENTS

LIST OF FIGURES

LIST OF TABLES

LIST OF SYMBOLS/ABBREVIATIONS

A Dimensional model parameter

A_{50} A dimensionless model parameter

B Channel width (m)

B Weir width

C_m, C_1, C_2, s_k, s_e empirical constants

c_s A dimensional coefficient

d Mean size of particles of bed material (m)

d_{50} Mean particle diameter (m)

E   Wall roughness parameter

F_1 Upstream Froude number

F_{rd} The densimetric Froude number

f_c Roughness coefficient

g Gravitational acceleration (m/s^2)

G   Turbulence production term

h   Depth of water in the channel (m)

h_s Water depth on the sill (m)

J   Jacobian

K   Kinetic energy

$\boldsymbol{k}$ Von Karman constant

K   A parameter

L,   Length of scour profile

l_m Mixing length (m)

L_p Length of rigid apron (m)

L_s Maximum scour length (m)

MAE Mean absolute error

MAPE   Mean absolute percentage error

MSE Mean square error

N   Number of data

n Trial value of power of the relative magnitude of kinetic enrgy

to the potential energy

p Instantaneous pressure (Pa)

$\bar{p}$ Mean value of fluctuating pressures (Pa)

p_c Pressure correction

Pe   Peclet number

P_k The volumetric production rate of k

q_1 to q_9 Tranformation coefficients given in Equation (3.40)

Q Unit discharge (m^2/s)

Q Water discharge (m^3/s)

R   The jet area divided by the perimeter of the jet

Re   Reynolds number

R^2 Coefficient of determination

R Coefficient of correlation

S   Submergence factor

S_l Ordinate of bed profile (m)

S_{max} Maximum scour depth (m)

S_u, S_v, S_k, S_e, S_p Source terms in transformed plane

t Time

T   Test duration

u Streamwise component of velocity

u_c, v_c Velocity corrections

$\left(\sqrt{\overline{u'^2}} \right)$ Longitudinal turbulent intensity

$-\overline{u'v'}$ Turbulent shear stress

U, V   Velocities in boundary fitted coordinates (m/s)

U_1 Initial velocity of entering jet

V_s Volume of scour hole per unith width

u*   Friction velocity

u_o Surface velocity

u_1 Inlet velocity

u_2 Downstream velocity (m/s)

u_m Streamwise maximum mean velocity (m/s)

u', v' and p' Fluctuating components of u, v and p

v Vertical component of velocity (m/s)

$\left(\sqrt{\overline{v'^2}} \right)$ Vertical turbulent intensity

x, y   Cartesian coordinate axis in the horizontal and vertical directions

XS Location of maximum scour depth

x_x, x_h Differentiation of x with respect to ξ, η

y_x, y_h Differentiation of y with respect to ξ, η

y_1 Upstream depth of water (m)

y_2 Downstream depth of water (m)

y' Distance between the maximum velocity and corresponding mean velocity (m)

y_t Tailwater depth (m)

z Height of sill (m)

f Functional symbol

ρ Mass density of water (kg/m^3)

ρ_s Mass density of sediment (kg/m^3)

$\dot{a}$ Relaxation factor

a,b   Normalization factors

b_1 Length scale for inner layer

γ Unit weight of water (N/m^3)

δij Kronecker delta, =1 for i=j and =0 for i≠j

ε Dissipation rate of kinetic energy

η, ξ Curvilinear coordinate axis

v_t Turbulent kinematic viscosity

ρ Density of water (kg/m^3)

r_s The density of sediment particle (kg/m^3)

d_{1a} Length scale for outer layer

σ Standard deviations or r.m.s value of data

τ Reynolds turbulent shear stress (Pa)

τ_{cr} Critical shear stress (Pa)

τ_{hydr} Hydrodiynamic shear stress (Pa)

τ_w Wall shear stress (Pa)

Φ Dependent variable stands for u, v, k and ε

CHAPTER 1

INTRODUCTION

1.1 General

Scouring is a natural phenomenon caused by the flow of water in rivers and streams. Turbulent water jet flowing over erodible bed nearby and downstream of hydraulic structures causes *local scour* at and/or downstream of these structures. Moreover, it may undermine the foundations of these structures and cause fatal structural collapses. Thus, the control and prediction of local scour is of immense importance, because the foundations of these structures are not designed taking into consideration the extent of local scour. Because complete protection against scouring is generally expensive, the designer should seek ways to guide and control the scouring process in order to minimize the risk of failure (Breusers and Raudkivi, 1991).

Numerous studies have been carried out to investigate the local scour phenomena. These studies try to give a better understanding of the complex structure of local scour together with the rag bags present in the soil-structure-water interaction. Local scour downstream of spillways, stilling basins, slip-buckets, sluice gates, grade control structures, turbulent jets, etc., and around bridge piers, bridge abutments have been theoretically and experimentally investigated. The literature review on theoretical and experimental studies on local scour is given in further sections of this thesis, in detail.

Ade and Rajaratnam (1998), Liriano and Day (2000) and more recently Sarkar and Dey (2004) summarize the experimental studies on local scour beneath two- and

three-dimensional wall jets and inclined ones, from different sources downstream of hydraulic structures. In fact, most of these studies aim to derive an empirical relation between the depth, s, and the location, XS, of the maximum scour depth, and the soil characteristics such as sediment diameter, d, and its density, ρ_s; inflow conditions such as the initial velocity of the entering jet, U_1, the apron length, L_p, the sluice gate opening, y_1, the tailwater depth, y_t and the incoming unit discharge, q; and the density of fluid, ρ, the viscosity of the fluid. In general, the functional relationship involved in the local scour process can be presented as

$$s, XS = f(\boldsymbol{r}, \boldsymbol{r}_s, g, \boldsymbol{n}, d, y_1, y_t, U_1, L_p) \tag{1.1}$$

Different sub-groups of the above relation have been proposed by the researchers for variant scour forms. But, due to the complexity of the process, none of them can be used universally, or even for the same scour problems with different geometric and hydraulic scales. Moreover, the proposed equations, most of which are based on regression analysis, suffer from very low generalization capacity and high errors in prediction of laboratory scale experimental data. Their accuracy in prediction of field data is questionable (Adduce, 2004).

In present study, new techniques alternative to the conventional regression analysis will be proposed in order to eliminate the above mentioned deficiencies in prediction of local scour data. Namely, artificial neural networks (ANNs) and genetic programming (GP), which is an extension to genetic algorithms, are utilized as the two intelligent soft computing techniques. Also, the explicit formulations of the proposed soft computing models will be presented.

The difficulties in physical modeling of local scour such as time consumed, economical restrictions and difficulty in many cases to repeat with the same experimental condition with high precision, call for use of numerical and analytical modeling that is well established and widely accepted technique.

In this study a hybrid analytical-numerical model will be developed which consists of an analytical model that simulates the temporal evolution of scour profile downstream of hydraulic structure and a k-ε turbulence model that simulates the flow

patterns in corresponding instantaneous scour profile. The two models will be capable of working independently as well as working in co-operation.

The analytical model will use information related both to the measured velocity fields and to the physical and mechanical properties of the sand, constituting the mobile bed. The analytical structure of the model will consist of a second order partial differential parabolic equation whose unknown is the shape of the mobile bed. The numerical integration of this equation is carried out using Mac-Cormack scheme.

The calculated scour profile data will be transferred to the numerical model. The model will use a finite volume method to solve the equations of motion and transport equations for two dimensions on a transformed rectangular domain using boundary-fitted coordinates. The internal characteristics of the mean flow of submerged horizontal jets including surface profiles on frozen scoured beds will be computed by a two-dimensional k–ε turbulence model. Computations will be carried out at different frozen-scoured bed profiles. A staggered grid system will be adapted for variable arrangements to avoid the well-known checkerboard oscillations in pressure and velocity. The SIMPLE algorithm will be adapted for the computation.

The proposed hybrid model and the soft computing models will be calibrated and validated using experimental data taken from several research papers from the literature and two Ph.D. works. The proposed hybrid model will also be compared with FLUENT commercial software and the other numerical studies in the literature.

Some of the experimental data of other studies, used in this thesis, have been determined in tabular form in related researches, whereas the rest of the experimental data, in graphical form. The experimental data in graphical form have been converted into numerical values using a digital software, Graph-Digger. The accuracy of the software has been evaluated by several figures composed of already known numerical data. The results showed that the software digs the numerical data from the digital figures with high precision.

1.2 Scope of the Thesis

The main aim of this thesis is to investigate the use of a new approach to numerical modeling, namely hybrid modeling, based on combining a analytical and a numerical model, in simulation of complex local scour problems downstream of hydraulic structures. By using hybrid modeling technique, it is aimed to improve the accuracy in prediction of local scour profile by using explicit analytical model and secondly, the flow patterns in the corresponding computed scour profile will be simulated by a well-established and widely used and validated k-ε turbulence model.

Two new approaches alternative to conventional regression analysis, namely artificial neural networks and genetic programming will be used in prediction of scour profile, depth and location of maximum scour depth based on experimental and field data taken from the literature. The explicit formulation of the proposed soft computing models will also be presented. To the knowledge of the author, these explicit formulation techniques will be the pioneering studies in the subject area of this thesis.

1.3 Contribution of the Thesis

This study is expected to contribute to the understanding of the new techniques in simulation of local scour downstream of hydraulic structures, beneath different types of jet flow. The emphasis will be given on a) development of a powerful hybrid model that will be used in numerical simulation of scour process by using more than one numerical models in co-operation b) derivation of more robust and generalized explicit formulation of depth and location of maximum scour depth using soft computing techniques and comparing these proposed formulas with most widely used and more conventional equations. The explicit formulations of proposed soft computing models will be the most up-date development in prediction of local scour parameters.

1.4 Layout of the Thesis

This thesis is composed of six chapters. Brief descriptions of each chapter are given as:

Chapter 1 Introduction

A description of mechanics behind local scour beneath turbulent jets and numerical modeling of local scour, scope and contribution of this research and a general framework of this thesis are given.

Chapter 2 Local scour beneath turbulent jets

General description of scour process, mechanism of scour by turbulent jets and a detailed review on experimental studies on local scour beneath horizontal and plunging turbulent jets is given.

Chapter 3 Hybrid numerical-analytical modeling of local scour

Review on numerical and analytical studies on local scour, description of the proposed hybrid model and validation of its components with experimental data are given.

Chapter 4 Prediction of local scour using soft computing techniques

General description of soft computing, overview of artificial neural networks and genetic programming, description of the proposed models and their explicit formulations, and validation of these models with experimental and field data are given.

Chapter 5 Results and discussions

The predictions of the proposed hybrid model to the experimental data of instantaneous scour profiles, free surface profiles, the distribution of velocity components, bed shear stress and the Reynolds stress over rigid apron and scoured zone are given and discussions are made based on the results of the numerical predictions and its comparison with measured ones. The proposed hybrid model is

compared with FLUENT commercial software and Artificial Neural Networks technique.

Chapter 6 Conclusions and suggestions for further research

The general conclusions which are drawn from the results of this research are given and some considerations for possible further research are proposed.

CHAPTER 2

LOCAL SCOUR BENEATH TURBULENT JETS

2.1   General

Scour is naturally caused by the erosive action of the flowing water on the erodible sediment beds. Local scour downstream of a hydraulic structure due to turbulent jet poses an immense problem in designing the foundation of the hydraulic structure. Collapse of an apron downstream of a hydraulic structure may occur as a result of the excessive scour. Also, there are environmental concerns as a result of the deposition that takes place in the downstream of a channel due to large-scale scour in a plunging pool type energy dissipator. Hence, local scour caused by the jets has been a topic of continued interest to the researchers and the design engineers as well (Sarkar and Dey, 2004). The pioneering investigation on scour due to vertical submerged jet in uniform sediments was conducted by Rouse (1939). Thus, a large number of researches have been carried out to study the scour due to different types of jets (Hoffmans and Verhrij, 1997; Raudkivi, 1998; Graf, 1998). Sarkar and Dey (2004) presented an state-of-art review of the up-to-date investigations on local scour due to horizontal and impinging jets, including all possible aspects.

This section briefly presents the mechanism of local scour beneath turbulent jets, and most relevant researches on local scour due to turbulent jets. Also, the studies on scouring process, parameters affecting local scour, time variation of local scour, and local scour estimation formulas are briefly reviewed.

2.2 Mechanism of Scour by Turbulent Jet

In general, localised scour can occur in two ways:

> (1) clear-water scour

> (2) live-bed scour.

Clear-water scour refers to the situation where no sediment is supplied from upstream into the scour zone. Live-bed scour, on the other hand, occurs when there is general bed load transport by the stream. Sediment is continuously being supplied to the areas subjected to scour. This thesis mainly deals with the clear-water scour.

As the diffused jet starts to flow over the initially flat erodible bed, the scouring potential of the jet, created by the high incoming velocity, is usually so strong that the sand grains are immediately dislodged from the surface and transported downstream at a rapid rate. For a small time period, the vertical dimensions of the scour hole increase at a faster rate than the horizontal dimensions and the bed material is transported mainly as bed loads. As the scour hole gradually enlarges with time, the depth of water also increases. From the principle of continuity, the expanding cross sectional area would require a reduction in the mean flow velocity. Accordingly, the local velocity near the scoured bed decreases as the depth of the hole increases. Hence, the rate of erosion decreases as time progresses. For larger time periods, the bed velocity eventually reduces to a certain "critical" value when the flow (near the bed) becomes incapable of removing further bed material from the scour area. At this point, it could be said that the scour geometry has reached its "equilibrium" or "asymptotic" state. Implicitly, this suggests that the local bed velocity is directly related to the concept of a threshold of a particular movement. It has been accepted that the boundary shear stress is a logical choice of a key variable to characterise the incipient motion of particles for a given bed slope. The bed shear stress is a function of the local bed velocity and the friction factor, which is often assumed to be constant, thus, measurements of the bed velocity and distributions in a scour hole enables the scouring process to be examined (Karim and Ali 2000)

2.3 Local Scour beneath Horizontal Jets

2.3.1 Scouring process

Scouring starts downstream of a hydraulic structure (beneath a water jet) in case of without apron or an apron when the bed shear stress induced by the horizontal jet exceeds the critical bed shear stress for the initiation of bed particle motion. The scouring process downstream of a hydraulic structure is complex in nature owing to the abrupt change of the flow characteristics over the erodible bed and the complex nature of the turbulent jet itself. Different cases of local scour due to horizontal jets are depicted in Figure 2.1(a) – 2.1(d). Figure 2.1(a) presents a schematic diagram of a typical scour hole developed due to the submerged horizontal jet issuing from a sluice opening downstream of an apron (Hassan and Narayanan, 1985), whereas Figure 2.1(b) depicts a typical scour hole developed due to a submerged horizontal jet issuing from a sluice opening (without apron) directly on the erodible bed (Rajaratnam, 1981a). Also, Figure 2.1(c) shows a schematic diagram of a scour hole downstream of a spillway apron (Dargahi, 2003), and Figure 2.1(d) presents a scour hole developed due to the flow simultaneously over and under a sluice gate (Uyumaz, 1988).

Many experimental studies of scour downstream of hydraulic structures are available in literature. Bormann and Julien (1991) reviewed the experimental researches on scour downstream of hydraulic structures below free and submerged jets, being pioneered by Schoklitsch (1932) and Laursen (1952). Bormann and Julien (1991) investigated the scour downstream of grade control structures with large scale experiments using unit discharge up to 2.5 m^2/s and scour depths exceeding 1.4 m. Sarkar and Dey (2004) presented a comprehensive review of the up-to-date investigations on local scour due to horizontal and impinging jets is presented including all possible aspects, such as scouring process, parameters affecting scour, time variation of scour, velocity distribution on the apron and within the scour hole, development of boundary layer thickness, bed shear stress, scour estimation formulas and protection works. Additional to experimental studies reviewed in abovementioned studies, Sarkar and Dey (2004) conducted experiments on characteristics of scour holes in uniform and nonuniform sediments downstream of an apron due to a submerged horizontal jet issuing from a sluice opening, Adduce

and Sciortino (2006) investigated both experimentally and numerically the local scour downstream of a sill followed by a rigid apron.

Most of these experimental studies have sought to empirically correlate parameters such as maximum scour depth, maximum dune height, and the streamwise distances to the maximum scour depth point and dune with forcing parameters such as the mean grain size, density, incoming flow velocity, unit discharge, etc., as given in next section.

2.3.2 Parameters affecting on local scour

Ali and Neyshaboury (1991) studied local scour downstream of a deeply submerged horizontal jet. They described the effect of densimetric Froude number F_d on the extent of scour. The equilibrium scour depth was observed to increase with increase in F_d. They observed that the equilibrium scour depth increases with decrease in height of jet above the bed level.

Ali and Neyshaboury (1991) found that at a given time, the volume of scour hole increases with decrease in sediment size for a constant jet height and velocity. Farhoudi and Smith (1985) showed that for coarse sediments, a dune was formed at the downstream end of the scour hole. But the dune gradually diminished with time with increase in volume of the scour hole. On the other hand, there was no formation of dune with smaller sediment sizes. The effect of sediment size on scour below a sluice gate was investigated by Kells et al. (2001). Keeping all other parameters fixed, the equilibrium scour depth and the area of scour hole decreases with the increase in the sediment size.

Farhoudi and Smith (1985) conducted experiments on scour downstream of spillway to find the height of the dune, which was found significantly high for high tailwater condition. As time progressed, the longitudinal extension of the scour hole became more pronounced. Ali and Lim (1986) experimentally studied the scour due to two and three-dimensional submerged wall jets under shallow tailwater condition. The existence of a critical tailwater depth was noticed, beyond which the asymptotic scour depth always increases irrespective of the variation of tailwater depth. In

shallow tailwater condition, the process of development of scour hole is complex compared to relatively deep tailwater conditions.

Comparing the different tailwater conditions, Johnston (1990) reported that the process of the development of scour hole is a methodical one in case of high tailwater conditions leading to a well-defined equilibrium state (beyond which the scour depth does not increase), whereas in shallow tailwater conditions, the asymptotic state seldom reaches.

Balachandar et al. (2000) studied the effect of tailwater depth on the scour downstream of a sluice gate. The equilibrium scour depth, achieved for a particular set of hydraulic parameters, increases with the increase in the tailwater depth. But the magnitude and the rate of increase of the ratio of equilibrium scour depth to tailwater depth decreases with the increase in the tailwater depth.

Ade and Rajaratnam (1998) observed the differences in the scouring process and the formation of scour profile due to the effect of relative density difference. The longitudinal extension was more in comparison with the dune height when the scour hole was produced by the air jets. They stated that the high value of the relative density difference is to be the most plausible reason for the aforesaid case.

Aderibigbe and Rajaratnam (1998) experimentally studied the effect of sediment gradations on scour due to plane turbulent wall jets. The nonuniformity of sediment particles significantly affects the scour hole development. The portion of the scour hole bearing the coarser particles laid between 0.37 to 0.75 of the length of the scour hole and the median size of the sediment particles present in this zone was d_{95} of the initial sediment mixture, where d_{95} is the 95 % finer particle diameter. There was also a reduction of the maximum scour depth and height of dune due to armoring. The average reductions of the dune height and the maximum scour depth were found to be 50 % and 60 %, respectively. Scour by circular wall jets with nonuniform sediments was studied by Lim and Chin (1992). Kells et al. (2001) also investigated the effect of sediment gradations on scour below sluice gate. The asymptotic scour depth reduces more in nonuniform sediments than that in uniform sediments.
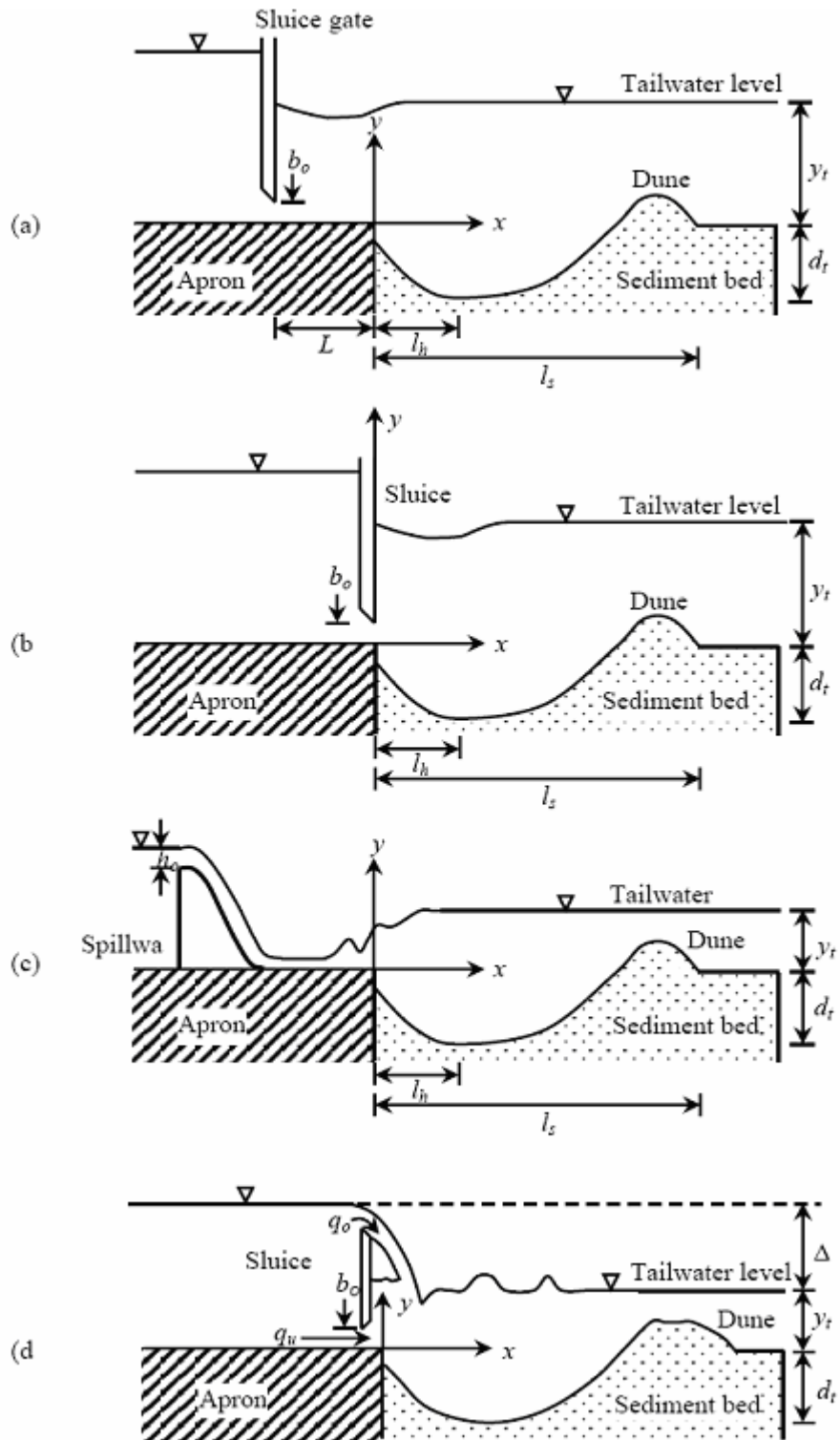
Figure 2.1 Local scour: (a) downstream of an apron after Hassan and Narayanan (1985), (b) due to a submerged horizontal jet without apron (Rajaratnam, 1981a), (c) downstream of a spillway apron (Dargahi, 2003) and (d) due to simultaneous flow over and under a sluice gate after Uyumaz (1988) (Sarkar and Dey 2004).

12

2.3.3 Time variation of scour profiles

Rajaratnam and Berry (1977) experimentally studied the scour caused by circular wall jets of air and water in polystyrene and sand beds, respectively. The scour profiles were approximately similar with some noticeable deviations in the region of the dune at the downstream end of the scour hole. The similarity existed even during the unsteady state and the formation of scour hole. The maximum scour depth (s) and distance of the zone of maximum scour depth from the nozzle, made nondimensional by the diameter of the jet, are functions of the densimetric Froude number.

Rajaratnam (1981a,b) studied the scour of sand and polystyrene beds by plane turbulent wall jets of air and water. He observed the scour profiles being similar for air-sand and air-polystyrene combinations but different for water-sand combination. He also observed that s/b_0 (b_0=sluice gate opening) was larger for the air jets in comparison with the water jets. Scour due to plane wall jet with minimum tailwater was experimentally investigated by Rajaratnam and Macdougall (1983). The maximum scour depth s, and the zone of maximum scour were expressed as functions of densimetric Froude number F_d. However, the magnitude of the maximum scour depth in low tailwater was much less in comparison with that in high tailwater. The zone of maximum scour was located at further downstream section and the dune, which existed for high tailwater condition, was not found for low tailwater depth.

Farhoudi and Smith (1985) plotted the nondimensional coordinates of the profiles and found that the scour profiles are similar. They concluded that a simple parabolic (polynomial) relationship could be used to express the common nondimensional scour profile as

$$y = ax^2 + bx + c \tag{2.1}$$

where a, b and c = constants.

Ali and Lim (1986) obtained the scour profiles along the centerline of the scour hole. For three-dimensional jets, the scour holes were slightly deflected from the central axis of the jet. A ridge, formed at the downstream end of the scour hole, became

flatter with decrease in tailwater depth for two and three-dimensional jets. For two-dimensional jet, the ridge was washed out when the duration of scour was too long. They proposed a relationship for expressing the nondimensional scoured bed profiles as

$$\frac{d_s}{d_t} = -\exp\left(-a\left(\frac{x}{x_n} - b\right)^2\right) \qquad (2.2)$$

where d_s = depth of scour at any distance x, d_t = depth of scour at any time t, and x_n = value of x where $d_s = 0.5\ d_t$.

Chatterjee et al. (1994) investigated the scour downstream of an apron caused by a horizontal jet issuing from a sluice opening. They cited that there was a slight deviation of their proposed profile from the profile given by Hassan and Narayanan (1985) in the downstream ridge of the scour hole, which was mainly due to the effect of sediment particle size on the scouring process.

Ade and Rajaratnam (1998) performed a generalized study of scour due to horizontal circular turbulent jets. The asymptotic state was reached earlier at the zone closer to the nozzle. They concluded that the similarity of the bed profiles in the unsteady and asymptotic states exists.

The similarity of the scour profiles by plotting the nondimensional coordinates was established by Dey and Westrich (2003), where the maximum scour depth at any time was used for the normalization. They proposed that the nondimensional scour profiles can be represented by a simple polynomial. Another important observation was the sediments at the edge of the apron being washed out owing to the reversed flow along the upstream face of the scour hole. Also, the similarity of scour profiles for different time intervals was shown by Carstens (1966) and Mazurek et al. (2003).

On the other hand, Dargahi (2003) found a considerable difference in the shape of the scour profiles at different times. He considered the entire scoured area for investigating the existence of similarity of the scour profiles. His observation contradicts the opinion of previous researchers regarding the similarity of the profiles

at different times. Balachandar and Kells (1998) studied the instantaneous water surface and scour profiles, using the technique of video image analysis.

Hogg et al. (1997) analytically studied the scour of sand bed by planar turbulent wall jets. They presented their own scaling laws representing the spatial variation of the mean velocity and the lateral extent of a two-dimensional turbulent wall jet. These laws were used to develop an analytical model of the progressive scour of the initially flat bed. They compared the predicted scoured bed profiles with the experimental observations of Rajaratnam (1981a) and found that the predictions were in good agreement.

Adduce and Sciortino (2006) both experimentally and numerically studied the scour due to a horizontal jet occuring downstream of a sill followed by rigid apron. Their model uses information related both to measured velocity fields and to the physical and mechanical properties of the sand constituting the mobile bed. The analytical structure of the model consists of a second order partial differential equation whose unknown is the shape of the mobile bed. The numerical integration of this nonlinear equation, with suitable boundary conditions, is in agreement with the measured scour profiles at the end of the run. Upon comparing experimental and numerical data, a similar temporal evolution of the maximum scour depth was observed by the researchers.

2.3.4   Time variation of scour depth

Time variation of scour depth for the flow over and under a structure was investigated by Breusers (1966), Kotoulas (1967) and Dietz (1969). Breusers (1966) recommended a power law type relationship for calculating the time variation of scour depth. Kotoulas (1967) observed that 64 % of the equilibrium scour depth occurred in the first 20 seconds and 97 % of the equilibrium scour depth reached in 2 hours.

The time variation of the scour depth was represented by the following equation:

$$y_t + s = \left[\frac{1.9}{g^{0.35}} \left(\frac{\Delta h^{0.35} q^{0.7}}{d_{95}^{0.4}} \right) \right] \left(1 - e^{-0.55 t^{0.2}}\right) \qquad (2.3)$$

where y_t= tailwater depth, Δh = difference between the upstream water depth and tailwater depth; q = unit discharge of jet; and g= gravitational acceleration.

Most of the analytical methods developed for predicting the time variation of scour depth attempt to find a solution of the sediment continuity equation, which is

$$\frac{dv_s}{s} = Q_s \qquad (2.4)$$

where v_s = volume of scour per unit width; and Q_s = volume rate of sediment transport out of scour hole per unit width.

Hassan and Narayanan (1985) developed a semiempirical theory to predict the temporal variation of scour depth downstream of an apron due to submerged jets based on the measured mean velocity distributions in the scour hole. They proposed the following equation for the rate of scour:

$$\frac{ds}{dt} = b_1 U_m \frac{U_m^2}{g(s_r - 1)d_m} \left(\frac{U_m^2}{g(s_r - 1)d_t} \right)^n \qquad (2.5)$$

where β_1 = nondimensional coefficient, U_m= maximum mean velocity, d_m= median size of sediment particles, s_r=relative density of sediment particles, and n = constant.

Ali and Neyshaboury (1991) observed that at long duration of scour, the rate of scour at the zone of maximum scour depth was negligibly small. But the longitudinal extension of the scour hole enlarged continuously without altering the maximum scour depth.

Chatterjee et al. (1994) measured the maximum scour depth s at different times for various bed sediments and found that s is approximately equal for the same value of v_s measured for different bed sediments.

Dey and Westrich (2003) used the Buckingham π-theorem to give an expression of time variation of scour depth in nondimensional form. For scour depth downstream of a spillway, Dargahi (2003) studied the effects of flow and sediment parameters on the temporal variation of the scour profiles, existence of similarity of the scour profiles at different times and prediction of the maximum scour depth at a given time. The scour cavity increased in size and shape with increase in operating head or discharge. He concluded that the time variation of maximum scour depth might be described by a power law.

Balachandar and Kells (1997) investigated the time variation of scour in uniform sediments downstream of an apron due to submerged jet issuing from a sluice opening. Application of the various scaling laws for a turbulent wall jet was studied by Breusers (1965), Farhoudi and Smith (1982) and Wygnanski et al. (1992).

2.3.5 Prediction of scour depth

Schoklitsch (1932, 1935) studied on the local scour downstream of a gate due to flow over a gate without apron. The following equation was proposed for computing equilibrium scour depth:

$$s + y_t = 4.75 \Delta h^{0.2} q_0^{0.57} d_{90}^{-0.32} \tag{2.6}$$

where q_o = overflow discharge.

Eggenberger and Mueller (1944) investigated the development of scour hole downstream of an apron by a two-dimensional horizontal jet issuing from a sluice gate. They presented an empirical relationship for the equilibrium scour depth.

$$s + y_t = w_e \frac{\Delta h^{0.5} q_0^{0.6}}{d_{90}^{0.4}} \tag{2.7}$$

where w_e = a coefficient. They observed that the above equation overestimated the measured scour depth in general.

The scour resulting from the combination of flow over and under a hydraulic structure was also investigated by Eggenberger and Mueller (1944). They proposed the following equation for calculating the coefficient w_e in case of combination of flow over and under a structure:

$$w_e = 22.88 - \frac{1}{0.0049R_q^3 - 0.0063R_q^2 + 0.026R_q + 0.064} \tag{2.8}$$

where R_q = ratio of the overflow to underflow unit discharge.

Scour downstream of river barrages, sills and stilling basins was investigated by Novak (1956, 1961). He proposed an equation for calculating the maximum scour depth as

$$s + y_a = K_1 \left[6\Delta h^{0.25} q^{0.5} \left(\frac{y_t}{d_{90}} \right)^{1(3} - y_t \right] \tag{2.9}$$

where y_a = flow depth over apron; and K_1 = constant. The value of K_1 = 0.45 for y_t/y_c = 1.6, and K_1 = 0.65 for y_t/y_c = 1; where y_c = critical of flow depth.

Shalash (1959) did experimentally investigatedthe development of scour downstream of an apron. He included the effect of apron length in the proposed equation for computing the equilibrium scour depth as

$$s + y_a = 9.65H_1^{0.5} q_u^{0.6} d_{90}^{-0.4} \left(\frac{L_{min}}{L} \right)^{0.6} \tag{2.10}$$

where H_1 = upstream water depth, q_u = underflow discharge, L=length of apron and L_{min} = $1.5H_1$.

Clarke (1962) presented an empirical formula predicting the length of scour hole as

$$\frac{l_s}{s} = 4.3 \left[\frac{U_1}{(gd_n)^{0.5}} \right]^{0.467} \left(\frac{U_1}{w} \right)^{0.2} \left(\frac{gt}{w} \right)^{0.067} \tag{2.11}$$

where l_s = longitudinal extension of scour hole including dune from the edge of apron, d_n = diameter of nozzle, U_1 = issuing velocity of jet, and ω = mean fall velocity of sediment particles.

Kotoulas (1967) experimentally investigated scour downstream of an apron when the flow takes place over or under a structure. He suggested the following relationship for the equilibrium scour depth:

$$s + y_t = \frac{1.9}{g^{0.35}} \left(\frac{\Delta h^{0.35} q_0^{0.7}}{d_{95}^{0.4}} \right)$$
(2.12)

Scour depth obtained from Eqn. (2.7) is approximately 85 % larger than that from Eqn.(2.12). Philips (1984) studied the temporal lag effect in bed load sediment transport. He suggested an equation for computing the nondimensional maximum scour depth. Dietz (1969) carried out an experimental investigation on scour downstream of a hydraulically rough apron.

Whittaker and Schleiss (1984) put forward the following relationship for the length of scour hole:

$$\frac{l_s}{2b_0} = 35 \left(\frac{U_1}{w} \right)^{0.57} U_1^{0.86}$$
(2.13)

Ali and Lim (1986) found that the time evolution of scour follows a power law relationship and the semi-logarithmic law as well. They proposed the following relationship for the equilibrium scour depth:

$$\frac{s}{L_0} = 2.3 \left(\frac{U}{w} \right)^{0.5} \left(\frac{d_m}{L_a} \right)^{0.375} F_d^{0.75} - 1.19$$
(2.14)

where U = mean velocity of jet; and L_a = length scale, defined as (a) $L_a = b_o$ for a deeply submerged two-dimensional jet issuing from a sluice gate opening with a well rounded lip; (b) $L_a = Y_v$ for a deeply submerged two-dimensional jet issuing from a sharp sluice gate; and (c) L_a = ratio of jet area to its perimeter for two- and three-

dimensional jets with shallow tailwater depth; where Y_v = thickness of jet at vena-contracta.

Analyzing the available laboratory data, Breusers (1991) proposed the following relationship for calculating the equilibrium scour depth:

$$\frac{s}{b_0} = 0.008 \left(\frac{U_1}{u_{*c}} \right)^2$$ (2.15)

where u_{*c} = critical velocity for sediment particles.

Breusers and Raudkivi (1991) analysed the scour data due to horizontal submerged jets of Clarke (1962), Rajaratnam and Berry (1977) and Rajaratnam (1981a) and suggested the following equations:

$$\frac{s}{d_n} = 0.08 \frac{U_1}{u_{*c}} \qquad \text{for round jets}$$

$$\frac{s}{2b_0} = 0.008 \left(\frac{U_1}{u_{*c}} \right)^2 \qquad \text{for plane jets}$$ (2.16)

Chatterjee et al. (1994) reported that the maximum scour depth at equilibrium is independent of the sediment particle size which contrasts the dependence of maximum scour depth at any time during the scouring process on the particle size of bed sediment. They put forward the following expression for the maximum equilibrium scour depth:

$$\frac{s}{b_0} = 0.775 \frac{U_0}{(gb_0)^{0.5}}$$ (2.17)

In order to develop scour depth equations, Dargahi (2003) avoided the nonlinear multiple regression analysis due to its inherent difficulty in generating a simple equation. He found the major parameters and put forward simple equations for calculating the maximum scour depth and its location separately for the side (near the flume walls) and centerline sections (along the middle of the flume), which are as follows:

$$\frac{s}{h_0} = \left(\frac{h_0}{d_m}\right)^{1/3} \tag{2.18}$$

$$\frac{x_m}{h_0} = 10\left(\frac{h_0}{d_m}\right)^{1/12} \tag{2.19}$$

$$\frac{s}{h_0} = 1.7\left(\frac{h_0}{d_m}\right)^{1/4.5} \tag{2.20}$$

$$\frac{x_m}{h_0} = 5\left(\frac{h_0}{d_m}\right)^{1/3} \tag{2.21}$$

where x_m = location of maximum scour depth from the edge of the apron, and h_0=operating head. The first two equations are valid for the side sections and the remaining equations are valid for the centerline section. He compared the measured maximum scour depths with the ones predicted by the existing equations and the equation given by Jaeger (1939), which was found to be a good estimate of the measured scour depths.

2.4   Local Scour beneath Impinging or Plunging Jets

2.4.1   Scouring process

Scour of sand, clay, gravel and weak rock beds by impinging jets has significant importance in hydraulic engineering, as it is indispensable to predict and control erosion near hydraulic structures, which may otherwise damage the structures. Impinging (or plunging) jet refers to the jets of water striking on or inside the free surface issuing from an outlet situated above or below the free surface. Figures 2.2 and 2.3 present the schematic views of the typical scour holes developed due to the submerged vertical impinging and plunging jets, respectively.

Mih and Kabir (1983) experimentally investigated the impinging action of the water jet on nonuniform sediment beds. In the initial stages, the jet penetrated the

streambed very fast. The jet was deflected upward from the deepest point of the scour hole forming a vertical circulation. The vertical circulation carried out the sediments from the scour hole to deposit on the adjacent bed. The circulation expanded gradually outward from the jet centerline. Sorting of bed particles was observed as the smaller particles had a larger velocity and tended to rotate at a larger radius of curvature than the larger particles.

Jia et al. (2001) numerically simulated the scouring process of a plunging pool with bed sediments. Considering an unsteady three-dimensional model, they applied the finite element method for solving the problem. The effects of bed shear stress and fluctuating lift force were incorporated in the computation. They found the hybrid (numerical-empirical) model to be very efficient to simulate the scouring process.

Mazurek et al. (2001) investigated the scour of cohesive sediment by submerged circular impinging jets. They observed three different types of erosion. Initially, the erosion of small flakes was observed. The flakes were circular in shape having a diameter of 1-3 mm and thickness 0.5 mm. The critical shear stress during flake erosion was 15 Pa. The mode of transport changed when the critical shear stress was increased. Both small and large chunks of soil were eroded during this phase. Rapid surface erosion occurred when the critical shear stress exceeded 200 Pa.

2.4.2   Parameters affecting on local scour

Doddiah et al. (1953) experimentally investigated the scouring of sediment bed due to hollow and circular impinging jets. The resaerchers witnessed the existence of a critical impinging distance beyond which the maximum static scour depth decreased with the increase or decrease in the impinging distance.

Westrich and Kobus (1973) studied the erosion of a uniform sediment bed by continuous pulsating jets. The variation of the asymptotic scour depth with impinging distance has multiple peaks. The effect of the impinging distance on the scour profile due to submerged vertical circular jets of water was experimentally
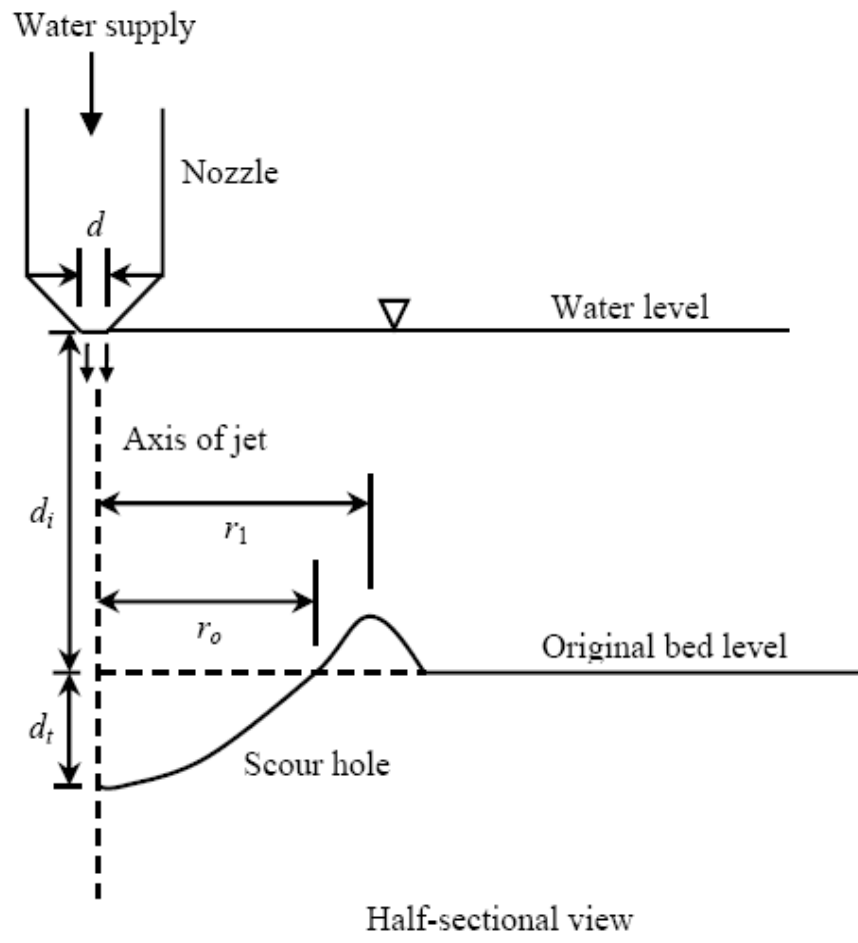
Figure 2.2 Definition sketch of local scour due to a submerged vertical impinging jet (Aderibigbe and Rajaratnam 1996)
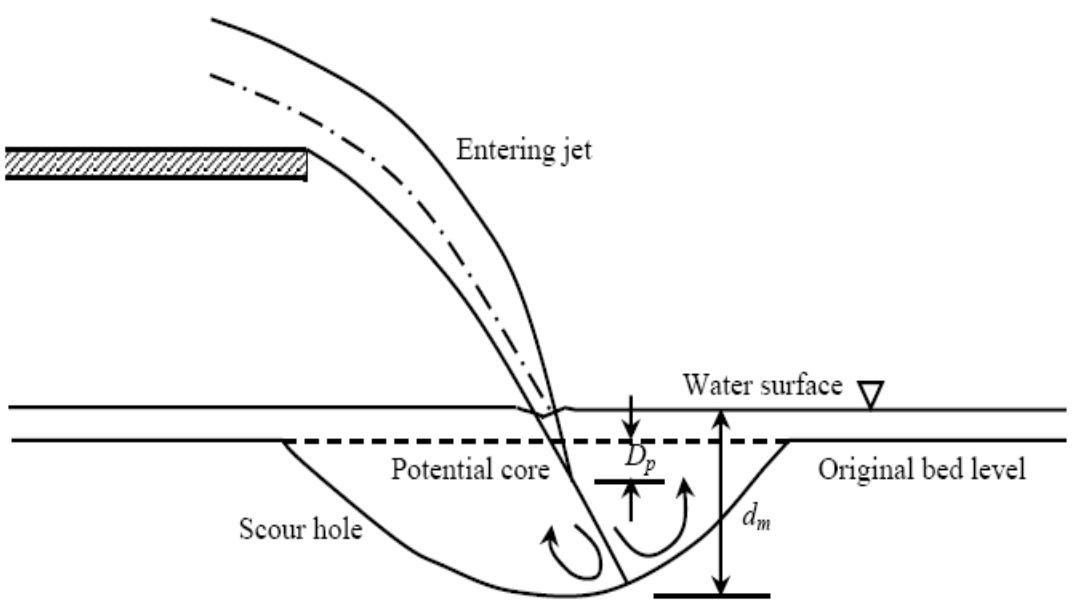
Figure 2.3 Definition sketch of scour in a plunging pool (Stein et al. 1993)

studied by Aderibigbe and Rajaratnam (1996). They witnessed the existence of the critical impinging distance, at which the static scour depth attains maximum value.

Aderibigbe and Rajaratnam (1996) stated that the equilibrium characteristic lengths of the scoured bed are functions of the scour parameter E_c and the relative density difference. They proposed the following equation of the maximum scour depth, which can be used for different values of the relative density difference:

$$\frac{s}{d_i} = 0.05(E_c - 0.14)^{0.16} \frac{(\Delta + 1)^{3.1}}{\Delta^{2.8}} \tag{2.22}$$

where d_i=impinging distance, E_c=scour parameter, and $\Delta = (r_s / r) - 1$.

They also proposed the equation of the radius of scour hole as

$$\frac{r_m}{d_i} = 11E_c^{0.65} \frac{\Delta^{6.2}}{(\Delta + 1)^{6.6}} \tag{2.23}$$

where r_m = asymptotic value of scour hole radius.

2.4.3   Time variation of scour profiles

Rajaratnam (1982) analyzed the scour profiles in the asymptotic state and concluded that the profiles are similar. The similarity of the profiles is described by the following equation:

$$\frac{d_t}{s} = \exp\left(-0.693\left(\frac{r}{x_n}\right)^2\right) \tag{2.24}$$

where r = radius of the scour hole at a given time.

Blaisdell and Anderson (1991) determined the shape of the scour hole measuring the longitudinal and transverse sections of the hole along the centerline. The maximum scour hole dimensions were determined from the projections of the slopes of the

longitudinal and transverse sections. They found the scour hole contours to be elliptical. Aderibigbe and Rajaratnam (1996) also studied the evolution of the scour profiles with time. The similarity of the asymptotic scour profiles exists. They found Eqn. (2.24) to be effective in describing the nondimensional asymptotic scour profiles.

Rajaratnam and Mazurek (2002) analyzed the asymptotic scour profiles of the eroded bed and came into a conclusion that the profiles are similar and could be represented by the early proposed exponential equation (2.24) by Rajaratnam (1982) .

2.4.4   Time variation of scour depth

Rouse (1939) conducted the first experimental study on scouring of uniform sediments caused by vertical submerged impinging water jets. He observed that the depth of scour in uniform sediments varies linearly with the logarithm of the impinging time for an appreciable zone of the scouring process. Keeping in view the risk of future repair and maintenance costs, Blaisdell and Anderson (1991) used the hyperbolic technique of Blaisdell et al. (1981) to compute the scour depth at any time. They plotted the ratio of asymptotic maximum scour depth below tailwater relative to nozzle diameter Z_{mu}/d_n as a function of the densimetric Froude number F_o and found the curve to be hyperbolic. They proposed the following set of equations for computing the scour depth at any time:

$$x_h + y_h - \sqrt{x_h^2 + a_h^2} = \log\frac{-Z_m}{d_n} \tag{2.25}$$

$$x_h = \log\frac{tu_e}{Y_0} \tag{2.26}$$

$$y_h = \log\frac{-Z_{mu}}{d_n} \tag{2.27}$$

where Z_m = maximum scour depth below tailwater (-ve); x_h = abscissa of hyperbola; y_h = offset of origin of hyperbola on y-axis; a_h = semimajor axis of hyperbola; and Z_{mu} = asymptotic maximum scour depth below tailwater. The value of Z_{mu}/d_n can be calculated from the following expressions:

$$\frac{Z_{mu}}{d_n} = -7.5\left(1 - \exp(-0.6(F_d - 2))\right) \quad for\, Z_p/d_n \le 1 \tag{2.28}$$

$$\frac{Z_{mu}}{d_n} = -10.5\left(1 - \exp(-0.35(F_d - 2))\right) \quad for\, Z_p/d_n > 1 \tag{2.29}$$

where Z_p = height of the pipe invert from tailwater.

Stein et al. (1993) put forward an analytical approach to determine the time variation of scour depth. They equated the sediment continuity equation to the excess shear equation and integrated the resulting nonlinear differential equation to get a nondimensional equation from which the maximum scour depth at a given time can be determined. The equations of nondimensional times are given below:

$$T^* = D^*\left(\frac{D_p^*}{1 - D_p^*}\right)^x \tag{2.30}$$

$$T_p^* = D_p^*\left(\frac{D_p^*}{1 - D_p^*}\right)^x \tag{2.31}$$

where T^* = nondimensional time, that is t/T_r; T_r = reference time; D^* = nondimensional maximum scour depth, that is d_t/d_m; D_p^* = nondimensional depth of potential core, that is D_p/d_m; ξ = sediment detachment exponent; T_p^* = nondimensional time, that is T_p/T_r; and T_p = time required to reach the scour depth D_p.

Mazurek et al. (2001) stated that the growth of the scour hole has a definite relationship with the logarithm of time except during the initial stages and at times when it approaches equilibrium. They put forward the following equation for the nondimensional time scale:

$$t^* = \frac{t_{80} U_0}{d_i} \left(\frac{d_n}{d_i} \right) \tag{2.32}$$

where t^* = nondimensional time scale; and t_{80} = time to reach 80 % of the maximum scour depth.

Neyshaboury et al. (2003) numerically simulated the turbulent flow and the progressive erosion of the bed due to a free falling jet. They used the finite volume method together with a non-staggered grid pattern for the solution of the momentum, continuity and k-ε turbulence model equations to simulate the turbulent flow field. The progressive erosion of the bed was computed using the sediment continuity equation.

2.4.5   Prediction of scour depth

Veronese (1937) studied on the scouring process in a plunging pool and proposed the following equation for calculating the equilibrium scour depth:

$$s + y_0 = 3.68 H^{0.225} q^{0.54} d_e^{-0.42} \tag{2.33}$$

where y_o = water depth in the plunge pool; and H = height of upstream energy level above pool level. The above equation was also used by USBR for calculating the equilibrium scour depth (Sarkar and Dey 2004). Later, the equation was modified by Jaeger (1939) in the following form:

$$s + y_0 = 6 H^{0.25} q^{0.5} \left(\frac{y_0}{d_{90}} \right)^{0.33} \tag{2.34}$$

The experiments of Veronese (1937) were repeated by Hartung (1957), who modified the equation suggested by Veronese (1937) as

$$s + y_0 = 12.4 H^{0.36} q^{0.64} d_{85}^{-0.32} \qquad (2.35)$$

where d_{85} = 85 % finer particle diameter.

Damle et al. (1966) also suggested an equation for the computation of equilibrium scour depth caused by a plunging jet

$$s + y_0 = 0.55(gH)^{0.5} \qquad (2.36)$$

Chian (1973) and Martins (1975) experimentally studied on the development of scour due to plunging jets and suggested the following relations for estimating the equilibrium scour depth:

$$s + y_0 = 1.18 q^{0.6} H^{0.235} \qquad (2.37)$$

$$s + y_0 = 1.5 q^{0.6} z^{0.1} \qquad (2.38)$$

where z = difference between the free surface and the lip of the flip bucket elevation.

Akashi and Saito (1984) performed an investigation on local scour due to submerged vertical plane jets and proposed the following relationship:

$$\frac{s}{2b_0} = 0.0065 \left(\frac{U_0}{u_{*c}} \right)^{1.28} \qquad (2.39)$$

Most of the formulas to estimate the scour due to an impinging jet are of the following form:

$$s = K \frac{q^a h_0^b}{d_m^{\,g}} \qquad (2.40)$$

where K, α, β and γ = constants.

Mason and Arumugam (1985) summarized the formulas which have been developed for estimating the maximum scour depth under a falling jet. The accuracy of the formulas was evaluated by using each to process sets of scour data from prototypes and models of such prototypes. The authors proposed a comprehensive model and prototype equation which can be rewritten as:

$$\frac{s}{\left(\frac{q^2}{g}\right)^{1/3}} = (6.42 - 3.10H^{0.1})g^{-H/600} \times \left(\frac{gH^3}{q^2}\right)^{20+H/600} \left(\frac{H}{d_s}\right)^{1/10} \left(\frac{h}{H}\right)^{3/20} \tag{2.41}$$

where q is unit discharge (m^2/s), H is drop between upstream water level and tailwater depth (m), g is gravitational acceleration and d_s is representative bed grain size (m).

Mason and Arumugam (1985) obtained the best agreements between the selected equations and measurements for the model data by using d_s equal to d_m (mean bed grain size).

Bormann and Julien (1991) carried out a large-scale study in order to calibrate their semi-theoretical equation for calculating maximum scour depth, under a wide range of conditions: wall jets, vertical jets, free jets, submerged jets and flow over large-scale grade control structures. Their proposed equation is remarkably similar to the regression based equations proposed in the literature:

$$s = \left[\frac{0.611}{[\sin(0.436 + b')]^{0.8}} q^{0.6} \frac{U_0}{g^{0.8}d_{90}^{0.4}} \sin b'\right] - z \tag{2.42}$$

where d_{90} is bed grain size for which 90% of sampled particles are finer (m) and U_0 is jet velocity impinging on the tailwater (m/s).

Stein et al. (1993) developed the following analytical equation to determine the equilibrium scour depth:

$$s = \frac{C_d^2 c_f r U_0^2 Y_0}{t_{0c}} \sin q \tag{2.43}$$

where C_d=jet diffusion coefficient, c_f = coefficient of friction. They assumed that beyond the depth of the potential core of the jet, the shear stress decreases until it approaches the critical shear stress for the bed sediments.

Aderibigbe and Rajaratnam (1996) put forward the following relationship for calculating the equilibrium scour depth:

$$\frac{s}{d_i} = 1.26 E_c^{0.11} - 1 \qquad (2.44)$$

Rajaratnam and Mazurek (2002) observed that the maximum equilibrium scour depth due to the oblique impinging jet was more than that for the vertical impinging jet. They cited the greater transport capability of the component of the flow parallel to the bed as the main reason for getting the enhanced scour depth. They presented the following set of equations for calculating the maximum equilibrium scour depth:

$$\frac{s}{d_i} = 0.73 \frac{F_d}{d_i / d_n} - 0.1 \quad for\ 30^0 < q < 60^0 \qquad (2.45)$$

$$\frac{s}{d_i} = 0.77 \frac{F_d}{d_i / d_n} - 0.2 \quad for\ 15^0 < q < 30^0 \qquad (2.46)$$

where θ=impingement angle.

Altinbilek and Okyay (1973) investigated the scour in a sediment bed due to vertical jets. And various studies concerning the other aspects of impinging jets were performed by Cola (1965), Poreh and Hefez (1967), Beltaos (1972), Beltaos and Rajaratnam (1973), Hartung and Hausler (1973), Martins (1973), Beltaos (1974), Beltaos and Rajaratnam (1974), Martins (1975), Beltaos (1976a), Beltaos (1976b), Beltaos and Rajaratnam (1977), Kobus et al. (1979), Chee and Yuen (1985), Salehi-Neyshaboury (1988), Fahlbusch (1994), Hoffmans (1998), and Mazurek et al. (2001).

Agostino and Ferro (2004) developed a methodology for prediction of scour downstream of grade-control structures by applying the incomplete self-similarity theory for deriving the nondimensional groups influencing the scour process. Using a

forward stepwise regression on all nondimensional groups, they proposed the following relationship:

$$\frac{s}{z} = 0.54 A_{50}^{0.544} \left(\frac{b_w}{z} \right)^{0.593} \left(\frac{\Delta h}{y_t} \right)^{-0.126} \left(\frac{d_{90}}{d_{50}} \right)^{-0.856} \left(\frac{B}{b_w} \right)^{-0.751} \tag{2.47}$$

where z=height of the weir, d_{50}=50% finer particle diameter, A_{50} = non-dimensional associated with median sediment particles; b_w = weir width.

CHAPTER 3

NUMERICAL-ANALYTICAL ANALYSIS OF LOCAL SCOUR

3.1   General

In hydraulic engineering, the prediction and control of erosion are important consideration in safe design of hydraulic structures, for example, near cooling pools of power plants, around bridge piers, in spillway and culvert outlets and in irrigation channels. Large scale erosion caused by fluid flow to hydraulic structures is of obvious concern because the foundations can be undermined leading to structural failure (Gunal and Guven 2006).

Expensive and time consuming experimental studies of scouring processes supported numerical modeling of this process. Scour modeling is also a time consuming process, even when recently developed computer software and hardware technology are used. The designers require detailed flow patterns of the scoured bed profile to minimize the risk of failure of hydraulic structures.

The standard k-ε model has been successively applied and well validated in local scour and sediment transport problems (Devantier and Larock 1986, Toro et al. 1989, Çelik and Rodi 1991, Ushijima et al. 1992, Olsen and Melaaen 1993, Olsen and Kjellesvig 1998, Garcia-Martinez, et al. 1999, Karim and Ali 2000, Neyshabouri et al. 2001, 2003, Barron and Neyshabouri 2003, Gunal and Guven 2006).

Because of the popularity and high efficiency of the k-ε model, different and improved versions of this model have been proposed. The basic scope of the improvements was the remedying of deficiency of the standard model in under-predicting flows past steps and obstacles and flows in recirculation region (Yap 1987, Yakhot and Orszag 1986, Chen and Kim 1987, and Lam and Bremhorst 1981).

In this thesis, a hybrid numerical-analytical model is presented, which consists of a analytical modeling of temporal evolution of local scour profile, and a standard k-ε turbulence model which simulates the temporal and spatial flow patterns in the corresponding instantaneous local scour profile. Several experimental studies in the literature together with two Ph.D. works are used to calibrate the proposed hybrid model and evaluate the efficiency and accuracy of its predictions to the experimentally observed data.

3.2   Review on Numerical Studies on Local Scour Due to Turbulent Jets

In recent years, with the ever increasing capabilities of computer hardware and software, and due to the time consuming and expensive nature of experimental research on scouring processes caused by flowing water,   several authors have focused attention on the numerical simulation of the interaction of the fluid flow and the movable bed (Neyshabouri et al. 2001).

Zaghloul and McCorquodale (1975) proposed a numerical model that predicts the depth and shape of the local scour hole. The model involves two relaxation stages: (a) two dimensional relaxation in time, (b) relaxation of the depth i.e. the third dimension. The first stage utilizes the Helmholtz-Poisson form of the Reynolds equations with constant eddy viscosity and proceeds until a stable separation pattern is obtained. The second stage permits the depth to change in such a way as to balance applied shear and the bed resistance. At this stage the stream functions and vortices are relaxed in space only. A stability analysis of the numerical model has been completed. They confirmed the numerical model with several experimental flume studies.

Guohou and Peisheng (1988) simulated local scouring downstream of stilling basin. They solved simultaneously equations consisting of motion and continuity equations for flow equation for bed-load transport (Einstein equation) and continuity equation for the bed material. In computation, they used the method of characteristics considering large scale vortex. Experiments with gravel particles (as bed-load) were selected to calibrate the analytical model. Verification analysis showed that their model gave good approximation for local scouring.

Ushijima et al. (1992) considered 2- and 3-dimensional scouring by warmed jets. The unsteady continuity and momentum equations, with the k-ε turbulence closure model, were solved using the finite difference method. Both bed-load and suspended-load were considered in the solution of the equation for sediment at the bed. The convection–diffusion equation for suspended-load concentration was solved numerically. Sediment concentration at the bed was calculated with the aid of the Lane and Kalinske (1941) relation. Although the results were, in general, satisfactory, the computed bed profiles exhibited some undulations which were not present in the experimental results.

To reduce above-mentioned problems, Ushijima (1996) subsequently used an arbitrary Lagrangian-Eulerian approach in which three-dimensional body-fitted coordinates were generated for the sand bed profile, as it was unsteadily deformed by the flow.

Hoffmans and Booij (1993) presented a model for the flow in a trench based on the solution of the 2-D Reynolds equation and the convection-diffusion equation. Bed-load and suspended-load were computed by the stochastic method proposed by Van Rijn (1987). The results were satisfactory, even though it was necessary to calibrate some parameters in the sediment transport formula for different flow zones.

Olsen and Melaaen (1993) predicted local scour developing processes using a three-dimensional flow and sediment transport model. They solved the Reynolds equations with the k-ε model for turbulence closure. Considering both suspended load and bed load, they solved the bed sediment conservation equation by iterating the procedure until the scour hole at an equilibrium state is obtained. Comparison of the numerical results with experimental data showed fairly good agreement.

Hogg et al. (1997) developed an analytical model predicting local scour of an initially flat bed of grains by two-dimensional turbulent wall jet. The steady-state profile was calculated by applying critical conditions along the bed surface for the incipient motion of a particle. The temporal evolution of the scour hole was obtained by integrating a sediment-volume conservation equation. The predicted profiles were compared with experimental studies by Rajaratnam (1981).

Olsen and Kjellesvig (1998) modeled numerically in three dimensions the water flow around a circular cylinder placed vertically in a flume. They used k-ε turbulence model in solving the Navier-Stokes equations, and this gave the shear stress on the bed. They solved the water flow field simultaneously with the sediment calculation. They used an adaptive grid which follows the changes in bed and water surface elevations. The predicted scour hole and a maximum scour depth compared well with empirical formulas for local scour.

Hoffmans (1998) used a different approach to compute the practical equilibrium scour process caused by plunging or horizontal jets when no bed protection is present. He applied Newton's second law of motion to mass of particles of fluid to derive relations for the maximum scour depth in the equilibrium phase (no sediment is tranported downstream anymore). Hoffman used the equations found previously by other researchers and the accuracy of these equations was evaluated using numerous of data of both prototype situations and flume experiments. He used a significant amount of work from other researchers by drawing them together to calibrate and verify the predictors for the scour depth caused by horizontal jets. Although the simplifications were made in applying the momentum principle to a short horizontal reach of a scour hole, reasonable results were obtained for both 2-D and 3-D jet scour compared with other scour relations.

Garcia-Martinez, et al. (1999) presented a two-dimensional computational model to simulate suspended sediment transport and bed changes using standard k-ε turbulence model.

Karim and Ali (2000) simulated the flow patterns generated by turbulent water jets impinging on rigid horizontal and scoured beds. They compared three turbulence closure models incorporated in FLUENT CFD package: the Standard k-ε model, the Reynolds Stress model (RSM) and the Re-normalized Group (RNG) k-ε model. In general, flowfields, velocities and shear stresses predicted by FLUENT showed good agreement with relevant experimental results.

Salehi Neyshabouri et al. (2001) simulated the scouring process caused by a wall jet without a solid apron. Their results showed good agreement with experimental data

on evolution of the scour with time. The predicted shape and position of scour hole and the deposition of the bed material downstream of the hole appeared realistic.

Jia et al. (2001) developed a numerical model simulating the local scour in a plunge pool of loose bed due to a 2-dimensional plane impinging jet. They modified the sediment transport model of Nakagawa and Tsujimono (1980) by including the effects of shear stress and a fluctuating lift force, the latter was related to pressure fluctuations by using empirical functions. They solved the flow field by CCHE3D, a finite element based unsteady 3-dimensional model, with a k-ε turbulence model.

Barron and Salehi Neyshabouri (2003) presented the numerical modeling of the 2-D scour process caused by a wall jet, occurring downstream of a solid apron. This type of scour occurs frequently in practice (scour downstream of a stilling basin, sluice gate, etc.), and thus forms a problem of considerable importance in hydraulic engineering. Comparison of the simulation results with available experimental data showed favorable agreement for the time evolution of the scour hole and for the maximum scour depth.

Neyshabouri et al. (2004) simulated scour by a free falling two-dimensional jet on cohesionless alluvium. The momentum equations, the continuity equation and the k-ε equations for turbulent flows were applied. First the turbulent flow due to a free falling jet was computed, then the distribution of the sand concentration was determined and the scoured bed was predicted. The results of numerical simulation appeared to compare favourably with experiment.

Gunal and Guven (2006) simulated the turbulent water flow issued on frozen scoured beds. They used a finite volume method to solve the equations of motion and transport equations for two dimensions on a transformed rectangular domain using boundary-fitted coordinates. The internal characteristics of the mean flow of submerged horizontal jets including surface profiles on frozen scoured beds are computed by a two-dimensional k–ε turbulence model. Computations are carried out at different frozen-scoured bed profiles. They investigated the diffusion characteristics of the submerged jet, growth of boundary layer thickness, velocity distribution within the boundary layer, and shear stress at the scour and compared with the results of others.

Adduce and Sciortino (2006) developed an analytical-numerical model that simulates local scour downstream of a sill followed by a rigid apron. The model uses information related both to the measured velocity fields and to the physical and mechanical properties of the sand constituting the mobile bed. The analytical structure of the model consists of a second order partial differential parabolic equation whose unknown is the shape of the mobile bed. The numerical integration of this nonlinear equation, with suitable boundary conditions, is in agreement with the measured scour profiles. Upon comparing experimental and numerical data, a similar temporal evolution of the maximum scour depth was observed.

3.3   Hybrid Numerical-Analytical Modeling of Local Scour

In this thesis, it is aimed to analyze physics and mechanics behind local scour phenomenon together with the mean flow patterns using numerical and analytical methods in co-operation. Namely, an analytical model is developed in order to simulate the temporal and spatial variation of scour profile downstream of hydraulic structure based on shear-stress modeling, and then, the time-dependent developments of mean flow components (mean velocity components in two-dimension, pressure distribution, free surface profile, bed-shear stress distribution and velocity decay, etc.) are simulated in the scouring zone using the standard k-ε turbulence modeling.

By using a hybrid model, we aim to get more accurate predictions of time-dependent local scour profiles by utilizing an explicit analytical model that directly analyzes the external forces acting on a soil particle and relates the shape of instantaneous bed profile to the action of these forces and the mechanic characteristics of the soil particle. Unlike the proposed model, the other k-ε models in the literature, firstly the solve the internal flow patterns occurring on erodible soil and then and derive the shape of mobile bed profile by applying the sediment transport continuity equation to the cells closest to the bed (Olsen and Melaaen 1997, Garcia-Martinez et al. 1999, Karim and Ali 2000 and Neyshabouri et al. 2001, 2004).

The latter part of the proposed hybrid model is k-ε turbulence modeling of the flow patterns in the instantaneous bed profile. The proposed model works efficiently with

the analytical model and it is not needed to run for deriving the instantaneous shape of bed profile, thus lots of computing time are gained contrary to the other models that must solve all functionalities included to get the scour profile.

3.3.1 The standard k-ε model

The k-ε turbulence model proposed by Harlow and Nakayama (1968) is still the most widely-used two-equation eddy-viscosity turbulence model, mainly because the energy dissipation, ε, was long believed to require no extra terms near walls. The popularity of the model, and its wide use and testing, has thrown light on both its capabilities and its short-comings, which are well-documented in the literature.

The basic assumption of this method is that the local state of turbulence is characterized by the two parameters k and ε, which are equivalent to the parameter pair k and L because ε is proportional to $k^{3/2}/L$. The model employs the eddy viscosity/diffusivity concept and the parameters k and ε is dictated by dimensional analysis:

$$u_t = C_m \frac{k^2}{e} \tag{3.1}$$

$$\Gamma = \frac{u_t}{s_t} \tag{3.2}$$

where C_μ is an empirical constant and σ_t is again the turbulent Prandtl/Schmidt number ($\sigma_t=0.7$).

The Standard k-ε model employs the Boussinesq eddy viscosity concepts for Reynolds stresses:

$$-\overline{u'^2} = 2v_t \frac{\partial u}{\partial x} - \frac{2}{3}k \tag{3.3}$$

$$-\overline{v'^2} = 2v_t \frac{\partial v}{\partial y} - \frac{2}{3}k \tag{3.4}$$

$$-\overline{u'v'} = v_t\left(\frac{\partial u}{\partial y} + \frac{\partial v}{\partial x}\right) \tag{3.5}$$

where v_t is determined from dimensional analysis of (k, ε) and approximated by Equation (3.1). Here, u and v represent the mean velocity components, and x and y are the space coordinates. The distributions of k and ε are determined from:

Transport equation of Turbulent Energy:

$$u\frac{\partial k}{\partial x} + v\frac{\partial k}{\partial y} = \frac{\partial}{\partial x}\left(\frac{v_t}{s_k}\frac{\partial k}{\partial x}\right) + \frac{\partial}{\partial y}\left(\frac{v_t}{s_k}\frac{\partial k}{\partial y}\right) + G - e \tag{3.6}$$

Transport equation of Turbulence Energy Dissipation:

$$u\frac{\partial e}{\partial x} + v\frac{\partial e}{\partial y} = \frac{\partial}{\partial x}\left(\frac{v_t}{s_e}\frac{\partial e}{\partial x}\right) + \frac{\partial}{\partial y}\left(\frac{v_t}{s_e}\frac{\partial e}{\partial y}\right) + C_1\frac{e}{k}G - C_2\frac{e^2}{k} \tag{3.7}$$

where; G is the turbulence energy production term and defined as:

$$G = v_t\left[\left(\frac{\partial u}{\partial y} + \frac{\partial v}{\partial x}\right)^2 + 2\left(\frac{\partial u}{\partial x}\right)^2 + 2\left(\frac{\partial v}{\partial y}\right)^2\right] \tag{3.8}$$

The turbulence model coefficients, σ_k, σ_ε, C_1, C_2 and C_μ, were determined from the results of some specific experiments and computational optimization (Hanjalic, 1970; Launder et al., 1972 and Jaw, 1991), and more recently from renormalization analysis (Yakhot and Orszag 1986) or statistical analysis (Yoshizawa 1987, Takemitsu, 1990). The values used in the standard k- ε model are provided in Table 3.1.

The k-ε method has been applied to many different flow situations, perhaps not so much in the area of surface water problems but in mechanical, aeronautical engineering and many subjects in hydraulic engineering has been found to work well with the standard constants in many cases. However, the model does not work very well for some complex flows such as separated flows and flows in curved geometries (Versteeg and Malalasekera 1995, Wilcox 1998). Therefore corrections to the

constants have been introduced for the round jet and for weak shear layers occurring mainly in far wakes (Rodi 1980).

Table 3.1 Model constants used in standard k-ε method

Model Constant	Value
C_μ	0.09
C_1	1.44
C_2	1.92
σ_k	1.0
$\sigma\varepsilon$	1.3

The model has a tendency to under-predict the size of separation regions in unconfined flow (e.g. behind bluff bodies), but various modifications to the ε-equation have been suggested to improve the performance, for example, by making the production of ε more sensitive to normal stress than to shear stress (Hanjalic and Launder 1972), but none of the proposals work entirely satisfactorily (Rodi 1980, Launder and Spalding 1974).

The standard k-ε model has been successively applied and well validated in local scour and sediment transport problems (Devantier and Larock 1986, Toro et al. 1989, Celik and Rodi 1991, Ushijima et al. 1992, Olsen and Melaaen 1993, Olsen and Kjellesvig 1998, Garcia-Martinez, et al. 1999, Karim and Ali 2000, Neyshabouri et al. 2001, 2003, Barron and Neyshabouri 2003, Gunal and Guven 2006).

3.3.1.1 Main equations governing fluid flow

The main equations governing the fluid flow are the continuity equation (3.9) and the Reynolds averaged Navier-Stokes equations (3.10), (3.11), i.e.:

$$\frac{\partial u}{\partial x} + \frac{\partial v}{\partial y} = 0 \qquad (3.9)$$

and

$$u\frac{\partial u}{\partial x} + v\frac{\partial u}{\partial y} = -\frac{1}{r}\frac{\partial r}{\partial x} + \frac{\partial(\overline{-u'^2})}{\partial x} + \frac{\partial(\overline{-u'v'})}{\partial y} \qquad (3.10)$$

$$u\frac{\partial v}{\partial x} + v\frac{\partial v}{\partial y} = -\frac{1}{r}\frac{\partial r}{\partial y} + \frac{\partial(\overline{-v'^2})}{\partial y} + \frac{\partial(\overline{-u'v'})}{\partial x} \qquad (3.11)$$

The momentum equations (3.10) and (3.11) are also known as the Reynolds equations, and the fluctuating-velocity terms $\overline{u'^2}, \overline{v'^2}$ and $-\overline{u'v'}$ are also the Reynolds (turbulent kinematic) Stresses. As it is obviously seen, the continuity (3.9) and the momentum equations (3.10) and (3.11) form 3 equations with six unknown variables (u, v, p, $-\overline{u'^2}, -\overline{v'^2}$ and $-\overline{u'v'}$). Therefore these equations do not form a closed set. In order to solve these equations, additional relationships are needed to express Reynolds Stresses in terms of known or determinable quantities and these relationships are determined through the turbulence model.

The turbulent eddy viscosity (v_t) is modeled using the standard k-ε turbulence model (See Equation (3.1)).

3.3.1.2 Boundary conditions

3.3.1.2.1 Inlet conditions

The velocity and turbulence quantities are specified at the inlet. At the inlet, the streamwise velocity u is assumed to be uniform and vertical velocity v is assumed as zero for the cases of sluice gate without apron, whereas for the cases of hydraulic structures followed by a rigid apron, the streamwise velocity u is calculated using the exponential equation proposed by Karim and Ali (2000), which was developed based on the experimental and tehoritical study of Rajaratnam and Berry (1977) (see Eqn. (3.12)).

$$\frac{u}{u_m} = e^{-0.693(y/d)^2} \qquad (3.12)$$

41

where u_m is the maximum velocity of the velocity profile at any x distance from the inlet, and y is vertical distance from the axis of jet at any x direction, $d = 0.7x$ is verrtical distance from the axis to the point where $u=u_m/2$.

Zero pressure gradient is assumed in the streamwise direction next to the inlet. With the assumption of turbulence being locally isotropic and in equilibrium at the inlet, turbulence quantities k and ε are taken from the experimental measurements of Long et al.(1991) as:

$$k_{inlet} = 1.4 \times 10^{-3} u_1^2 \tag{3.13}$$

$$e_{inlet} = 2.2 \times 10^{-5} \frac{u_1^3}{y_1} \tag{3.14}$$

3.3.1.2.2 Outlet conditions

At the outflow boundary, zero-gradient boundary conditions are used and velocities are set equal to the values in the elements closest to the outflow.

$$\frac{\partial U}{\partial x} = \frac{\partial V}{\partial x} = \frac{\partial k}{\partial x} = \frac{\partial e}{\partial x} = 0 \tag{3.15}$$

3.3.1.2.3 Free surface conditions

The velocity normal to the free surface and the pressure on the surface are taken zero. First derivatives of U, V, k and ε with respect to η are taken to vanish on the free surface. Thus the surface conditions are:

$$P_{surface} = 0 \tag{3.16}$$

$$V_{surface} = 0 \tag{3.17}$$

$$\frac{\partial U}{\partial y} = \frac{\partial V}{\partial y} = \frac{\partial e}{\partial y} = \frac{\partial k}{\partial y} = 0 \tag{3.18}$$

42

3.3.1.2.4 Wall conditions

At high Reynolds number, the viscous layer of a boundary layer is so thin it would require large computational resources to resolve flows at such small scale. In order to avoid this problem in CFD, wall functions are applied in the near wall region that rely on the existence of the logarithmic region in the velocity profile. Wall functions are commonly used to provide the boundary conditions for nodes nearest to the channel bed; they are proposed by Launder and Spalding (1974).

Implementation of wall boundary conditions for turbulence model is accessed by evaluating the scaled wall distance, y^+, between the wall surface and the computational node nearest the wall. For distances where $y^+ \geq 11.63$, the flow is turbulent and the wall function approach is used, for y^+ values les than 11.63 the near wall flow is taken as laminar.

From this assumption and the eddy viscosity formula, the following wall functions are developed.

$$u^+ = \frac{1}{k} \ln(Ey^+) \tag{3.19}$$

$$k_{wall} = \frac{u_*^2}{\sqrt{C_m}} \tag{3.20}$$

$$e_{wall} = \frac{u_*^3}{ky} \tag{3.21}$$

where; $k = 0.41$ is the Von Karman constant (for smooth surfaces) but $k = 0.43$ is taken in present study; and E is a wall roughness parameter = 9.0 (E value is taken smaller than 9.0 for rough surfaces (Versteeg and Malalasekera, 1995). In present study, E value is shifted between 8.5 and 9.0, for calibration purpose); $u^+ = u/u_*$; $y^+ = yu_*/v$ and u_* is the friction velocity defined by $u_* = (t_w/r)^{1/2}$ where t_w is the wall shear stress.

The wall shear stress is the most important issue in wall functions. When the shear stress is estimated velocity in the fully developed outer region can be found easily through the wall functions (Gunal, 1996). Benim and Zinser (1985) proposed a wall model iteration technique for estimating the wall shear stress (see Eqn.(3.22). Long et al. (1991) implemented this model and reported good results. So it is decided to use their model in this study.

$$t_w = \frac{k_{n1} C_m^{1/4} r u_{n2} k_{n1}^{1/2}}{\ln\left(\dfrac{E C_m^{1/4} y_{n2} k_{n1}^{1/2}}{n}\right)}$$

(3.22)

The logic of this model is that first two grid points in the solution domain are away from the viscous layer, but within the logarithmic layer. At the beginning, u_* is assumed and u_{n1}, v_{n1}, k_{n1}, ε_{n1} at node 1 can be determined. This will be used as wall conditions. After each iteration, the information at node 2 is fed back to node 1 through the following relationship for the wall shear stress (Benim and Zinser 1985).

3.3.2 Governing equations in boundary-fitted coordinates

The governing equations presented in this chapter are in Cartesian coordinates. However, owing to the curvature of the free and bed surfaces, a cartesian coordinate system is less effective as approximations have to be made at the surface for a rectangular grid. Such approximations make it necessary to use fine mesh in cartesian coordinates, but this is computationally expensive. In order to overcome this difficulty, the continuity and momentum equations with transport equations were transformed into the boundary fitted coordinate system.

Having already mentioned, the basic idea is that a curvilinear coordinate transformation is used to map the complex flow domain in the physical domain to a simpler rectangular flow domain in the computational domain. The case of submerged horizontal jet requires only a simple transformation from the non-rectangular physical plane into a rectangular computational plane. Our particular case of submerged horizontal jet occurring on frozen scoured bed requires finer mesh in coordinate system and different transformation logic owing to the differentiation in

the coordinates of channel bed due to the scouring process. This modified transformation is:

$$\xi = x \tag{3.23}$$

$$\eta = \frac{y - y_o}{y_t - y_o} \tag{3.24}$$

where ξ and η are the coordinates of the transformed plane and y_o is the ordinate of the bed profile for the correspondent ordinate value, y, of any point in physical plane, and y_t is the tailwater depth. In this way, we will transform the independent variables in the physical plane (x, y) to a new set of independent variables in transformed plane (ξ, η) as below:

$$\xi = \xi(x, y) \tag{3.25}$$

$$\eta = \eta(x, y) \tag{3.26}$$

The inverse transformation is given by:

$$x = x(\xi, \eta) \tag{3.27}$$

$$y = y(\xi, \eta) \tag{3.28}$$

After performing the chain rule of differentiation, the following relations between the operators of two coordinate systems can be obtained.

$$\frac{\partial}{\partial x} = \frac{1}{J} \left(y_\eta \frac{\partial}{\partial \xi} - y_\xi \frac{\partial}{\partial \eta} \right) \tag{3.29}$$

$$\frac{\partial}{\partial y} = \frac{1}{J} \left(x_\xi \frac{\partial}{\partial \eta} - x_\eta \frac{\partial}{\partial \xi} \right) \tag{3.30}$$

where

$$J = x_\xi y_\eta - x_\eta y_\xi \tag{3.31}$$

45

$$x_x = \frac{\partial x}{\partial x} \quad , \quad y_x = \frac{\partial y}{\partial x}$$

(3.32)

$$x_h = \frac{\partial x}{\partial h} \quad , \quad y_h = \frac{\partial y}{\partial h}$$

(3.33)

The continuity, momentum and transport equations (3.6)-(3.11) can be rewritten in the (ξ,η) coordinates using the above operators (equations (3.32)-(3.33)):

Continuity Equation:

$$\frac{\partial U}{\partial x} + \frac{\partial V}{\partial h} = 0$$

(3.34)

u-Momentum Equation:

$$U\frac{\partial u}{\partial x} + V\frac{\partial u}{\partial h} = \frac{\partial}{\partial x}\left[\frac{v_t}{J}(q_1\frac{\partial u}{\partial x} + q_2\frac{\partial u}{\partial h})\right]$$
$$+ \frac{\partial}{\partial h}\left[\frac{v_t}{J}(q_2\frac{\partial u}{\partial x} + q_3\frac{\partial u}{\partial h})\right] + JS_u(x,h)$$

(3.35)

v-Momentum Equation :

$$U\frac{\partial v}{\partial x} + V\frac{\partial v}{\partial h} = \frac{\partial}{\partial x}\left[\frac{v_t}{J}(q_4\frac{\partial v}{\partial x} + q_5\frac{\partial v}{\partial h})\right]$$
$$+ \frac{\partial}{\partial h}\left[\frac{v_t}{J}(q_5\frac{\partial v}{\partial x} + q_6\frac{\partial v}{\partial h})\right] + JS_v(x,h)$$

(3.36)

Tranport Equation of Turbulent Energy k:

$$U\frac{\partial k}{\partial x} + V\frac{\partial k}{\partial h} = \frac{\partial}{\partial x}\left[\frac{v_t}{Js_k}(q_7\frac{\partial k}{\partial x} + q_8\frac{\partial k}{\partial h})\right]$$
$$+ \frac{\partial}{\partial h}\left[\frac{v_t}{Js_k}(q_8\frac{\partial k}{\partial x} + q_9\frac{\partial k}{\partial h})\right] + JS_k(x,h)$$

(3.37)

Transport of Turbulent Energy Dissipation ε:

46

$$U \frac{\partial e}{\partial x} + V \frac{\partial e}{\partial h} = \frac{\partial}{\partial x}\left[\frac{v_t}{Js_e}(q_7 \frac{\partial e}{\partial x} + q_8 \frac{\partial e}{\partial h}) \right]$$

$$+ \frac{\partial}{\partial h}\left[\frac{v_t}{Js_e}(q_8 \frac{\partial e}{\partial x} + q_9 \frac{\partial e}{\partial h}) \right] + JS_e(x,h)$$

(3.38)

where

$$U = uy_h - vx_h$$

$$V = vx_x - uy_x$$

(3.39)

and

$$
\begin{aligned}
q_1 &= 2y_h y_h + x_h x_h & q_6 &= y_x y_x + 2x_x x_x \\
q_2 &= -2y_h y_x + x_h x_x & q_7 &= y_h y_h + x_h x_h \\
q_3 &= 2y_x y_x + x_x x_x & q_8 &= -y_x y_h - x_h x_x \\
q_4 &= y_h y_h + 2x_h x_h & q_9 &= y_x y_x + x_x x_x \\
q_5 &= -y_h y_x - 2x_x x_h
\end{aligned}
$$

(3.40)

S (ξ, η) is the source term im transformed (ξ, η) coordinates and they can be written for each dependent variable (u, v, k and ε) as follows,

$$S_u = \frac{1}{J}\left[\frac{\partial}{\partial x}\left(-\frac{1}{r}y_h p - \frac{2}{3}y_h k \right) + \frac{\partial}{\partial h}\left(\frac{1}{r}y_x p + \frac{2}{3}y_x k \right) \right] +$$

$$\frac{1}{J}\left[\frac{\partial}{\partial x}\left[\frac{1}{J}v_t\left(x_h y_x \frac{\partial v}{\partial h} - y_h x_h \frac{\partial v}{\partial x} \right) \right] + \frac{\partial}{\partial h}\left[\frac{1}{J}v_t\left(y_h x_x \frac{\partial v}{\partial x} - y_x x_x \frac{\partial v}{\partial h} \right) \right] \right]$$

(3.41)

$$S_v = \frac{1}{J}\left[\frac{\partial}{\partial x}\left(\frac{1}{r}x_h p + \frac{2}{3}x_h k \right) + \frac{\partial}{\partial h}\left(-\frac{1}{r}x_x p - \frac{2}{3}x_x k \right) \right] +$$

$$\frac{1}{J}\left[\frac{\partial}{\partial x}\left[\frac{1}{J}v_t\left(x_x y_h \frac{\partial u}{\partial h} - x_h y_h \frac{\partial u}{\partial x} \right) \right] + \frac{\partial}{\partial h}\left[\frac{1}{J}v_t\left(y_x x_h \frac{\partial u}{\partial x} - y_x x_x \frac{\partial u}{\partial h} \right) \right] \right]$$

(3.42)

$$S_k = G(x,h) - e$$

(3.43)

47

$$S_e = C_1 \frac{e}{k} G(x,h) - C_2 \frac{e^2}{k} \qquad (3.44)$$

It is seen from equations (3.43) and (3.44) that S_k and S_ε contain production of kinetic energy term G which is due to interactions of turbulent stresses with horizontal mean-velocity gradients (Rodi 1980). G can be represented in the transformed plane by using the relations (Equations (3.30)-(3.32)) between the two coordinate systems.

3.3.3   Numerical solution of the partial differential equations: Finite Volume Method

The transformed governing equations in (x,h) plane should be transformed into corresponding discrete forms in order to be solved. The Finite Volume Method (FVM) was chosen for the present study because it is easy to implement and conservation can always to be obtained in the computational cells. In FVM, the domain is first overlaid with cells which divide the whole domain into a number of control volumes. In the present formulation, a grid system is first generated numerically at the corner of each control volume. The velocities are calculated at a point half way between these grid nodes and the pressures are calculated at the center of each control volume. This staggered grid system as shown in Figure 3.1 is adopted for variable arrangement to avoid the well known chequerboard oscillations in the pressure and velocity. Since a staggered grid system has been employed for all velocity components (U, V) and scalar quantities (p, k, ε), a separate control volume is to be considered for the integration of each governing equations. As an example of the procedure of the integration the transformed governing equation (3.35) for a dependent variable, f (given in Equatin (3.45)) whose control volume is the same as that of pressure, is described in the following section. The dimension of the control volume is Δx to Δh.

Firstly the convection part (left side) of the equation (3.36) is taken and integrated over the control volume as shown in Figure 3.1:

$$\int_e^w \int_s^n \left[\frac{\partial}{\partial x}(U\Phi) + \frac{\partial}{\partial h}(V\Phi) \right] dxdh \qquad (3.45)$$

where Φ stands for any dependent variable (u , v, k or ε) and assume that Φ varies uniformly along the control volume faces. Using the linear interpolation between the control volume faces then the above expression (3.45) will look as follows:

$$\left[U_e \frac{(\Phi_p + \Phi_e)}{2} - U_w \frac{(\Phi_p + \Phi_w)}{2} \right] \Delta h + \left[V_n \frac{(\Phi_N + \Phi p)}{2} - V_s \frac{(\Phi_s + \Phi_p)}{2} \right] \Delta x \qquad (3.46)$$

The right hand side (the diffusion part) of the equation (3.36) can be integrated and described as:

$$\int_e^w \int_s^n \frac{\partial}{\partial x} \left[\frac{v_t}{JS_\Phi}(q_1 \frac{\partial \Phi}{\partial x} + q_2 \frac{\partial \Phi}{\partial h}) \right] dxdh$$
$$+ \int_e^w \int_s^n \frac{\partial}{\partial x} \left[\frac{v_t}{JS_\Phi}(q_1 \frac{\partial \Phi}{\partial x} + q_2 \frac{\partial \Phi}{\partial h}) \right] dxdh \qquad (3.47)$$

Making the same assumption that is made in equation (3.45), it can be written as follows:

$$\left[\frac{v_t}{JS_\Phi} \left(q_1(\frac{\Phi_E - \Phi_P}{\Delta x_e}) + q_2(\frac{\Phi_{NE} - \Phi_{SE}}{\Delta h}) \right) \right]_w \Delta h$$
$$+ \left[\frac{v_t}{JS_\Phi} \left(q_1(\frac{\Phi_p - \Phi_w}{\Delta x_w}) + q_2(\frac{\Phi_{Nw} - \Phi_{Sw}}{\Delta h}) \right) \right]_w \Delta h \qquad (3.48)$$
$$- \left[\frac{v_t}{JS_\Phi} \left(q_1(\frac{\Phi_p - \Phi_w}{\Delta x_w}) + q_2(\frac{\Phi_{Nw} - \Phi_{Sw}}{\Delta h}) \right) \right]_w \Delta h$$

In the same way, source term can be integrated and the terms which cannot be written in terms of five nodes (P, E, W, S and N as shown in Figure 3.1) are moved into the source term. After rearrangement, the following discretization equation for Φ_P and neighboring variables can be written as follows (Patankar, 1980):

$$A_p \Phi_p = A_E \Phi_E + A_W \Phi_W + A_N \Phi_N + A_S \Phi_S + S_\Phi \qquad (3.49)$$

3.3.4 Pressure correction equation

The momentum equations can be solved only when the pressure field is given or estimated. Unless the correct pressure field is employed the resulting velocity field will not satisfy the continuity equation. Thus, the aim here is to find a way of improving the guessed pressure such that the resulting velocity field satisfies the continuity equation.
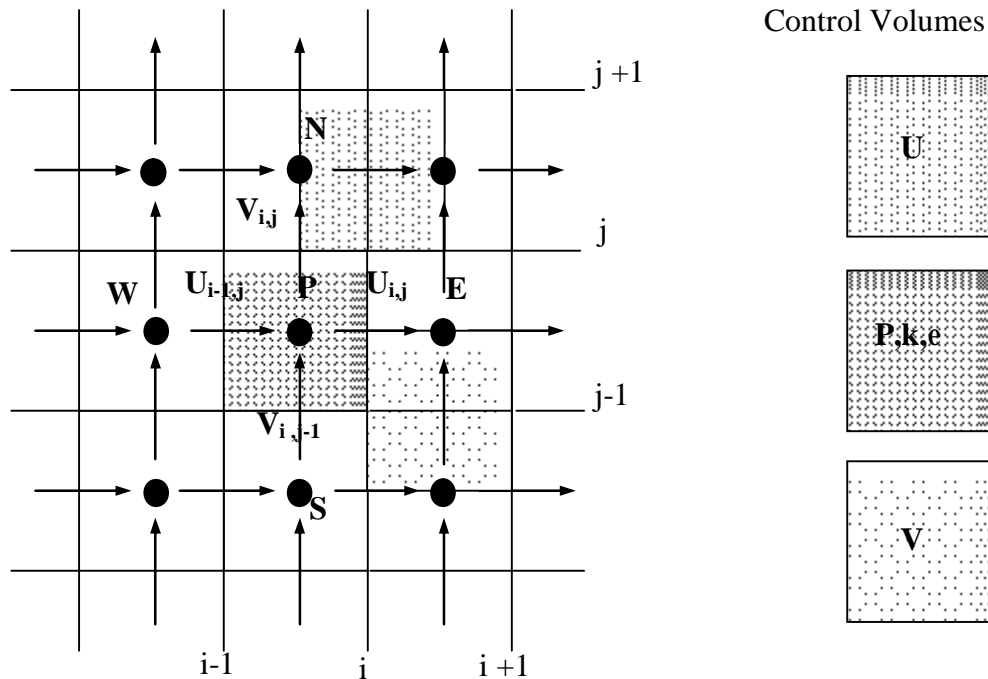
Figure 3.1 Arrangement of control volumes in computational domain.

The continuity equation (3.34) in the computational plane can be written in a discretisized form over each control volume as follows (see Figure 3.1).

$$(U_e - U_W)\Delta h + (V_n - V_S)\Delta x = 0 \qquad (3.50)$$

If we assume that u^* and v^* will satisfy the momentum equations in the physical plane with a given distribution of p^*. Since the pressure will not satisfy the

continuity equation, the pressure p^* must be corrected. The correct pressure p is obtained from:

$$p = p^* + p_c \qquad (3.51)$$

where p_c is called the pressure correction. The corresponding velocity corrections u_c, v_c can be introduced as

$$u = u^* + u_c \qquad\qquad v = v^* + v_c \qquad (3.52)$$

Shy et al (1985) have derived the pressure correction assuming that u^* and v^* can be obtained from

$$u_p^* = \sum_{i=E,W,S,N} A_i^u u_i^* + D^u + (B^u p_x^* + C^u p)_h^* \qquad (3.53)$$

$$v_p^* = \sum_{i=E,W,S,N} A_i^v v_i^* + D^v + (B^v p_x^* + Cvp)_h^* \qquad (3.54)$$

where $D^u and D^v$ are the derivative viscous terms in the u and v momentum equations, and

$$B^u = -\frac{y_h}{A_p^u}\Delta x\Delta h \qquad\qquad C^u = \frac{y_x}{A_p^u}\Delta x\Delta h \qquad (3.55)$$

$$B^v = -\frac{x_h}{A_p^v}\Delta x\Delta h \qquad\qquad C^v = -\frac{x_x}{A_p^v}\Delta x\Delta h \qquad (3.56)$$

Shy et al. (1985) assumed that the velocity components can be corrected by the following formulas:

$$u = u^* + (B^u p_{cx} + C^u p_{ch}) \qquad (3.57)$$

$$v = v^* + (B^v p_{cx} + C^v p_{ch}) \qquad (3.58)$$

The above equation is derived to correct the velocities in Cartesian coordinates. The velocity corrections for U and V in the computational plane can be obtained by substituting equations (3.57)-(3.58) to (3.59)-(3.60) as follows :

$$U = U^* + (B^u y_h - B^v x_h) p_{cx} \tag{3.59}$$

$$V = V^* + (C^v x_x - C^u y_x) p_{ch} \tag{3.60}$$

By substituting equations (3.59)-(3.60) into discretized continuity equation (3.61), the pressure correction equation can be written as follows:

$$A_p p_p = A_E p_E + A_W p_w + A_S p_s + A_N p_N + S_p \tag{3.61}$$

3.3.5 Hybrid numerical scheme

In the literature, various types of interpolation practice can be found in order to avoid the faults while discretization of governing equations. In the model of the present study the most widely-used interpolation practice known as the Hybrid Differencing Scheme that was proposed by Spalding (1972) has been used. It is the combination of central and upwind differencing scheme. The hybrid differencing scheme basically switches from upwind to central differencing or vice versa in evaluating the convection term according to the cell peclet number (p_e). For example, the flux across the east face of the control volume (see Figure 3.1) is evaluated by

$$
\begin{aligned}
&\left[U_P \left(\frac{\Phi_P + \Phi_E}{2} \right) - \left(\frac{v_t q_1}{J s_\Phi} \right) \left(\frac{\Phi_E - \Phi_P}{\Delta x_e} \right) \right] \Delta h \quad \text{when} \ -2 < p_e < 2 \\
&U_p \Phi_p \Delta_h \qquad\qquad\qquad\qquad\qquad\qquad \text{when} \quad p_e \geq 2 \\
&U_p \Phi_E \Delta_n \qquad\qquad\qquad\qquad\qquad\qquad \text{when} \quad p_e \leq 2
\end{aligned}
\tag{3.62}
$$

where Φ is the dependent variable, J is the Jacobian and v_t is the turbulent viscosity and s_Φ is the model constant and p_e is the cell Peclet number and defined as :

$$p_e = \frac{U_E \Delta x_e}{\left(\dfrac{v_t q_1}{J S_\Phi} \right)} \qquad\qquad (3.63)$$

In the present study, the equations (3.49) and (3.61) are formulated using the hybrid finite difference formulation proposed by Runchal (1972).

3.3.6 Solution technique: Tri- Diagonal Matrix Algorithm

The algebraic equations (3.49) and (3.61) exist for every computational node in the computational domain. There are (M x N) equations with (M x N) unknowns. These equations can be solved by a direct or iterative method. The direct solution by matrix inversion would consume more time and demands more computer storage than the iterative method. The linearized algebraic equations (3.49) and (3.61) are themselves approximations of the partial differential equations and it would be inappropriate to adopt a direct solution method.

The system of equations are solved by Tri-diagonal Matrix Algorithm (TDMA), a line iterative method, with alternating sweep directions. In an iterative scheme it is often desirable to speed up or slow down the changes of dependent variables from iteration to iteration, which is known as over-relaxation or under-relaxation. Because the Navier Stokes equations are non-linear, the process of convergence needs to be slowed down. In the present study, in order to avoid divergence, under relaxation factor with changeable values in each run of program was used for velocities and pressures. The under relaxation factors are mainly problem dependent and have no influence on the converged solution.

3.3.7 Solution algorithm: Semi-Implicit Method for Pressure-Linked Equations (SIMPLE)

The pressure gradients which are present in the momentum equations must be known in order to solve the momentum equations by the pre-mentioned iterative method. Thus, the derived pressure correction equation (3.61) is solved after solving discretized governing equation (3.49) for new velocity field based on a guessed

pressure. The pressure and velocity fields are then corrected respectively before starting to the next iteration. This algorithm is known as SIMPLE, which stands for Semi-Implicit Method for Pressure-Linked Equations. The SIMPLE algorithm has been described by Patankar and Spalding (1972) and Patankar (1980). The procedure of SIMPLE algorithm for the governing equations can be summarized as follows:

1. Initialize all dependent variables in the domain including pressure,
2. Solve the discretized governing equation (3.49) to obtain new velocities based on a guessed pressure field.
3. Solve the discretized pressure correction equation (3.61).
4. Correct the pressure field (Eqn. 3.51).
5. Calculate a new velocity field using the velocity correction equations (Eqn. 3.48)
6. Solve the transport equations and update the turbulent viscosity v_t.
7. Return the step 2 and repeat the whole procedure until a converged solution is obtained.

The convergence is monitored by the absolute residual sum for the continuity equation (Eqn. (3.9)). The program stops when the residual sum is 0.0001. The computer program is written in Fortran 90, by Developer Studio, which is a visual fortran developing software. The iterations are carried out using the super-computer, gul3, provided by the computer system of Gaziantep University. Gul3 utilizes the Linux Kernel 2.6 operation system with Intel Core 2 6600 at 2.4 GHz processor and 3.3 giga-bytes memory.

3.4   Application of k-ε Turbulence Model on Prediction of Flow Patterns in Rigid Scoured Bed Downstream of Sluice Gates

3.4.1   Rigid scour models

Figure 3.2, shows local scour caused by a horizontal jet referred to as a flow below a gate, followed by a rigid apron. These flows are two-dimensional and usually have a considerable potential of scour. Experimental studies of Ali and Lim (1986) showed that the scouring process almost stops, when letting water jet over the erodible bed

54

for a period of 400 minutes, a phase known as "equilibrium stage" or "asymptotic stage." Some researchers observed the presence of equilibrium scour condition (Rajaratnam and Macdoughal 1983, Ali and Lim 1986, Johnston 1990, Ade and Rajaratnam 1998) while the investigation by Balachandar and Kells (1997), observed the absence of an equilibrium state even after five or more days of testing in laboratory setting for one tailwater depth. Following this study, Balachandar et al. (2000) also did not observe an equilibrium state. Johnston (1990) stated that while in deep tailwater conditions the development of the scour depth reaches a well-defined asymptotic state, in shallow tailwater conditions such a state is sometimes absent. The solution of this discrepancy may be achieved by more investigation of local scour caused by horizontal jets with different tailwater and flow regime conditions.

3.4.2 Simulation using k-ε turbulence model

3.4.2.1 Governing equations

Flow due to a submerged horizontal jet is considered as two-dimensional, steady and incompressible. The k-ε turbulence model uses four equations apart from the continuity equation (Eqn. 3.9), namely two momentum equations (Eqns.(3.10)-(3.11)), a transport equation for the turbulent kinetic energy k (Eqn. (3.6)) and another transport equation for the dissipation of turbulent energy ε (Eqn.(3.7)

The other unknown terms and the algorithm of the numerical method is already given from section **3.3.1** to section **3.3.2**. Thus, in this section, only the application of the model is given in further sections. The boundary conditions (Eqns(2.13)-(3.22)) needed for solution of governing equations were driven from experimental results of Dey and Westrich (2003). The experimental conditions used in validation of the proposed numerical model are given in Table 3.2.
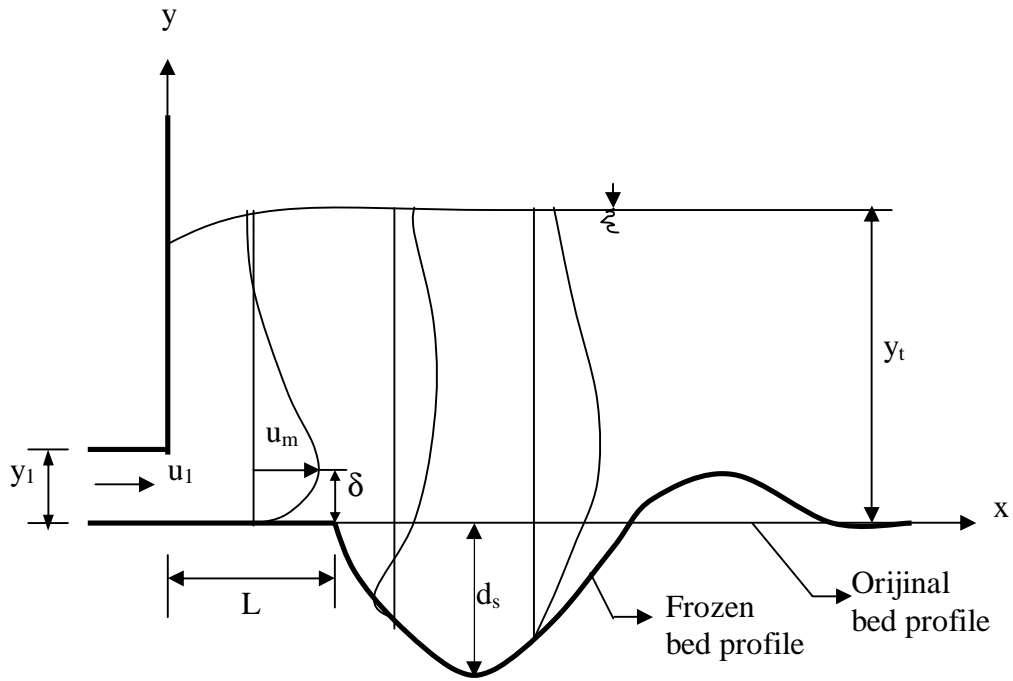
Figure 3.2 Definition sketch of local scour by a horizontal jet

3.4.2.2 Model validation with experimental data

This section reports the results obtained from the present numerical simulation. The present predictions were compared with the experimental results of Dey and Westrich (2003). They were performed 12 tests in a glass-walled flume of 0.25 m wide, 0.60 m deep and 8 m long. A sediment trap of 0.20 m thick and 1 m long was constructed downstream the apron. They used cohesive sediment that has a relative density of 2.49, a mean size of 1.733 X 10^{-5}, and a porosity of 65 %.

Figure 3.3 shows the numerical prediction of bed shear stress along the streamwise direction. The frozen bed profile was taken from the experimental results of Dey and Westrich (2003). It is observed that the decay of bed shear stress is more rapid in the scour region then the apron.

Table 3.2 Conditions used in numerical prediction

Run	y_1 (m)	u_1 (m/s)	y_t (m)	$F_1 = \dfrac{u_1}{\sqrt{gy_1}}$	$S = \dfrac{y_t}{y_1}$
1	0.04	0.699	0.127	1.12	3.175
2	0.04	0.484	0.120	0.77	3.00

Figure 3.4 shows the diffusion characteristics of submerged jet for the present numerical Run 1 and 2 with empirical curves of Dey and Westrich (2003). Two distinct zones for the diffusion of submerged jet are clearly seen downstream of the sluice gate. The jet diffusion is more rapid over the apron than the scour-hole region. The present numerical results are in good agreement with the empirical curve of Dey and Westrich (2003).

The variation of boundary layer thickness δ at different streamwise locations from the sluice gate opening is shown in Figure 3.5 with the present numerical results and the empirical curve of Dey and Westrich (2003). It is observed that there is a difference between present predicted results and their empirical curve. The reason is that the present numerical model does not predict well the reverse flow region comparing the experimental results of them. Present numerical results show that there is a sudden increase in boundary layer thickness just after the sluice gate, but after that it reduces for a short distance then increase slowly over the apron and the scour region.

The variation of inner layer velocity with vertical distance over the apron is shown in Figure 3.6 with the present predictions and the empirical curve of Dey and Westrich (2003). It was observed that the decay of inner layer velocity for the present predictions is higher than their empirical curve. The differences between the predictions and empirical curve are due to the poor predictions of reverse flow velocity in the region near to the scored bed.
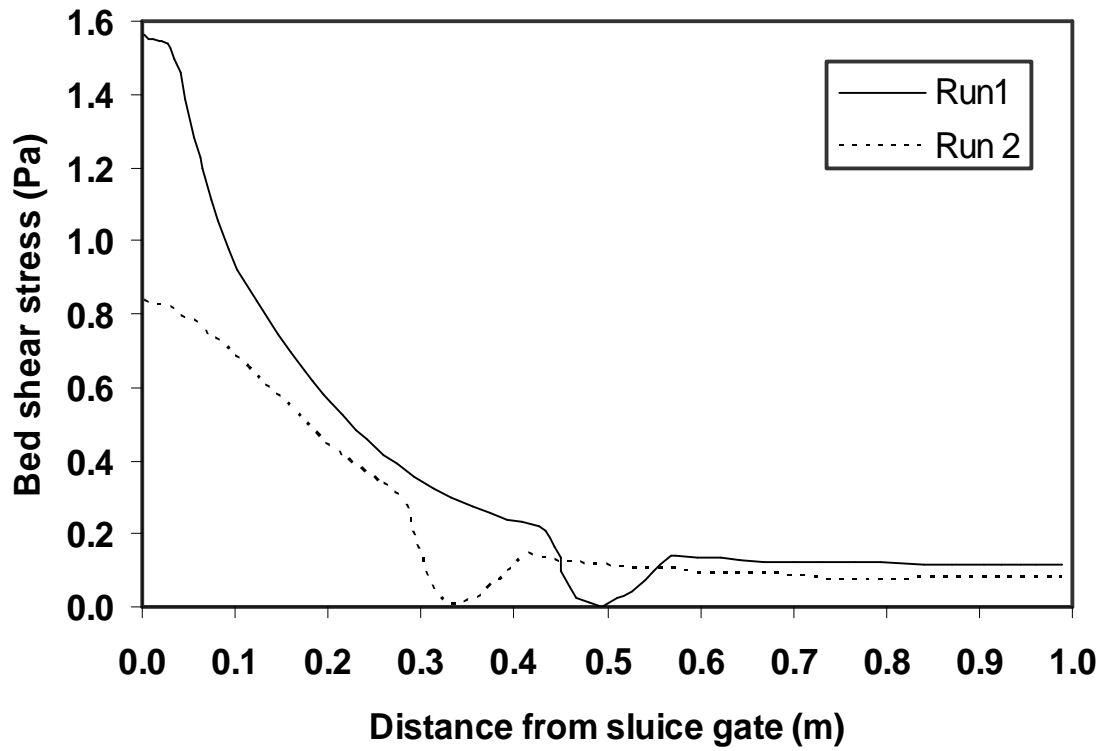
Figure 3.3 Variation of predicted bed shear stress distribution against the distance from the sluice gate
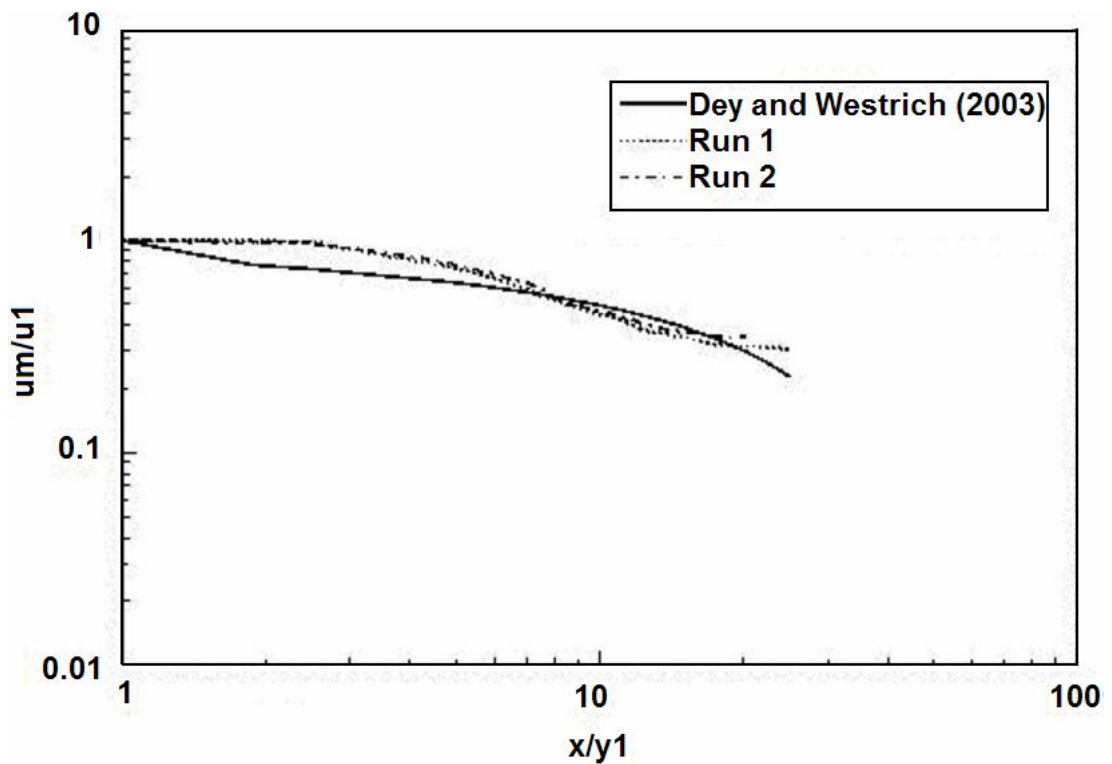
Figure 3.4 Inner layer variations for Run 1 and Run 2 with experimental results of Dey and Westrich (2003)
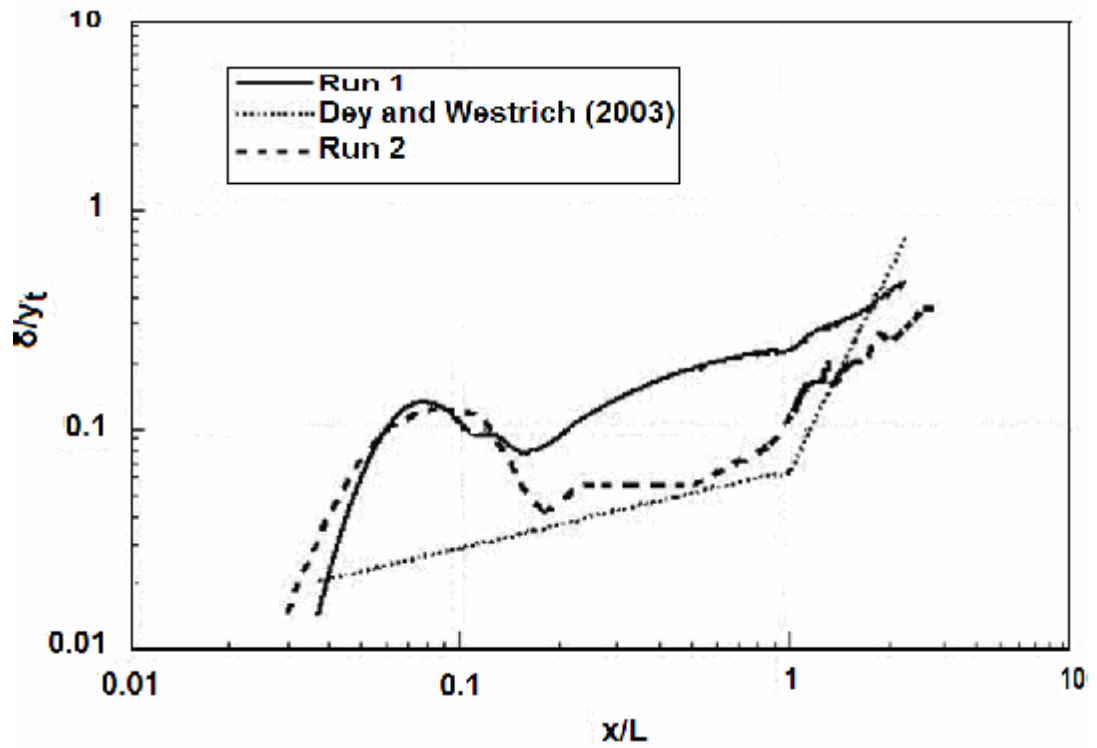
Figure 3.5 Streamwise variation of boundary layer thickness for Run 1 and Run 2 with experimental results of Dey and Westrich (2003)
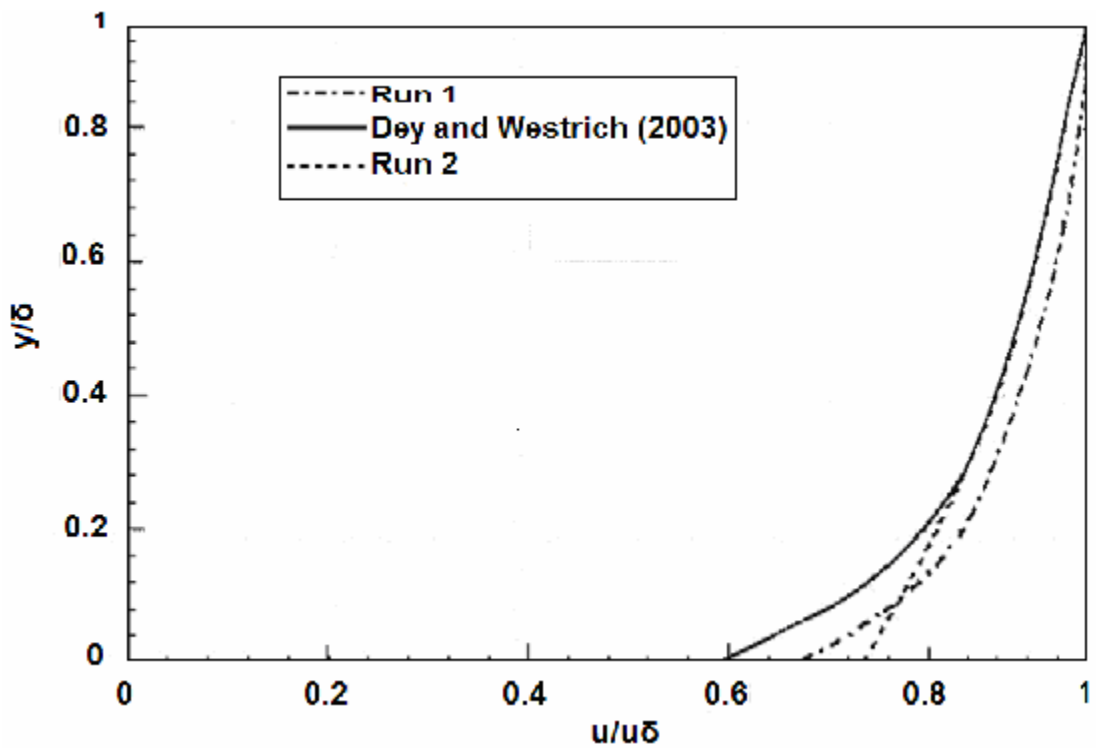
Figure 3.6 Variation of inner layer velocity with vertical distance for Run 1 and Run2 with experimental results of Dey and Westrich (2003)

3.4.2.3 Conclusions

1. The flow characteristics of a submerged horizontal jet over a rigid scoured bed were studied numerically using a two-dimensional k-ε model and a boundary-fitted coordinate system. The advantages of using boundary-fitted coordinate system are mentioned in Gunal and Narayanan (1998).

2. Present numerical predictions of bed shear stress agree with both the experimental results of Ali and Lim (1986) and the numerical results of Karim and Ali (2000). The present numerical predictions of bed shear distribution fell just between those of the experimental and numerical results.

3. The present numerical predictions of boundary layer thickness and velocity profiles with an apron are compared with the experimental results of Dey and Westrich (2003). It is concluded that the prediction of reverse flow properties are poor comparing to their experimental result. This is some extent expected result because k-ε turbulence model is not good for predicting recirculating flows.

3.5 Numerical-Analytical Modeling of Time-Dependent Downstream Local Scour Profile

3.5.1 Analytical modeling of mobile bed profile

In this section, a 2-dimesional numerical-analytical model is developed, which simulates the temporal and spatial evolution of local scour profile under a horizontal wall jet. The proposed model utilizes the continuity equation for local solid discharge together with the mechanical properties of the sand subjected to scouring. The model analyzes the forces acting on a sand particle, considering the angle of repose of the sand, the critical shear stress beyond which the particle is dislodged and the hydrodynamic shear stress induced by the impinging water jet.

The method of the proposed model while deriving the instantaneous shape of mobile bed and modeling the bed shear stress is similar to Hogg et al. (1997) followed by Adduce (2004). The proposed model differs from Hogg et al. (1997) in numerical integration of a partial differential equation representing the shape of mobile bed based of local solid discharge, while Hogg et al. (1997) integrates a sediment-volume

conservation equation. As it is described in the following parts of this section, the proposed model uses the same partial differential equation with Adduce (2004), but it integrates the non-conservative form of the equation, unlike Adduce (2004) who used the conservative form, in order to improve the accuracy of the model.

As the hydro dynamic shear stress acting on the sand particle (t_{hydr}) exceeds the critical shear stress (t_{cr}), the sand particle is dislodged and transported beyond, the condition, for horizontal bed, can be written as:

$$t_{hydr} > t_{cr} = W_s \tan(j)$$ (3.64)

where $W_s = (r_s - r_w)g$ is the saturated weight of sand particle, r_s is mass density of sand particle, r_w is mass density of water, g is gravitational acceleration, φ is angle of repose of sand particle, and $t_{cr} = 0.047(r_s - r_w)gd_{50}$ (Simons and Senturk, 1992).

As the scour hole progresses, the soil bed is no longer flat, which can be described as:

$$S_l = S_l(x,t)$$ (3.65)

The above expression represents the evolution of bed profile, S_l, in horizontal axis x and with time t. The transport conditions have to be modified to account for the effect of the bottom slope (see Figure 3.7). In this case, the critical shear stress becomes:

$$t_{cri} = \frac{t_{cr}}{\sqrt{1 + S_{lx}^2}}$$ (3.66)

where S_{lx} is the derivative of S_l with respect to x axis. t_{cri} can be rewritten as:

$$t_{cri} = \frac{W_s \tan(j)}{\sqrt{1 + S_{lx}^2}}$$ (3.67)

Adding the hydrodynamic bed shear stress and the shear stress due to gravity (t_s), the condition of incipient motion of sand particle becomes:

$$t_{hydr} > t_{cri} - t_g = \frac{t_{cr}(\tan(j) + S_{lx})}{\tan(j)\sqrt{1+S_{lx}^2}}$$

(3.68)

Referring to Figure 3.7, the local solid discharge can be simply supposed as:

$$Q_{sd} = f(y) \text{ where } y = t_{hydr} - \frac{t_{cr}(\tan(j) + S_{lx})}{\tan(j)\sqrt{1+S_{lx}^2}}$$

(3.69)

where ψ is an independent variable. Similar to Hogg et al.(1997) and Adduce (2004), the Meyer-Peter and Muller transport formula is used in this study:

$$Q_{sd} = \frac{8}{\sqrt{r(g_s - g)}} y^{3/2} \quad for \ y > 0$$
$$Q_{sd} = 0 \qquad\qquad for \ y \leq 0$$

(3.70)
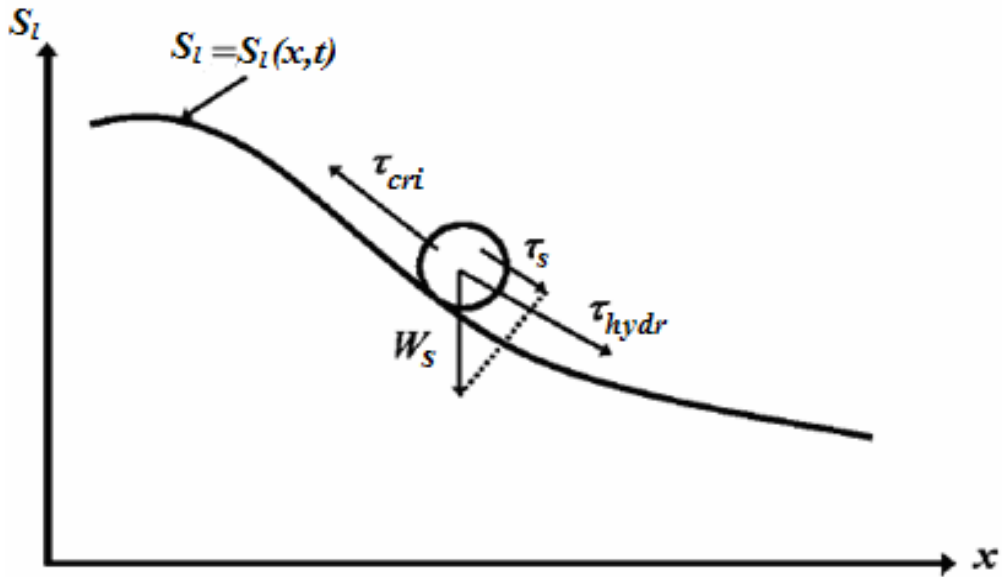
Figure 3.7 Sketch of shear stress acting on a sand particle on sloping bed (After Adduce (2004), modified)

In this study, the 2-dimensional and time dependent transportation of solid particle is assumed to be due to Q_{sd}, in other words, suspended sediment load is neglected. So, the velocity of sand particle is assumed to be locally parallel to the bed inclination. Finally, the continuity equation for local solid discharge is supposed as (Adduce 2004):

$$\frac{\partial S_l}{\partial t} + \left(\frac{1}{1-p}\right)\frac{\partial}{\partial x}\left(\frac{Q_{sd}}{\sqrt{1+S_{lx}^2}}\right) = 0 \qquad (3.71)$$

where p is he porosity of sand. Referring to Eqn.(3.69) and taking the spatial derivative of the expression in brackets in Eqn. (3.71), the equation becomes:

$$\frac{\partial S_l}{\partial t} + \frac{1}{1-p}\left[\frac{\partial Q_{sd}/\partial y}{\sqrt{1+S_{lx}^2}}\left(\frac{\partial t_{hydr}}{\partial x} - \frac{t_{cr}(1-\tan(j)S_{lx})}{\tan(j)(1+S_{lx}^2)^{3/2}}\frac{\partial^2 S_l}{\partial x^2}\right) - Q_{sd}\frac{\partial S_l}{\partial x}\frac{\partial^2 S_l/\partial x^2}{(1+S_{lx}^2)^{3/2}}\right] = 0$$

$$(3.72)$$

The above equation possesses a non-linear and parabolic structure. Therefore it can be solved by applying appropriate numerical integral method with realistic boundary conditions.

The hydrodynamic shear stress, at a distance δ from the bed surface, by a turbulent 2-dimensional horizontal wall jet is modeled following Schlichting (1979) as:

$$t_{hydr} = \frac{arU_m^2}{U_m^{1/4}(d/n)^{1/4}} \qquad (3.73)$$

where α= 0.00283 is a numerical constant, U_m is maximum velocity of jet and v is the kinematic viscosity of the fluid. δ, the viscous sublayer thickness is modeled in order to predict the motion of bed load as:

$$d = \frac{N_i v\left(2.49\sqrt{g}\,\ln(13.3Rf_r/d_{50})\right)}{U_m\sqrt{g}} \qquad (3.74)$$

where N_i=11.5 is the Nikuradse number, R is the hydraulic radius and f_r is the shape factor of channel cross-section (f_r=width of channel/height of channel). Referring to Eqn.(3.74),

$$(d/v) = \frac{N_i\left(2.49\sqrt{g}\ \ln(13.3Rf_r/d_{50})\right)}{U_m\sqrt{g}}$$

(3.75)

is adapted in Eqn.(3.73) and is rewritten as:

$$t_{hydr} = \frac{abU_m^2}{N_i^{1/4}\left(2.49\ln(13.3Rf_r/d_{50}\right)^{1/4}}$$

(3.76)

Following Schlichting (1979), Hogg et al. (1997) and Adduce (2004), the decay of maximum velocity is expressed as:

$$U_m = C_1\frac{M}{v}\left(\frac{v^2}{M(x+L_p)}\right)^k$$

(3.77)

and taking $k \cong 0.5$ (Schlicting 1979, Hogg et al. 1997), the above equation reduces to:

$$U_m = C_1\left(\frac{M}{x+L_p}\right)^{1/2}$$

(3.78)

where

$$M = \int_{S_l}^{y_t} U^2 dS_l$$

(3.79)

and C_1 is a constant, which is calculated by the measured velocity profile of the wall jet at the end of apron, y_t is tailwater depth and L_p is length of rigid apron. Assuming $h+S_l=y_t$, where h is instantaneous water depth above the bed, and assuming $M = q^2/(y_t - S_l)$, where q is the unit discharge, the final form of Eqn.(3.75) becomes:

$$t_{hydr} = \frac{raC_1^2 q^2}{N_i^{1/4}\left(2.49\ln(13.3Rf_r/d_{50})\right)^{1/4}(x/L_p)(y_t - S_l)}$$ (3.80)

The above formulation approximately predicts the bed shear stress at a distance from the initial bed profile for the case of rigid bed. When a horizontal wall jet, flowing firstly on a rigid apron, impinges on originally flat soil, the scouring starts (see Figure 3.8). Just as the scouring starts, the behavior of the jet becomes like a free jet, rather than a wall jet, the transport action of which gets weaker than that of wall jet. The free jet then becomes like a wall jet after a length scale of the same order of magnitude of one half of the maximum scour length (Adduce, 2004).
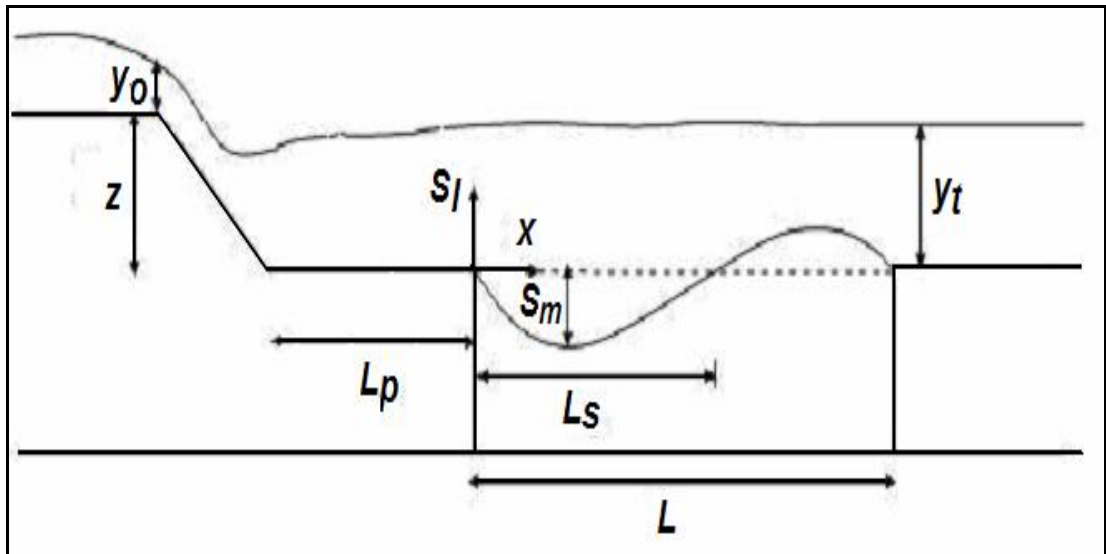
Figure 3.8 Definition sketch for local scour downstream of a sill followed by a rigid Apron (after Adduce (2004), modified)

Hogg et al. (1997) proposed a Gaussian-like approximation in order to simulate the different transport action of the free jet from the edge of apron till maximum scour depth abscissa (XS) and that of a wall jet from that point till the end of dune section. They multiplied the Eqn.(3.80) by a Gaussian function $G(x,S_l)$ in order to simulate the evolution of bed shear stress, $G(x, 0)=1$ in absence of scour, while it simulates the transition from a free-like jet to a wall-like jet in the region from the end of rigid apron to XS. Namely, the Gaussian function becomes weaker when simulating the

free-like jet and becomes stronger and stronger as the free jet changes into wall jet as:

$$G(x,S_l) = \begin{cases} 1 \quad for \ x > XS \ \ or \ in \ absence \ of \ scour \\ \exp\left(-\left[\dfrac{x-XS}{XS}\right]^2 \ln(1/V)\right) for \ x \leq XS \ \ or \ in \ presence \ of \ scour \end{cases}$$ (3.81)

where $G(0,S_l)=\varsigma$, $0 < \varsigma < 1$ is a calibration parameter of the proposed model, which considers the transport action of free jet is weaker than that of wall jet in region of end of rigid apron.

As it is clear in the Eqn.(3.81), in order to apply the Gaussian-like transport action, the abscissa of the maximum scour depth has to be already known. As Adduce (2004) experimentally detected, the scour profile is assumed to be self similar when XS(t) and S_m(t) are taken as horizontal and vertical length scales, where XS(t) and S_{max}(t) are the instantaneous abscissa and the depth of maximum scour depth, respectively (see Figure 3.9). Thus, the instantaneous shape of mobile bed can be formulated as:

$$S_l(x,t) = S_{max}(t) f\left(\frac{x}{XS(t)}\right)$$ (3.82)

where f is a functional symbol. And the area of the instantaneous scour hole, A_i, is calculated as:

$$A_i = \int_0^{L_s} S_l(x,t)\,dx = S_{max} XSC_2$$ (3.83)

where L_s is instantaneous maximum scour length and C_2 is a model constant, linked to the self similarity of the local scour profile.

Adduce (2004) defined A_L as:

$$A_L = \int_0^L S_l^2(x,t)\,dx = S_{max}^2 XSC_3$$ (3.84)

where C_3 is a model constant, linked to the self similarity of the canal and L is the instantaneous total scoured plus dune length. If we combine Eqns.(3.82) and (3.84), we get:

$$XS = \frac{C_3}{(C_2)^2}\frac{A_i^2}{A_L} = C_u\frac{A_i^2}{A_L}$$

(3.85)

where C_u is a universal constant, which is a control parameter of the proposed model. C_u values used in this study are derived by introducing the empirical equations defining A_i and A_L areas derived from experimental data, and taking their numerical integration using Mathematica 4.0 commercial software.

We initially assumed clear-water conditions (without sediment supply from upstream to the scoured zone) and a 2-dimensional scour profile. In this case, the scoured area should be equal to the dune area:

$$A_i = \int_0^{L_s} S_l(x,t)\,dx = \frac{1}{2}\int_0^L |S_l(x,t)|\,dx$$

(3.86)

so,

$$XS = C_u\frac{\left[\frac{1}{2}\int_0^L |S_l(x,t)|\,dx\right]}{\int_0^L S_l^2(x,t)\,dx}$$

(3.87)

Eqn.(3.87) calculates the abscissa of instantaneous maximum scour depth as a functions of corresponding scour profile and it is used in evaluation of $G(x,S_l)$.

The final shape of hydraulic bed shear stress, taking into account the Gaussian law proposed by Hogg et al. (1997), becomes:

$$t_{hydr} = \frac{raC_1^2 q^2}{N_i^{1/4}\left(2.49\ln(13.3Rf_r/d_{50})\right)^{1/4}(x/L_p)(y_t - S_l)}G(x,S_l)$$

(3.88)
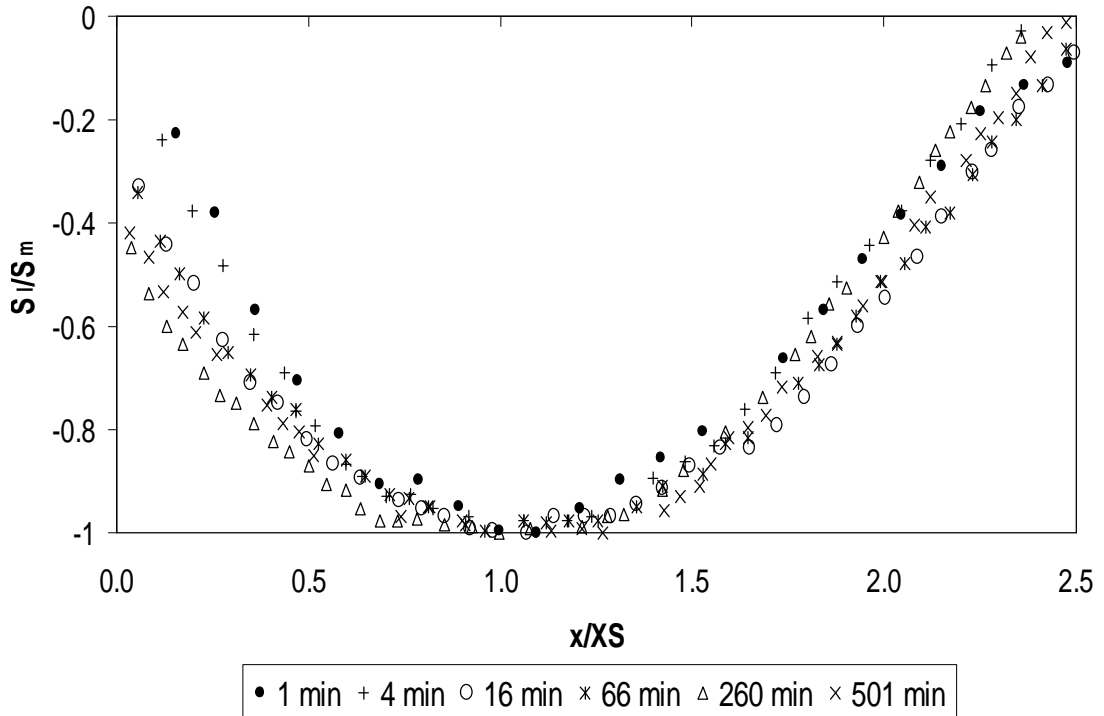
Figure 3.9 Similarity of dimensionless instantaneous scour profiles caused by submerged jet (after Adduce 2004, modified)

3.5.2 Numerical integration of the proposed analytical model: The Mac-Cormack Finite Difference Scheme

The proposed analytical model, Eqn.(3.72) has a parabolic partial differential structure. Thus, the integration equation requires specific numerical integral methods, with implication of proper bundary conditions. Eqn. (3.72) is non-conservative form of the Eqn. (3.71), which Adduce (2004) used as modeling the mobile bed profile. However, as Adduce (2004) admitted, numerical integration of Eqn. (3.72) would give more realistic and accurate results. Hence, this study is assumed to improve the model proposed by Adduce (2004).

Following Garcia and Kahawita (1985) and Adduce (2004), we used a Mac-Cormack Scheme in numerical integration of Eqn. (3.72). We used two difference operators, namely backward (B) and forward (F) functioning as:

$$B(S_l)_i^n \equiv \frac{(S_l)_i^n - (S_l)_{i-1}^n}{\Delta x} \tag{3.89}$$

$$F(S_l)_i^n \equiv \frac{(S_l)_{i+1}^n - (S_l)_i^n}{\Delta x} \tag{3.90}$$

where $(S_l)_i^n \equiv S_l|x = i\Delta x, t = n\Delta t$, i and n are spatial and temporal indexes, respectively, used in present scheme. $\Delta x = L/M$ is the spatial step of integral, M is the number of the discretization and Δt temporal step of integration. In this study, M is taken as 100 and Δt as 0.02 seconds.

The proposed Mac-Cormack scheme uses a predictor-corrector numerical scheme according to following integration scheme:

$$(S_l)_i^P = (S_l)_i^n - \Delta t \left(\frac{1}{1-p}\right) B \left[\frac{\frac{\partial Qs}{\partial x}\sqrt{1 + F(S_l)_i^n} - Qs\left(\frac{1}{2}\left(1 + F(S_l)_i^n\right)^{-1/2}\left(\frac{\partial F(S_l)_i^n}{\partial x}\right)\right)}{1 + F(S_l)_i^n}\right]$$

$$\tag{3.91}$$

$$(S_l)_i^C = (S_l)_i^p - \Delta t \left(\frac{1}{1-p}\right) F \left[\frac{\frac{\partial Qs}{\partial x}\sqrt{1 + B(S_l)_i^p} - Qs\left(\frac{1}{2}\left(1 + B(S_l)_i^p\right)^{-1/2}\left(\frac{\partial B(S_l)_i^p}{\partial x}\right)\right)}{1 + B(S_l)_i^p}\right]$$

$$\tag{3.92}$$

$$(S_l)_i^{n+1} = \frac{1}{2}\left((S_l)_i^C + (S_l)_i^n\right) \tag{3.93}$$

where P and C stand fort the predictor and the corrector step, respectively.

As explained in the beginning of this section, the numerical integral algorithm explained above needs being closed by using appropriate boundary conditions.

Namely, these boundary conditions are clear-water scour condition at the inlet of the mobile bed and absence of the local solid discharge at the end of it ($x=0$ and $x=L$).

The clear water condition at the inlet and the end of the mobile bed is defined as:

$$t_{hydr}(S_l) = \lambda\, t_{eff}(S_{lx})$$

(3.94)

where $t_{eff} = t_{cri} - t_s$ is the effective shear resistance of sediment and λ is a model parameter the value of which should be properly chosen. In this study, the values of λ are calibrated according to experimental results.

The clear water condition at the inlet is discretized as:

$$t_{hydr}(S_l)_0^{n+1} = \lambda_0 t_{eff}\left(B(S_l)_1^{n+1}\right)$$

(3.95)

where $(S_l)_1^{n+1}$ is known, since it is calculated in the internal grid point. Thus, in the above equation the only unknown is $(S_l)_0^{n+1}$. Eqn.(3.95) can be numerically solved for assigned the value of λ_0.

At the outlet boundary, zero-gradient boundary condition is used and the hydraulic shear stress is set equal to the value in the element closest to the outlet:

$$t_{hydr}(S_l)_m^{n+1} = t_{hydr}(S_l)_{m-1}^{n+1}$$

(3.96)

where the only unknown is $(S_l)_m^{n+1}$, and is equalized to $t_{hydr}(S_l)_{m-1}^{n+1}$ value.

3.6   Application of the Analytical Model on Prediction of Local Scour Profile Downstream of a Sluice Gate

3.6.1   Local scour downstream of a sluice gate

Prediction of local scour downstream of sluice gates is of considerable importance and has been subject of numerous researches in the literature. These studies were

generally interested in the experimental investigation of the maximum scour depth, S_{max}, and its location XS with respect to the sluice gate.

The jet issuing from the sluice get has a considerable potential of eroding the initially flat soil. The extent of this erosion may be so vital that both the foundation and the structure itself may be undermined causing structural collapses (Gunal and Guven 2006, Liriano et al. 2002, Karim and Ali 2000). Thus, a well-planned design of these structures against the scouring problem can prevent both the high rebuild costs and repairs from possible structural damage. In this sense, the design of the hydraulic structures must not only include the optimum sizes to provide the desired hydraulic capacity, but must also include the protection upstream and downstream of the structure against scouring.

In this section, the prediction of temporal evolution of local scour downstream of a sluice gate is presented. The experimental data were taken from Kurniawan et al. (2001). The predictions to development of sour profile in time increments and the so-called asymptotic-sate scour profile versus the measured one are presented.

3.6.2   Experimental conditions

Kurniawan et al. (2001) carried out their experiments using a 17 m-long tilting flume with a 0.8 m-high and 0.5 m-wide rectangular cross-section. They artificially raised the upstream and downstream ends of the flume bed in order to create a 0.35m-deep and 3.8m-long test section, beginning at a distance of 5.0m from the inlet. They filled the test section with a uniformly graded sand with a mean diameter of $d_{50}=2$mm.

The jet issued from a sluice gate, which was installed directly upstream end of the test section. A slightly submerged jet was created by setting the tailwater, y_t, controlled by a weir at the downstream end of the flume. The experiment started at $t=0$, when the pump discharge was increased rapidly to the predefined discharge, Q, which is maintained constant until the formation of "asymptotic scour hole". Until achieving the asymptotic scour profile, the temporal evolution of bed profile was measured at different time intervals. The asymptotic profile was measured by a point gauge installed on carriage.

3.6.3   Analytical modeling of local scour downstream of a sluice gate

In this section the proposed analytical model, explained in section **3.5**, is applied on prediction of the experimental scour profile downstream of a sluice gate, measured by Kurniawan et al. (2001). The inlet flow conditions, the boundary conditions and the corresponding soil characteristics were taken from the experimental study in order to calibrate the proposed model according to the corresponding experimental case.

Figure 3.10 shows the temporal evolution of the scour profile predicted by the model for different time intervals, starting from $t=10$ minutes to $t=5000$ minutes. Figure 3.11 compares the predictions of the proposed analytical model to the measured scour profile in equilibrium stage. The figure proves a strictly good agreement between the predicted and the measured values, except the dune zone. This discrepancy can be explained by the fact that the predicted scour profile is two-dimensional, while the measured scour profile showed a three-dimensional behavior as explained by Kurniawan et al. (2001).

Figure 3.12 shows the self-similarity of the predicted scour profiles for different time intervals and the asymptotic scour profile measured by Kurniawan (2001). The horizontal and vertical axes are normalized by taking XS and s_{max} as the horizontal and the vertical scales, respectively. It is clearly seen that all predicted profiles and the measured asymptotic one fall into one curve as also observed by the other researchers (Chatterjee and Ghosh ,1980, Ali and Lim ,1986, Adduce, 2004, Adduce and Sciortino, 2006, Kurniawan et al. 2001, 2003)

3.6.4   Conclusions

1. An analytical model was developed in order to simulate the temporal evolution of scour profile downstream of hydraulic structures.

2. The experimental scour profiles measured by Kurniawan et al. (2001) were used in order to to evaluate the performance of the proposed analytical model while simulating the local scour downstream of a submerged sluice gate..

3. The self-similarity of instantaneous scour profiles, when scaled with proper parameters, was also proved by the predictions the proposed model. The proposed model also simulated the asymptotic scour profile observed by Kurniawan et al. (2001) with strictly good agreement.

4. These findings prove the efficiency of the proposed model in simulation of complex scouring problem and promise to be used in local scour prediction in preliminary design of hydraulic structures.
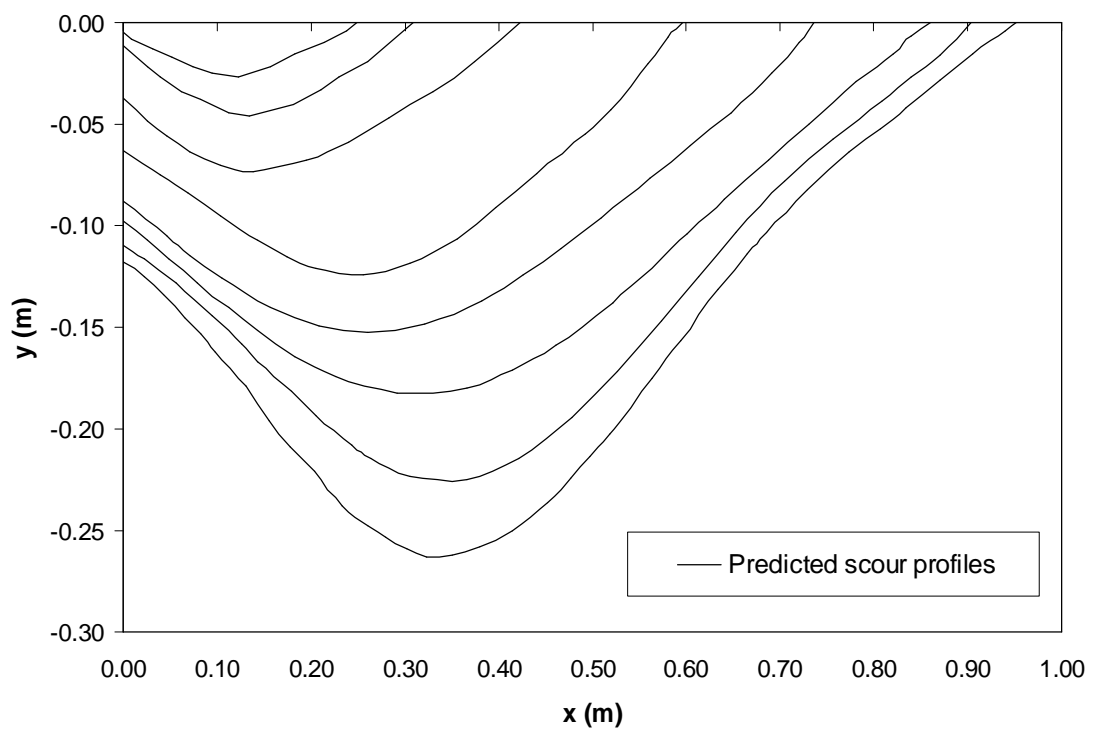
Figure 3.10 Temporal evolution of predicted scour profiles for t=100, 250, 500, 1000, 2000, 3000, 4000 and 5000 minutes
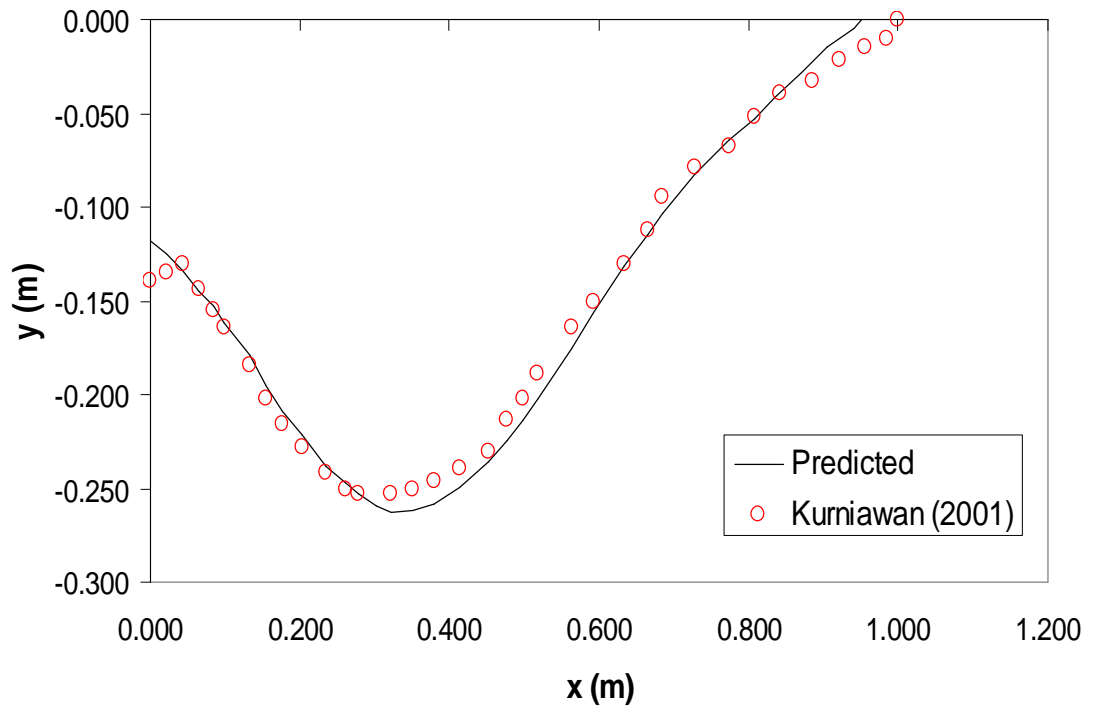
Figure 3.11 Predicted and measured scour profiles at asymptotic stage
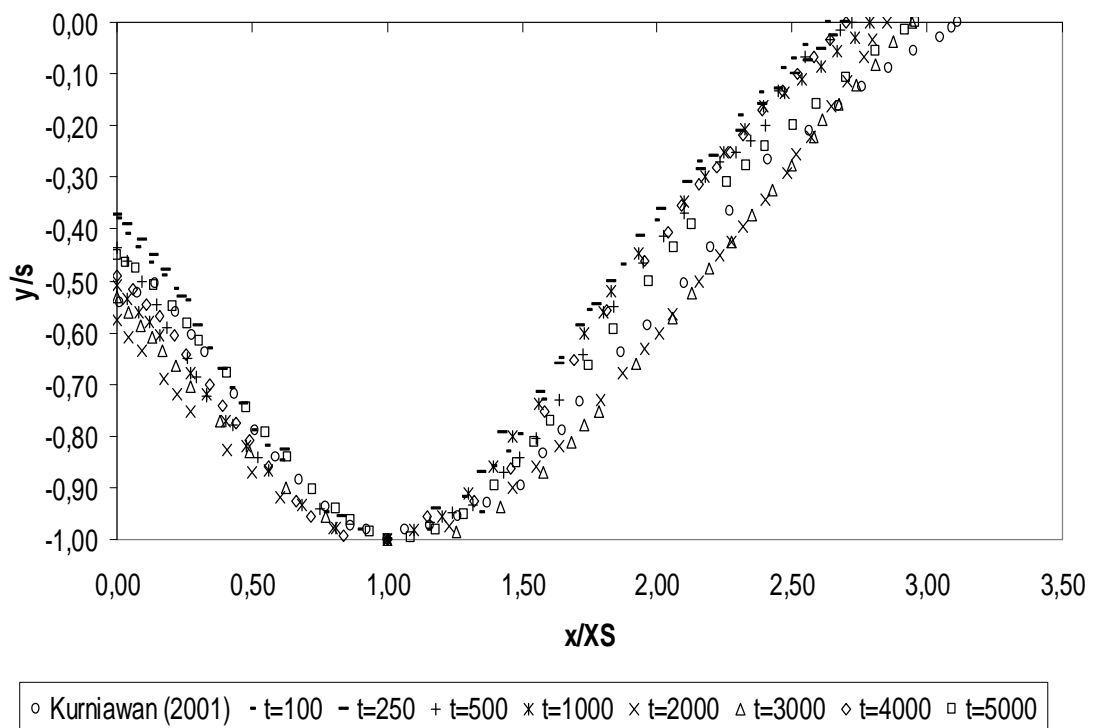
Figure 3.12 Self-similarity of predicted scour profiles and the measured asymptotic

scour profile by Kurniawan (2001)

3.7   Solution Algorithm of the Proposed Hybrid Model and its Calculation Flowchart

The proposed hybrid numerical model is combination of the analytical modeling of mobile scour profile and k-ε turbulence modeling of internal flow characteristics (u, v, k, ε, p, etc.) in scoured zone. Both models are capable of functioning separately on their own, also when used together, the latter model derives the instantaneous scour profile from the former and solve the flow patterns in corresponding scour profile. The algorithm of the proposed hybrid model can be listed as follows:

1. The inlet flow conditions, characteristic parameters of soil and the model parameters are defined.

2. For $t=0$, the Eqn.(3.72) is solved and the ordinate of bed profile for $t = t + \Delta t$ are calculated for internal grid points.

3. The boundary conditions for the inlet and end of mobile bed for $t = t + \Delta t$ is calculated (Eqns. (3.94)-(3.95)).

4. Step 2 and 3 are repeated for Δt temporal steps until there is no a significant difference between the shape of scour profile for t^n and t^{n+1}.

5. The abscissa and ordinate values of scour profile for corresponding time are stored in a pre-defined file.

6. The abscissa and ordinate values of scour profile for corresponding time are derived from the pre-defined file.

7. The physical domain is generated using the stored data in step 6.

8. Grid for solution domain is generated using Eqns. (3.25)-(3.26).

9. The boundary conditions are calculated (Eqns. (3.12)-(3.22)).

10. All independent variables are initialized.

11. The governing equations are solved (Eqns. (3.6)-(3.8)).

12. Surface profile is corrected and grid is re-generated.

13. For $t = t + Dt$, bed profile is comuted abd stored in a pre-defined file (steps 1-6).

14. Grid is re-generated.

15. The new boundary conditions are calculated.

16. The governing equations are solved with new boundary conditions.

17. Return to step 5 and repeat the whole procedure between step 5 and step 11 until a converged solution is obtained.

18. The governing equations are solved for equilibrium scour profile conditions (step 5 to step 11).

19. The program stops.

The convergence is monitored by the absolute residual sum for the continuity equation. The program stops when the residual sum equals or smaller than 0.0001. The computer program is written in Fortran 90. The calculation flow chart of the proposed hybrid model is given in Figure 3.13. The grey boxes represent the analytical model, whereas the dotted ones represent the k-ε turbulence model.
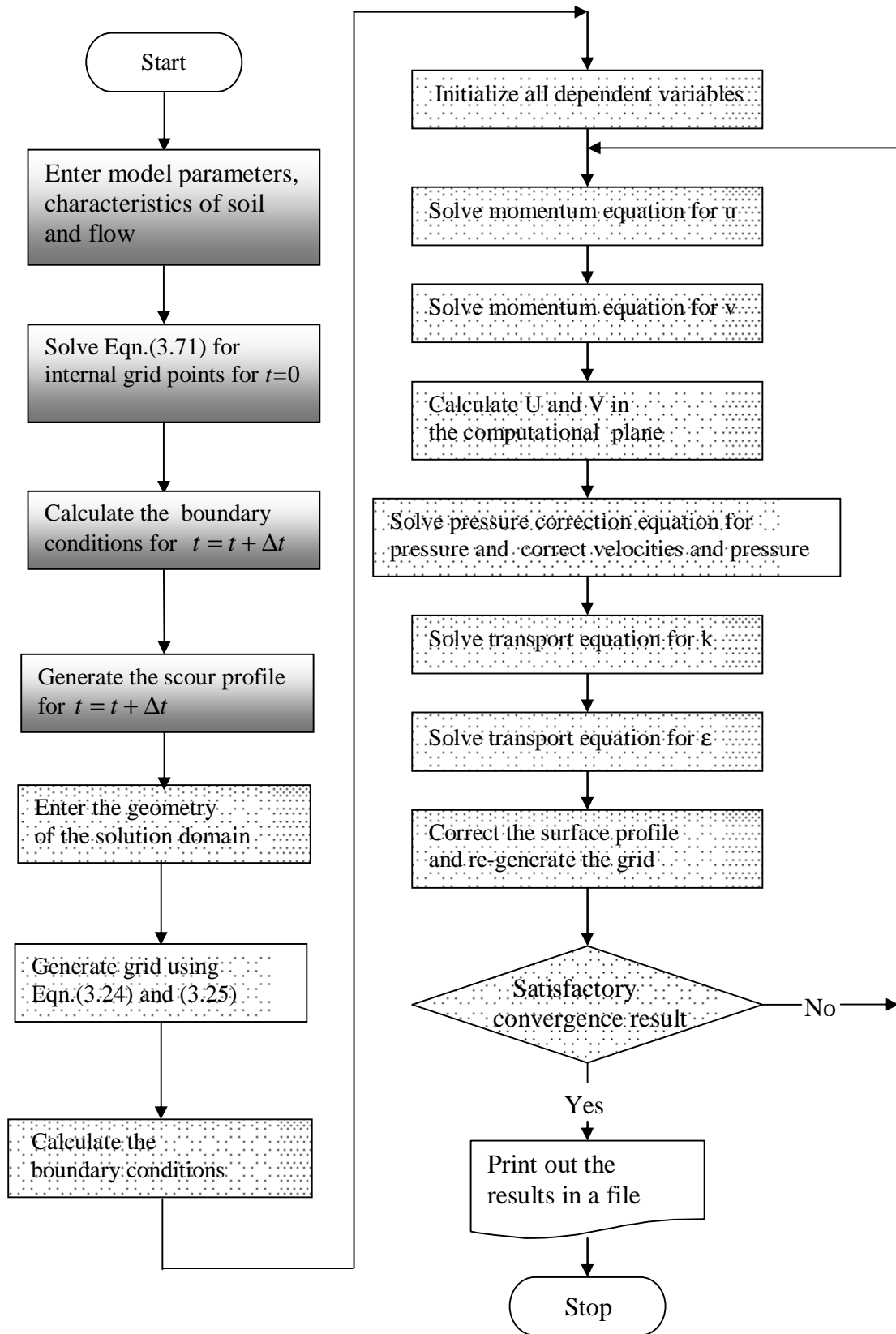
Figure 3.13 The calculation flowchart of the proposed hybrid model

CHAPTER 4

PREDICTION OF LOCAL SCOUR USING SOFT COMPUTING TECHNIQUES

4.1   Soft Computing Techniques

The definition of soft computing does not have determinate limitations. Lotfi A. Zadeh, the researcher who invented the term soft computing, describes it as a collection of methodologies that aim to exploit the tolerance for imprecision and uncertainty to achieve tractability, robustness, and low solution cost. The principal constituents of soft computing are fuzzy logic, neurocomputing, and probabilistic reasoning. Soft computing is likely to play an increasingly important role in many application areas, including software engineering (Zadeh, 1994).

Soft computing techniques mimic living organisms: plants, animals, human beings, which are soft, flexible, adaptive and clever. It can be described as a family of problem-solving methods that have analogy with biological reasoning and problem solving. It includes basic methods such as fuzzy logic, artificial neural networks (ANNs), genetic algorithms (GA) and genetic programming (GP) methods which do not derive from classical theories. Soft computing can also be seen as a foundation for the growing field of computational intelligence as an alternative to traditional Artificial Intelligence (AI) which is based on hard computing (Koivo, 2000). Soft computing represents a significant paradigm shift in the aims of computing, unlike present day computers, possesses a remarkable ability to store and process information which is pervasively imprecise, uncertain and lacking in categorization (Hun and Changha, 2004). Two soft computing approaches based on ANNs and GP are within the scope of this study and will be described in this section.

4.2   Overview of Artificial Neural Networks (ANNs)

ANNs technique is a data processing tool that mimics the function of the human brain and nerves built on the so-called neurons – processing elements – connected to each other. A biological neuron is made up of four main parts: dendrites, synapses, axon and the cell body (see Figure 4.1). The dendrites receive signals from other neurons. The axon of a single neuron serves to form synaptic connections with other neurons. The cell body of a neuron sums the incoming signals from dendrites. If input signals are sufficient to stimulate the neuron to its threshold level, the neuron sends an impulse to its axon. On the other hand if the inputs do not reach the required level, no impulse will occur.
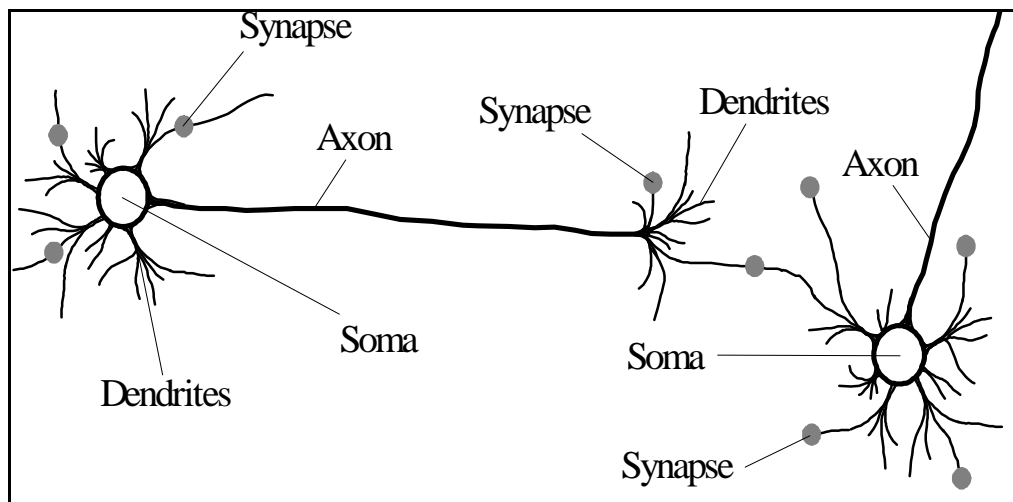
Figure 4.1 A biological neuron

Biological neuron model is also the basis of the artificial neuron model. Artificial neurons are organized in such a way that the structure resembles a network. This technique differs from the traditional data processing; it learns the relationship between the input and output data (Hecht-Nielsen, 1990). ANNs, like people, learn by example. An ANN is configured for a specific application, such as pattern recognition or data classification, through a learning process. Learning in biological systems involves adjustments to the synaptic connections that exist between the neurons.

ANN models have been used as an alternative method in engineering analysis and predictions during last two decades (Guven et al. 2006). ANNs mimic somewhat the learning process of a human brain. They operate requiring no detailed information about the system. Instead, they learn the relationship between the input parameters and the controlled and uncontrolled variables by studying previously recorded data. ANNs have ability to handle large and complex systems with many interrelated parameters. They seem simply to ignore excess data that are of minimal significance and concentrate instead on the more important inputs (Kalogirou, 1999).

4.2.1 Basic Elements of artificial neural networks

4.2.1.1 Artificial neuron

The basic element of a neural network is the artificial neuron as shown in Figure 4.2, which often consists of a body which acts as a basic function, with a set of inputs represented by the number of incoming links (McCulloch-Pitts unit) or real values. These values are passed to the neuron through abstract links, which might be associated with weights as in the case of synaptic weights in the biological neuron. The neuron computed the function of the inputs, and emits an output value, which is transmitted to other components in the network. Hence, the artificial neurons can be thought as simplified versions of biological neurons or primitive analytical functions.

Artificial neuron consists of three main components; weights, bias, and an activation function. Each neuron receives inputs x_i ($i = 1, 2, …, n$) attached with a weight w_{ij} ($j \geq 1$) which shows the connection strength for a particular input for each connection.

Every input is then multiplied by the corresponding weight of the neuron connection and summed as

$$W_i = \sum_{j=1}^{n} w_{ij}.x_j \qquad (4.1)$$
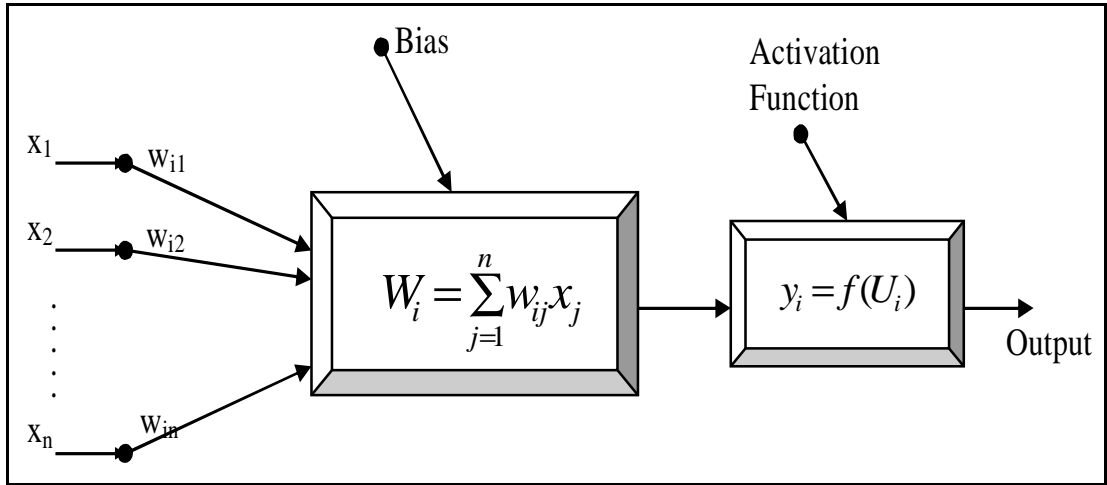
Figure 4.2 Basic elements of artificial neuron

A bias b_i, a type of correction weight with a constant non-zero value, is added to the summation in Equation (4.1) as

$$U_i = W_i + b_i \qquad (4.2)$$

In other word, W_i in Equation (4.1) is the weighted sum of the ith neuron for the input received from the preceding layer with n neurons, w_{ij} is the weight between the ith neuron in the hidden layer and the jth neuron in the preceding (input) layer, and x_j is the output of the jth neuron in the input layer. After being corrected by a bias as in Equation (4.2), the summation is transferred using a scalar-to-scalar function called "activation or transfer function", $f(U_i)$, to yield a value called the unit's "activation", given as

$$y_i = f(U_i) \qquad (4.3)$$

Activation functions serve to introduce nonlinearity into NNs which makes it more powerful than the linear transformation. In Figure 4.3, the most common types of activation function are shown. In this study, I used the sigmoid and tangent hyperbolic functions. The advantages of these functions are their easy differentiable forms and symmetry around the origin as shown in Figure 4.3.

Linear function	Sign function	Sigmoid function	Tangent hyperbolic function
$Y^{linear} = X$	$Y^{sign} = \begin{cases} +1, \text{if } X \geq 0 \\ -1, \text{if } X < 0 \end{cases}$	$Y^{sigmoid} = \dfrac{1}{1+e^{-X}}$	$Y^{\tan-hyp} = \dfrac{2}{1+e^{-2X}} - 1$
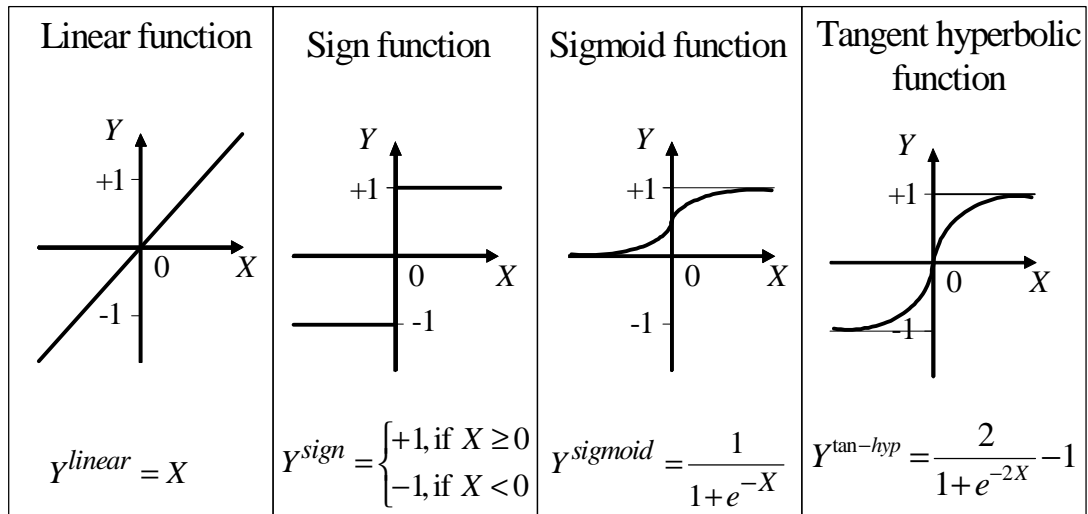
Figure 4.3 Activation functions

4.2.1.2 Learning algorithms

There are three basic types of learning algorithms, namely, supervised, unsupervised and reinforcement learning. These three types differ from each other according to the degree of dependence of the system on the prior knowledge regarding the behavior function (depending in that order from fully dependent to independent). Supervised learning requires a priori knowledge in the training phase, i.e. the "user" has to set up a set of inputs with their corresponding output values. On the contrary, unsupervised learning requires no priori knowledge. Reinforcement learning also does not require an explicit prior knowledge, it rather receives knowledge from the environment, i.e. the system constructs a trial network, and observes the reaction in the environment, using its observations to adjust the weights (Haykin 2000). The scope of this thesis is limited to supervised learning.

4.2.1.3 Artificial neural network architecture

ANNs are commonly classified by their network architecture, (i.e. feedback, feed forward) and learning or training algorithms (i.e., evolutionary, back propagated).

For example, a multilayer feed forward neural network with back propagation indicates the architecture and learning algorithm of the neural network (Figure 4.4). In this study, multilayer feed forward neural network with back propagation algorithm is used.

4.2.1.3.1 Multi layer perceptron

A multilayer perceptron has an input layer of source nodes and an output layer of neurons (i.e., computation nodes); these two layers connect the network to the outside world (see Figure 4.4). In addition to these two layers, the multilayer perceptron usually has one or more layers of hidden neurons, which are so called because these neurons are not directly accessible. The hidden neurons extract important features contained in the input data.

4.2.1.3.2 Feed forward neural networks (FFNNs)

In FFNNs, the direction of signal flow is from input to output units, strictly in a feed-forward direction. The data processing can extend over multiple (layers of) units, but no feedback connections are present, that is, connections extending from outputs of units to inputs of units in the same layer or previous layers. FFNN is the most popular architecture used in engineering problems. There are other types of architectures such as recurrent neural networks, associative networks, and redial basis functions. This thesis is scoped on multilayer FFNN.

4.2.1.3.3 Back propagation algorithm

ANNs are composed of a complex function of the input signals. The key issue is how to derive a suitable set of parameters, i.e. synaptic weights, to fit the function to a particular problem. Among the specific number of learning algorithms proposed in the literature, Back Propagation (BP) is the most popular most widely validated one.

The BP algorithm looks for the minimum error function in the weight space, using iterative gradient descent method. In other words, the set of weights are considered to be the solution if it minimizes the error function. The BP algorithm can be summarized as follows:

- A set of zero or random values fort he synaptic weight and thresholds are fired.

- The mode of training pattern (i.e. sequential, batch mode) is selected.

- Given a pattern, x_j is forwarded to the ANN and output of each node is computed. The computation can be divided into three sub-steps:

- The weighted sum of the inputs to node is computed (Eqn.(4.1)).

- The output signal of node j is computed by applying the activation function (Eqn.(4.3)).

- The errors at the output layer, depending on the error function in use, are computed.

- The error is propagated backward to the nodes in hidden layers. A logical gradient is defined and computed for each node.

- The weights are updated in the negative gradient direction.

- The learning (training) process is halted when a certain stopping criterion is achieved. The simple stopping criterion is fixing the number of iterations to a predefined value. But during this thesis, some more accurate types of stopping criteria such as Genetic Algorithm or Akaike Information Criterion are utilized.

4.2.1.4 Testing (validation) of artificial neural networks

As the training process is stopped, the weights that give the best training performance are freezed to test the generalization capacity of the network with a set of data that is not used in training process. This data set is called as testing data. If the training is successful and the network's architecture is correct, it will apply its 'past experience' to this data and still produce a good solution. If this is the case, then the network will be able to generalize based on the training set. What is interesting is that a network with enough weights will always learn the training set

better as the number of iterations is increased. However, neural network researchers have found that this decrease in the training set error was not always coupled to better performance in the test set. When the network is trained with too much number of synaptic weights, the network 'memorizes' the training patterns and does not generalize well.
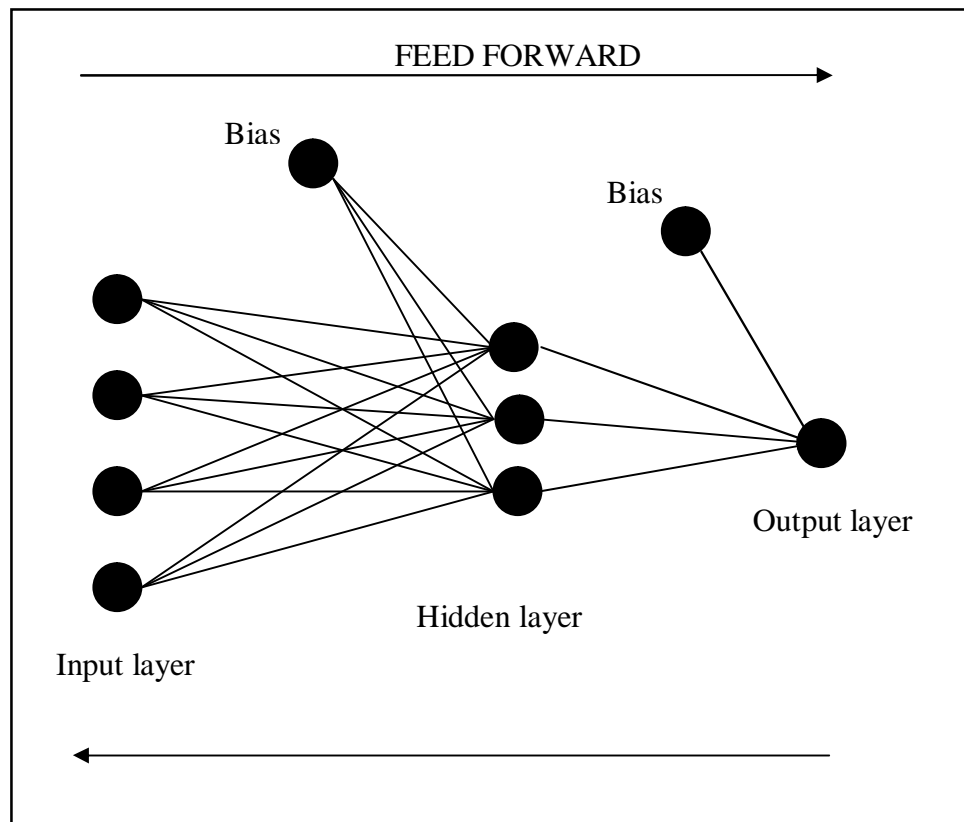
Figure 4.4 Multilayer Feed Forward Neural Network with Back Propagation

During training phase, the network is going to search for the best mapping between the input data and the desired performance. If the data used in the training set is not representative of the input data class, it can expect poor performance with the test set, even though performance can be excellent with the training set. This is called "over-generalization", and several methods have been proposed to overcome this problem, in the literature. In this thesis, a Genetic Algorithm and some other

techniques are used to obtain the optimum neural network architecture with high generalization capacity.

4.2.1.5 Performance measures of ANNs

It is important to define the criteria by which the performance of the model and its prediction accuracy will be evaluated in model development process. Various statistical measures have been developed and used to assess the model performance. The correlation coefficient (*R*), the mean square error (*MSE*), mean absolute error (*MAE*), and the mean absolute percentage error (*MAPE*) are used in this thesis. Statistical formulations of these parameters are given in Equations (4.4) to (4.7), respectively. The smaller the *MSE* of the both train and test sets, the higher the predictive quality is. *R* describes the fit of the ANNs output variable approximation curve to the actual test data output variable curve. Higher *R* coefficients indicate an ANN with better output approximation capabilities. Lower *MAE* and *MAPE* values are also show the robustness of the proposed ANN models.

$$MSE = \frac{\sum_{i=0}^{n}(o_i - p_i)^2}{n} \tag{4.4}$$

$$R = \frac{\sum o_i - o')(p_i - p')}{\sqrt{\sum(o_i - o')^2 \sum(p_i - p')^2}} \tag{4.5}$$

$$MAE = \left(\sum \left|\frac{o_i - p_i}{o_i}\right|\right) / n \tag{4.6}$$

$$MAPE = \frac{1}{n}\sum_{i=1}^{n}\left|\frac{o_i - p_i}{o_i}\right| *100 \tag{4.7}$$

where o' and p' are mean values of observed (o_i) and predicted (p_i) values

4.2.2 History of ANNs and Applications in Hydraulic Engineering

The first step toward artificial neural network came in 1943 by Warren McCulloch, a neurophysiologist, and a young mathematician, Walter Pitts (McCulloch and Pits 1949). They modeled a simple neural network with electrical circuits. In 1949, Donald Hebb proposed 'Hebb rule' which states that nets can learn from their experience in a training environment. 'Hebb rule' has always played a striking role in the field of ANN studies (Hebb 1949). Throughout 1950s scientists implemented models called perceptrons based on the work of McCulloch and Pitts. In 1957 Rosenblatt invented the *Perceptron* which has been a milestone in ANN studies (Rosenblatt 1957). Widrow and Hoff developed the models called ADALINE and MADALINE in 1960 which was the first neural network to be applied to a real world problem (Widrow and Hoff 1960). In 1969, Marvin Minsky published some intrinsic limitations of neural Networks which slowed down the implementations of ANN drastically (Minsky and Pappert 1969).

The studies in the field ANN almost stopped for more than a decade until Hopfield invented the Hopfield Network in 1982 whose dynamics were guaranteed to converge (Hopfield 1982). After this novel invention ANN studies have raised again. Back propagation was invented in 1986 by Rumelhart, Hinton and Williams which opened a new area in ANN applications (Rumelhart et al. 1986).

However, the first application in Civil Engineering only goes back to the late of 1980s, Levitt et al. (1988) and Flood (1989). Some of the first applications of artificial neural network in water engineering were carried out by Karunanithi and co-workers in 1994 in predicting the river flow (Karunanithi et al. 1994) and Grubert in 1995 in the stability analysis of stratified flow (Grubert 1995). Most of the ANN applications in water engineering can be found in ASCE task Committee (2000), Maier and Dandy (2000), and Dolling and Varas (2002). Therefore, some recent studies were additionally reviewed in this study. ANNs were applied by Liu and James (2000) in estimation of discharge capacity in meandering compound channels, by Baxter et al. (2001) in evaluating the drinking water quality, by Nagy et al. (2002) in prediction of sediment load concentration in rivers, by Sarghini et al. (2003) in modeling of turbulent flows in co-operation with large eddy simulation, by Azmatullah et al. (2006) in prediction of scour below spillways, and by Guven et. al

(2006) in prediction of pressure fluctuations beneath hydraulic jumps occurring on sloping stilling basins.

4.2.3 Local scour and artificial neural networks

Liriano and Day (2001) predicted the scour depth at culvert outlets, Azinfar et al. (2004) predicted the scour depth downstream sluice gate and Negm et al. 2004 predicted scour depth downstream of rectangular basin using neural networks. Azmatullah et al. 2005 and Azmatullah et al. 2006 estimated the scour downstream of a ski jump and below spillways using neural networks, respectively. Bateni et al. (2007) estimated the maximum scour depth around bridge piers at both equilibrium and time-dependent cases using NNs and adaptive neuro-fuzzy interference system (ANFIS).

4.2.4 Explicit formulation of neural networks (ENNF)

The main focus is to obtain an explicit formulation of output variable (y_i) as a function of input variables (x_j), transfer function and weights of the proposed ANN model (w_{ij}). All necessary parameters were obtained from the trained ANN, and the explicit expression is formed from the weights of the trained ANN model. Each input is multiplied by a connection weight, namely products and biases are simply summed, then transformed through a transfer function to generate a result, and finally outputs are obtained more easily. Inputs and outputs are normalized before the learning process of the ANN. To get an accurate result from ENNF, normalization values have to be considered as well. Input and output variables are normalized in the range (i.e. 0.05-0.95 for sigmoid function and -0.95-0.95 for tangent hyperbolic function) as follows:

$$\Phi_{normalised} = a \times \Phi + b \tag{4.8}$$

where Φ represents the variables used in ANN training, a and b are normalization coefficients of correspondent variable and calculated as given in Eqn.(4.9).

$$a = \frac{0.95}{Max(i) - Min(i)} \quad , \quad b = 0.95 - a \times Max(i) \tag{4.9}$$

where *Max(i)* and *Min(i)* are maximum and minimum values of correspondent variable.

The goal is to obtain the output in a functional form in terms of measured input variables as:

$$y_i = \frac{f(W) - b_o}{a_o} \tag{4.10}$$

where a_o and b_o are the normalization coefficients of output variable, f is symbol of activation function.

As a summary of this section, ENNF is composed of linear equations (U_i) used in input layer and the transfer function used in hidden layer (Eqn.(4.2)). The same equations (U_i) are repeated for each neuron in input layer, and then the sum-up equation (Eqn.(4.1)) is found in hidden layer. Finally, the output of the optimum network is de-normalized to get the actual output (Eqn.(4.10)). It should be noted that ENNF is valid between the maximum and minimum values of the input and output variables utilized in corresponding ANN application.

4.3   Overview of Genetic Programming

GP is a search technique which allows the solution of problems by automatically generating algorithms and expressions. These expressions are coded or represented as a tree structure with its terminals (leaves) and nodes (functions) (Koza, 1992). GP applies Genetic Algorithms (GAs) to a "population" of programs - typically encoded as tree-structures. Trial programs are evaluated against a "fitness function" and the best solutions selected for modification and re-evaluation. This modification-evaluation cycle is repeated until a "correct" program is produced.

There are five major preliminary steps for solving a problem by using GP; (i) the set of terminals, (ii) the set of functions, (iii) the fitness measure, (iv) the values of the

numerical parameters and qualitative variables for controlling the run, and (v) the criterion for designating a result and terminating a run (Koza, 1992).

The first major step in preparing to employ the GP paradigm is to identify the set of terminals to be used in the individual computer programs in the population. The major types of terminal sets contain the independent variables of the problem, the state variables of the system and the functions with no arguments. These types of terminal sets are given in a table by Koza (1992). The second major step is the set of functions; arithmetic operations, testing functions, (such as `IF` and `CASE` statements) and boolean functions. The third major step is fitness measure which identifies the way of evaluating how good a given program solves a particular problem. The terminals and the functions are the components of the programs which form the junctions in the tree. The choice of components of terminals and functions (the program) and the fitness function establishes the space that GP searches for. The fourth major step is the selection of certain parameters to control the runs. The control parameters contain the size of the population, the rate of crossover *etc*. The fifth and the last step is the criteria to terminate the run. For most of the problems, if the sum of the differences becomes zero (or reasonably close to zero), then, the solution is considered acceptable. The termination criterion is basically a rule for stopping. Characteristically the rule is to stop either on finding a program which solves the problem or after a certain number of generations.

Once the terminal and non-terminal operators are specified, it is possible to establish the types. Each node will have a type, and the construction of child expressions with crossover and mutation operations needs to follow the rules of the nodal type (Montana 1995), i.e., respect those grammatical rules specified by the user or investigator. Moreover, both specified operator sets must fulfill two requirements: closure and sufficiency. That is, it must be possible to build right trees with the specified operators, and the solution to the problem (the expression desired) must be able to be expressed by means of those operators.

The automatic program generation is carried out by means of a process derived from Darwin's evolution theory, in which, after subsequent generations, new trees (individuals) are produced from old ones via crossover, copy, and mutation (Fuchs 1998; Luke and Spector 1998). Based on natural selection, the best trees will have

more chances of being chosen to become part of the next generation. Thus, a stochastic process is established where, after successive generations, a well-adapted tree is obtained.

4.4   Review on GP Applications in Water Engineering

Genetic programming (GP) is a new technique used in water engineering. Only a few applications of GP fall into field of hydraulic engineering. Babovic et al. (2001a,b) applied GP to sedimentary particle settling velocity equations. Savic et. al (1999), Whigham and Crapper (1999, 2001), Keijzer and Babovic (2002) applied GP to rainfall-runoff modeling. Raju and Kumar (2004) studied on irrigation planning using genetic algorithms. Dorado et al. (2003) studied on prediction and modeling of the rainfall-runoff transformation of a typical urban basin using artificial neural networks (ANNs) and GP. Rabunal et al. (2006) determined the unit hydrograph of a typical urban basin using GP and ANNs. Giustolisi (2004) determined resistance coefficient in corrugated channels by using GP.

4.5   Gene-Expression Programming

Gene expression programming (GEP) software used in this thesis is developed by Ferreira (2001). GEP is an extension to GP that evolves computer programs of different sizes and shapes encoded in linear chromosomes of fixed length. The chromosomes are composed of multiple genes, each gene encoding a smaller subprogram. Furthermore, the structural and functional organization of the linear chromosomes allows the unconstrained operation of important genetic operators such as mutation, transposition, and recombination. One strength of the GEP approach is that the creation of genetic diversity is extremely simplified as genetic operators work at the chromosome level. Another strength of GEP consists of its unique, multigenic nature which allows the evolution of more complex programs composed of several subprograms. As a result GEP surpasses the old GP system in 100–10,000 times (Ferreria 2001a,b, 2002). GeneXproTools 4.0, a GEP software developed by Ferreira (2001a,b) is used in this thesis.

The fundamental difference between GA, GP and GEP is due to the nature of the individuals, namely in GAs the individuals are linear strings of fixed length (chromosomes); in GP the individuals are nonlinear entities of different sizes and shapes (parse trees); and in GEP the individuals are encoded as linear strings of fixed length (the genome or chromosomes) which are afterwards expressed as nonlinear entities of different sizes and shapes (i.e. simple diagram representations or expression trees).

4.5.1 Architecture of GEP

Two main parameters of GEP are the chromosomes and expression trees (ETs). The process of information decoding (from the chromosomes to the ETs) is called translation which is based on a set of rules. The genetic code is very simple where there exist one-by-one relationships between the symbols of the chromosome and the functions or terminals they represent. The rules also very simply determine the spatial organization of the functions and terminals in the ETs and the type of interaction between sub-ETs (Ferreria 2001a, b, 2002). That is the reason why two languages are utilized in GEP: the language of the genes and the language of ETs. A significant advantage of GEP is that it makes possible to infer exactly the phenotype given the sequence of a gene, and vice versa which is termed as Karva language. For example, an algebraic expression $(b-(b*a))+(a*b)$ was represented by Lopes and Weinert (2004) by a two-gene chromosome and an ET as shown in Figure 4.5.
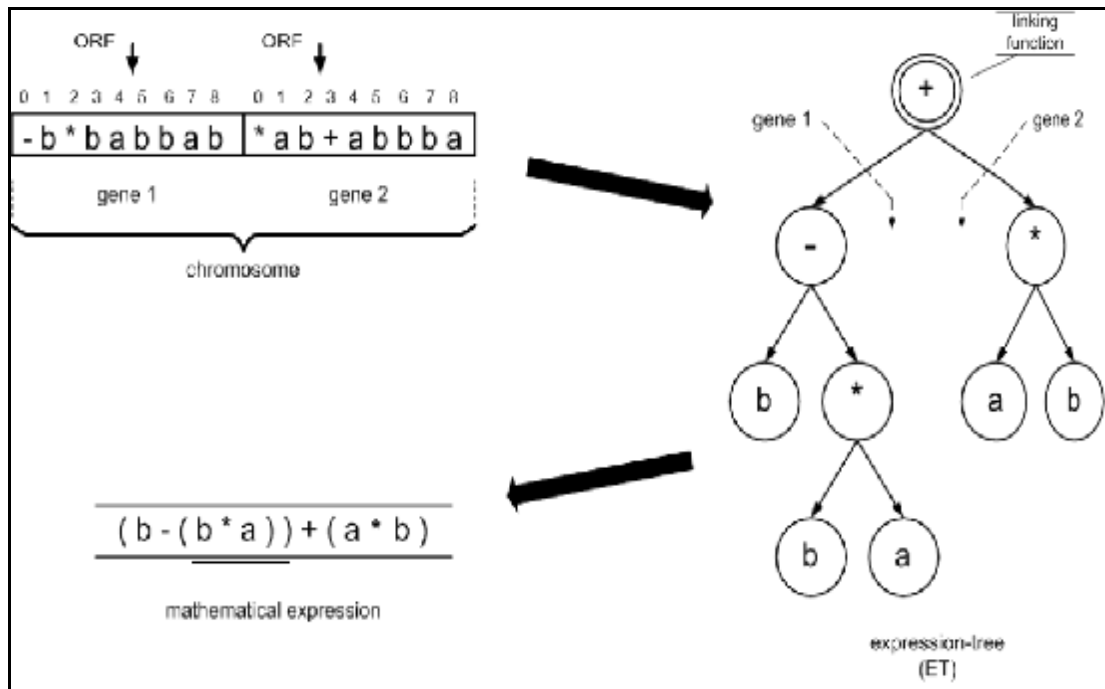
Figure 4.5 Example for GEP: two-genes chromosome, expression tree and corresponding analytical expression (Lopes and Weinert, 2004)

4.5.2 GEP algorithm and genetic operators

GEP modeling begins with the random generation of the chromosomes of a certain number of individuals or programs (the initial population). Then these chromosomes are expressed and the fitness of each program is evaluated against a set of fitness cases (also called selection environment or training set). The programs are then selected according to their fitnesses (their performance in that particular environment) to reproduce with modification, leaving progeny with new traits. These new programs are, in their turn, subjected to the same developmental process: expression of the chromosomes, confrontation of the selection environment, selection, and reproduction with modification. The process is repeated for a certain number of generations or until a good solution has been found (Ferreira 2001a).

In GEP, the individuals are often selected and copied into the next generation according to the fitness by roulette-wheel sampling with elitism, which guarantees the survival and cloning of the best individual to the next generation. Variation in the

population is introduced by conducting single or several genetic operators on selected chromosomes, which include (Baykasoğlu et al. 2007):

• Recombination (Crossover), in which two parent genomes are randomly chosen and paired to exchange some elements between them. There are two kinds of crossover; one-point, and two-point crossover, working in the same fashion as that in GAs.

• Mutation, which can happen with any times at any position in a genome, as long as that the mutated individual, passes the validity test. Note that like crossover, a mutation in the coding sequence of a gene usually drastically reshapes the ET.

• Inversion (Rotation), in which two subparts of element sequence in a genome are rotated with respect to a randomly chosen point (this is similar to the inversion in GAs).

4.5.3 Sub-expression trees and linking functions

The chromosomes of GEP are usually composed of more than one gene of equal length. For each problem or run the number of genes, as well as the size of the head, are a priori chosen. Each gene codes for a sub-expression tree (sub-ET) and the sub-ETs (see Figure 4.6) interact with one another forming a more complex multi-subunit expression tree.

The sub-ETs or sub-programs interact with one another through special functions, the so called linking functions: addition, subtraction, multiplication, and division for mathematical models and And, Or, Nand, Nor, Xor, Nxor, Less Than, Greater Than, Less Or Equal, and Greater Or Equal for Logic Synthesis problems.
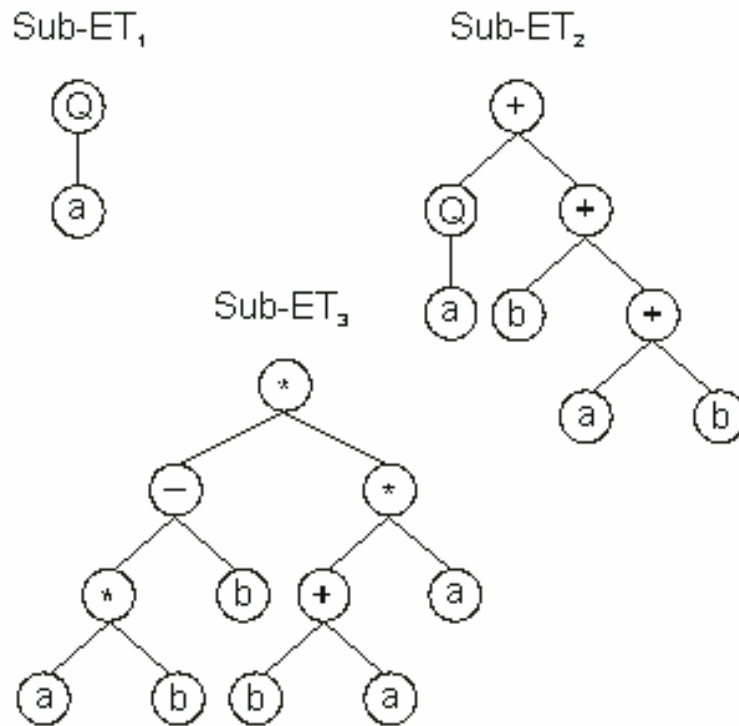
Figure 4.6 Sub-expression trees (sub ETs)

4.6 Soft Computing Applications on Local Scour Downstream of Grade-Control Structures

4.6.1 Local scour downstream of grade-control structures

Grade-control structures, having a weir width b and a fall height z (Figure 4.7) are built in order to prevent excessive channel-bed degradation in alluvial channels. The erosive action of the weir overflow may, however, cause significant local scour and may undermine these structures (Bormann and Julien 1991). Thus, the structural design of grade control structures must include sufficient protective provisions against local scour. An appropriate structural design of grade-control structure requires an understanding of the mechanics, location and extent of the downstream scour.

Consider the grade control structure in Figure 4.7. As the flow over the weir and impinges the tailwater, a neutrally buoyant jet occurs, which diffuses between point

A and B. Flow separates from the structure at point A and a vortex is formed in the separation zone. The diffused flow velocity in the vicinity of point B exerts a shear stress on bed sediment particles. When the applied shear stress exceeds the critical shear stress, sediment is dislodged and transported beyond the impingement zone (Bormann and Julien 1991). Local scour progresses until the equilibrium conditions are ultimately reached and the rate of scour approaches zero (Ali and Lim 1986, Rajaratnam and MacDoughall 1983, Johnston 1990, Bormann and Julien 1991). This state is characterized by maximum scour depth, *s*. Mason and Arumugam (1985) carried out a comprehensive literature review and data analysis and proved that the concept of an "maximum (ultimate) scour depth" is, for all practical purposes, valid. Estimation of *s* has been subject to numerous investigations in the literature.
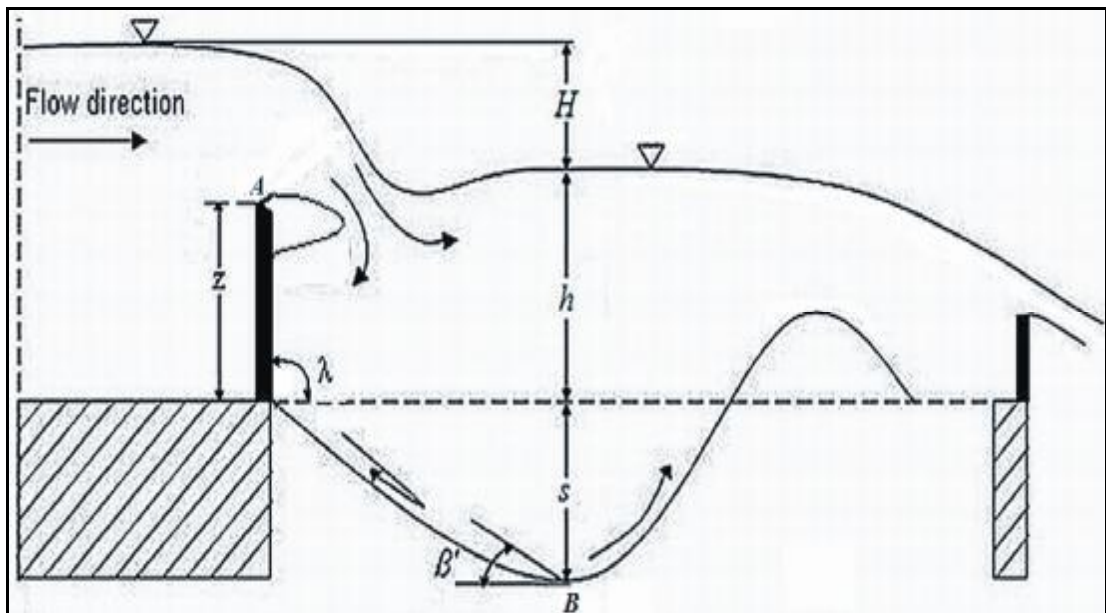
Figure 4.7 Sketch of scour downstream of sharp-crested grade-control structure

Bormann and Julien (1991) reviewed the experimental studies on scour downstream of hydraulic structures below free and submerged jets, being pioneered by Schoklitsch (1932) and Laursen (1952). Bormann and Julien (1988, 1991) investigated the scour downstream of grade control structures with large scale experiments using unit discharge up to 2.5 m^2/s and scour depths exceeding 1.4 m.

More recently, Lenzi and Comiti (2003) analyzed local scouring downstream of 29 drop structures and Marion et al. 2004 conducted a series of tests to determine the effect of bed sill spacing and sediment grading on the potential erosion by jets flowing over the sills.

4.6.2 Proposed maximum scour depth formulas to date

Mason and Arumugam (1985) summarized the formulas which have been developed for estimating the maximum scour depth under a falling jet. The accuracy of the formulas was evaluated by using each to process sets of scour data from prototypes and models of such prototypes. The authors proposed a comprehensive model and prototype equation which can be rewritten as:

$$\frac{s}{\left(\frac{q^2}{g}\right)^{1/3}} = (6.42 - 3.10H^{0.1})g^{-H/600} \times \left(\frac{gH^3}{q^2}\right)^{20+H/600} \left(\frac{H}{d_s}\right)^{1/10} \left(\frac{h}{H}\right)^{3/20} \qquad (4.11)$$

where q is unit discharge (m^2/s), H is drop between upstream water level and tailwater depth (m), g is gravitational acceleration and d_s is representative bed grain size (m).

Mason and Arumugam (1985) obtained the best agreements between the selected equations and measurements for the model data by using d_s equal to d_m (mean bed grain size).

Bormann and Julien (1991) carried out a large-scale study in order to calibrate their semi-theoretical equation for calculating maximum scour depth, under a wide range of conditions: wall jets, vertical jets, free jets, submerged jets and flow over large-scale grade control structures. Their proposed equation is remarkably similar to the regression based equations proposed in the literature:

$$s = \left[\frac{0.611}{[\sin(0.436 + b')]^{0.8}} q^{0.6} \frac{U_0}{g^{0.8} d_{90}^{0.4}} \sin b'\right] - z \qquad (4.12)$$

where d_{90} is bed grain size for which 90% of sampled particles are finer (m) and U_0 is jet velocity impinging on the tailwater (m/s).

The angle b' (Figure 4.7) is experimentally inferred by Bormann and Julien (1991) as:

$$b' = 0.316\sin l + 0.15\ln\left(\frac{z+y_0}{y_0}\right) + 0.13\ln\left(\frac{h}{y_0}\right) - 0.05\ln\left(\frac{U_0}{\sqrt{gy_0}}\right) \quad (4.13)$$

where l is downstream face angle of the grade-control structure (radian), y_0 is water depth at the crest (m). Eqn.(4.13) was obtained through a regression analysis also including 21 experimental data by Tarapore (1956) and Rajaratnam (1981).

Although Eqn.(4.12) was tested using large-scale experiments (88 data), the mathematical shape of Eqn.(4.13) limits its applicability to the cases for which the drop height z is less than the term of Eqn.(4.13) within the square brackets.

D'Agostino and Ferro (2004) used incomplete self similarity theory and some experimental scour depth data for deducing some relationships describing the geometrical pattern of scour profile (maximum scour depth, location of maximum scour depth). They expressed the scour phenomena due to the erosive action of flowing water by following functional relationship:

$$s = f(z, b, h, Q, r_s, r, g, d_{50}, d_{90}) \quad (4.14)$$

where r_s is mass density of sediments, r is mass density of water, d_{50} is diameter for which 50% of particles are finer.

They did not introduce the gradation coefficient in Eqn.(4.14), which is usually used to characterize non-uniform sediments, because it can be replaced by d_{50}/d_{90} with no significant loss of accuracy.

Because the relation in Eqn.(4.14) represents a physical phenomenon that does not depend on the choice of measurement unit, D'Agostino and Ferro (2004) used

Buckingham p theorem to represent physical parameters given in Eqn.(4.14) in dimensionless form. They chose z, Q and r as dimensional independent variable and deduced following eight dimensionless groups $\prod_i$ ($i=1,\ldots,8$):

$$\prod_1 = s/z \qquad \prod_2 = \frac{b}{z} \qquad \prod_3 = \frac{B}{z} \qquad \prod_4 = \frac{h}{z}$$

$$\prod_5 = \frac{(r_s - r)}{r} \qquad \prod_6 = \frac{gz^5}{Q^2} \qquad \prod_7 = \frac{d_{50}}{z} \qquad \prod_8 = \frac{d_{90}}{z}$$

(4.15)

Eleven dimensional parameters in Eqn.(4.14) were reduced to eight dimensionless groups in Eqn.(4.15) Additionally, d_{90}/z and d_{50}/z in Eqn.(4.14) were reduced to a new dimensionless group d_{90}/d_{50} ($\prod_8/\prod_7$), b/z and B/z were reduced to b/B ($\prod_2/\prod_3$). Combining b/z, $(r_s - r)/r$, gz^5/Q^2 and d_{50}/z, the following dimensionless group A_{50} is obtained:

$$A_{50} = \frac{1}{\dfrac{b}{z}}\left(\frac{1}{\dfrac{(r_s - r)}{r}\dfrac{gz^5}{Q^2}\dfrac{d_{50}}{z}}\right) = \frac{Q}{bz\left[gd_{50}\left(\dfrac{r_s - r}{r}\right)\right]^{1/2}}$$

(4.16)

From dimensional analysis, D'Agostino and Ferro (2004) suggested that,

$$\frac{s}{z} = f(\frac{b}{z}, \frac{h}{H}, A_{50}, \frac{d_{90}}{d_{50}}, \frac{b}{B})$$

(4.17)

and proposed following equation:

$$\frac{s}{z} = 0.54\left(\frac{b}{z}\right)^{0.593}\left(\frac{h}{H}\right)^{-0.126}(A_{50})^{0.544}\left(\frac{d_{90}}{d_{50}}\right)^{-0.856}\left(\frac{b}{B}\right)^{-0.751}$$

(4.18)

4.6.3 Data collection and data set analysis

Experimental measurements of Veronese (1937) (36 data sets), Bormann and Julien (1991) (88 data sets), D'Agostino (1994) (114 data sets) and Mossa (1998) (19 data sets) are used as training and testing sets of the proposed NNs and GEP models. Considerable scale difference is observed in these data sets (see Table 4.1). Veronese (1937), D'Agostino (1994) and Mossa (1998) carried out experiments in medium- or small- scale flume, while Bormann and Julien (1991) worked with a large-scale flume. Experimental discharges used in the combination of above-mentioned studies range between 0.001 to 2.5 m^2/s, producing maximum scour depths between 0.0352 to 1.40 m. Furthermore, the data sets range widely in bed grain size distributions. Veronese (1937) and Mossa (1998) focused on uniform size ($d_{90}=d_{50}$) sand, while the tests of Bormann and Julien (1991) and D'Agostino (1994) were characterized by a range $1.5<d_{90}/d_{50}<5.3$.

The functional relationship of scour downstream of sharp crested weir due to erosive action of impinging water is given in Eqn.(4.17). In this study, the dimensionless parameters given in Eqn.(4.17) were used order to construct empirical models and to show the generalization capability of ANN and GEP, the database produced in the experimental part is subdivided into two sets so called training and test sets. The empirical formulations were developed based on the former while the latter was employed to test the proposed models so as to measure their generalization capabilities. Of all 257 data sets, the training and testing sets consisted of randomly selected 206 (80% of whole data) and 51 (20% of whole data) sets, respectively. Table 4.1 reports the ranges of input and output parameters i.e. maximum and minimum values of dimensionless groups, which are used in this study.

4.6.4 Explicit formulation of local scour downstream of grade-control structures using neural networks

The objective of this section is to predict maximum scour depth using neural networks. The best architecture of the network was derived using Genetic Algorithm (GA). The model was trained with experimental data driven from four different

researches. The explicit formulation of neural networks (ENNF) is also presented. The proposed ENNF was compared with other equations in the literature. The results showed that ENNF estimated the maximum scour depth compared well to other formulations based on multiple non-linear regression analysis.

4.6.4.1 Construction of neural network model

In this study, the multi-layer perceptron network with back-propagation training algorithm is used. The Levenberg-Marquardt algorithm was used to minimize the global error (mean squared error (*MSE*) of the train set).

The optimal architecture of the proposed network was found using Genetic Algorithm (GA). GAs are used in order to avoid finding a local optimum solution that is closest to the starting point, since they are well suited to find, as in many cases, global optimum solution with high probability (Rao 1996). The genetic search for an optimal NN architecture starts from defining a population size for initializing the procedure. The objective function is chosen as *MSE* of train set (Eqn.(4.4)). Several networks are produced as individual strings and each individual string is assigned a probability of being selected:

$$P_i = \frac{f_i}{\sum_{i=1}^{K} f_i} \tag{4.19}$$

where f_i is objective function value of ith individual and K is the size of population.

In every generation, a new set of string is produced by using randomized parents selection and crossover from the old generation (old set of strings). Finally, the genetic optimization stops when the value of objective function is lower than a predefined value.

The optimal NN architecture in this study, as shown in Figure 4.8, was found to be 5-9-1 (no. of input parameters – no. of hidden nodes - no. of output parameters), with sigmoid transfer function:

$$f(W_j) = \frac{1}{1 + e^{-w_j}} \qquad (4.20)$$

where $W_j = \sum_1^n w_{ij} x_i$ is the weighted sum-up equation of j th neuron for the input received from the preceding layer with n neurons, w_{ij} is the weight between the j th neuron and the i th neuron in the preceding layer, and x_i is the output of the i th neuron in the preceding layer. The output of the j th neuron, out_j, is calculated using a sigmoid function as follows:

$$out_j = \frac{1}{1 + e^{-kW_j}} \qquad (4.21)$$

where k is a constant used to control the slope of the semi-linear region. The sigmoid non-linearity activates in every layer except the input layer.

4.6.4.2 Results of neural network training and sensitivity analysis

The experimental data taken from corresponding researches were used as training and test sets for NN modeling. The overall performances of both sets are evaluated by *MSE*, the mean absolute percentage error (*MAPE*).

Firstly, an attempt was made to assess the significance or influence of the input parameters on performance of NN modeling. NNs based on single input parameter were tried and the NNs based on dimensionless parameter *b/z* gave the best result with *MSE*=0.028 and *R*=0.864. Then different input parameter combinations are tried by adding input parameters one by one and their influence on testing data sets was evaluated in terms of *MSE*, *MAPE* and *R* criteria. The results given in Table 4.2 suggest that each parameter has a notable influence on the performance of NNs. Starting from single parameter, adding each parameter one by one improved the performance of NNs, with the best result obtained from NN5 model containing all dimensionless parameters given in Eqn.(4.17).
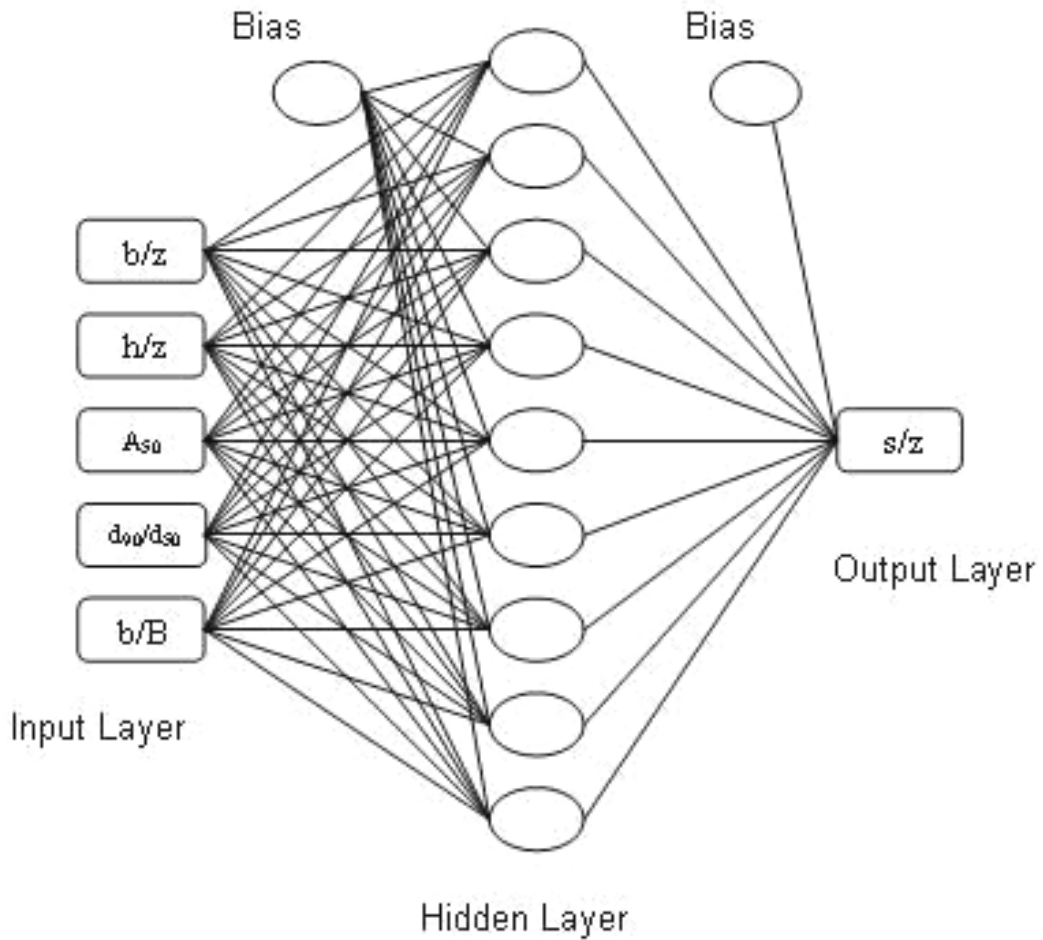
Figure 4.8 Optimal neural network architecture

Figures 4.9 and 4.10 compare the NN5 model predictions of s/z with the observations and scatter plot of measured s/z versus the predicted ones for training and testing sets, respectively. From Figure 4.9, it is clearly seen how well the proposed NN model learned the non-linear and complex interrelation between the inputs and output ($R=0.991$, $MAPE=8.03$). Comparison of NN predictions with measured ones for testing set (Figure 4.10) demonstrated a high generalization capacity of proposed model with relative low error ($MAPE=10.98$) and high correlation ($R=0.986$).

Table 4.1 Minimum and maximum values of physical variables

Physical parameters (unit)	Minimum value	Maximum value
b (m)	0.150	0.910
z (m)	0.090	2.130
h (m)	0.025	1.650
H (m)	0.044	3.260
Q (m^3/s)	0.001	2.247
d_{90} (m)	0.002	1.710
d_{50} (m)	0.002	0.45
B (m)	0.300	0.910
s (m)	0.035	1.520

Table 4.2 Sensitivity analysis of dimensionless input parameters

NN Model	Input parameters	*MSE*	*MAE*	*R*
NN1	b/z	0.028	25.122	0.864
NN2	b/z, A_{50}	0.017	16.470	0.906
NN3	b/z, A_{50}, h/H	0.012	15.224	0.939
NN4	b/z, A_{50}, h/H, d_{90}/d_{50}	0.008	11.769	0.958
NN5	b/z, A_{50}, h/H, d_{90}/d_{50}, b/B	0.002	10.982	0.986

4.6.4.3 Derivation of ENNF of maximum scour depth

The main focus is to obtain an explicit formulation of maximum scour depth (s) downstream of grade-control structures as a function of inputs, transfer function (sigmoid) and weights of the proposed NN5 model.

All necessary parameters were obtained from the trained NN, and the explicit expression is formed from the weights of the trained NN model. Each input is multiplied by a connection weight, namely products and biases are simply summed, then transformed through a transfer function (sigmoid) to generate a result, and finally outputs are obtained more easily. Inputs and outputs are normalized before the learning process of the NN. To get an accurate result from ENNF, normalization values have to be considered as well. Input and output parameters are normalized in the range (0.05-0.95) as given in Eqns. (4.8) and (4.9). The normalization coefficients of each parameter are given in Table 4.3.

Table 4.3 Minimum and maximum values of input and output parameters

Dimensionless parameters	Minimum value	Maximum value	Normalization coefficients	
			a	b
b/z	0.211	3.333	0.052	0.039
h/H	0.050	3.960	0.230	0.039
A_{50}	0.025	3.095	0.293	0.043
d_{90}/d_{50}	1.000	5.267	0.211	-0.161
b/B	0.300	1.000	1.286	-3.357
s/z	0.047	1.611	0.576	0.024

The goal is to obtain the s/z (normalized maximum scour depth) in a functional form in terms of measured dimensionless parameters:

$$\frac{s}{z} = \frac{1.737}{1 + e^{-W}} - 0.039 \tag{4.22}$$

where the coefficients (1.737) and (-0.039), come from de-normalization of output of proposed network, and

$$W=(4.05)*\left(\frac{1}{1+e^{-U1}}\right)+(-2.05)*\left(\frac{1}{1+e^{-U2}}\right)+2.59*\left(\frac{1}{1+e^{-U3}}\right)+2.73*\left(\frac{1}{1+e^{-U4}}\right)+0.63*\left(\frac{1}{1+e^{-U5}}\right)$$
$$+(-4.73)*\left(\frac{1}{1+e^{-U6}}\right)+(-2.88)*\left(\frac{1}{1+e^{-U7}}\right)+(-3.34*\left(\frac{1}{1+e^{-U8}}\right)+12.47*\left(\frac{1}{1+e^{-U9}}\right)-16.67 \tag{4.23}$$

and the values for U_i ($i=1,…,9$) are given as

$$U_1 =0.360b/z+9.215h/H-5.859A_{50}+2.729d_{90}/d_{50}-32.836b/B+10.067 \tag{4.24a}$$

$$U_2 =-1.587b/z+1.363h/H+1.616A_{50}-2.218d_{90}/d_{50}+17.302b/B-4.633 \tag{4.24b}$$

$$U_3 =2.224b/z+24.367h/H-5.464A_{50}-36.379d_{90}/d_{50}+31.318b/B-14.938 \tag{4.24c}$$

$$U_4 =-0.884b/z-17.295h/H+3.585A_{50}-0.384d_{90}/d_{50}+5.966b/B+24.221 \tag{4.24d}$$

$$U_5 =-1.879b/z+36.178h/H+11.5844A_{50}+15.374d_{90}/d_{50}+39.136b/B-357.567 \tag{4.24e}$$

$$U_6 =4.980b/z+8.282h/H-5.751A_{50}+2.210d_{90}/d_{50}-33.967b/B+7.880 \tag{4.24f}$$

$$U_7 =-0.009b/z+6.636h/H-4.096A_{50}+3.929d_{90}/d_{50}-22.546b/B+5.083 \tag{4.24g}$$

$$U_8 =0.328b/z-1.461h/H-0.627A_{50}+1.335d_{90}/d_{50}-9.657b/B+2.833 \tag{4.24h}$$

$$U_9 =0.724b/z-0.148h/H+1.295A_{50}+1.093d_{90}/d_{50}-5.376b/B+1.816 \tag{4.24i}$$

It should be noted that ENNF is valid within the range of input and output parameters given in Table 4.3.

4.6.4.4 Comparison of ENNF with other equations

The performance of ENNF (Eqn.(4.22)) is compared with Eqns.(4.11), (4.12), and (4.18) using the test set. The comparison of proposed equations is illustrated in Figure 4.11. Prediction of Eqn.(4.12), proposed by Bormann and Julien (1991), was not introduced, because the equation gave negative values for all of the data not included in their study. Scatter plot of measured *s* versus the predictions of proposed equations shows that the performance of ENNF (*R*=0.992, *MSE*=0.00001) is clearly better than Eqn.(4.11) (*R*=0.865, *MSE*=0.00175) and Eqn.(4.18) (*R*=0.746, *MSE*=0.00126).

In fact, the procedure of ENNF is longer than non-linear regression approach, but ENNF is such simple that it can be used, by anyone who is even not familiar with NNs, in a spreadsheet on a very simple PC or even in a hand calculator conditional that input parameters are measured.

ENNF uses a total of 64 fitting parameters, while Eqn.(4.11) uses 10 and Eqn.(4.18), 6 parameters. Viewed from this perspective, it is not entirely surprising that the ENNF produces better results compared to the other methods. But the important issue is the generalization capacity of a model when compared to another one. In this sense, two important performance measuring criteria were used to evaluate the generalization capacity ENNF combining its network size, compared to Eqn.(4.11) and Eqn.(4.18). Akaike's (1973) Information Criterion (*AIC*) is used to measure the tradeoff between generalization performance of a model and its network size, and Rissanen's (1978) Minimum Description Length (*MDL*) criterion tries to combine the model's error with the number of degrees of freedom to determine the level of generalization. The goal is to minimize these to terms.

$$AIC = N \ln(MSE) + 2p \qquad (4.25)$$

$$MDL = N \ln(MSE) + 0.5p \ln(N) \qquad (4.26)$$

where *N* number of data set used (*N*=51 for test set) and *p* is number of fitting parameters.

Evaluating ENNF with testing data gave AIC=-3342.54 and MDL=-3286.53, while Eqn.(4.11) gave AIC=-311.707, MDL=-311.911, and Eqn.(4.18), AIC=-328.616, MDL=-328.881. The results show that ENNF has the best generalization despite its more number of fitting parameters compared to the other equations.

4.6.4.5 Performance of ENNF in field data

The robustness of ENNF is evaluated with field data (13 sets) taken from the Missiaga stream in Italy (D'Agostino and Ferro 2004). The Missiaga stream lies on alluvial bed whose slope is 0.15 m/m. The degradation of stream is controlled by 13 check dams having broad crested weir with b in the range 7.5-10.8 (m) and z ranging from 0.55 to 1.35 m. The bed grain size distribution sampled between check dams yielded d_{50}=0.06 m and d_{90}=0.155m. The maximum discharge was recorded as 3.98 m^3/s. In spite of a unique bed grain-size distribution and a narrow range of q and z, observed data show a wide range of s values (see Table 4.4).

A comparison of proposed equations' predictions with measurements is shown in Figure 4.12. The figure shows that ENNF generally over-predicts the maximum scour depth. However the predictions of ENNF (R=0.942, $MAPE$=9.763) are clearly better than those of Eqn.(4.11) (R=0.730, $MAPE$=10.13) and Eqn.(4.18) (R=0.480, $MAPE$=21.30). Relatively small discrepancies between the predicted and measured values support the use of ENNF in obtaining preliminary maximum scour depth values in field studies.
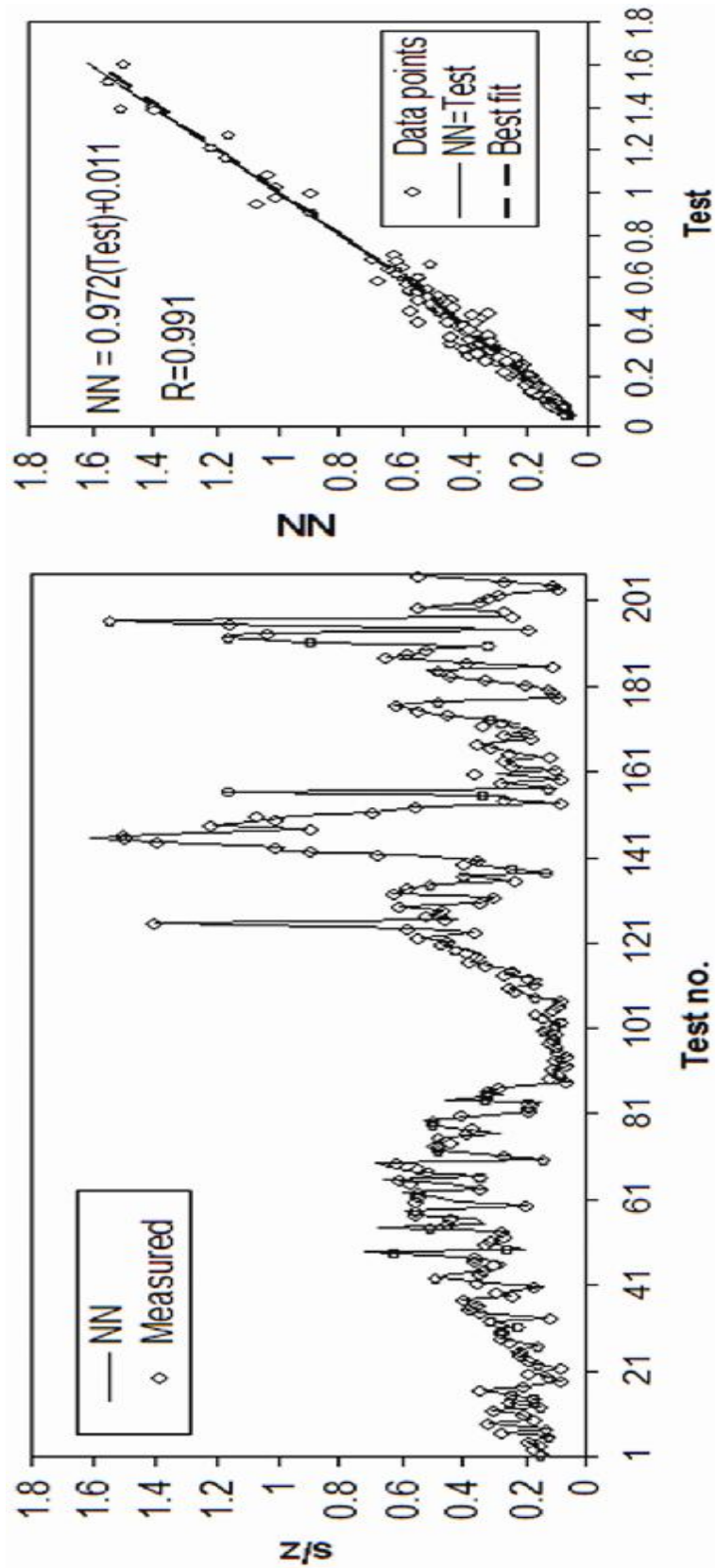
Figure 4.9 Comparison of NN estimations and measured ones for train set
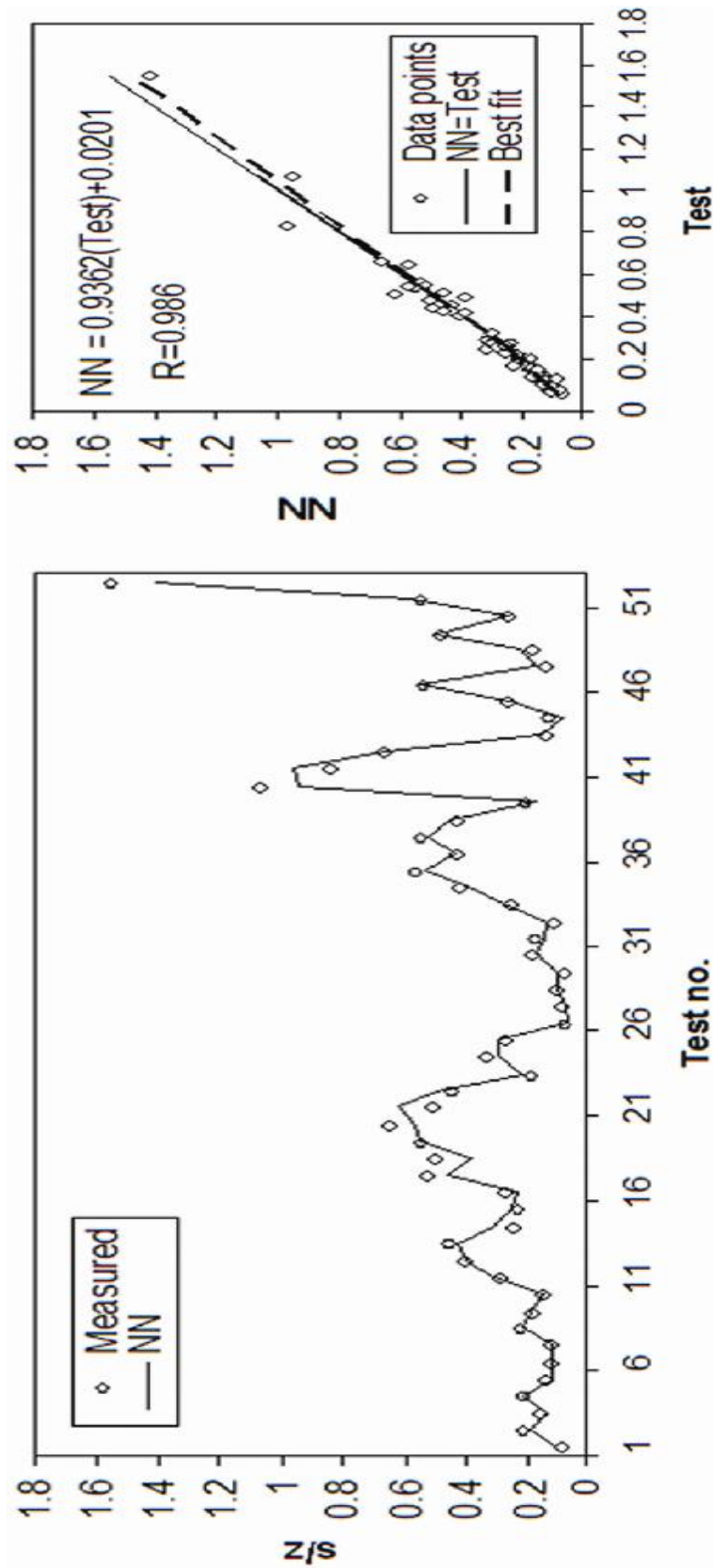
Figure 4.10 Comparison of NN estimations and measured ones for test set
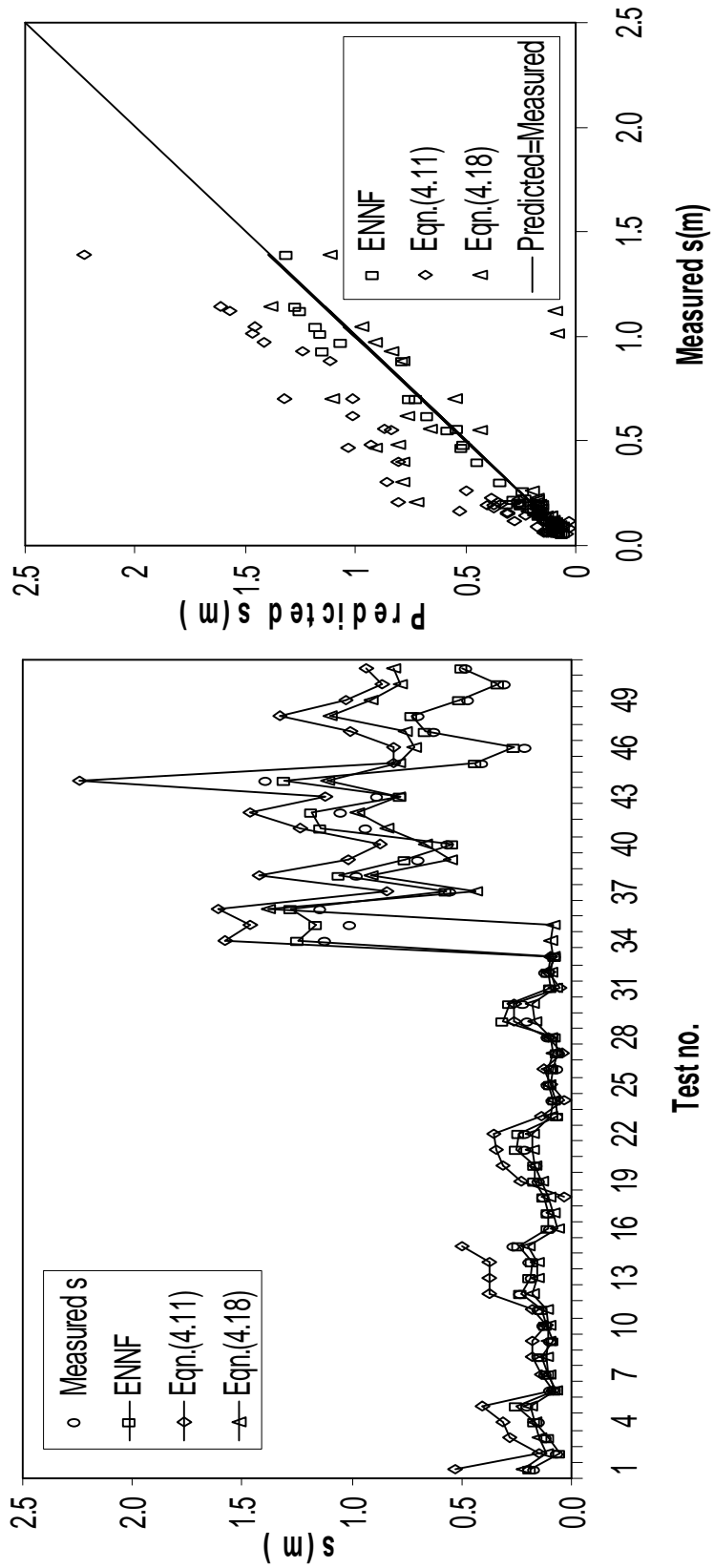
Figure 4.11 Comparison of estimations of proposed equations and measured ones for Test set
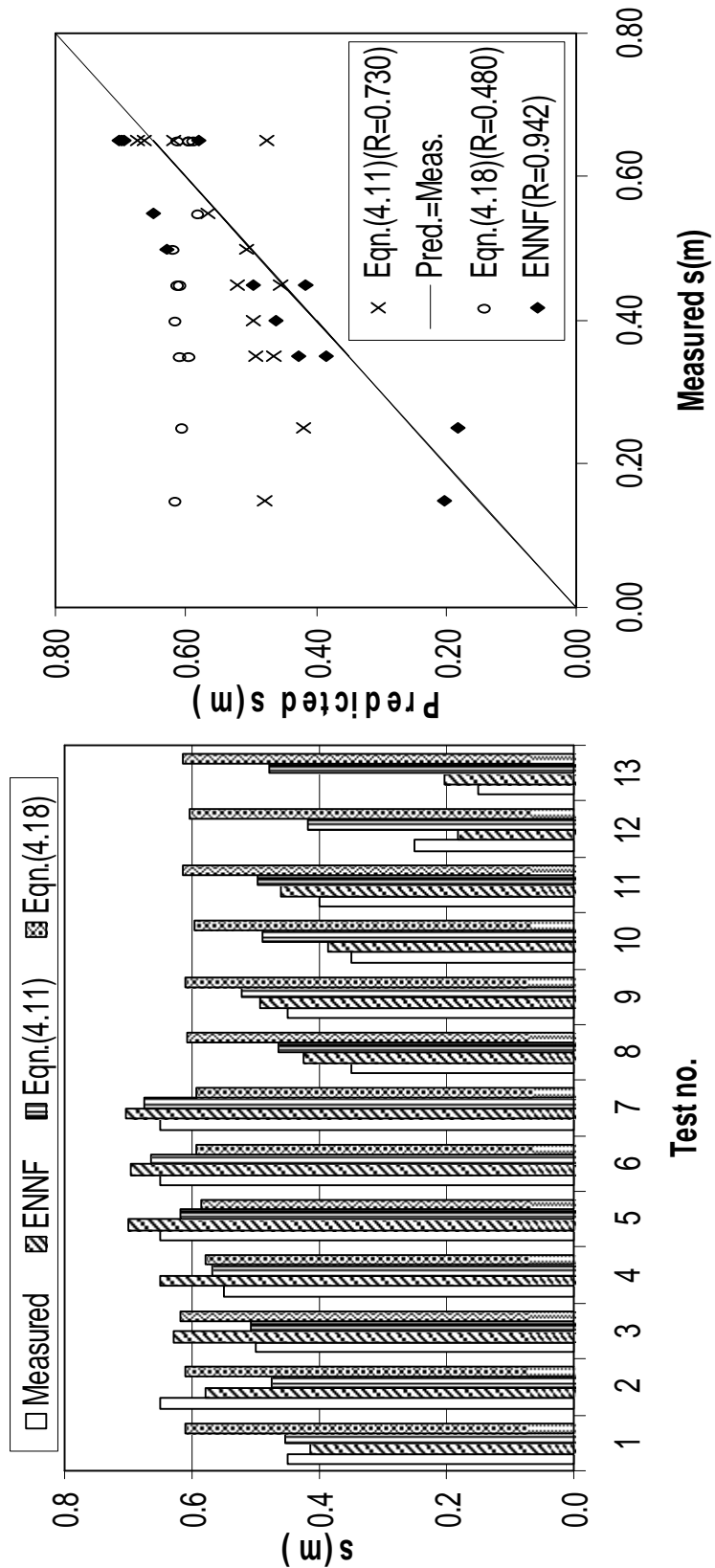
Figure 4.12 Comparison of estimations of proposed equations and field data

4.6.4.6 Parametric study

It is obvious from statistical results (R=0.991) above that the proposed NN model accurately learned to map the relationship between the dimensionless maximum depth of scour s/z and the dimensionless parameters representing the geometry of scouring, soil properties and the incoming flow characteristics. Thus the trained NN proposed in this study was used to conduct a parametric study to investigate the effect of changing input parameters on the dimensionless maximum scour depth. Keeping all input parameters but one as constants (at their average magnitudes) at a time, the variation of the dimensionless scour depth with respect to different input parameters was drawn. Figure 4.13 shows such a variation of s/z with b/z, h/H, A_{50}, d_{90}/d_{50} and b/B, respectively.

Interesting outcomes are observed on the graph of trends. As a general view, there are linear relationships between s/z depth and the other dimensionless groups. From Figure 4.13, increasing discharge (included in A_{50}, keeping the other included variables constant) results in deepening of the scour; the deepening of scour is very high at the beginning and gets lower after around the middle of the range of discharge. The geometrical parameters, b/z and b/B are directly proportional and linearly dependent to s/z; the increase in the former causes smaller depth of scour while the increase in the latter results in fast deepening of scour. From the physical point of view, it is easy to see that the scouring process is enhanced due the fact that the weir spans the entire width of the channel (b/B=1).

One of the most striking result is that the dimensionless parameter d_{90}/d_{50}, controlling the degree of soil uniformity, does not have a significant effect on s/z and can be neglected, which can be due to the fact that the available experimental data is generally of uniform soil type, in which the effect of non-uniformity is poorly included. It may thus been concluded that the proposed NN model produced physically consistent output.

Table 4.4 Field data of the Missiaga Stream ($b=B$)

z (m)	Q/B (m)	d_{50} (m)	d_{90} (m)	B (m)	H (m)	s (m)
1.000	0.379	0.060	0.155	10.500	0.837	0.450
0.820	0.379	0.060	0.155	10.500	0.677	0.650
0.600	0.379	0.060	0.155	10.500	0.486	0.500
1.300	0.531	0.060	0.155	7.500	1.091	0.550
0.900	0.531	0.060	0.155	7.500	0.736	0.650
0.600	0.531	0.060	0.155	7.500	0.482	0.650
0.550	0.531	0.060	0.155	7.500	0.442	0.650
1.000	0.386	0.060	0.155	10.300	0.836	0.350
0.650	0.398	0.060	0.155	10.000	0.528	0.450
1.200	0.437	0.060	0.155	9.100	1.011	0.350
0.680	0.379	0.060	0.155	10.500	0.555	0.400
1.350	0.375	0.060	0.155	10.600	1.156	0.250
0.720	0.369	0.060	0.155	10.800	0.590	0.150
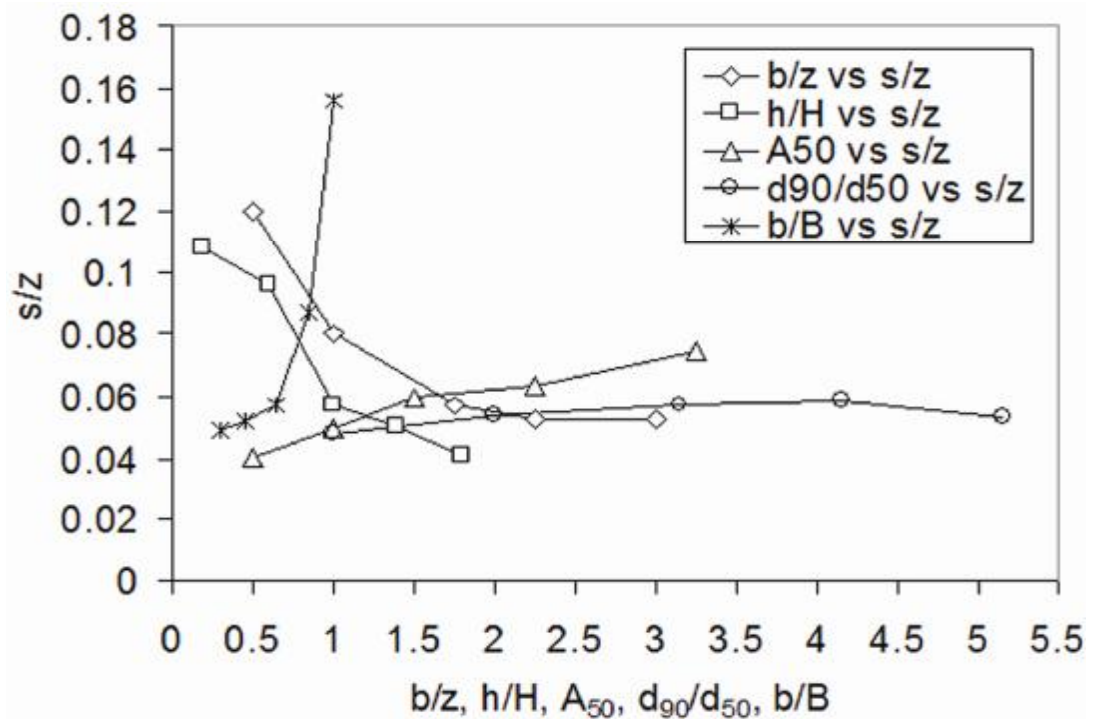
Figure 4.13 Variation of s/z with b/z, h/H, A_{50}, d_{90}/d_{50} and b/B

4.6.4.7 Conclusions

An alternative method to the conventional non-linear regression based formulation predicting maximum scour depth downstream of grade-control structures is introduced in this study. The method is based on explicit neural networks formulation (ENNF).

The experimental studies of others were used as training and testing sets in order to obtain the normalized maximum scour depth (s/z) as a function of the relevant dimensionless parameters. The best architecture of proposed neural networks was obtained using Genetic Algorithm. The optimal weights of input and output parameters were found by Levenberg-Marquardt back propagation algorithm. ENNF grows out of a transfer function (sigmoid) and the best weights obtained from training process.

NNs are found to be capable of predicting maximum scour depth downstream of grade-control structures. The estimations of ENNF were clearly better than those of conventional non-linear regression equations (Eqns.(4.11), (4.12), and (4.18)), with lower error (*MAPE*) and higher correlation coefficient (*R*).

The well trained NN model is also used to conduct parametric studies. The effect of dimensionless parameters regarding geometric, incoming flow and soil properties on scour is graphically presented. It is found the scouring process is enhanced when the weir spans the entire channel width ($b/B=1$), which can be an interesting outcome for researchers that deal with the effect of contraction of weir (b/B) on scour process.

ENNF predictions in field data which is not used in learning set gave satisfactory results and supported the use of neural networks modeling in preliminary estimations of field data. The results of this study are very promising.

4.6.5 A Genetic programming approach for prediction of local scour downstream of grade-control structures

The main focus of this section is to propose a new formulation technique for prediction of local scour by following a new approach, which is GEP which has not been applied in the literature so far. The proposed formulation was trained with experimental data explained in **section 4.4.3**. The explicit formulation of GEP is also presented. The proposed GEP models were compared to the developed regression-based equations and other equations available in the literature. The results showed that GEP estimated the maximum scour depth and horizontal distance between weir crest and the section of maximum scour depth well compared to other formulations.

4.6.5.1 Regression analysis

Regression analysis involves collecting predictor (independent variables) and response (dependent variables) values for common samples, and then fitting a predefined mathematical relationship to the collected data. Based on the predefined analytical model, regression analyses are classified as "linear" or "non-linear".

The dimensionless groups of parameters derived from dimensional analysis (Eqn.(4.17)) were related to each other in the present study on the basis of linear and non-linear regression analyses. The normalized maximum scour depth (s/z) was taken as dependent variable and the other parameters as independent variables. This yielded linear and nonlinear equations for prediction of s/z.

4.6.5.1.1 Multiple linear regression (MLR)

We considered a multi-linear relation of the form $\mathbf{y}=b_0+b_1\mathbf{x_1}+b_2\mathbf{x_2}+...+b_p\mathbf{x}_p$ between the non-dimensional pressure fluctuation parameter ($\mathbf{y}$) and the other non-dimensional parameters ($\mathbf{x_i}$) derived in dimensional analysis section (Eqn.(4.17)). The model coefficients (b_i) were calculated by least square regression with forward selection. Values of mean square error (*MSE*) were used in order to find the fitting

degrees of linear models with experimental data. The best model selection process stopped when the lowest *MSE* value was reached. MLR analysis yielded following equation:

$$s/z = 0.03b/z + 0.08h/H + 0.26A_{50} + 0.003d_{90}/d_{50} + 0.73b/B - 0.47 \qquad (4.27)$$

4.6.5.1.2 Multiple non-linear regression (MNLR)

Non-linear relationships between the dependent variable *s/z* and the independent variables based on tangent hyperbolic function, $y=2/(1+e^{-2z})-1$ where $z=b_0+b_1x_1+b_2x_2+...+b_px_p$, were considered. The model coefficients were calculated using Genetic Algorithm. The process of selecting optimal model stopped when the highest value of the correlation coefficient *R* was achieved. Following equation was derived:

$$s/z = \frac{1.74}{1+e^{\left(\frac{2.80}{1+e^{-0.01b/z-1.65h/H+9.53A_{50}-0.27d_{90}/d_{50}-44.10b/B-47.46}}-1.40\right)}} - 0.04 \qquad (4.28)$$

The statistical results of linear and non-linear regression analyses (Eqns.(4.27), (4.28)) in terms of mean squared error *MSE* (Eqn.(4.4)), correlation coefficient *R* (Eqn.(4.5)), and mean absolute percentage error *MAPE* (Eqn.(4.6)) between the measured and predicted scour are given in Table 4.5.

4.6.5.2 Construction of GEP model

The same experimental and field data used in neural network modeling was also utilized in this section. As described in **section 4.4.2**, among 257 test sets, 206 sets (80% of the total) were randomly chosen as training set for GEP modeling and the remaining 51 sets (20%) were used to evaluate the generalization capacity of the proposed GEP model. Once the training set is selected, the learning environment of the system has been defined.

There are five major steps in preparing to use gene expression programming, and the first is to choose the fitness function. For this problem we measured the fitness f_i of an individual program i by the following expression:

$$f_i = \sum_{j=1}^{C_t} \left(M - \left| C_{(i,j)} - T_j \right| \right) \tag{4.29}$$

where M is the range of selection, $C_{(i,j)}$ the value returned by the individual chromosome i for fitness case j (out of C_t fitness cases) and T_j is the target value for fitness case j. If $|C(i,j) - Tj|$ (the precision) less or equal to 0.01, then the precision is equal to zero, and $f_i = f_{max} = C_t M$. For our case, we used an $M = 100$ and, therefore, $f_{max} = 1000$. The advantage of this kind of fitness function is that the system can find the optimal solution for itself (Ferreira 2001a).

The second major step consists in choosing the set of terminals T and the set of functions F to create the chromosomes. In this problem, the terminal set consists obviously of the independent variable, i.e., T = {b/z, h/H, A_{50}, d_{90}/d_{50}, b/B}. The choice of the appropriate function set is not so obvious, but a good guess can always be done in order to include all the necessary functions. In this case, we used the four basic arithmetic operators (+, -, *, /), and some basic functions ($\sqrt{}$, $\ln(x)$, $\log(x)$, e^x, 10^x, power).

The third major step is to choose the chromosomal architecture, i.e., the length of the head and the number of genes. We used a length of the head, h=8, and three genes per chromosome. The fourth major is to choose the linking function. In this case, we linked the sub-ETs by addition. And finally, the fifth major step is to choose the set of genetic operators that cause variation and their rates. We used a combination of all genetic operators (mutation, the three kinds of transposition, and the three kinds of recombination). Parameters for the training of the GEP model are given in Table 4.6.

The best of generation individual, chromosome 9, has fitness 797. An explicit formulation based on GEP for normalized maximum scour depth as a function of dimensionless parameters most affecting the scour process (Eqn.(4.17) as follows:

Fig.4.14 shows the ET of the formulation which actually is (Karva Language):

$$(+.d0./.*.Pow1.0.d4.d0.Ln.Pow.+.d1.d3.d3.d3.d4.d3.d3.d3.d0.d3.G1C1)*$$
$$(/.d4.Pow1.0.Exp.+.G2C1.-.d1.-.Pow.d1.d1.d3.G2C1.d1.d1.d4.d4.d1.G2C1.d4) \quad (4.30)$$
$$*(/.Sqrt.+.d2.d0./.Ln.+.Pow1.0.-.d3.G3C1.d2.d0.G3C1.d1.d4.d1.d4.G3C1.d3)$$

where the constants in the formulation are:

$$G1C1=7.42, \; G2C1=-3.53, \; G3C1=0.32 \qquad (4.31)$$

and the actual parameters are:

$$d0=b/z, \; d1=h/H, \; d2=A_{50}, \; d3=d_{90}/d_{50}, \; d4=b/B \qquad (4.32)$$

After putting the corresponding values, the final equation becomes:

$$s/z = \left((b/z) + \frac{(b/B)(b/z)}{10^{(h/H)(\ln(d_{90}/d_{50})-0.69)}} \right) \left(\frac{(b/B)}{10^{-3.53-(h/H)(d_{90}/d_{50})}} \right) \left(\frac{(\sqrt{A_{50}})}{(b/z)+\dfrac{0.74}{(A_{50})-(b/z)+(d_{90}/d_{50})}} \right) \quad (4.33)$$

It should be noted that the proposed GEP formulation is valid for the ranges of training set given in Table 4.3, thus it covers a wide range of possible cases that can be faced in practice.

Statistical parameters of the test and training sets of GEP formulation are presented in Table 4.5. The prediction of the proposed GP formulation vs. actual experimental values for training and testing sets are given in Fig. 4.15 -4.16. Fig.4. 15 shows how good GEP learned the nonlinear relation between parameters and Fig.4.16 proves the high generalization capacity of the proposed GEP formulation.

4.6.5.3 Comparison of GEP with other equations

The performance of GEP (Eqn. 4.33) is compared to Eqns. (4.11), (4.12) and (4.18) using experimental data of Veronese (1937) and Mossa (1998). The comparison of the proposed equations is illustrated in Figure (4.17). Prediction of Eqn.(4.12) was

not introduced, because the equation gave negative values for whole data. The scatter plot proves that the performance of GEP (Eqn.(4.34)) (R=0.97, $MAPE$=7.94) are dominant to Eqn. (4.11) (R=0.73, MAPE=37.77) and Eqn.(4.18) (R=0.79, $MAPE$=23.20).

4.6.5.4 Performance of GEP in field data

The robustness of GEP is evaluated with field data (13 sets) taken from Missiaga stream in Italy (D'Agostino and Ferro 2004). The Missiaga stream lies on alluvial bed whose slope is 0.15. The degradation of stream is controlled by 13 check dams having a broad crested weir width b varying in the range 7.5-10.8 m and a fall height ranging from 0.55 to 1.35 m. Bed grain size distribution sampled between check dams represent d_{50}=0.06 m and d_{90}=0.155 m. The maximum discharge was recorded as 3.98 m^3/s.

Comparison of the proposed equations' estimations to the measured ones is shown in Figure 4.18. The black bars show that GEP generally over-predicts the maximum scour depth. However the predictions of GEP (R=0.93, $MAPE$=8.66) are dominantly better than those of Eqn.(4.11) (R=0.74, MAPE=21.08) and Eqn.(4.18) (R=0.75, $MAPE$=14.24). Relatively small discrepancies between the estimation of GEP and measured values encourage use of GEP in obtaining preliminary maximum scour depth values in field studies.

4.6.5.5 Conclusions

This study reports a new and efficient approach for the formulation of local scour downstream of grade-control structures using GEP for the first time in the literature. Explicit formulation is proposed for the maximum scour depth s.

The proposed GEP formulation is empirical and based on experimental results collected from the literature. The proposed GEP formulation shows excellent agreement with experimental results.

Also, linear and non-linear regression based formulations are proposed for *s*. The results of the proposed GEP formulation are compared to results of proposed regression based equations and existing equations in the literature, and the GEP formulation was found to be more accurate than others.

GEP may serve as a robust approach and it may open a new area for the accurate and effective explicit formulation of many water engineering problems. It should be noted that empirical formulations in local scour case are mostly based on predefined functions where regression analysis of these functions are later performed. However in the case of GEP approach there is no predefined function to be considered i.e. GEP creates randomly formed functions and selects the one that best fits the experimental results.

Moreover there is no restriction in the complexity and structure of the randomly formed functions as well. Evaluation of proposed GEP formulation for maximum scour depth in field data yielded relatively good results. The outcomes of this study are very promising and encourage the use of GEP in complex water engineering problems.

Table 4.5 Statistical parameters of local scour equations

Equation	MSE	MAPE (%)	Correlation coefficient (R)
GEP(Eqn.(4.33)) Train	0.004	12.061	0.98
GEP(Eqn.(4.33)) Test	0.005	17.559	0.97
MNLR(Eqn.(4.28))	0.028	48.148	0.85
MLR(Eqn.(4.27))	0.042	63.004	0.68
Eqn.(4.(11))	0.060	55.399	0.64

Table 4.6 Parameters of the GEP model

Function set	$+, -, *, /, \sqrt{}, \ln(x), e^x, 10^x$, power
Chromosomes	30
Head size	8
Number of genes	3
Linking function	Multiplication
Fitness function error type	MAE(Mean absolute error), Custom fitness error function
Mutation rate	0.044
Inversion rate	0.1
One-point recombination rate	0.3
Two-point recombination rate	0.3
Gene recombination rate	0.1
Gene transposition rate	0.1
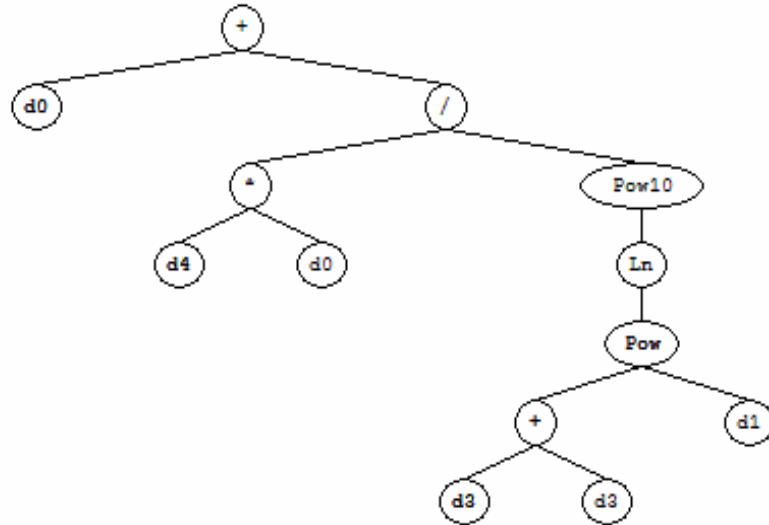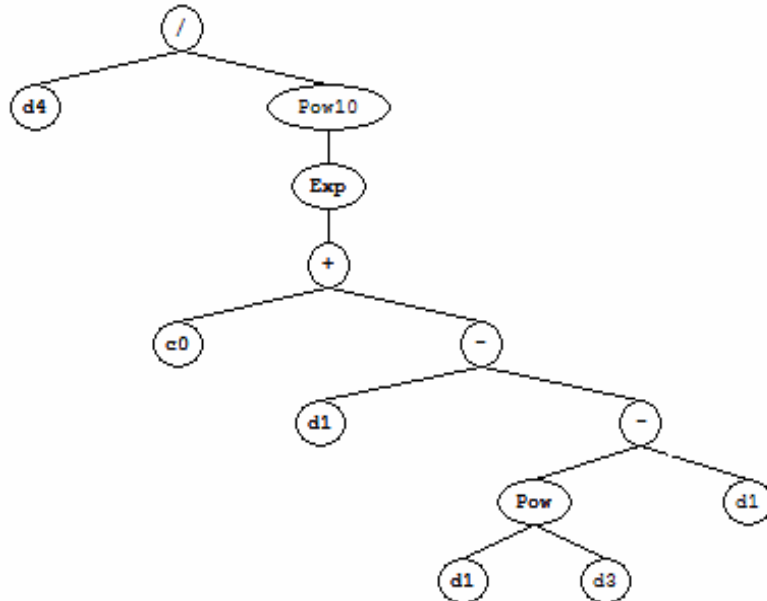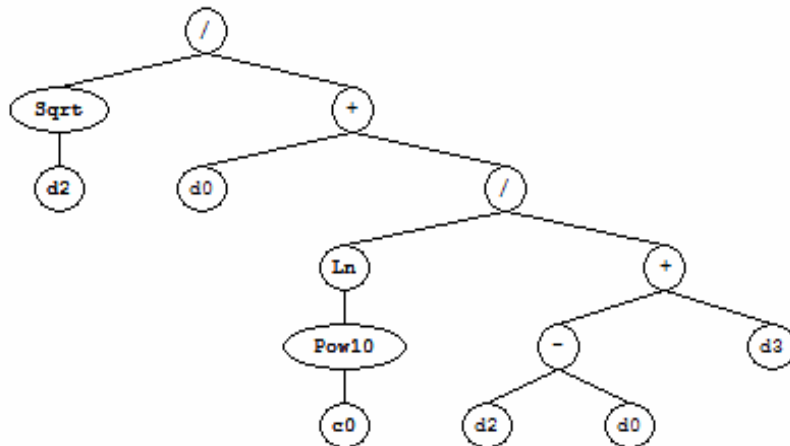
Figure 4.14 Expression tree (ET) for the proposed GEP formulation.
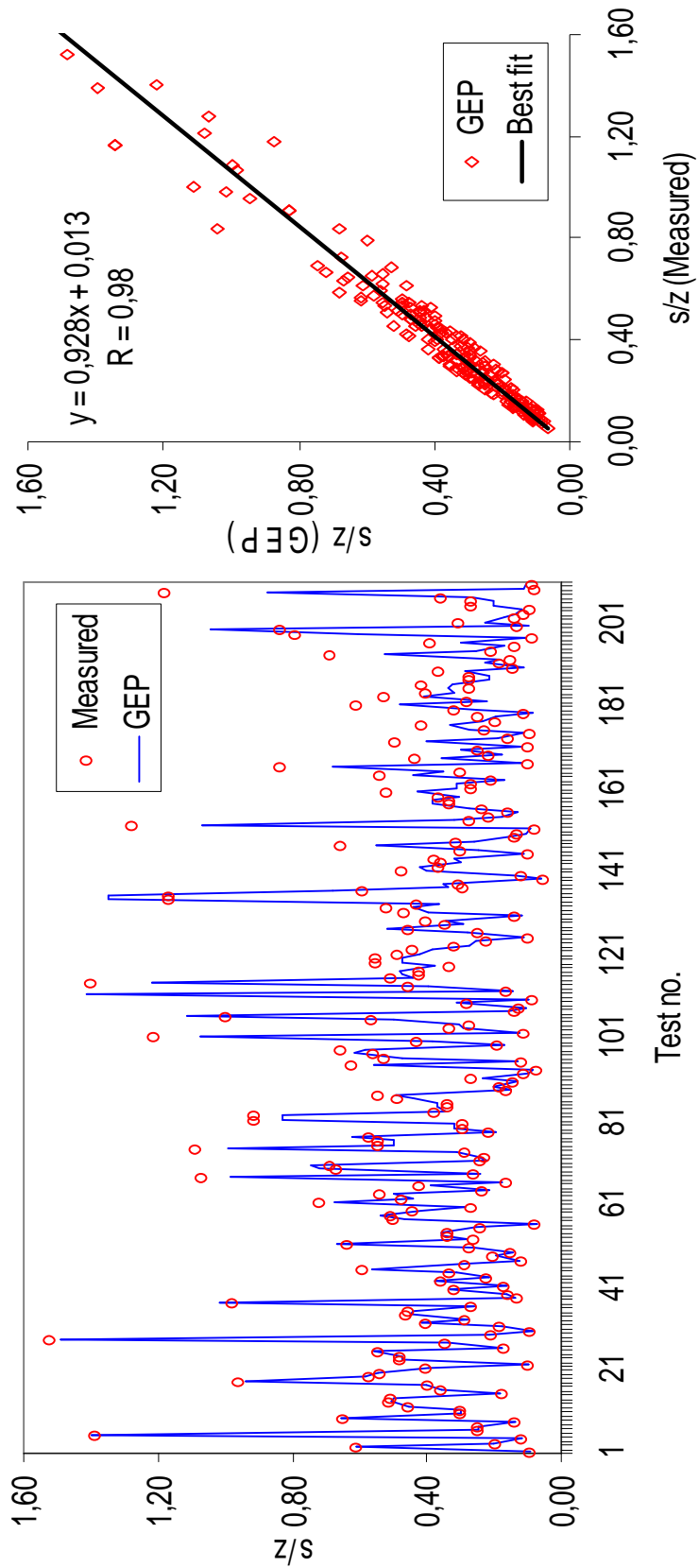
Figure 4.15 GEP estimations of *s/z* vs measured ones for train set

124
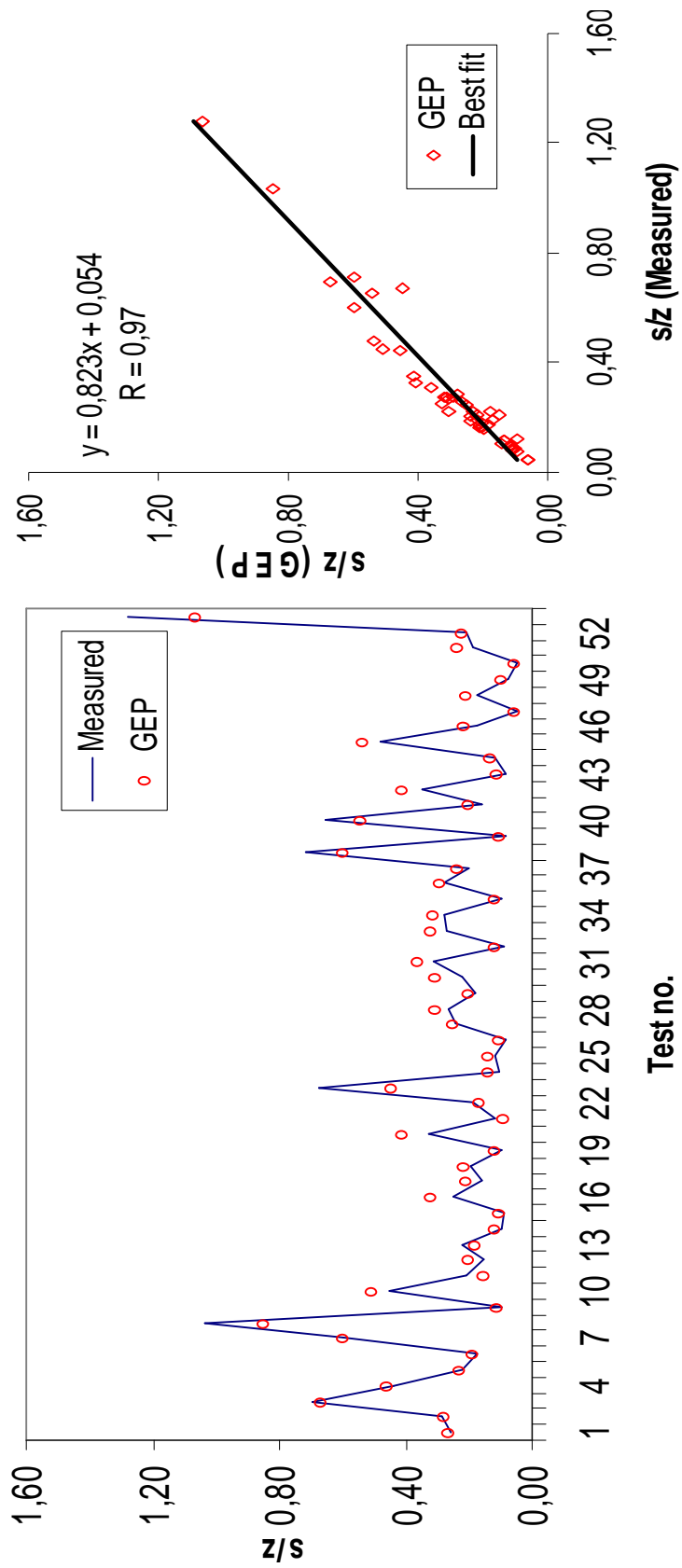
Figure 4.16 GEP estimations of *s/z* vs measured ones for test set.
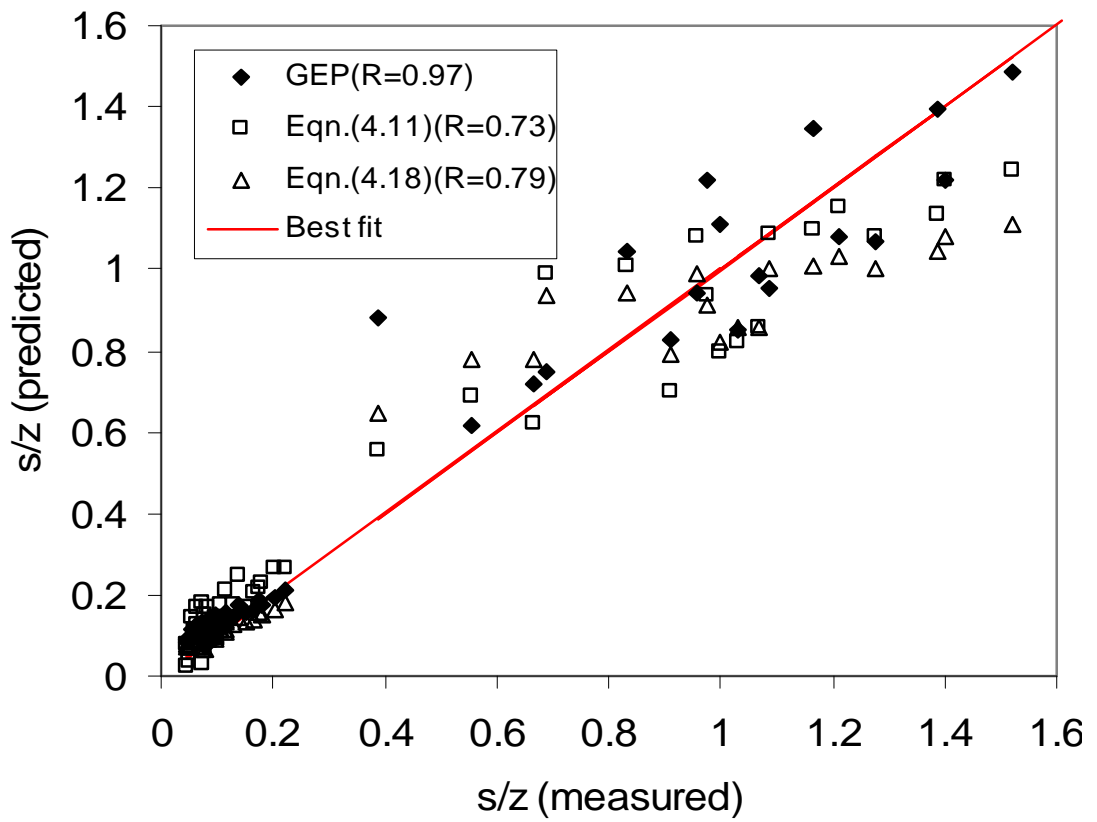
Figure 4.17 Comparison of estimations of proposed equations and measured ones
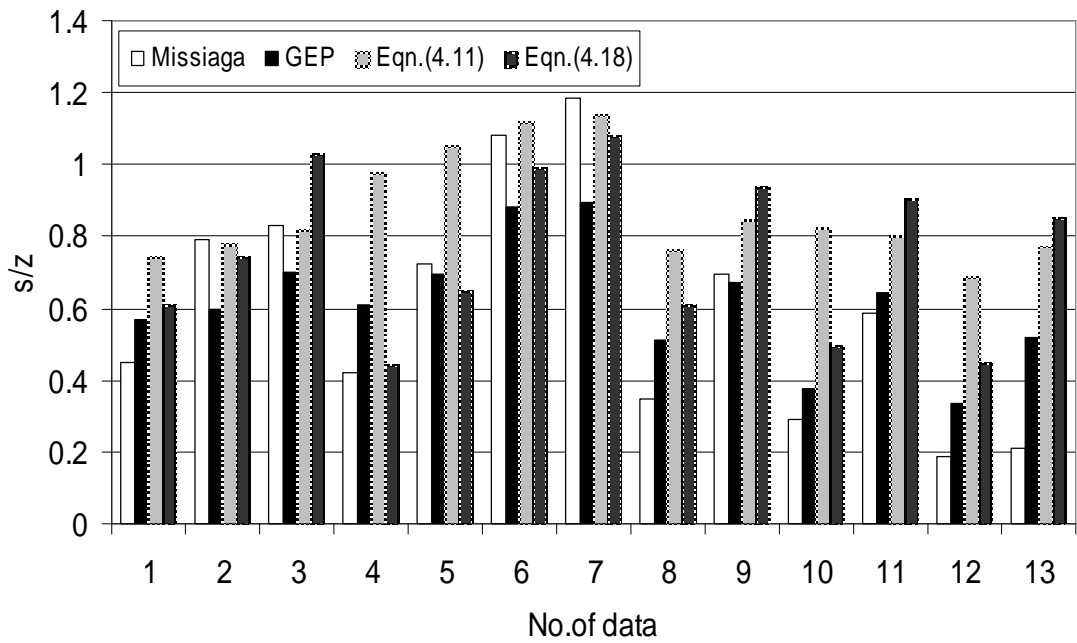
Figure 4.18 Comparison of estimations of proposed equations and field data

CHAPTER 5

RESULTS AND DISCUSSIONS

5.1 General

In this chapter, the performance of the proposed hybrid numerical-analytical model is evaluated based on experimental data taken from two Ph.D. studies, namely the first one carried out by Adduce (2004) on local scour downstream of a sill followed by a rigid apron, and the second one by Kurniawan (2003) on local scour downstream of a sluice gate. To the knowledge of the author, based on a detailed literature review, these two Ph.D. studies are the most relevant and the most up-to-date researches. The details on the experimental set-up and the measured data of these two researches are given in the next section.

Also, the predictions of the present hybrid model and those of FLUENT commercial software, which is the most widely used and well-established commercial software used in solving hydrodynamic problems, based on the experimental data of Ali and Lim (1986).

An alternative technique, Artificial Neural Networks, which is recently the most popular soft computing technique used in prediction of water engineering data (Guven et al. 2006, Azmatullah et al. 2005,2006, Dolling and Varas 2002) is presented and compared with the proposed hybrid model.

In this chapter, the main aim is to numerically investigate flow characteristics of a two-dimensional turbulent jet in scoured zone, such as the velocity components, surface profile, Reynolds stresses, bed shear stress and pressure distributions. The proposed hybrid numerical-analytical model is calibrated with the experimental conditions observed by Adduce (2004) and Kurniawan (2003) in

asymptotic states and the predictions of the model to the measured flow patterns are presented.

5.2 The Experimental Data Used in Evaluation of the Proposed Model

5.2.1 Local scour downstream of a sill followed by rigid apron (Adduce 2004)

Adduce carried out the experimental research at the Hydraulics Laboratory of the University of Rome, in a 17 m long flume with a rectangular cross-section of 1 m height and 0.8 m width. She conducted the local scour tests in a 0.3 m high and 0.8 m wide and 3 m long test section, positioned 7 m downstream of the flume inlet. This test section was created artificially by raising the flume bed. A mobile bed of uniformly graded sand of mean diameter d_{50}=0.72 mm, d_{90}=0.96 mm, density ρ_s=2650 kg/m^3 and a porosity p=0.44, was used in test section. In order to produce a bed of homogenous roughness, the same sand was glued both to the upstream and downstream fixed-bed sections. Clear water scour conditions were conducted by supplying no sediment into scour zone. A sill of height z=0.15m, followed by a rigid apron of length Lp=0.5 m was installed upstream of the test section. The downstream water depth was controlled using a control gate at the end of the flume. The water levels in the flume were measured with point gauge of accuracy=0.10mm was mounted on a carriage which moved along the flume. The water discharge at the inlet was measured with an electromagnetic flowmeter, and controlled by an inlet valve. Prior to running the experiments, the level of mobile bed was set to the same height as the fixed bed. In order to avoid undesirable scour of the sediment bed, the control gate was completely closed and the flume was slowly filled with water pumped from the laboratory water reservoir. The movement of the sand bed was prevented by increasing the water discharge slowly and setting to the desired experimental value.

The experiments started when the downstream water depth was set to the desired experimental value, by opening the control gate. The water discharge was kept constant for the entire duration of the experiment. The evolution of the scour hole was recorded by a CCD camera connected to a digital videocassette recorder. A detailed study of the temporal evolution of the scour hole was made possible by an image analysis technique (see Adduce, 2004). The experiments were stopped when

the measured maximum scour depth, plotted versus log time was sensibly constant. At the end of the experiment velocity measurements were performed by an ultrasonic doppler velocimeter (UDV, Signal-Processing DOP2000).

Adduce (2004) performed nine experiments, varying with different values of the water discharge, Q, water depth on the sill (h_s) and of the water depth downstream of the sill (y_t). The experimental conditions are given in Table 5.1. In Table 5.1, also the maximum scour depth values (S_{max}), the maximum scour length (L_s), inlet velocity entering the mobile bed section, U_1, and the test duration (T) for each test are reported.

Table 5.1 Experimental conditions (Adduce 2004)

Test	Q (m³/s)	U_1 (m/s)	h_s (m)	y_t (m)	S_{max} (m)	L_s (m)	T (min)
A1	0.0110	2.966	0.022	0.126	0.042	0.350	500
A2	0.0123	3.074	0.023	0.129	0.044	0.375	580
A3	0.0142	3.153	0.024	0.134	0.050	0.525	500
A4	0.0162	3.089	0.026	0.137	0.061	0.600	480
A5	0.0184	3.072	0.028	0.143	0.067	0.630	580
A6	0.0205	3.112	0.029	0.145	0.069	0.650	660
A7	0.0248	3.159	0.032	0.151	0.077	0.750	570
A8	0.0263	3.146	0.033	0.156	0.082	0.800	450
A9	0.0312	3.063	0.036	0.163	0.107	0.950	540

5.2.2 Local scour downstream of a sluice gate (Kurniawan 2003)

Kurniawan (2003) conducted the experiments using a 17 m long tilting flume with rectangular cross section of 0.8 m high and 0.5 m wide. The upstream and downstream ends of the flume bed was artificially raised in order to create a 0.35 m deep and 3.8 m long test section, beginning at a distance of 5.0 m from the inlet of

the flume. The test section was filled with a uniformly graded sand with a mean diameter of $d_{50} = 2$ mm. The same sand was glued on the downstream fixed-bed section. The slope of the flume bed was close to 0.

The jet issued from a vertical sluice gate, which was installed directly at the upstream end of the test section. A slightly submerged jet was created by setting the tail-water depth, y_t, controlled by a weir at the downstream end of the flume. A constant water discharge, Q, was pumped into the flume from the general basin of the laboratory.

Prior to the experiment, the test section was filled with sand and leveled to the same height as the fixed bed. The sluice-gate opening, y_1, was adjusted and the weir height was set to obtain the desired tail water depth, y_t. In order not to disturb the mobile bed, the flume was slowly filled until the water level touches the gate lip.

The experiment started, t = 0, when the pump discharge was increased rapidly to the predefined discharge, Q, which was maintained constant until the formation of the *asymptotic scour hole*. During this period the bed profile was measured at different intervals. The water depths at the upstream and downstream of the sluice gate were also measured. After the formation of the asymptotic scour hole, the discharge was gradually decreased to zero by taking care not to disturb the bed. The channel was slowly emptied and left to dry. The scoured bed was then fixed by spraying a special glue on the sand. This provided a rigid scour hole profile with the correct sand grain roughness. This asymptotic profile was measured using a point gauge installed on a carriage.

In order to measure the flow pattern in the scour hole, this same discharge, Q, was fed into the flume by keeping the sluice-gate opening and the tail-water depth as before. Using the point-gauge the water-surface elevations were checked to make sure that the flow conditions are the same. The vertical profiles of instantaneous velocity components were then measured at selected stations using an Acoustic Doppler Velocimeter (ADV). The general circulation pattern in the scour hole was visualized using dye injection and a rod with small flags. The hydraulic conditions of the experiments are given in Table 5.2.

Table 5.2 Experimental conditions (Kurniawan, 2003)

Test	Q (m^3/s)	U_1 (m/s)	h_1 (m)	y_t (m)	S_{max} (m)	L_{max}	T (min)
K1	0.015	0.875	0.050	0.121	0.225	1.000	5508
K2	0.015	0.846	0.050	0.222	0.168	0.625	7074
K3	0.015	0.843	0.050	0.222	0.131	0.566	5628
K4	0.015	1.213	0.050	0.222	0.230	0.823	4320
K5	0.015	0.620	0.050	0.222	0.122	0.491	4320
K6	0.015	0.874	0.050	0.222	0.151	0.519	4320
K7	0.015	0.879	0.080	0.222	0.199	0.822	4320
K8	0.015	1.032	0.025	0.222	0.107	0.343	4320

5.3 Development of the Hybrid Numerical-Analytical Model for Simulation of Local Scour and Flow Patterns in Scoured Zone

In this section, the proposed hybrid numerical-analytical model is run for the experimental conditions of Adduce (2004) in Table 5.1, and those of Kurniawan (2003) in Table 5.2 and the experimental condition given in Karim and Ali (2000), a total of 18 experimental tests. As given in further sections, some of these experimental conditions are used for simulation of the temporal evolution of scouring downstream of hydraulic structures (sill, sluice gate, rigid apron, etc) and the rest for simulation of the flow patterns in scoured zone in so-called asymptotic state. The predictions of the proposed hybrid model to the measured ones are tabulated and illustrated in figures, and also compared with predictions of other researches, well-established commercial software, and proposed artificial neural networks model.

5.3.1 Development of physical and computational solution domains

The actual grid mesh in physical domain and the computational domain are given in Figures 5.1-5.3, for test A2 by Adduce (2004), K1 by Kurniawan (2003) and experimental condition of Ali and Lim (1986), respectively. The absolute size of

cells within the grid is an important issue, since if the cells are too large the solution obtained can be dependent on the cell size rather than the physical conditions of the solution domain and input conditions (Kariam and Ali, 2000; Guven, 2003). For each experimental condition, the proposed hybrid model was run for different grid arrangements and a grid arrangement of 101x51 was used for the tests A1-A9 by Adduce (2004), 71x31 for the tests K1-K8 by Kurniawan (2003) and 71x21 for the experimental condition of Ali and Lim (1986), respectively. It can be easily observed from the figures that, although the shape of the physical domain varies for different physical conditions, the computational domain is always rectangular. Hence, it makes easy to discretize the governing equations (Eqns.(3.1)-(3.11)). Moreover, the boundary conditions (Eqns.(3.12)-(3.22)) are able to be applied much more easily without any interpolation on boundary cells as needed when the physical domain is used as the solution domain.

5.3.2 Convergence of the hybrid model

As explained in section **3.3.6**, the equations in the proposed system are solved by Tri-diagonal Matrix Algorithm (TDMA), which is a line iterative method, with alternating sweep directions. In TDMA, it is often desirable to speed up or slow down the changes of dependent variables from iteration to iteration, which is known as over-relaxation or under-relaxation. Because the Navier Stokes equations are non-linear, the process of convergence needs to be slowed down. In the present study, in order to avoid divergence, under relaxation factor ($0<\Omega<1$) with changeable values in each run of program was used for velocities and pressures, which are given in Table 5.3 for Adduce (2004), Kurniawan (2003) and Ali and Lim (1986).

The under relaxation factors are mainly problem dependent and have no influence on the converged solution. The convergence is monitored by the absolute residual sum for the continuity equation (Eqn. (3.9)) for the solution domain. The program stops when the residual sum is 0.0001 or the iteration number, ii, reaches a value pre-defined by the user. The decay of the global error versus the iteration number for different experimental conditions is shown in Figure 5.4. From the figure it can be

seen that, although some fluctuations occur in the trend of error, as a general view, the trend of the line decreases.

The analytical model part of the proposed hybrid model, which simulates the temporal evolution of the local scour, is run for the time given in experimental studies to be simulated.
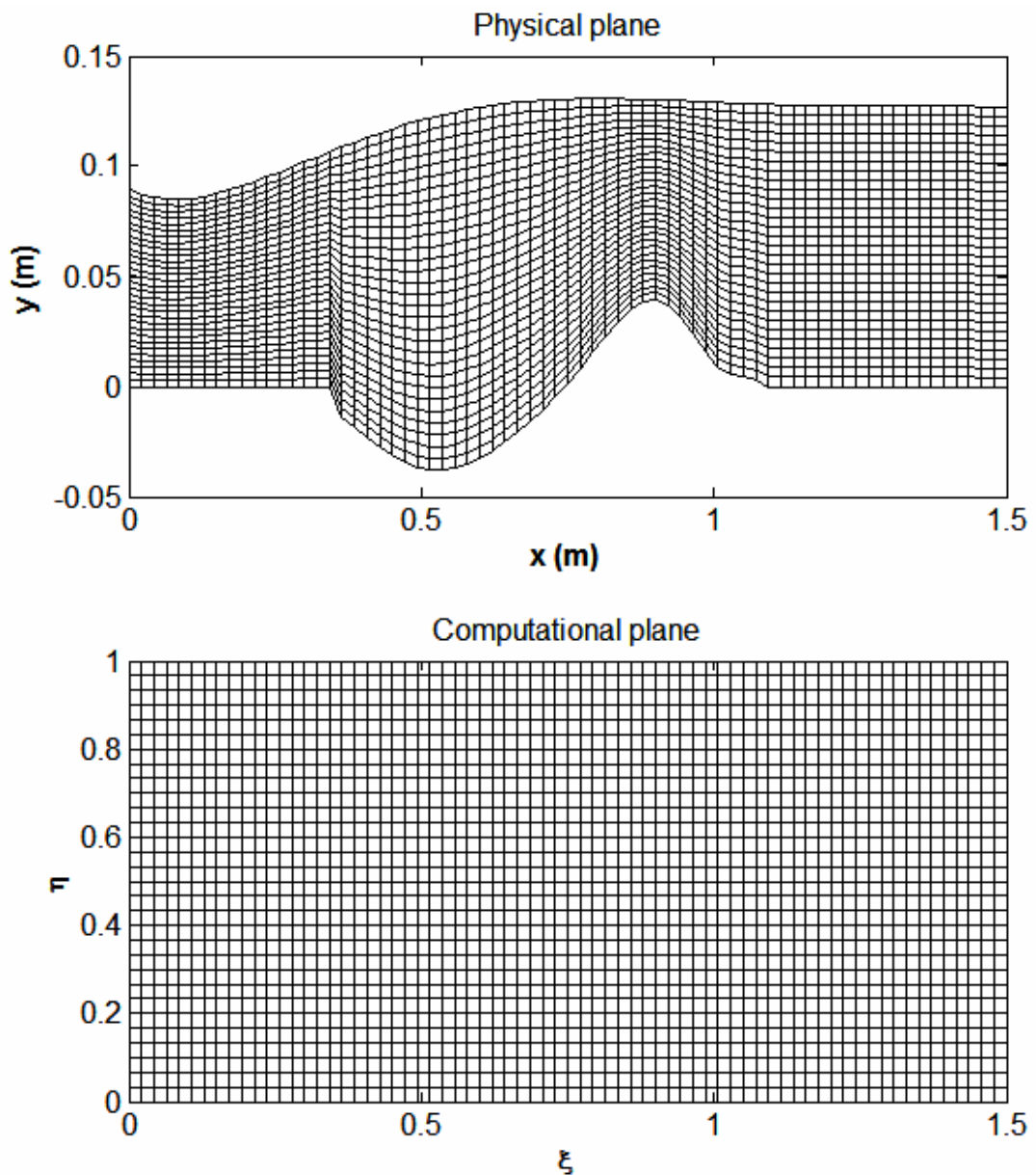
Figure 5.1 Grid transformation for test A2 by Adduce (2004)
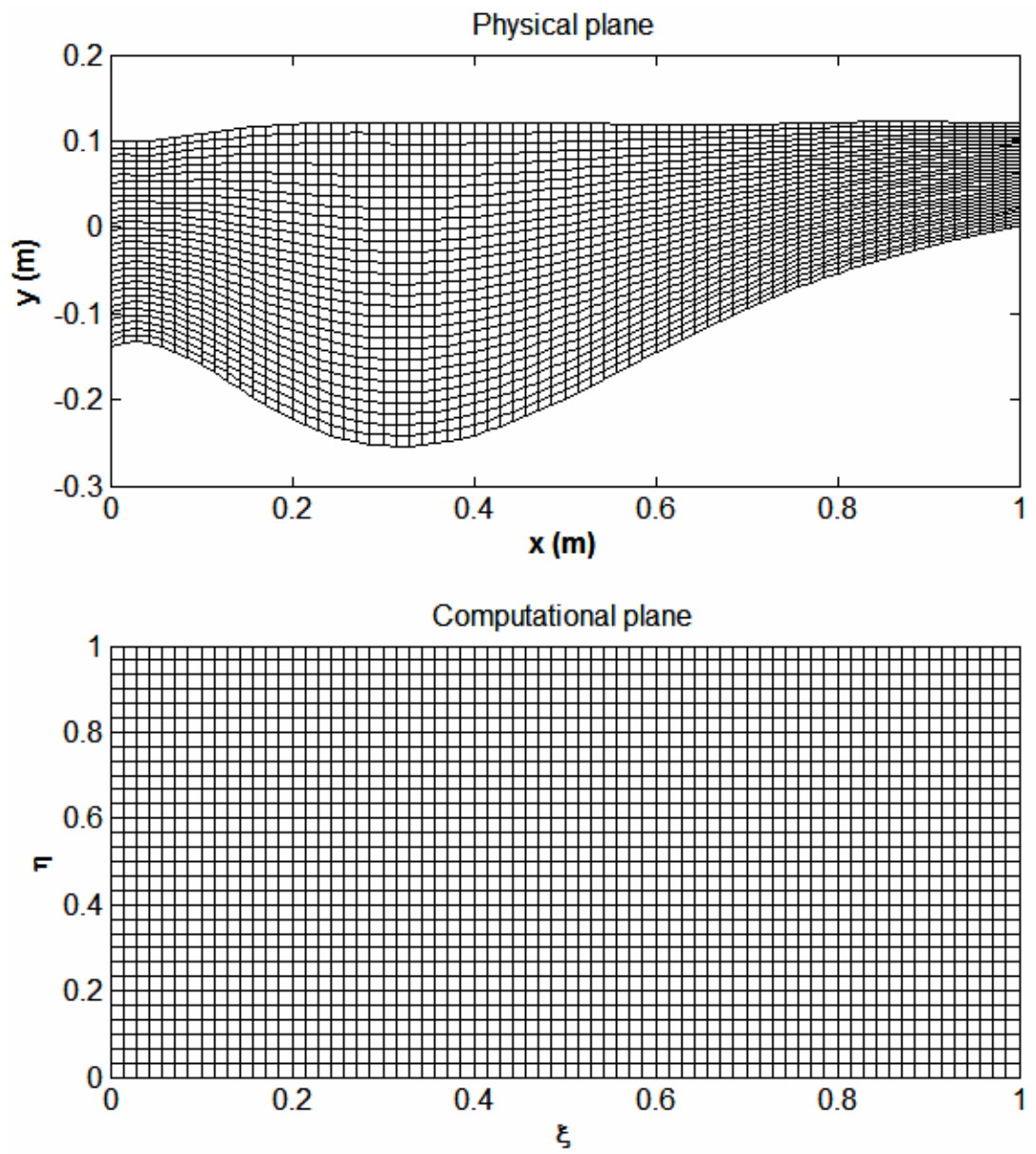
Figure 5.2 Grid transformation for test K1 by Kurrniawan (2003)
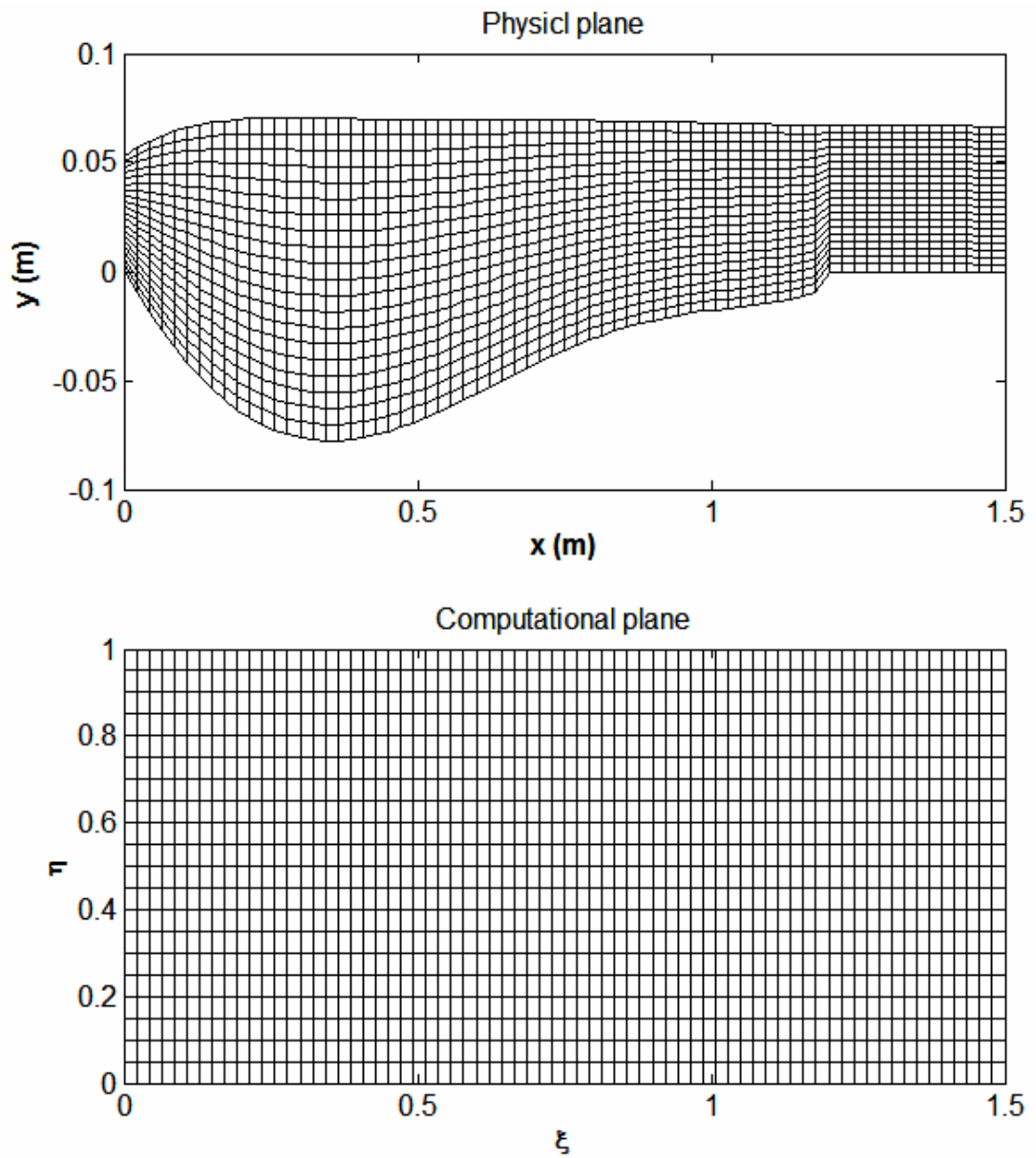
Figure 5.3 Grid transformation for test by Ali and Lim (1986)

Table 5.3 Under-relaxation factors for different experimental conditions

Experimantal study	Under-relaxation factor (Ω_i)						
	Ω_u	Ω_v	Ω_p	Ω_s	Ω_h	Ω_d	Ω_k
Adduce (2004)	0.3	0.3	0.2	0.2	0.2	0.1	0.1
Kurniawan (2003)	0.2	0.2	0.1	0.1	0.1	0.1	0.1
Ali and Lim (1986)	0.5	0.5	0.3	0.3	0.3	0.2	0.2
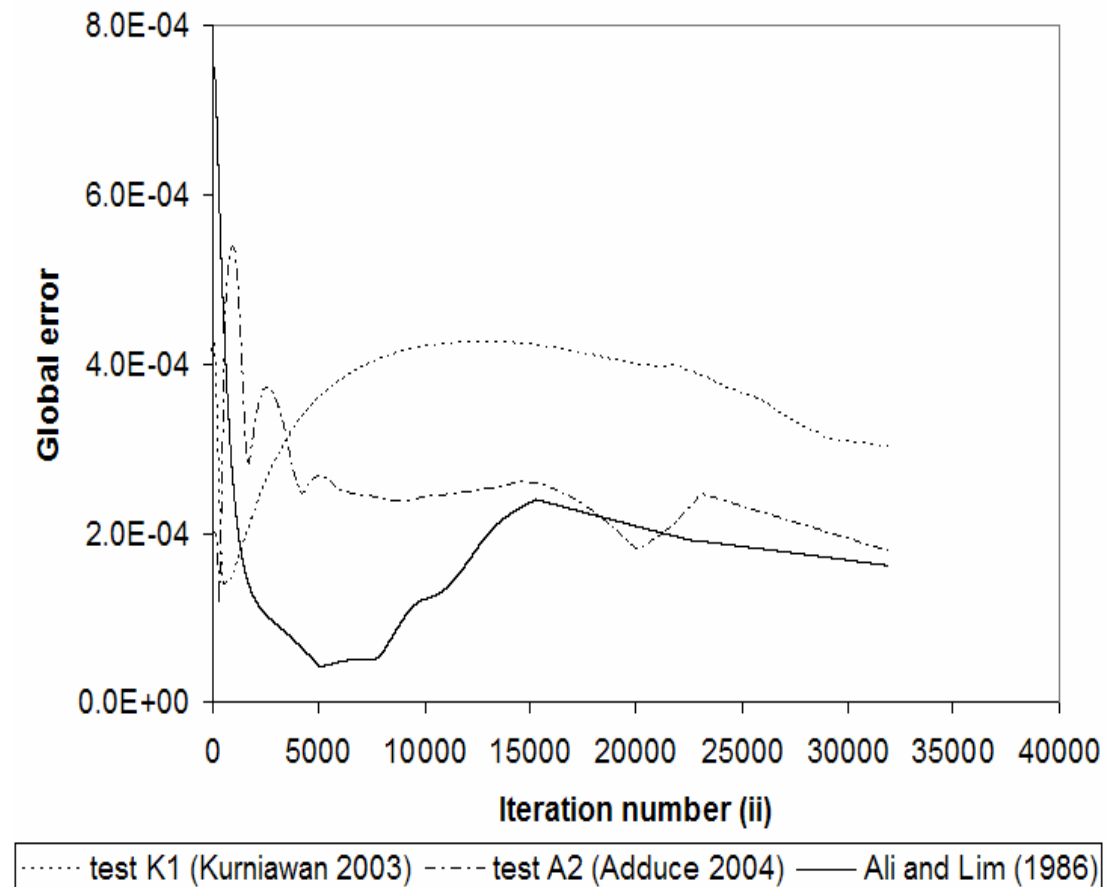
Figure 5.4 Decay of global error of present hybrid model

5.4   Prediction of Instantaneous Scour Profiles

In this section, the time evolution of scour profiles for three experimental runs carried out by Adduce (2004), namely the tests A2, A4 and A8, are simulated by the proposed hybrid model. For the tests A2 and A4 the predictions for eight time increments, t= 10, 50, 100, 200, 300, 400, 500 and 600 are presented (see Figures 5.5-5.6), and for the test A8 the evolution of scour profile for seven time increments, t=10, 50, 100, 200, 300, 400, 500 are presented (see Figure 5.7). As a general view in Figures 5.5-5.7, the geometry of the scour hole increases with increasing flow rates. As Adduce (2004) also admits, for small flow rates, a small dune with sharp crest follows the scour hole, and by increasing the flow rate, the dune becomes flatter and longer.

Figures 5.8-5.10 show the proposed model's predictions to the measured scour profiles by Adduce (2004) for asymptotic states for the tests A2, A4, and A8 respectively. From the figures, it is clear that there is perfect agreement between the predicted and the experimental scour profiles, especially in scoured zone. But the numerical predictions of dune section are observed to be longer than the measured ones for small flow rates (tests A2-A4) (see Figures 5.8 and 5.9), and for high discharges (A8), only very small discrepancies are observed between the predicted and the measured ones (see Figure 5.10). It can be concluded that when the flow rate increases, the numerical predictions of dune section get better, compared to the measured ones and the numerical predictions of the dune section for small discharges are always longer that the measured ones. This event was also observed by Adduce (2004) and it can be explained by the fact that the predicted scour profiles are two-dimensional, although the experimentally observed ones are quasi-two-dimensional when the flow rates are large (test A8), but no more quasi-two-dimensional for small flow rates (tests A2-A4) (Adduce 2004, 2006).

Figures 5.11 and 5.12 show the predicted scour profiles of present model and the numerical model proposed by Adduce (2004) compared with the measured asymptotic scour profiles of the tests A4, and A8. As explained in previous sections, our proposed numerical model calculates the non-conservative form of the equation for temporarily scour profile (Equation (3.72)) while the model by Adduce (2004) calculates the Eqn. (3.71), which is the conservative form of the Equation (3.72). By

this, we expect to achieve more realistic and accurate predictions. From both figures, it is obvious that we achieved our goal, because the predictions of our model are closer to the measured ones, compared to those of the model by Adduce (2004). Especially the proposed model's predictions to the measured dune section are quite better than those of Adduce (2004) for small discharge (A4). As a general view from the Figures 5.11 and 5.12, the proposed model predicted the measured scour profile with higher accuracy (R^2=0.964) and lower error (MSE=0.0001) when compared to the analytical model by Adduce (2004) (R^2=0.924, MSE=0.0020). Especially, the proposed model predicted the dune section much better than the model by Adduce (2004).

5.5 Prediction of Depth and Length of Maximum Scour at Asymptotic State

The shape of scour profile at asymptotic state is concave as stated by Rajaratnam (1981a) and Kurniawan (2003) (see Figures 5.11 and 5.12). This concave shape can be roughly predicted by second-degree polynomial relation:

$$S_l = ax^2 + bx + c \qquad (5.1)$$

where *a, b* and c can be calculated by regression analysis on experimental scour profile data. The higher the degree of the polynomial function, the more accurate predictions we get.

Prediction of depth and length of maximum scour has been subject to numerous researches in the literature carried out a state-of art review on studies of prediction of local scour parameters (Ali and Lim 1986, Chatterjee and Ghosh. 1980; Bormann and Julien, 1989; Chatterjee et al., 1994; D'Agostino, 1994; Mossa, 1998; D'Agostino and Ferro, 2004; Sarkar and Dey, 2005a.; Sarkar and Dey, 2005b).

In this section, the proposed hybrid model's predictions of the maximum scour depth, S_{max}, and the length of the scour, L_s, at asymptotic state are compared with measured ones by Kurniawan (2003) and the predictions of other researches. All the researches that will be compared assume that the asymptotic state of the scour profile is reached.

Eggenberger and Mueller (1994) studied on the scouring process due to a submerged horizontal jet, issuing from a sluice gate followed by a rigid apron of length varying between 0.025 and 0.145 m. They proposed following functional relationships for S_{max} and L_s:

$$S_{max} = w_e \frac{\Delta h^{0.5} q^{0.6}}{d_{90}^{0.4}} - y_t \tag{5.2}$$

and

$$L_s = f_e (s + y_t) \tag{5.3}$$

where w_e=10.35 and f_e=6. They carried out a series of experiments, which cover unit discharge, q, in the range $3.95 \cdot 10^{-3} - 25.53 \cdot 10^{-3} \, \text{m}^3/\text{s.m}$, particle size, d_{50}, in the range 0.43-3.67 mm, head difference, Δh, in the range 5.64-14.40 cm.

Rajaratnam (1981a) investigated the scouring by submerged plane jet without a rigid apron. They carried out experiments, covering a velocity range, $0.866 < U_1$ (m/s)< 2.217, a gate opening range, $0.36 < y_1$ (cm)< 2.49, and sediment sizes d_{50}=1.20 and 2.38 mm. They proposed a functional relationship for the maximum scour depth normalized by the gate opening (s/y_1) as:

$$\frac{S_{max}}{y_1} = 4.3 (F_{rd} - 4.0) \tag{5.4}$$

Ali and Lim (1986) studied on local scour beneath 2- and 3-dimensional horizontal jets in the literature, in detail, and presented following equation:

$$\frac{S_{max}}{R_j} = 2.30 \left(\frac{U_1}{w_s} \right)^{0.5} \left(\frac{d_{50}}{R_j} \right)^{0.375} F_{rd}^{0.75} - 1.19 \tag{5.5}$$

where Rj is the area of the jet divided by it perimeter. They used d_{50}=0.82 mm for non-cohesive bed material and a settling velocity, w_s=0.11 m/s. The plane jet had the dimension of 5.1 cm×60.7 cm and the discharge, Q ranged between 0.01 and 0.017 m^3/s.

Chatterjee and his co-workers investigated the local scour beneath a submerged jet, issuing from a sluice gate followed by a rigid apron 0.66 m long (Chatterjee et al. 1994). They studied a velocity range of 0.840<U1 (m/s)<2.016, a gate opeing range of 0.02<y1 (m)<0.05, a unit discharge range of 0.0159<q (m3/s/m)<0.0342, and a particle size of d_{50}=0.76 mm. Their analysis on the measured data revealed that there is no relationship between the maximum scour depth and the grain size. They issued following relationship:

$$\frac{S_{max}}{y_1} = 0.775F_1 \tag{5.6}$$

where F_1 is the Forude number at the sluice gate, $F_1 = U_1 / \sqrt{gy_1}$.

The proposed hybrid model is compared with the above-mentioned empirical formulations (Eqns (5.2)-(5.6)), based on the experimental data measured by Kurniawan (2003), given in Table 5.2. The results of the comparison are tabulated in Table 5.4. It can be said that the proposed hybrid model predicted S_{max} and L_s quite well compared to measured ones. As a general view, the proposed hybrid model predicted lower values for measured S_{max} values, while higher values for L_s. This event can be explained by under-prediction of hybrid model in free jet zone (XS<x<L_s) as explained in Chapter 3.

It is obvious that Eggenberger and Mueller (1944) generally predicts lower values than the measured ones and gave generally negative values, which are physically non-observable. (Eqn.(5.2)). Kurniawan (2003) offered a twice higher value for the proposed w_e value. The predictions of Chatterjee et al. (1994) are also observed to be under the measured data (Eqn.(5.6)). Eqn. (5.4) by Rajaratnam (1981a) gave relatively good results, except for the maxima and the minima. Ali and Lim (1986) also gave reasonable results. As a general view the proposed hybrid model performed quite better compared to other empirical models.

5.6   Prediction of Free Surface Profiles

Figure 5.13 shows the proposed model's predictions of free surface profile to the experimental ones measured by Adduce (2004) for tests A1, A4 and A7, at asymptotic stages. Over the rigid apron (-0.5<x<0) a gradually variations are observed in both measured and the predicted surface profiles, and at the end of the apron, the surface profiles start to jump until a peak in the region of 0<x<0.5. Downstream of this region (x>0.5 m), the flow decreases steadily and then the rate of variation is observed to approach zero. As a general view form the figure, it can be said that the proposed hybrid model predicted the measured free surface profiles with quite good agreement.
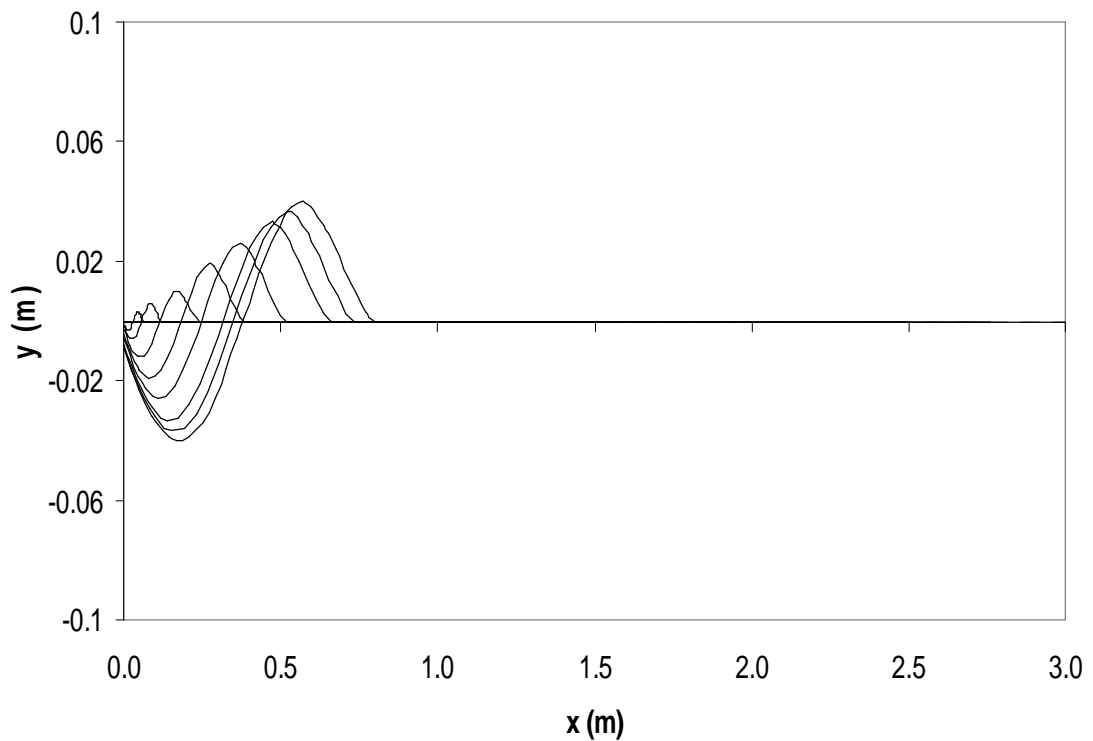
Figure 5.5 Predicted temporal evolution of local scour for test A2
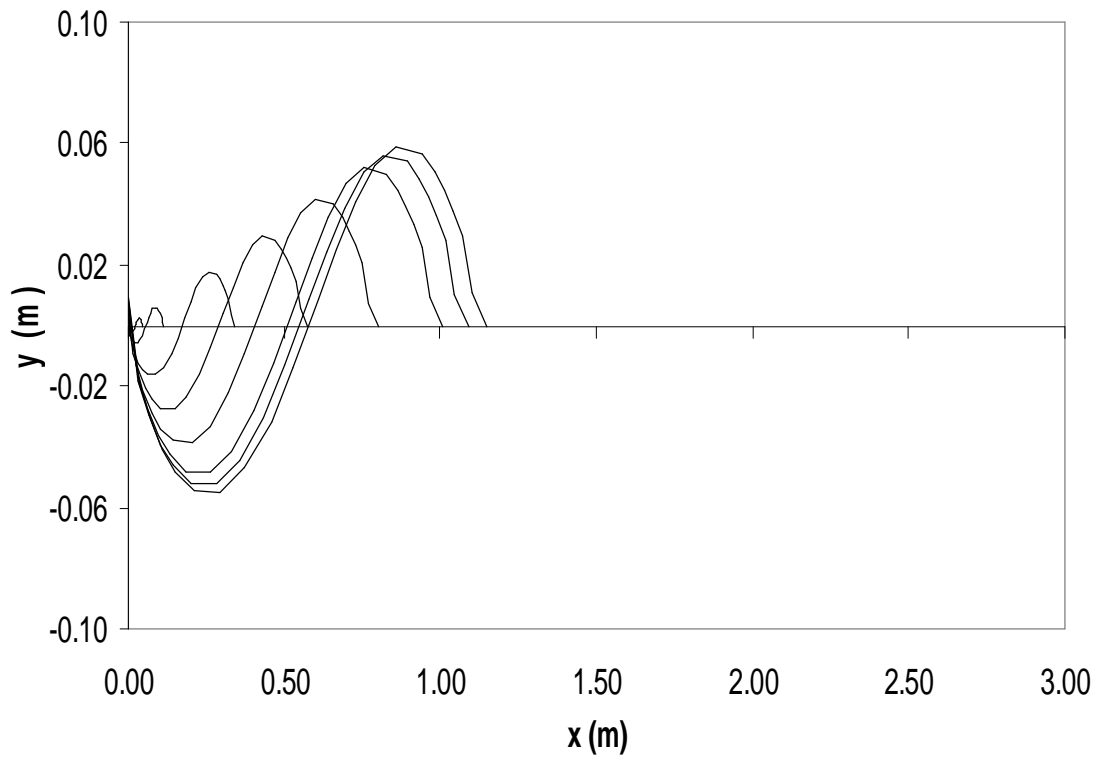
Figure 5.6 Predicted temporal evolution of local scour for test A4
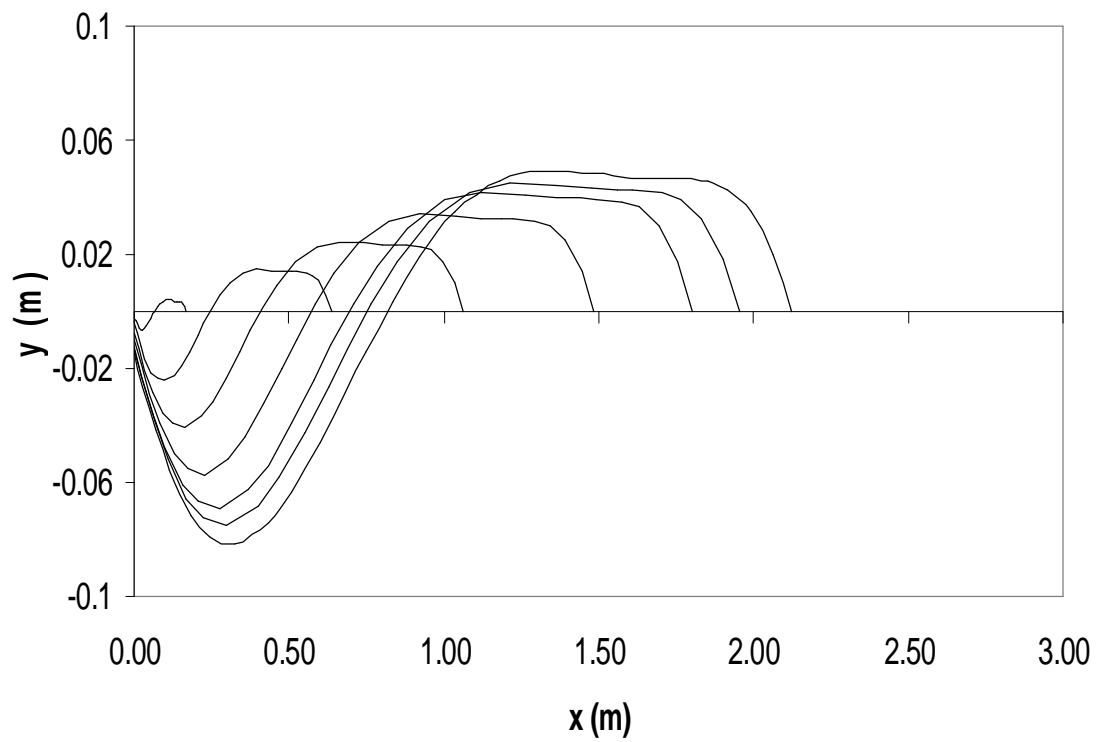
Figure 5.7 Predicted temporal evolution of local scour for test A8

142

Figure 5.8 Predicted scour profile vs. measured one for test A2

Figure 5.9 Predicted scour profile vs. measured one for test A4
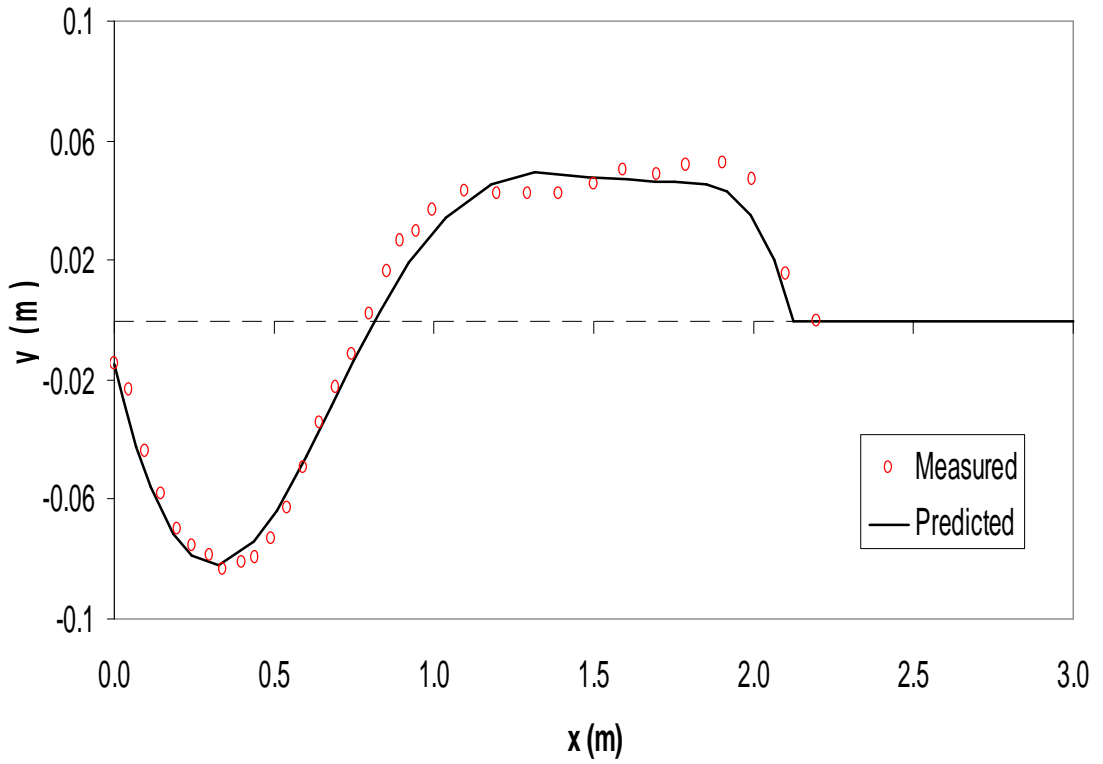
Figure 5.10 Predicted scour profile vs. measured one for test A8
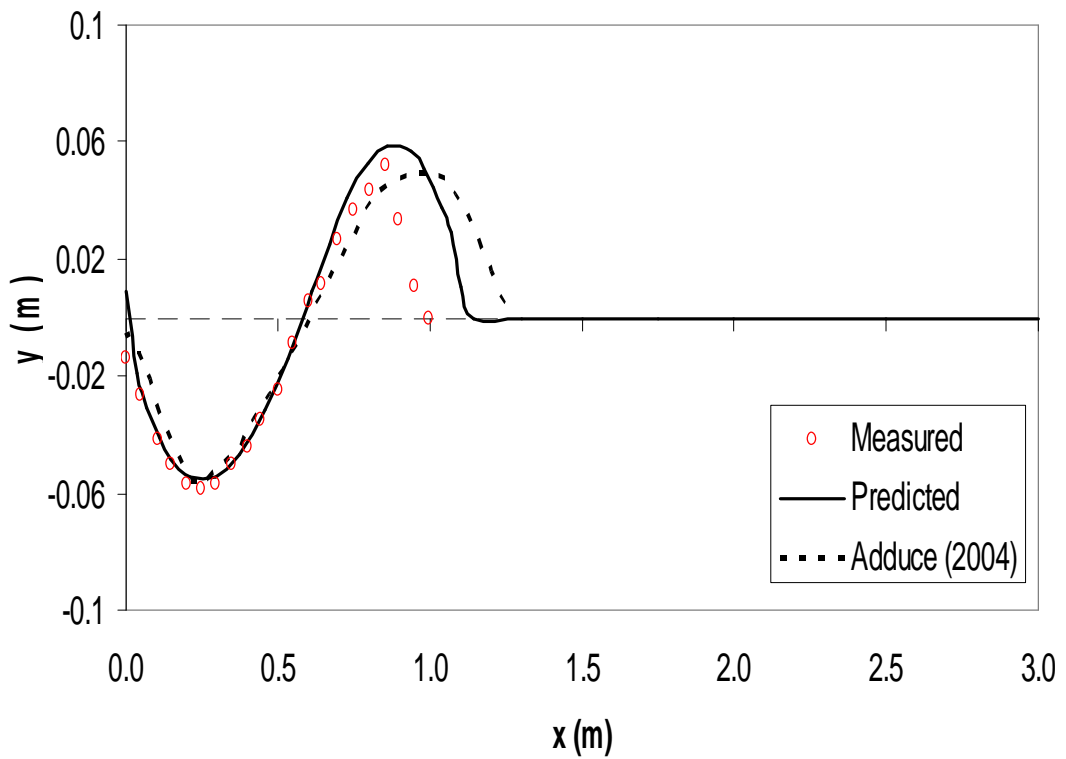
Figure 5.11 Comparison of predicted and scour profiles for test A4
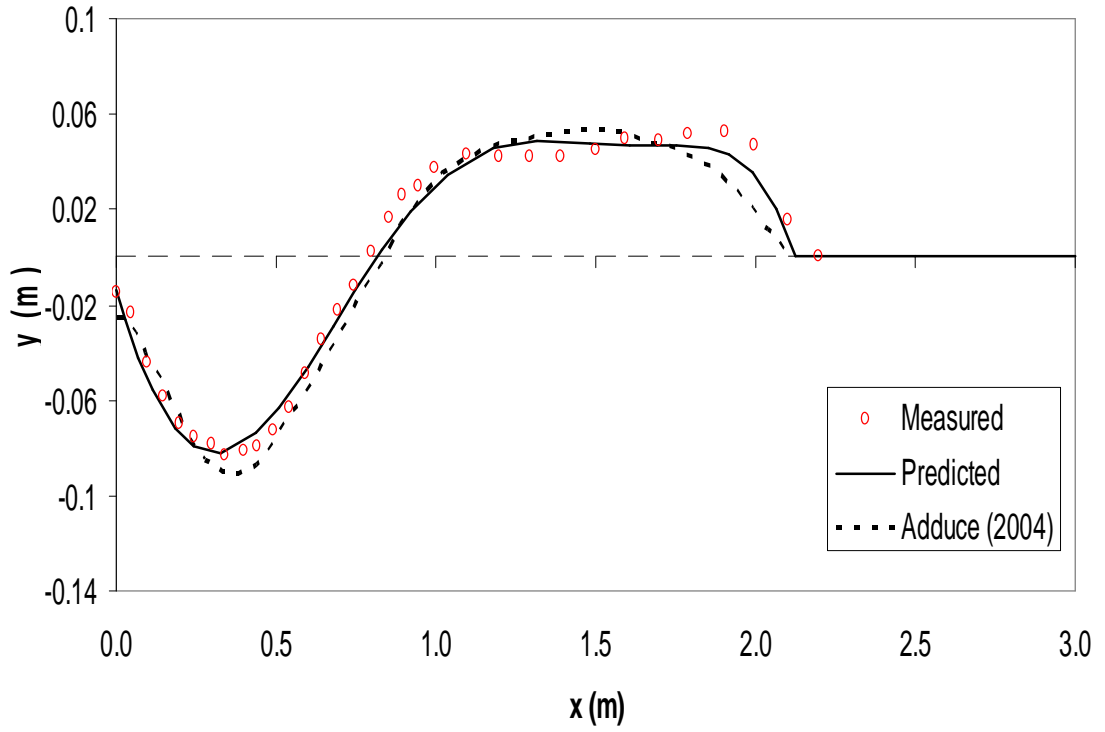
Figure 5.12 Comparison of predicted and scour profiles for test A8
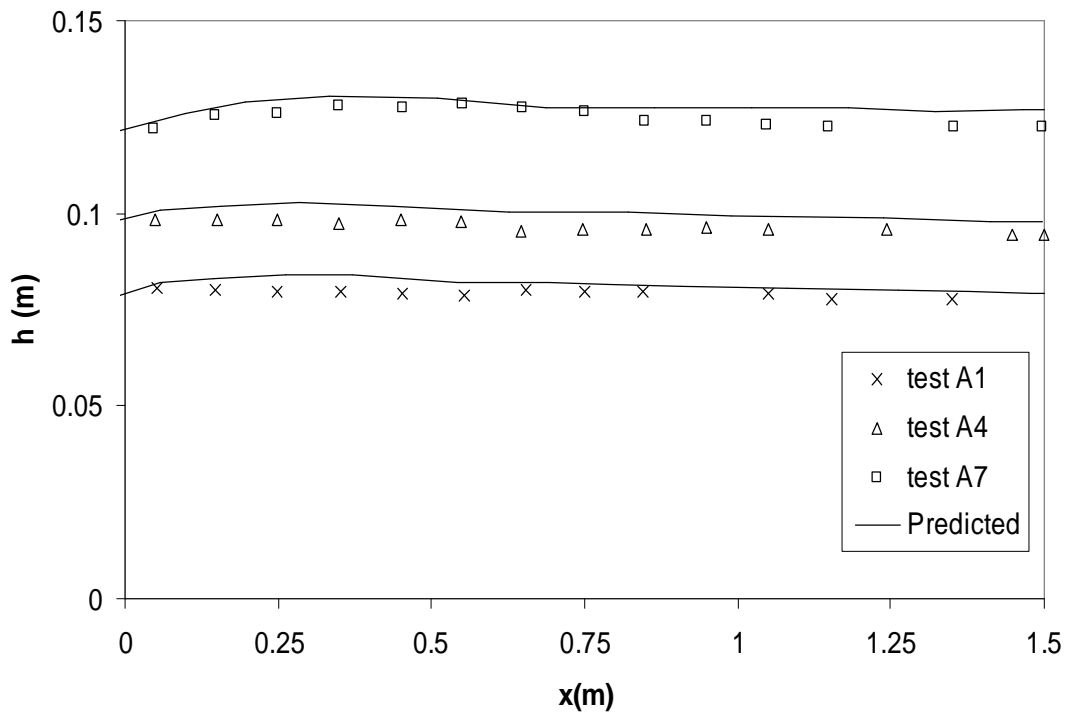
Figure 5.13 Predicted free surface profiles vs. measured ones

145

Table 5.4 Comparison of S_{max} and L_s predictions with measured data

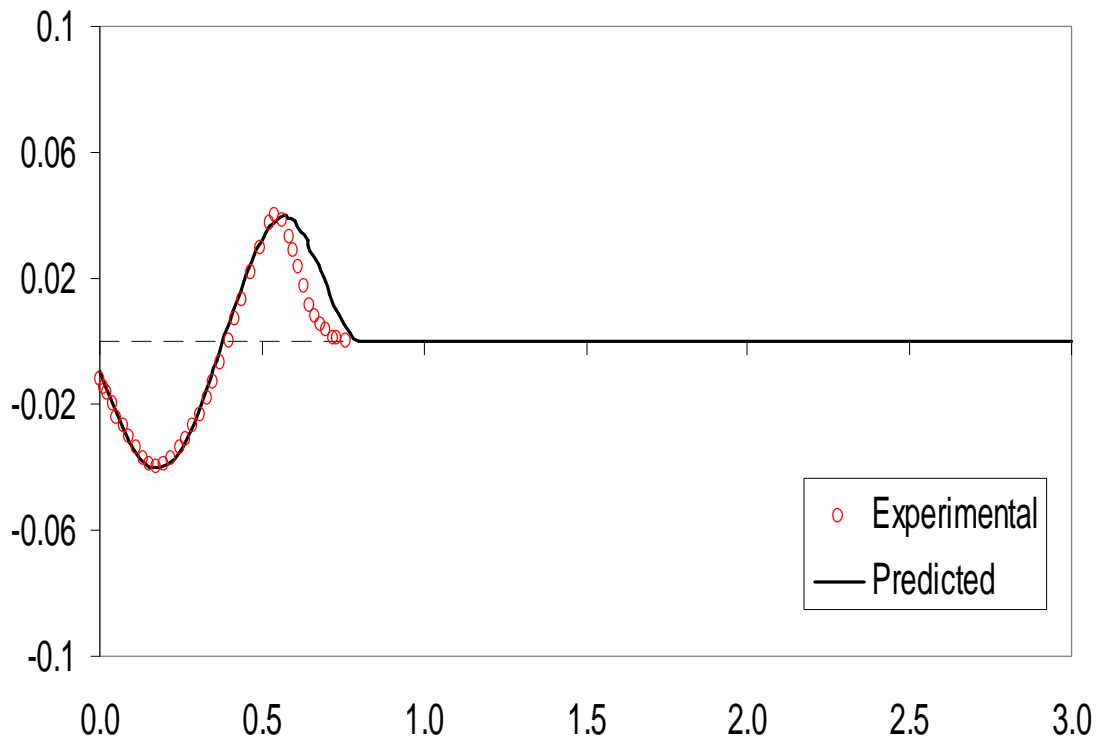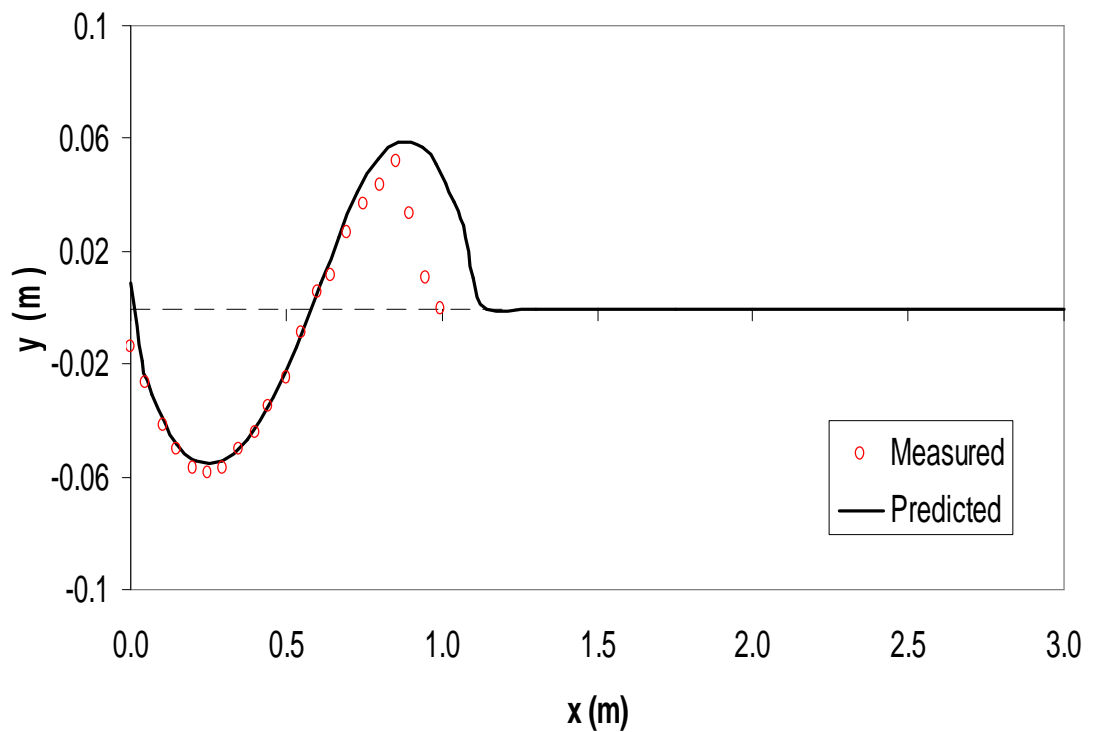| Test	Measured (Kurniawan, 2003)		Present Hybrid Model		Chatterjee et al. (2004)		Ali and Lim (1986)		Rajaratnam (1981a)		Eggenberger and Muelller (1944)	
	S_{max}	L_s	S_{max}	L_s	S_{max}	L_s	S_{max}	L_s	S_{max}	L_s	S_{max}	L_s
K1	0.255	1.00	0.263	0.952	0.048		0.117		0.186		0.064	1.112
K2	0.168	0.625	0.177	0.598	0.047		0.11		0.151		-0.041	1.076
K3	0.131	0.566	0.139	0.547	0.047		0.110		0.147		-0.041	1.071
K4	0.230	0.823	0.241	0.801	0.067		0.189		0.589		0.094	1.887
K5	0.120	0.491	0.127	0.469	0.034	NA	0.067	NA	-0.119	NA	-0.111	0.654
K6	0.151	0.519	0.160	0.501	0.048		0.117		0.185		-0.031	1.134
K7	0.199	0.822	0.208	0.796	0.062		0.147		0.306		0.030	1.500
K8	0.107	0.343	0.113	0.327	0.040		0.104		0.187		-0.059	0.966

5.7   Prediciton of Dimensionless Velocity Profiles

Figure 5.14 shows the definition sketch for typical velocity profile for a wall and a free jet. Following Adduce (2004), for the wall jet, the maximum mean velocity, U_m is used as velocity scale, and the distance, δ, from the plane of U_m to the plane of $U_m/2$, where $\partial u / \partial y < 0$, is used as length scale. (For the free jet, U_m is used as velocity scale, and δ_1, the distance from the plane of u_m to the plane of $U_m/2$, provided $\partial u / \partial y < 0$ is used as positive length scale; and δ_2, the distance from the plane of u_m to the plane of $U_m/2$, provided $\partial u / \partial y > 0$ is used as negative length scale (see Figure 5.14).

Figures 5.15, 5.16 an 5.17 show the proposed hybrid model's predictions to the measured dimensionless velocity profiles for tests A2, A4 and A8, for $XS<x<L_s$, carried out by Adduce (2004), respectively, and the theoretical curve of a wall jet proposed by Rajaratnam (1976). The velocities are made non-dimensional by u_m and the y-axis is made non-dimensional by δ, as described in previous paragraph and illustrated in Figure 5.14. Generally, almost perfect agreement is observed between the predicted and the measured dimensionless velocity profiles for 0.2 <y/δ<1.0 and fairly good one for 1< y/δ< 2. And also, the predicted and the measured dimensionless velocity profiles for 0.2 <y/δ<1.0 are observed to be over the theoretical curve, whereas they are totally below the theoretical curve for 1< y/δ< 2. The reason for the small discrepancies for 1< y/δ< 2 can be explained by under-predictions of the standard k-ε turbulence model especially in reverse flow regions. Both the predicted and the measured dimensionless velocity profiles can generally be said to be similar to the theoretical wall jet.

5.8   Prediction of Velocity Distribution in Scoured Zone

Adduce (2004) measured the velocity field in asymptotic scoured zones by Ultrasonic Doppler Velocity Profiler, and the bed profile and the free surface profiles by a point gauge in the centerline of the flume. In this section the experimental velocity profiles (u, v) for run A2 and A5, measured by Adduce (2004) are compared with the numerical predictions of the proposed model. Figures 5.18-5.21 show the

predicted velocity vector field for the tests A2, A4, A5 and A8 by Adduce (2004). Although it is not clearly visible, the formation of vortex in maximum scour depth, together with reverse flow in maximum scour depth region and near free surface profile for 0<x<0.3 m were observed in the four figures. The u-velocity values are observed to be relatively higher in upstream region and gradually decrease towards the dune sections. Also in dune sections, it can be observed that the flows are fully developed, and uniform.

Figures 5.22-5.25 show the present model's predictions of velocity distribution and the measured ones by Adduce (2004). The dots (○) represent the measured velocity, triangles (Δ) represent the measured surface profiles and the solid lines (─) represent the predictions of present model to the measured ones. From Figures 5.22-5.25 it is obvious that the horizontal component (u) of flow velocity is higher the vertical one (v) throughout the whole scour profile. In Figures 5.22 and 5.24, for the tests A2 and A5, it can be observed that the maximum velocity increases from the maximum scour depth region to the crest of dune, while it decreases beyond the crest of the dune. As general view, it can be concluded that the flow from the maximum scour depth to end of the dune can be modeled by plane wall jet analogy (Glauert, 1956; Schwartz and Cosart, 1961; Rajaratnam, 1976; Adduce, 2004).

As it is seen in Figures 5.22 and 5.24, for $0 \leq x \leq XS$, where XS=0.174 for run A2 and XS=0,285 for run A5, the jet behaves like a free jet, the erosive action of which is very weak compared to the wall jet (Adduce, 2004,2006; Balachandar and Kells, 1997; Kurniawan, 2001,2003). Beyond this zone to the end of dune section, the flow becomes a wall jet that erodes more aggressively and deepends the scour area faster. Figures 5.22-5.25 prove that the numerical predictions of the proposed model are in good agreement with the above findings by the experimental data measured by Adduce (2004). The weak effect of the free jet at the inlet of the scour hole is simulated based on a Gaussian-like relation as explained in Chapter 3.

5.9   Prediction of Distribution of Reynolds Stresses

The Reynolds stresses, $-\overline{u'^2}$ and $-\overline{v'^2}$ can be calculated from the measured u (x,y,t) and (x,y,t) data using Boussinesq relation (Eqn. (3.3)-(3.4). Figures 5.26-5.29 show the predictions of the present hybrid model to the spatial distribution of the Reynolds stresses, for the tests A2 and A5 measured by Micro ADV at the flume centerline by Adduce (2004 The dots ($\circ$) represent the measured velocity, triangles (Δ) represent the measured surface profiles and the solid lines ($-$) reprersent the predictions of present model to the measured ones. The Reynolds stresses are made non-dimensional by velocity scale U_0 (defined in Eqn.(5.7)) and by the length scale y_0 in horizontal plane (see Figure 3.8).

$$U_0 = \frac{Q}{b \times y_0} \qquad (5.7)$$

As a general view, the numerical predictions compare well with the measured data. From the figures, both the numerical predictions and the measured data prove that the turbulent flow is non-isotropic since $\sqrt{\overline{u'^2}}$ values are generally greater than $\sqrt{\overline{v'^2}}$ for the whole spatial distribution, ($\sqrt{\overline{u'^2}}$ =1.6 $\sqrt{\overline{v'^2}}$), which is also observed by Adduce (2004) and Liriano et al. (2002) and Gunal and Guven (2006). Liriano et al. (2002) observed that $\sqrt{\overline{u'^2}}$ =1.6 $\sqrt{\overline{v'^2}}$, where Gunal and Guven (2006)'s predictions revealed that $\sqrt{\overline{u'^2}}$ =1.69 $\sqrt{\overline{v'^2}}$, and Adduce (2004)'s measurements gave out that $\sqrt{\overline{u'^2}} = 1.65 \sqrt{\overline{v'^2}}$.

As a general view from Figures 5.26 and 5.28, as y increases, $\sqrt{\overline{u'^2}}$ increases till a maximum value, approximately at the point where the u-velocity distribution has also its maxima (see Figures 5.22 and 5.24), and then slightly decreases through the free surface. In the section between the maximum scour depth to the crest of dune, the $\sqrt{\overline{u'^2}}$ distribution shows a uniform profile. As explained in the previous paragraph, the $\sqrt{\overline{v'^2}}$ distribution in the whole scoured zone section showed smaller values than those of $\sqrt{\overline{u'^2}}$.
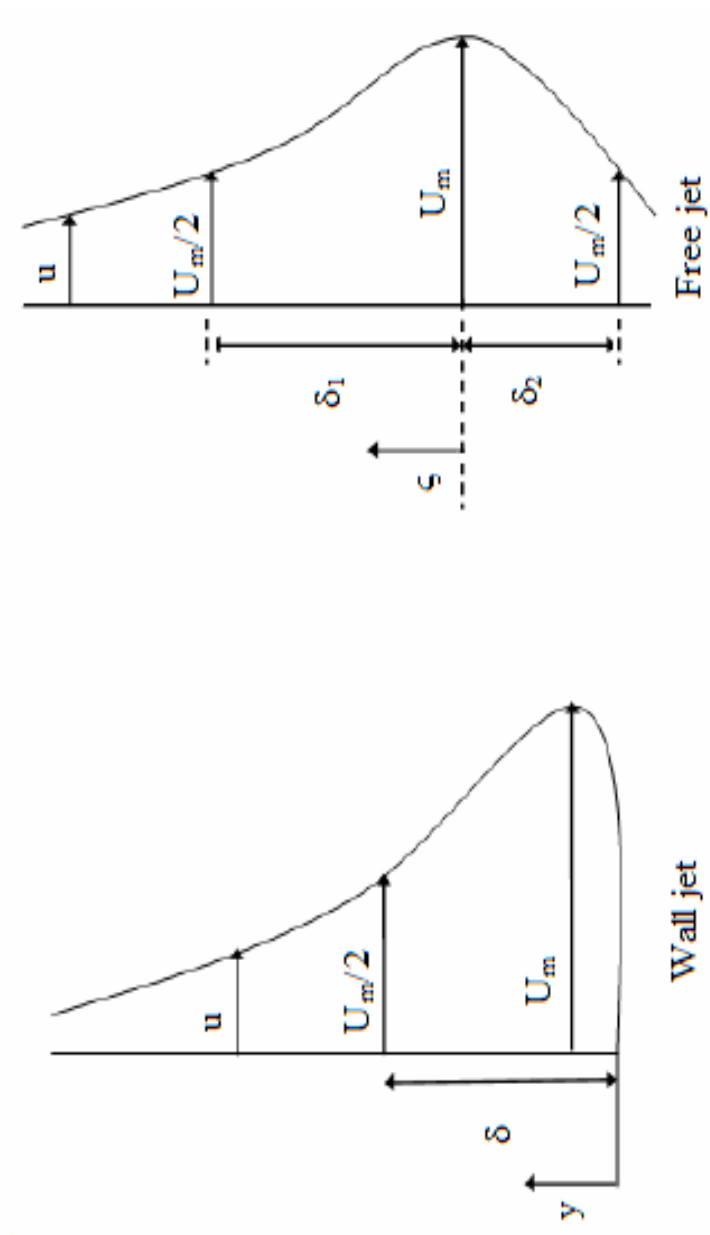
Figure 5.14 Definition sketch for typical velocity profiles for a wall and a free jet (After Adduce 2004, modified)
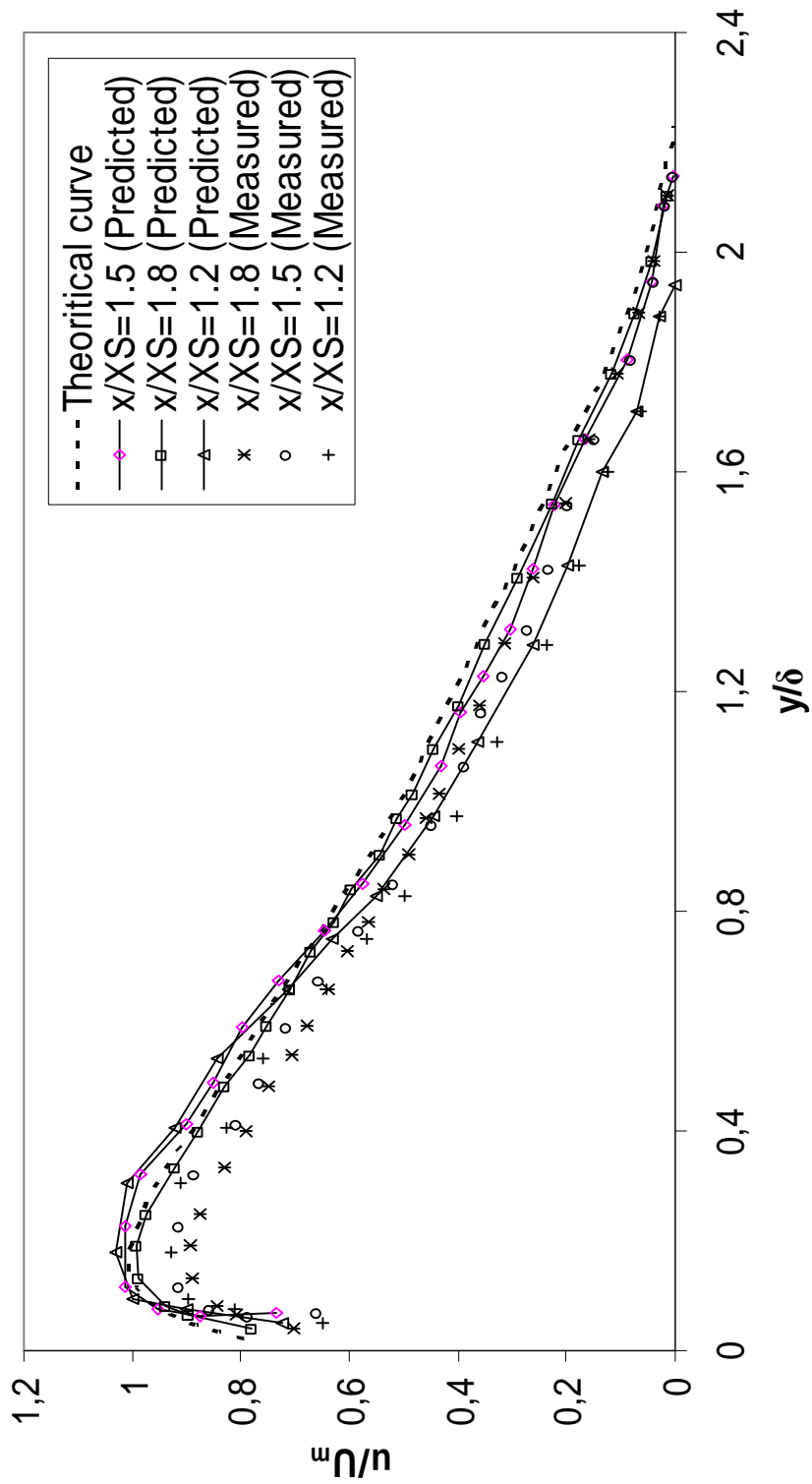
Figure 5.15 Predicted and measured dimensionless velocity profiles vs. theoretical curve for test A2
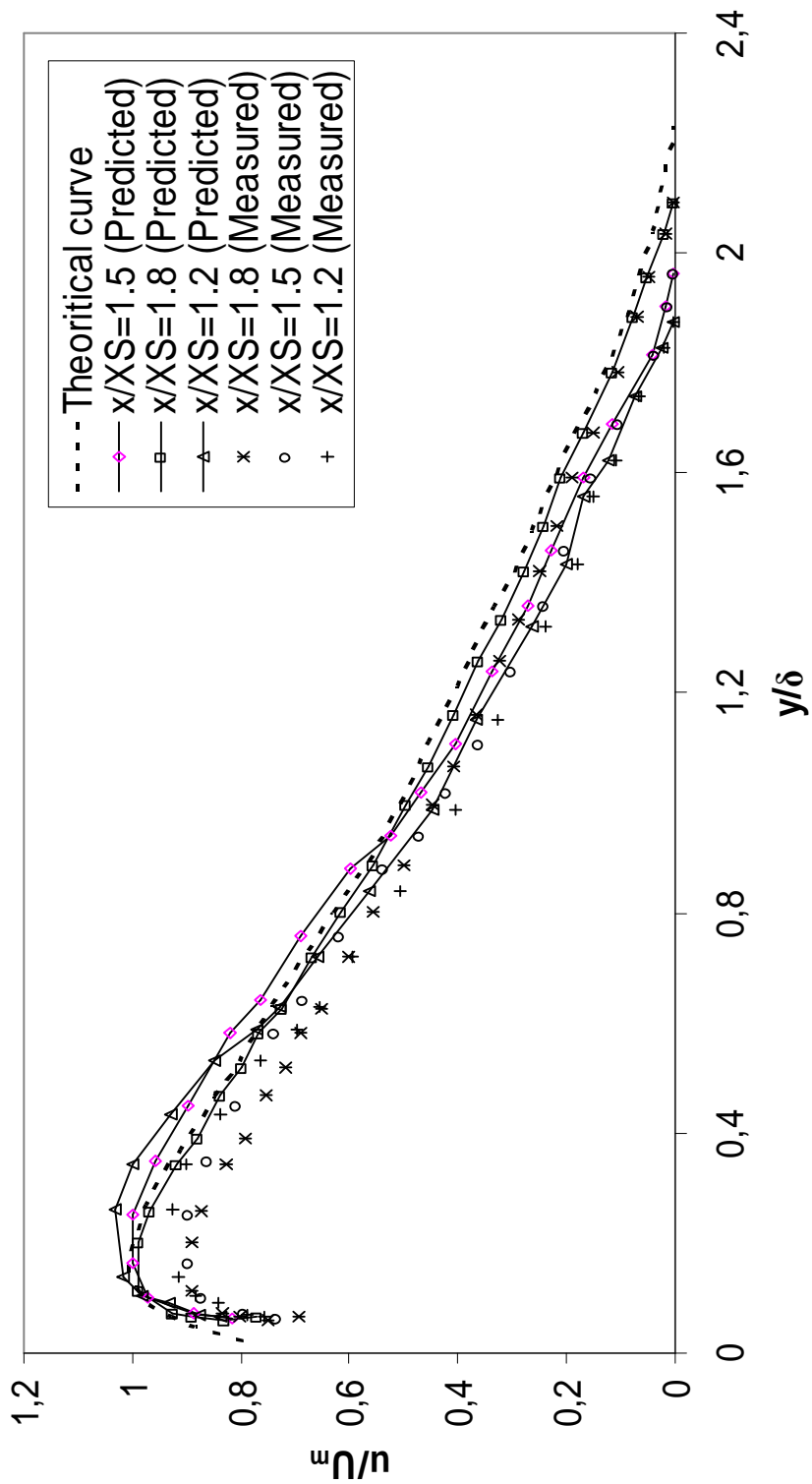
Figure 5.16 Predicted and measured dimensionless velocity profiles vs.

theoretical curve for test A4
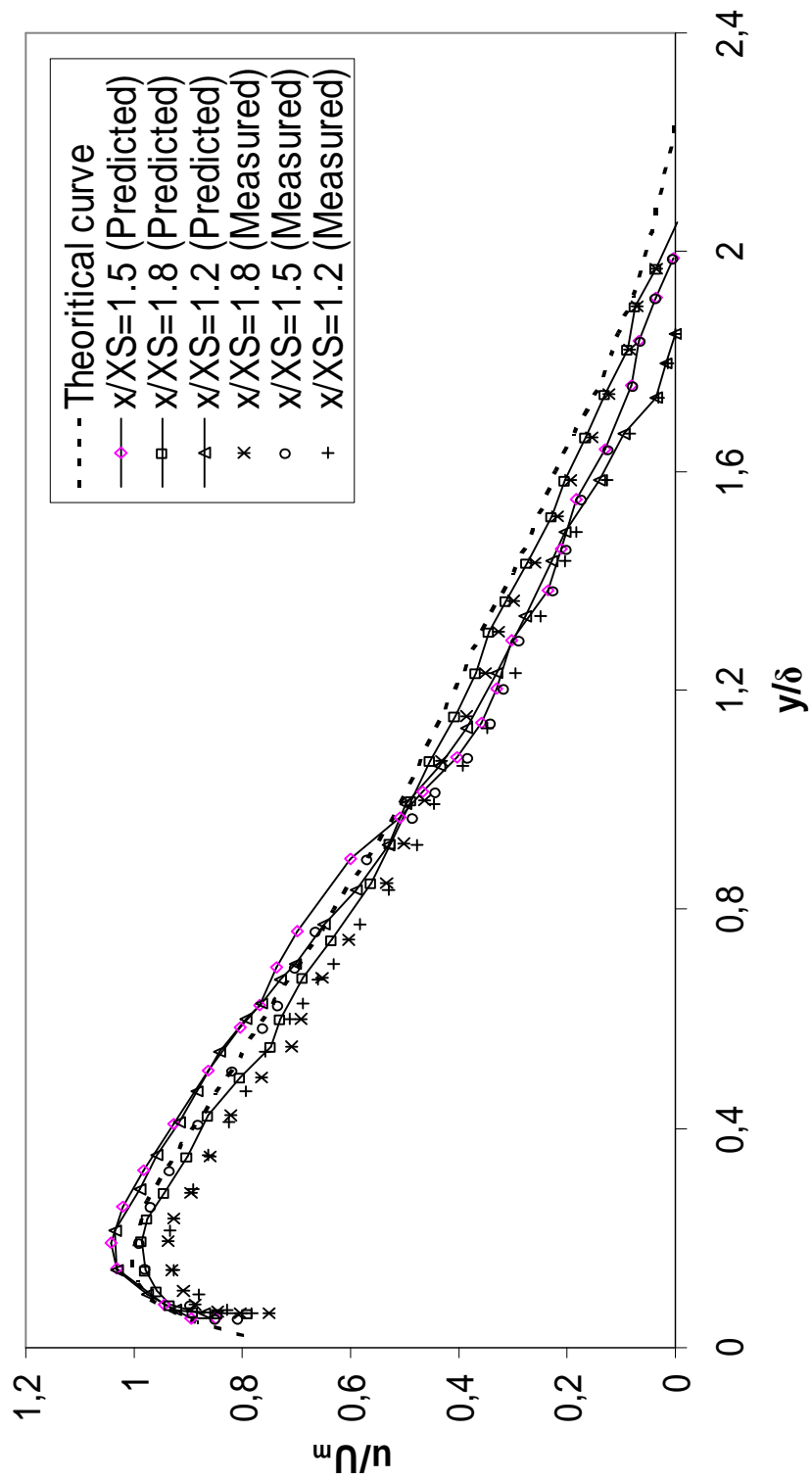
Figure 5.17 Predicted and measured dimensionless velocity profiles vs.

theoretical curve for test A8
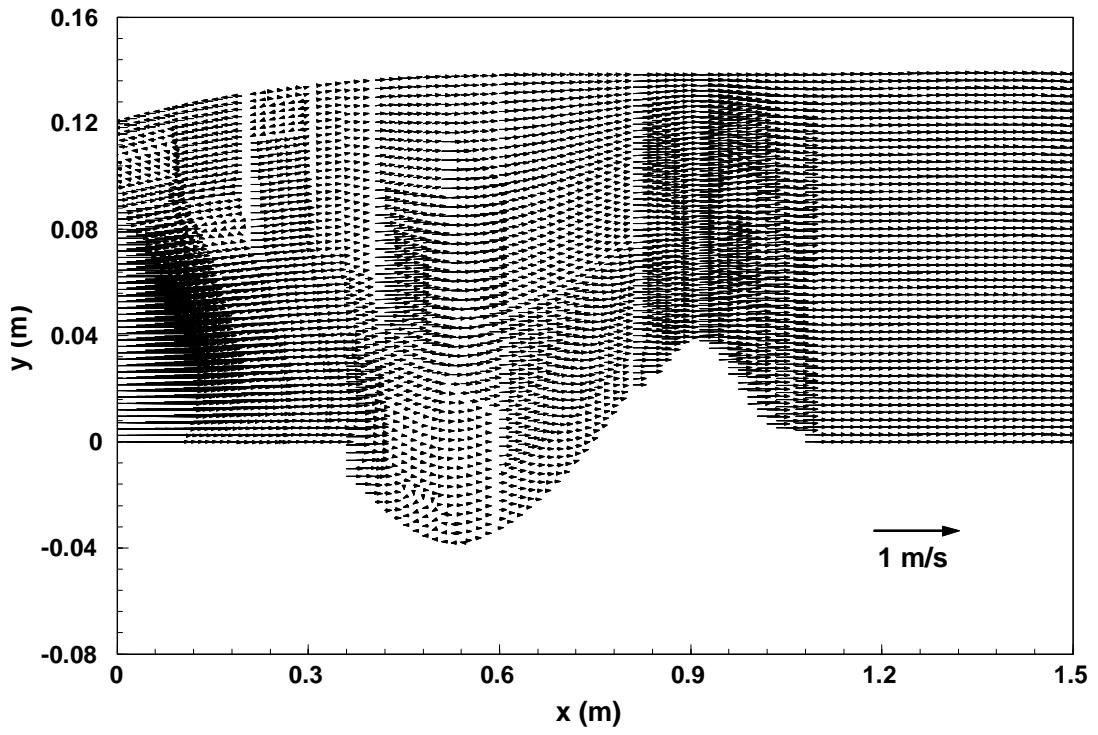
Figure 5.18 Predicted velocity vector field for test A2
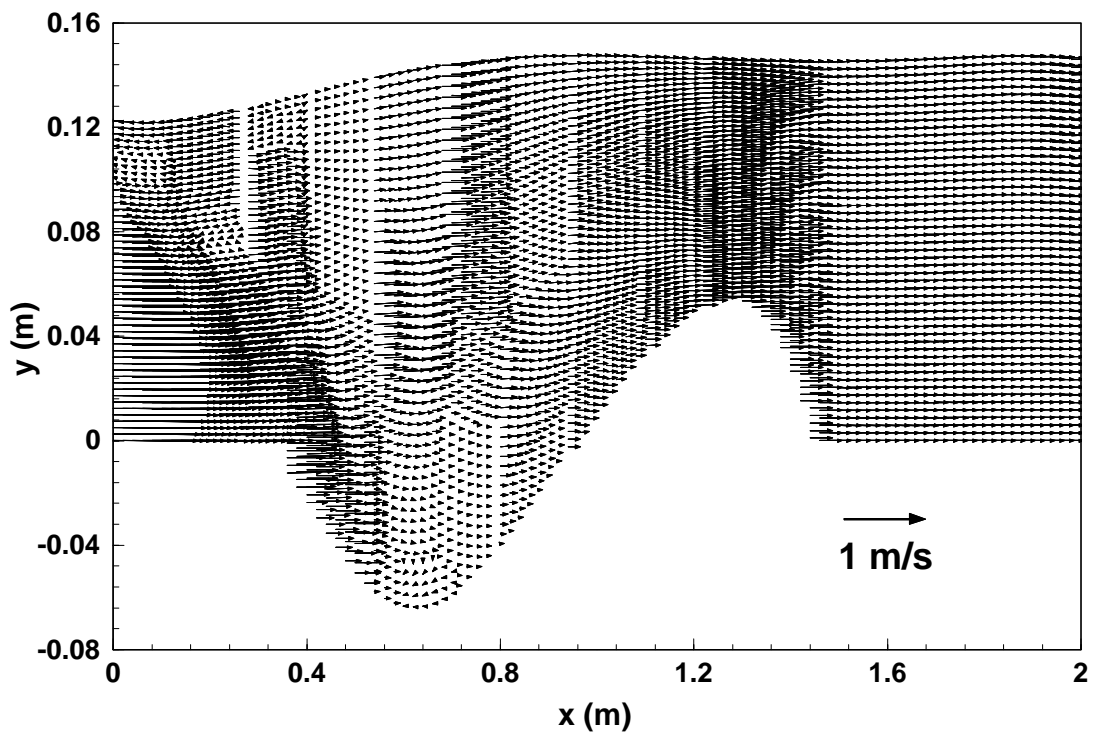
Figure 5.19 Predicted velocity vector field for test A4
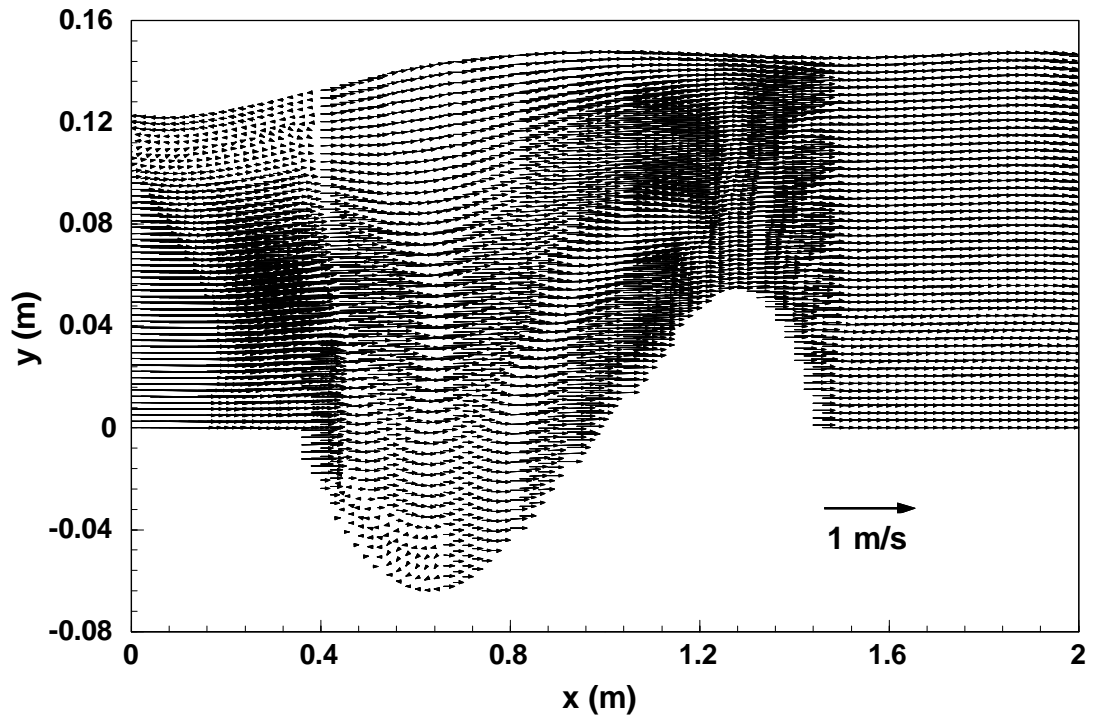
Figure 5.20 Predicted velocity vector field for test A5
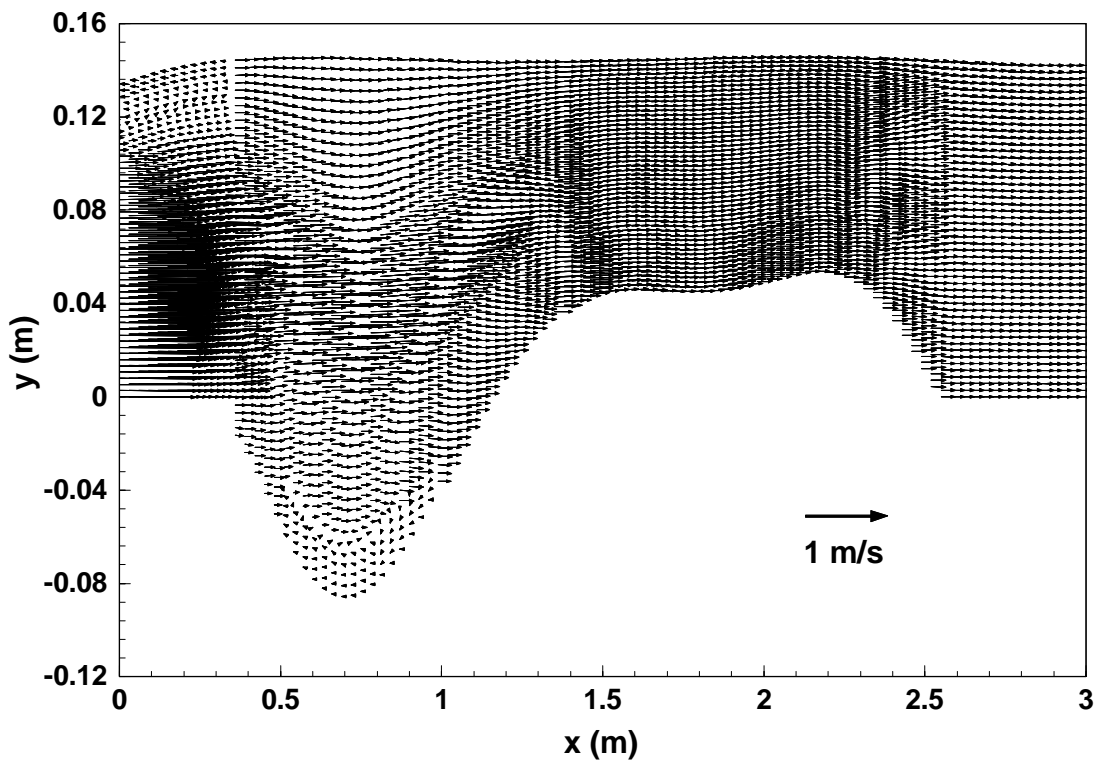
Figure 5.21 Predicted velocity vector field for test A9
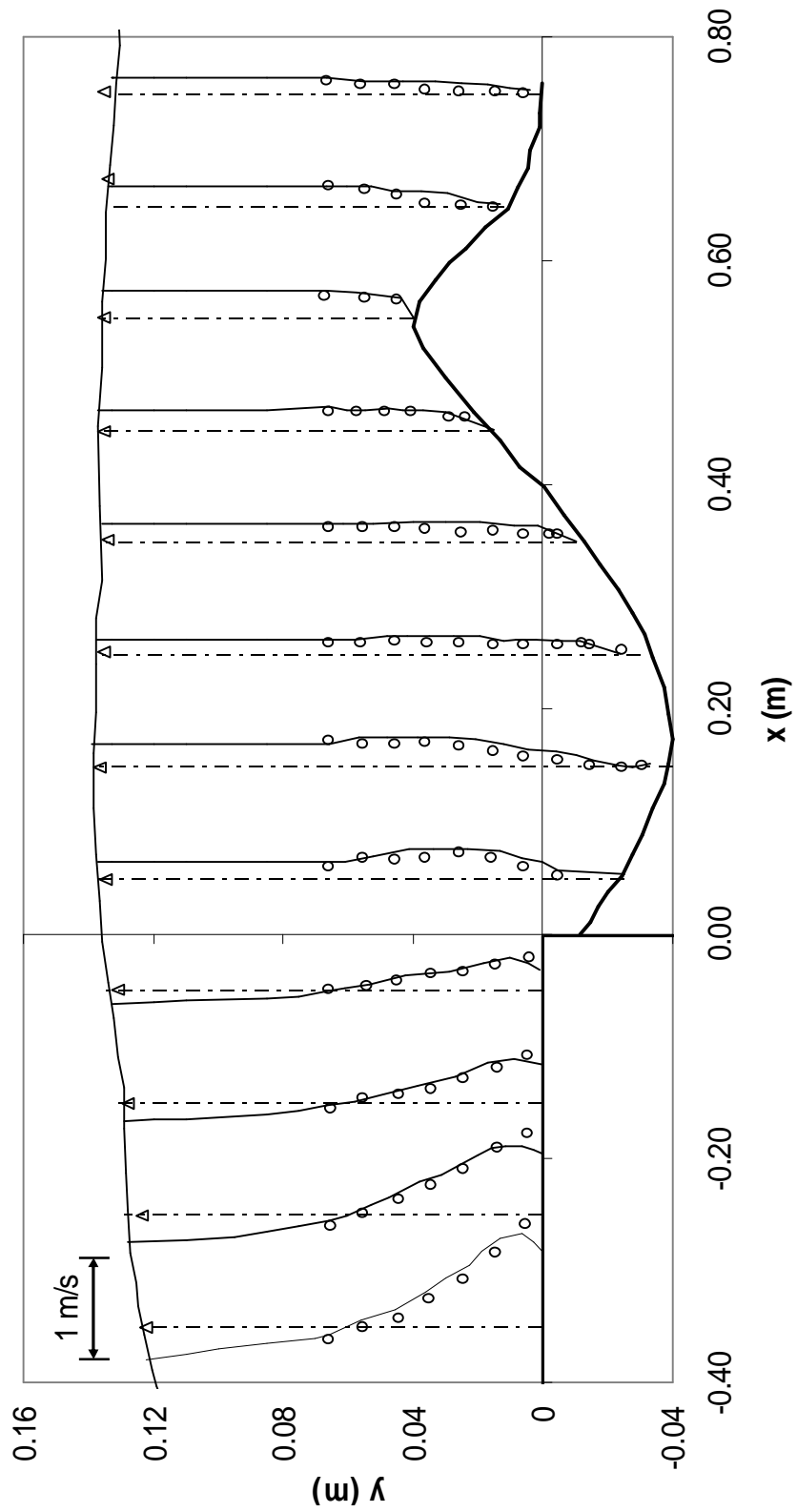
Figure 5.22 Predicted and measured u-velocity distribution over the rigid apron and scour profile for test A2
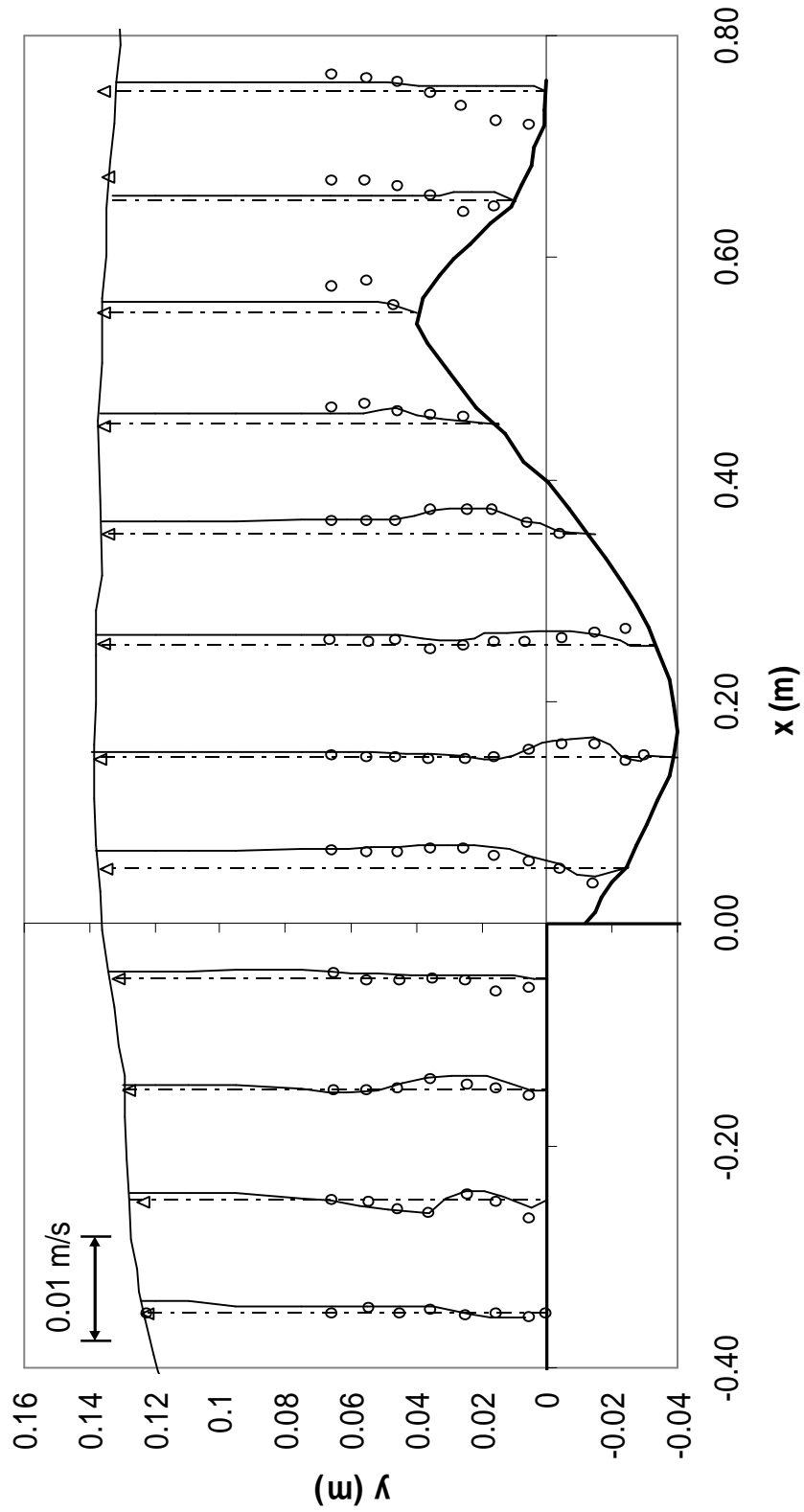
Figure 5.23 Predicted and measured v-velocity distribution over the rigid apron and scour profile for test A2
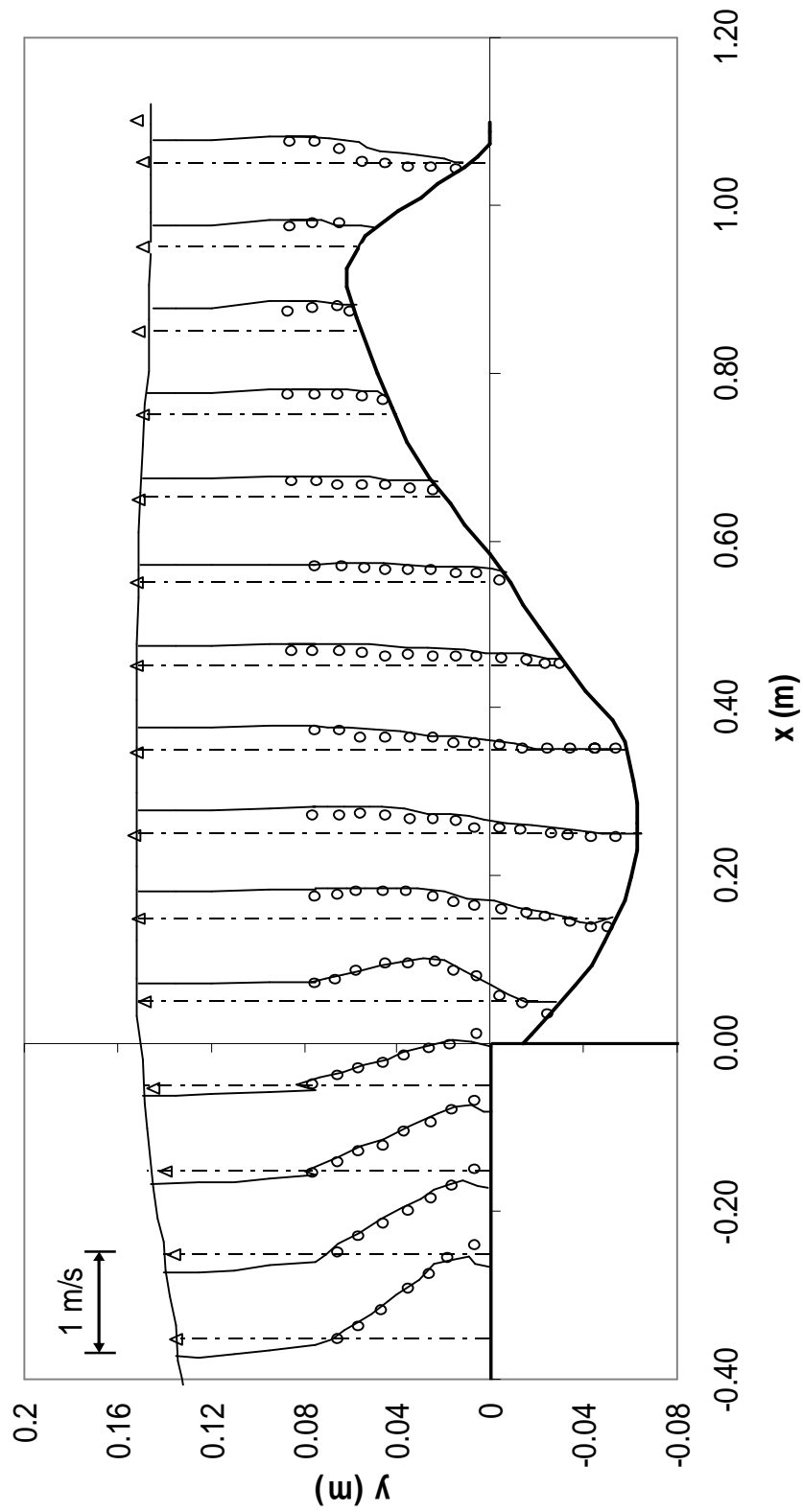
Figure 5.24 Predicted and measured u-velocity distribution over the rigid apron and scour profile for test A5
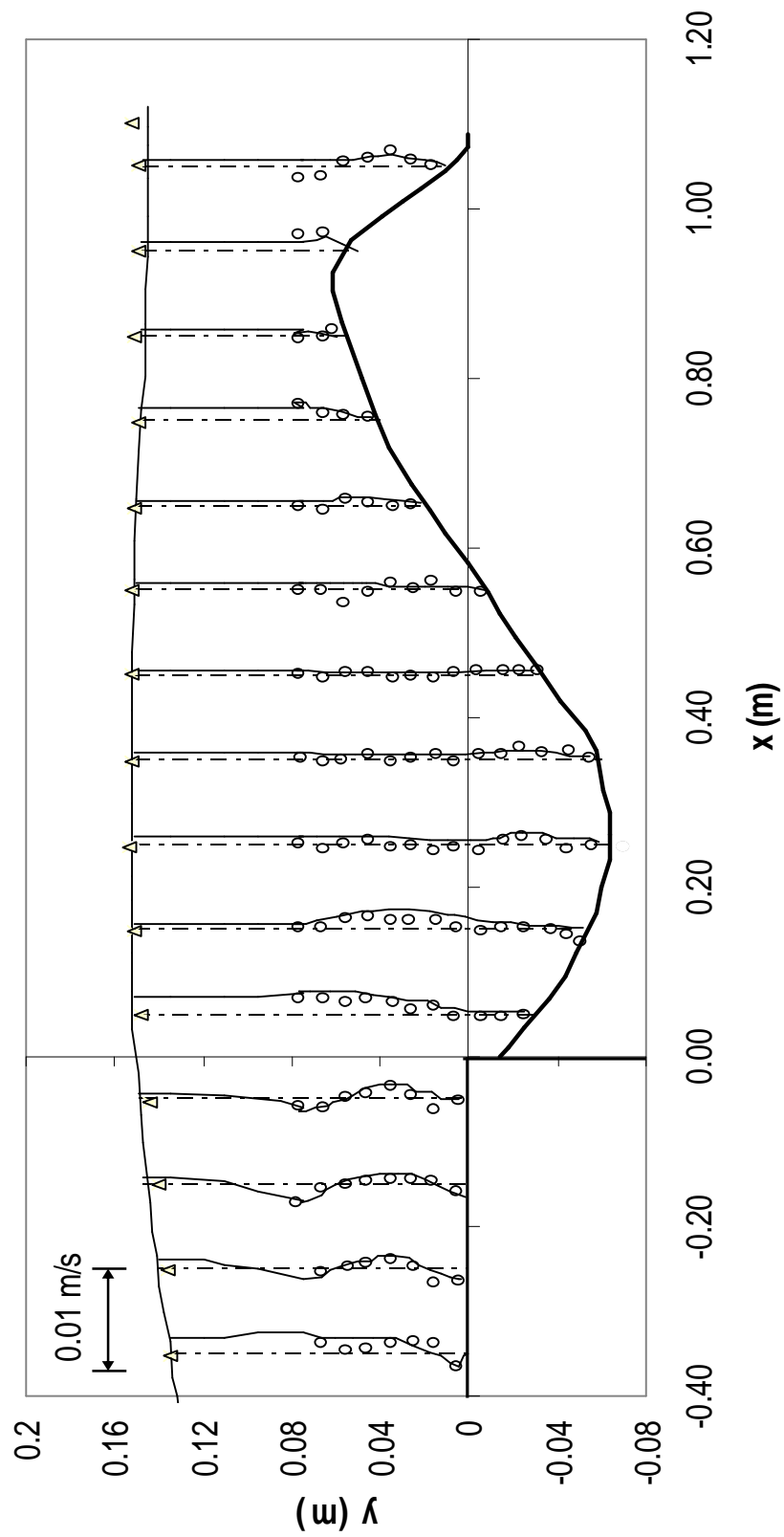
Figure 5.25 Predicted and measured v-velocity distribution over the rigid apron and scour profile for test A5
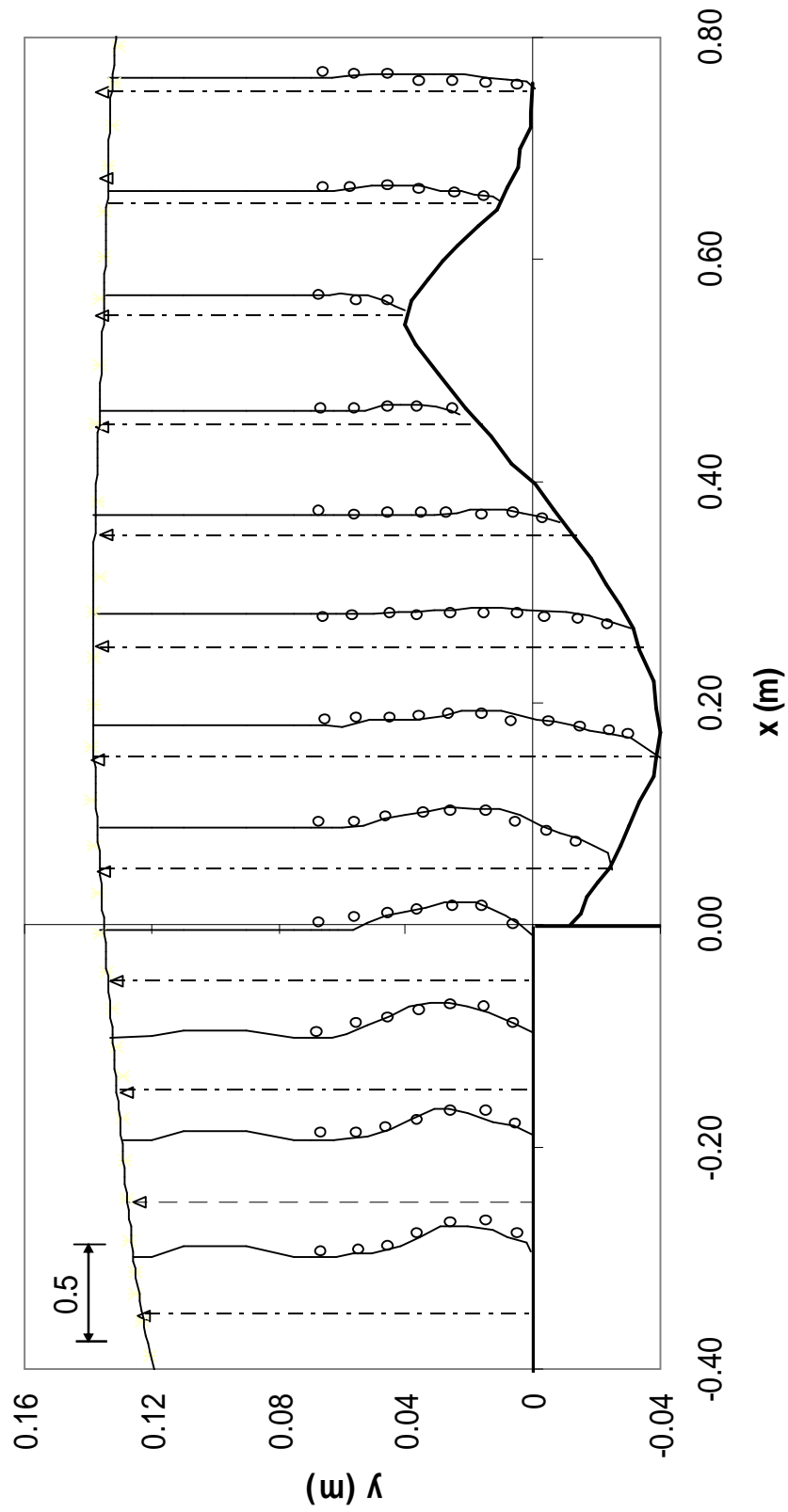
Figure 5.26 Predicted and measured $\sqrt{\overline{u'^2}}/U_0$ distribution over the rigid apron and scour profile for test A2
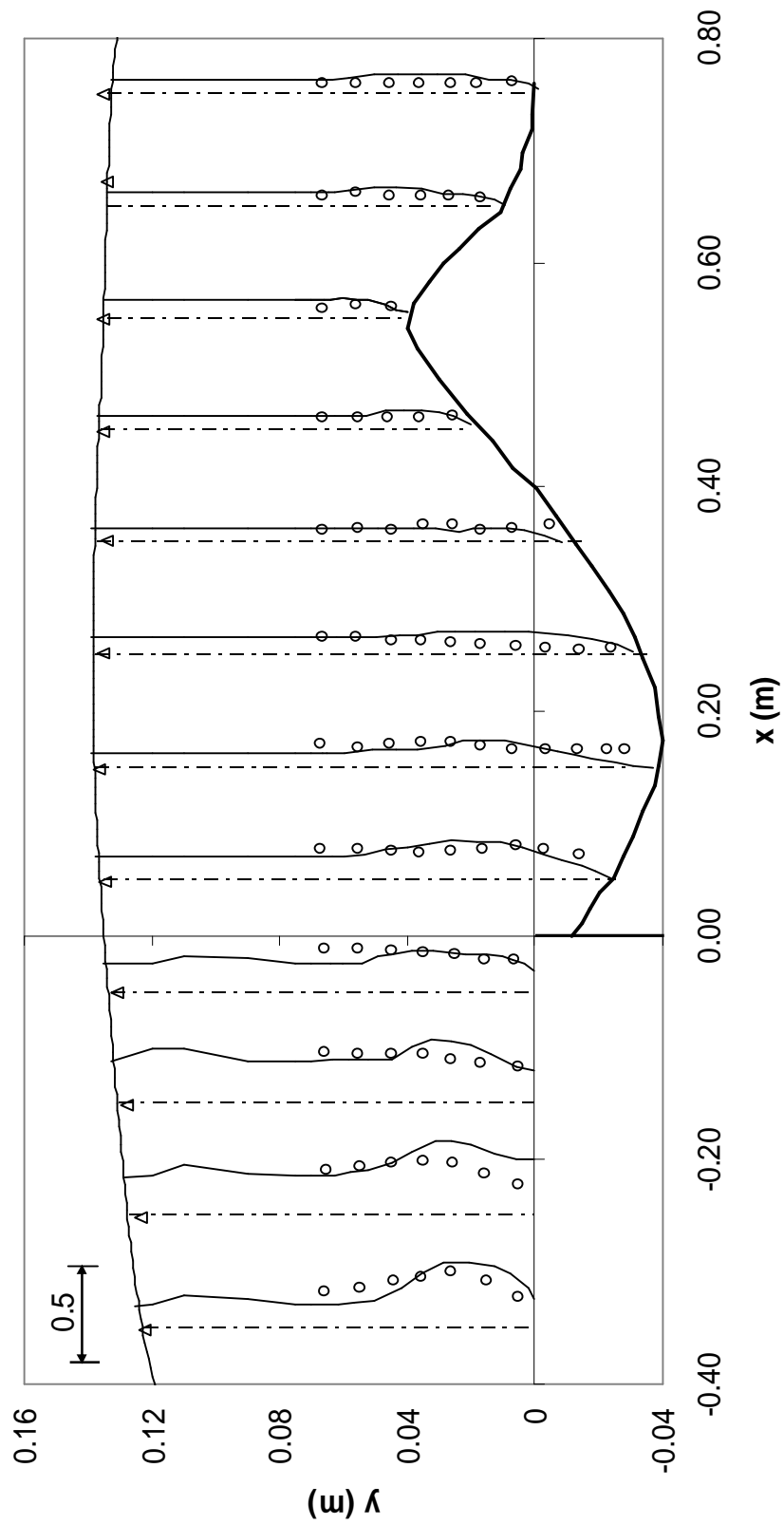
Figure 5.27 Predicted and measured $\sqrt{\overline{v'^2}}/U_0$ distribution over the rigid apron and scour profile for test A2
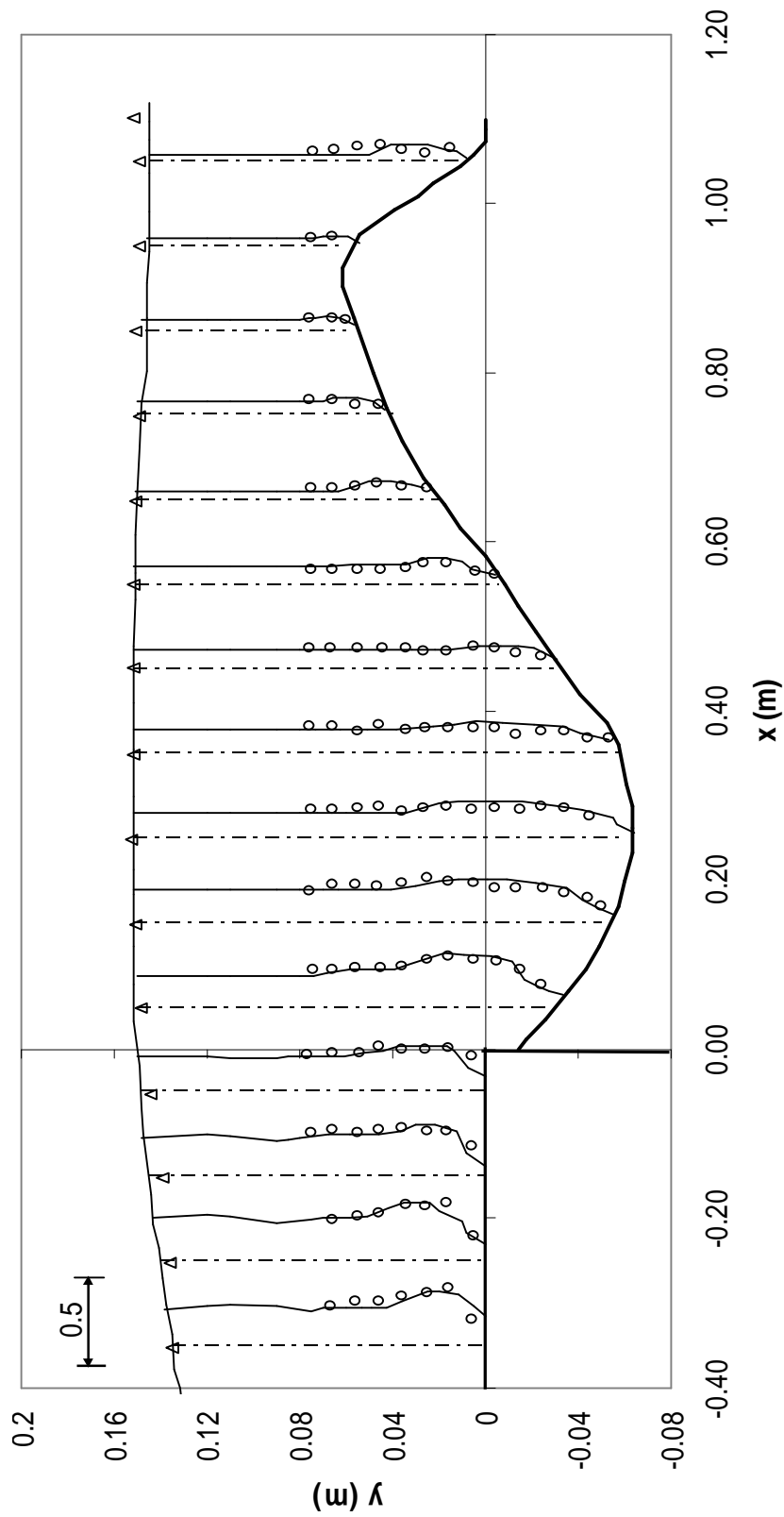
Figure 5.28 Predicted and measured $\sqrt{\overline{u'^2}}/U_0$ distribution over the rigid apron and scour profile for test A5
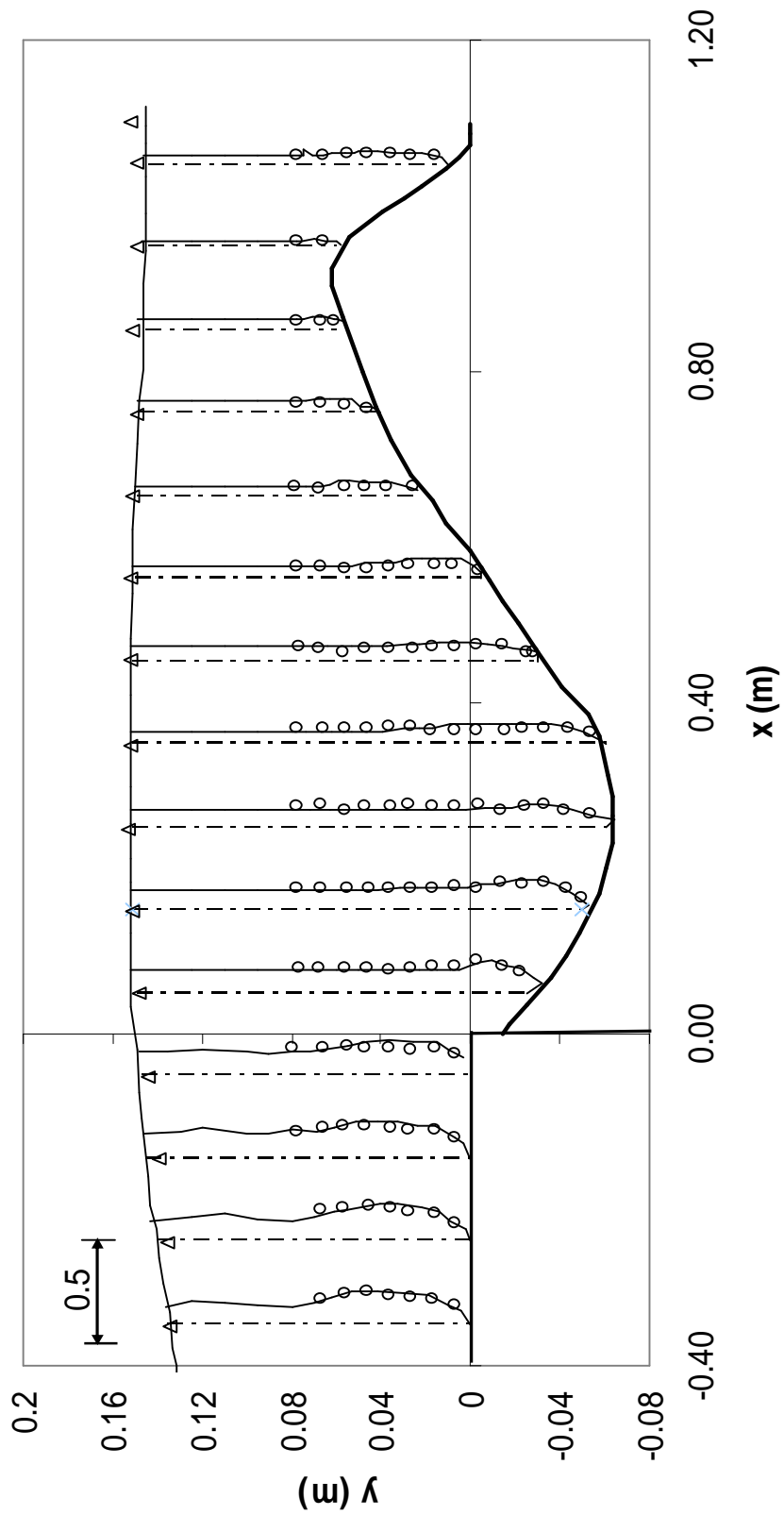
Figure 5.29 Predicted and measured $\sqrt{\overline{v'^2}}/U_0$ distribution over the rigid apron and scour profile for test A5

5.10 Comparison of Proposed Hybrid Model with FLUENT Software

In this section, the performance of the proposed hybrid model is evaluated by the most widely used, well-established FLUENT commercial software, based on the experimental observations of Ali and Lim (1986). The details on FLUENT and the experimental program of Ali and Lim (1986) are given in following sections.

5.10.1 Brief overview on FLUENT software

FLUENT (1993) is multipurpose commercial software for modeling fluid flow, heat transfer, and chemical reactions. It was used in simulating flow patterns, generated by a turbulent water jet impinging on rigid and scoured beds by Karim and Ali (2000). FLUENT applies computer simulation methods to analyse and solve practical design problems based on fundamental principles of computational fluid dynamics (CFD) such as the conservation of mass, momentum and energy. FLUENT (1993) is a two part program consisting of a pre-processor, PreBFC V4, and a main module, FLUENT. Karim and Ali (2000) used PreBFC V4 to define the geometry and a structured grid of the problem to be modelled, then they imported the grid information from PreBFC to FLUENT. The physical models, fluid/material properties, and boundary conditions that describe the problem to be modelled were next added to the grid information and stored in Case-File that is a record of all the inputs for problem definition (Karim and Ali 2000). The results of the calculations were stored in Data-File (Karim, 1996).

FLUENT underwent some updates since 2000 and the PreBFC V4 pre-processor was replaced by a more powerful grid generator GAMBIT. The other details on the new version of FLUENT software (FLUENT 6.3) and its applications can be found in web adress www.fluent.com, and the other details on application of FLUENT on local scour due to turbulent jets and simulation of flow patterns in scoured zone can be found in Karim and Ali (2000).

The main difference between the FLUENT (1993) package program and the present boundary-fitted coordinate model is the transformation of the governing equations

from the physical to the computational plane. In the present model, calculations were carried out at the computational plane, whereas FLUENT (1993) carries out calculation at the physical plane. FLUENT (1993) needs a grid development program, PreBFC V4, in order to generate the solution domain, whereas the present model generates the computaional domain itself.

5.10.2 Experimental study of Ali and Lim (1986)

Ali and Lim (1986) carried out their experimental research using a long channel of 5.0 m long, 0.61 m wide and 0.5 m deep. A well streamlined sluice gate was constructed in such a way so that it ensured uniform jet flow (Ali and Lim, 1986). Sand was filled to a height of 30 cm in the test section. The tailwater depth at the end of the channel was regulated using a sluice gate. The bed material used was uniform sand with d_{50}= 0.82 mm, specific gravity of 2.66, angle of response= 33°, and, porosity of 0.403. At the end of the experiment, the scour holes were measured using a depth gauge.

In order to investigate the transient non-uniform flow patterns, a steady-state flow model was necessary. Following (Lim, 1985), they converted the loose sand scour hole into a fixed-bed model so that the flow characteristics in the hole at that instant of time could be studied in detail. They by covered and moulded the scour hole with very thin aluminium foil. The foil was coated with the sand grains used in the experiment.The velocities were measured using a miniature streamflow current meter. The measuring hand of the current meter was 16 mm in diameter. The "floor velocity" was measured at y= 0.8 cm (equal to half of the diameter of the streamflow meter) above the bed of scoured hole. Since the probe only records positive velocity, reversed flow was judged by observing the direction in which the rotor turned. Based on a measured "floor" velocity, they calculated the boundary shear stress using a method developed by Melville and Raudkivi (1977). The further details can be found in Lim (1985) and Ali and Lim (1986).

5.10.3 Model validation with FLUENT software and experimental data

Figure 5.30 shows the time evolution of centreline bed-profiles obtained with tailwater depth, measured by Ali and Lim (1986) and the predictions of the present hybrid model. Based on available experimental data, a time peripod of $t = 0$ (initial bed), 15, 60, 150, 300, and 400 minutes (asymptotic) was used for numerical simulation by the proposed hybrid model. From the figure it is seen that, especially in the section from the inlet to the maximum scour depth ($0<x<XS$), there is perfect agreement between the experimental and the predicted values. From the maximum scour depth region to the end of scour profile ($XS<x<Ls$), the proposed model overpredicted the scour profiles with relatively small discrepancies. Also, the proposed model predicted the maximum scour depth S_{max} at asymptotic state as 0.082 m while it is experimentally observed as 0.078 m.

The predicted final velocity vector field for experimental conditions of Ali and Lim (1986) is plotted in Figure 5.31. This figure proves a strict agreement between the predictions of the proposed hybrid model (solid line) and those of FLUENT software (round points) presented in Karim and Ali (2000). The predicted surface profile is also presented in the figure. Although it is not clear in the figure, the proposed hybrid model predicted negative velocities in maximum scour depth region representing reverse flow. The reason for smaller negative velocity predictions is the under-predictions of reverse flow by the standard k-ε turbulence model (Rodi, 1980; Versteeg and Malalasekera, 1995; Gunal and Guven, 2006).

Figure 5.32 shows the dimensionless velocity profiles over the scoured profile for $XS<x<L_s$, predicted by the present model and FLUENT software and the measured ones by Karim and Ali (1986). Also, the theoretical curve of a wall jet, proposed by Rajaratnam (1976) is illustrated in the figure. The mean horizontal velocity, u and the distance y are normalized by maximum velocity U_m and the length scale δ, respectively. From the figure it is observed that predicted velocity distributions can be simulated by the theoretical wall jet. As it is seen from the figure, at $0<y/\delta<0.02$, both numerical predictions are under the theoretical curve, while there is strictly good agreement in section $0.02< y/\delta <1.0$. Beyond this to $y/\delta=2.4$, both numerical predictions are again under the theoretical curve, the predictions of present model being relatively better than those of FLUENT. Adduce (2004) also observed the

same event while analyzing her experimental velocity distributions and explains by the fact that u/U_m is affected by the reverse flow. It can certainly be said that there is a strict agreement between the numerical results of present study and those of FLUENT software that is presented in Karim and Ali (2000).

Figure 5.33 shows the comparison between the predicted bed shear stress of present model, those of FLUENT software (Karim and Ali, 2000) for two different turbulence models, RSM and RNG, respectively, and the experimental results of Lim (1985). A good agreement can easily be noticed between the present numerical predictions and the experimental ones, except for the maximum scour depth region. And also it is obviously seen that the experimental results of Lim (1985) falls just in the middle of present numerical predictions and those of FLUENT with RSM model. The reason of the distinction is the fact that FLUENT predicts much rougher bed surface than the prediction of present study. Although it cannot be easily observed from the figure that the present model predicted reverse horizontal velocities in the vicinity of maximum scour depth. But these values are much smaller that those of FLUENT. At $0<x/y_1<2$ very good agreement is observed and 15 % distinction is observed between present numerical results and those of FLUENT (RSM model) along $2<x/y_1<8$ region. 6 % distinction is observed at $8<x/y_1<24$ region between the two numerical results. The distinction between present numerical results and the experimental results of Lim (1985) is almost half of the above distinction values because the experimental results fall just between the two numerical results.

In Figure 5.34, the present predictions of surface profile and those of FLUENT are presented. A 1 % error is observed at $0<x/y_1<7$ region. And a very good agreement is achieved along the rest of surface profile. Also the present model's bed profile prediction is compared with the measured one by Karim amd Ali (1986). It should be noted that FLUENT software is not capable of simulating the mobile bed profile.
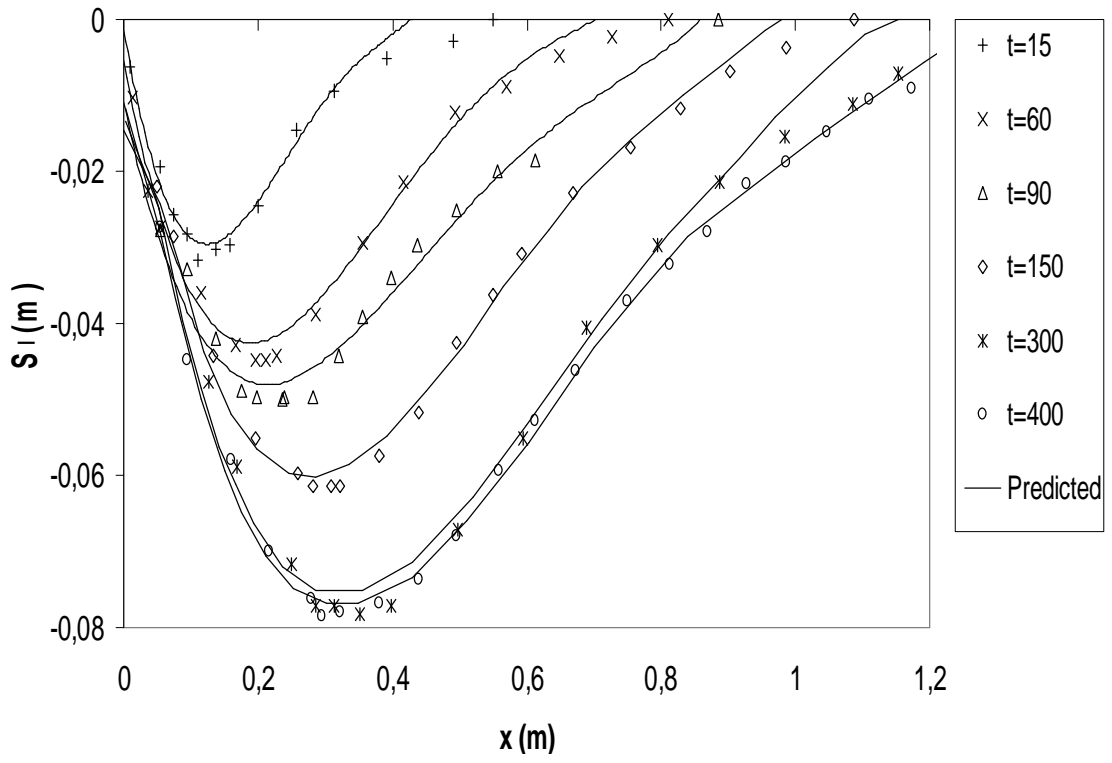
Figure 5.30 Predicted and measured temporal evolution of the scour profile
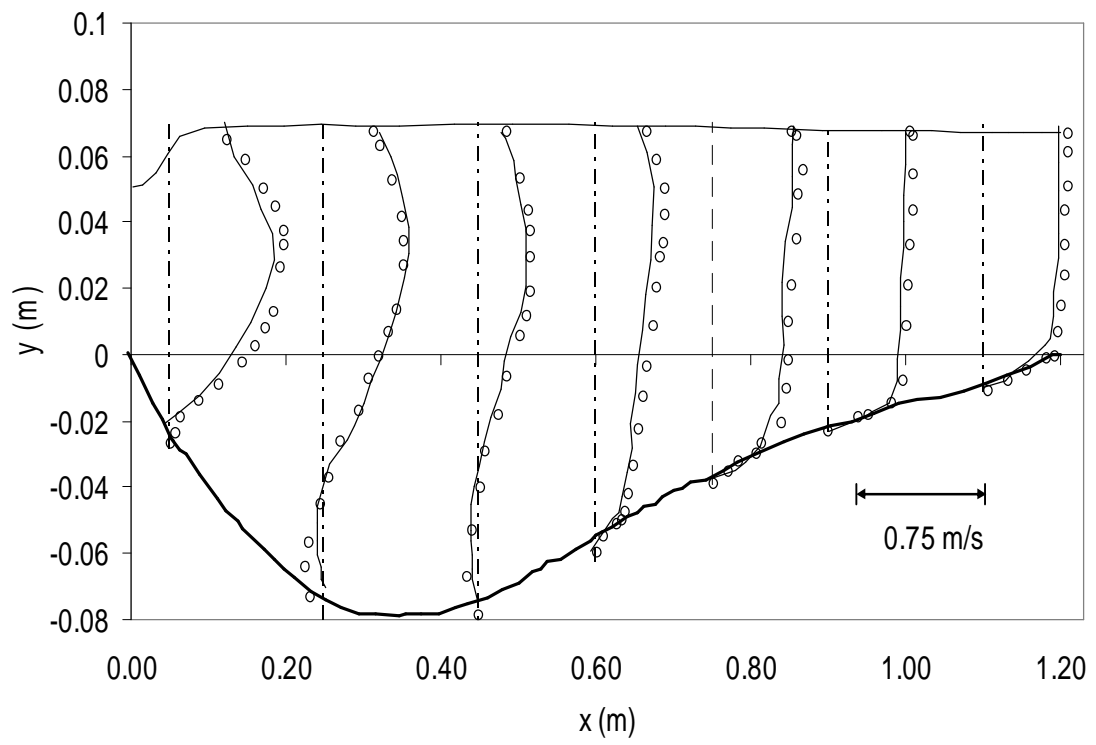
Figure 5.31 Predicted (─) and measured (○) u-velocity distribution over scoured zone

168
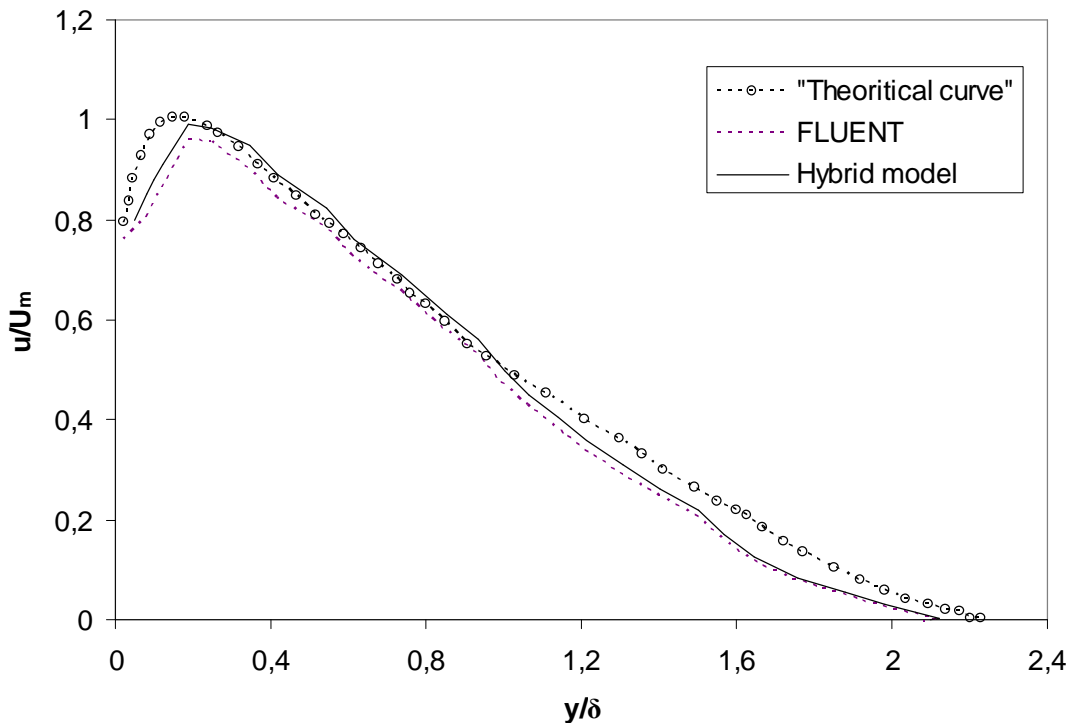
Figure 5.32 Dimensionless velocity profile predictions of present model and FLUENT vs. the theoretical curve
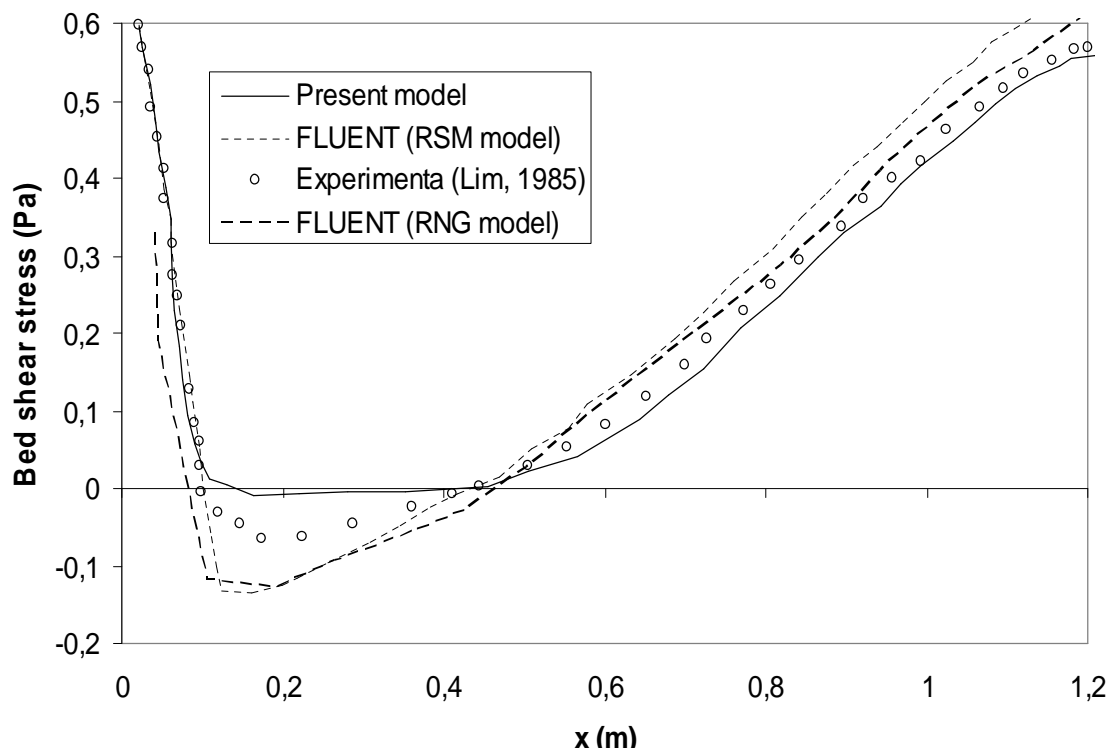
Figure 5.33 Predictions of of bed shear stress distribution and the measured one over scoured zone
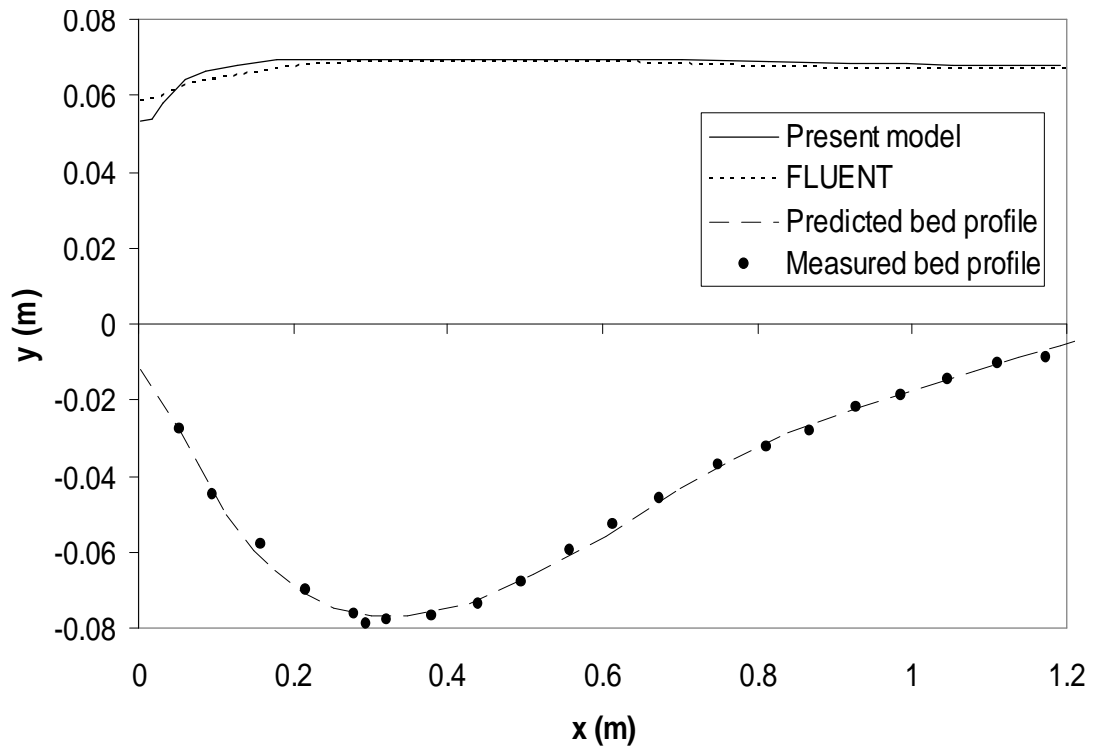
Figure 5.34 Present model's and FLUENT's predictions of free surface and bed profiles

5.11 Hybrid Numerical-Analytical Modeling versus Artificial Neural Networks

5.11.1 General

Physical modeling is doubtlessly a fundamental and effective method for understanding the mechanism of the scouring process. However, it is also associated with high costs and relatively long times. In addition, the inadequate knowledge of the scale effect in the model test poses a question mark on the application of experimental results to prototype. In comparison, the numerical modeling does not suffer from these defects. This provides us an alternative way to evaluate and understand the process of local scour downstream of hydraulic structures. It is therefore imperative that more effort is devoted to developing suitable numerical models (Karim and Ali 2000, Salehi-Neyshabouri et al. 2003, 2004). However, besides many successes of numerical modeling, its wider application is restrained by

its heavy demand in computing capacity and time. For some applications like real-time and nearly real-time control, the demand in computing time and resources are of such huge amount that numerical modeling is sometimes far from acceptable. Recent developments in soft computing techniques (artificial neural networks, genetic programming, fuzzy logic, etc.) have produced more potential in simulating physical processes, based on experimental data.

Neural Network (NN) modeling has been successively applied in prediction of hydraulic data in last ten years. NNs are more suited for dynamic adaptation with new data than general statistical and stochastic methods (Azmatullah et al. (2005). Furthermore, NNs are relatively stable with respect to noise in data and have a good generalization potential to represent input-output relationships (Guven et al. 2006). NNs have a structure where non-linear functions are present and the parameter identification process is based on techniques which search for global maximums in the space of feasible parameter values. Thus, NNs can represent the non-linear effects present in the scouring process. All these features of NN make it an intelligent tool in formulation of maximum depth of scour downstream hydraulic structures.

In this study, the asymptotic scour profiles downstream of a sill followed by rigid apron measured by Adduce (2004) (test A4-A9 in Table 5.1) are modeled using artificial neural networks. The explicit formulation of the proposed neural networks model (ENNF) is also presented. The proposed ENNF was compared with the proposed hybrid model.

5.11.2 Results of neural network training

The general procedure of the training and testing of the neural networks modeling is already given in Chapter 4. Therefore, in this section we only give brief information about the training and the testing stages of the proposed neural networks in order not to repeat the same details.

Referring to Figure 3.8, the ordinate of the scour profile (S_l) can be modeled as a function of the most affecting parameters, the fluid discharge (Q), gravitational, thickness of the sill (b), fluid density (ρ), density of the sediment (ρ_s) acceleration

(g), thickness of water at weir crest (h_s), length of the rigid apron (L_p), the sill height (z), tailwater depth (y_t) and the abscissa of the scour profile (x) from the edge of the rigid apron. The functional relationship can be given as follows:

$$S_l = f(Q, b, r, r_s, g, h_s, L_p, y_t, z, d_{50}, x) \tag{5.8}$$

Because the relation in Eqn.(5.8) represents a physical phenomenon that does not depend on the choice of measurement unit, we use Buckingham-p theorem to represent physical parameters given in Eqn.(5.8) in dimensionless form. We choose z, Q and r as repeating variables and deduce following non-dimensional groups $\prod_i$ ($i=1,\ldots,9$):

$$\prod_1 = S_l / z \qquad \prod_2 = \frac{b}{z} \qquad \prod_3 = \frac{h_s}{z} \qquad \prod_4 = \frac{L_p}{z}$$

$$\prod_5 = \frac{(r_s - r)}{r} \qquad \prod_6 = \frac{gz^5}{Q^2} \qquad \prod_7 = \frac{y_t}{z} \qquad \prod_8 = \frac{x}{z} \qquad \prod_9 = \frac{d_{50}}{z} \tag{5.9}$$

Twelve dimensional parameters in Eqn.(5.8) are reduced to nine dimensionless groups in Eqn.(5.9). By dividing L_p / z by h_s / z we derive a new dimensionless group, L_p / h_s. Combining b / z, h_s / z $(r_s - r)/r$, gz^5 / Q^2 and d_{50} / z, we obtain an important flow parameter, densimetric Froude number (F_{rd}), which most widely used in sediment transport problems:

$$F_{rd} = \frac{1}{\frac{b}{z} \frac{h_s}{z}} \left(\frac{1}{\frac{(r_s - r)}{r} \frac{gz^5}{Q^2} \frac{d_{50}}{z}} \right)^{1/2} = \frac{Q}{bh_s \left[gd_{50} \left(\frac{r_s - r}{r} \right) \right]^{1/2}} \tag{5.10}$$

Finally, we suggested that,

$$\frac{S_l}{z} = f(F_{rd}, \frac{h_s}{z}, \frac{L_p}{h_s}, \frac{y_t}{z}, \frac{x}{z}) \tag{5.11}$$

The functional relationship in Eqn.(5.11) is used in proposed NNs modeling, namely S_l/z is taken as output and the other ones as input parameters. The experimental data

(totally 178 tests) taken from Adduce (2004) are randomly divided into training (142 tests, 80% of all data) and testing (36 tests, 20% of all data) sets in present neural network modeling. The range of the physical variables used in present NNs modeling is given in Table 5.5.

Table 5.5 Minimum and maximum values input and output data

Physical variables (unit)	Minimum value	Maximum value
Q (m^3/s)	0.011	0.0364
h_s (m)	0.022	0.039
y_t (m)	0.126	0.168
x (m)	0.000	2.798
S_l (m)	-0.106	0.053

A multilayer feed forward neural network is used with back-propagation training algorithm. Levenberg&Marquardt training algorithm is used to optimize the network parameters. The optimal architecture of the proposed network is derived using Genetic Algorithm (GA). An optimal architecture, 5-9-1 (no. of input-no. of hidden neurons-no. of output), is derived after a number of iterations (see Figure 5.35). The training stage of the model is ceased after achieving satisfactorily high correlation ($R \geq 0.99$), if R value is less than the target value, the model is trained till the R value of the training stage gets no longer higher. The overall performances of both sets are evaluated by the coefficient of determination (R^2) and the mean square error (MSE).

5.11.3 Derivation of ENNF of scour profile

The general procedure of derivation of explicit formulation of corresponding neural networks is explained in Chapter 4, section 4.2.4, in detail. Thus, in this section we briefly explain how we obtain the ENNF of the proposed model.

The functional relation ship in Eqn.(5.11) is used between the normalized scour profile ordinate and the corresponding input variables. The neural networks model is trained for a number of iterations till predefined goal is achieved ($R>0.99$ or no. of iteration=10,000). After achieving the satisfactory training performance, the training is stopped and the optimal weights are taken. Each input is multiplied by corresponding model weight and summed for each neuron plus a bias (U_i, i=1, 9):

$$U_1 = 160.622F_{rd} - 90.059y_t/z + 192.617h_s/z - 2.958L_p/h_s - 0.364x/z - 42.682 \quad (5.12a)$$

$$U_2 = -7.174F_{rd} + 0.943y_t/z + 0.911h_s/z + 0.050L_p/h_s - 0.009x/z + 1.594 \quad (5.12b)$$

$$U_3 = -37.286F_{rd} - 152.667y_t/z - 114.178h_s/z - 3.649L_p/h_s + 3.126x/z + 126.391 \quad (5.12c)$$

$$U_4 = -137.055F_{rd} + 84.154y_t/z - 189.201h_s/z + 2.628L_p/h_s + 0.348x/z + 36.070 \quad (5.12d)$$

$$U_5 = -679.526F_{rd} + 95.720y_t/z - 170.5656h_s/z + 21.138L_p/h_s + 2.869x/z + 773.417 \quad (5.12e)$$

$$U_6 = 1.434F_{rd} + 208.462y_t/z - 285.349h_s/z + 2.888L_p/h_s - 1.686x/z - 102.428 \quad (5.12f)$$

$$U_7 = -163.177F_{rd} + 14.296y_t/z - 19.816h_s/z + 2.388L_p/h_s + 0.674x/z + 78.587 \quad (5.12g)$$

$$U_8 = -371.783F_{rd} - -12.171y_t/z + +497.849h_s/z - 0.247L_p/h_s - 0.036x/z + 8.092 \quad (5.12h)$$

$$U_9 = 301.785F_{rd} + 21.111y_t/z - 10.191h_s/z - 2.317L_p/h_s - 0.694x/z - 137.477 \quad (5.12j)$$

Then, the sum-up equations of each neuron (U_i) is transformed through a transfer function (tangent-hyperbolic) to generate a resultant equation W:

$$W = \left(\frac{-98.170}{1+e^{-2U1}}\right) + \left(\frac{225.297}{1+e^{-2U2}}\right) - \left(\frac{1.214}{1+e^{-2U3}}\right) - \left(\frac{104.100}{1+e^{-2U4}}\right) + \left(\frac{4.526}{1+e^{-2U5}}\right) - \left(\frac{2.453}{1+e^{-2U6}}\right) + \left(\frac{4.059}{1+e^{-2U7}}\right)$$
$$- \left(\frac{61.377}{1+e^{-2U8}}\right) - \left(\frac{5.897}{1+e^{-2U9}}\right) + 11.066 \quad (5.13)$$

Finally, output of the model is calculated as:

$$\frac{S_l}{z} = \frac{1.190}{1 + e^{-2W}} - 0.422 \qquad (5.14)$$

where the coefficients (1.190) and (-0.422) come from de-normalization of output of proposed network. It should be noted that the model weights in Eqns.(5.11)-(5.14) are the normalized form of the corresponding weights obtained from the training stage (see Eqns. (4.8) and (4.9)). The normalization coefficients of each parameter are given in Table 5.6. It should be noted that ENNF is valid within the range of input and output parameters given in Table 5.6

Table 5.6 Minimum and maximum values of input and output parameters

Input & output variables	Minimum value	Maximum value	Normalization coefficients	
			a	b
F_{rd}	0.228	0.317	20.225	-5.511
h_s/z	0.173	0.240	10.345	-10.345
y_t/z	0.913	1.087	26.866	-5.548
L_p/h_s	13.889	19.231	-0.337	-5.580
x/z	0.000	18.655	0.097	-0.090
S_l/z	-0.708	0.363	1.681	0.290

Figures 5.36 and 5.37 compare the proposed model predictions of S_l/z with the measured ones via the scatter plot of measured S_l/z versus the predicted ones for training and testing sets, respectively. It should be noted that the negative horizontal section in Figure 5.36 and 5.37 represents the scoured zone and the positive one represents the dune section. From Figure 5.36, it is clearly seen how well the proposed NNs model learned the non-linear and complex interrelation between the inputs and output (R^2=0.999, MSE=0.00008). Comparison of NN predictions with measured ones for testing set (Figure 5.37) revealed a high generalization capacity of proposed model with relative low error (MSE=0.004) and high correlation (R^2=0.996). The negative values represent the data points in scoured zone, while the positive ones represent those in dune section.
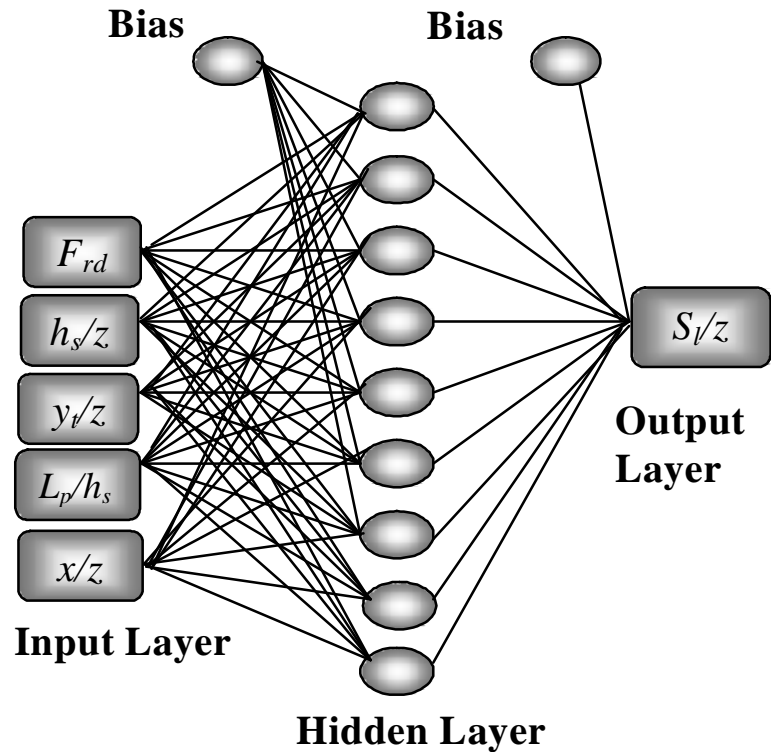
Figure 5.35 Optimal NNs architecture

Figures 5.38-5.41 show the predictions of the proposed hybrid numerical-analytical model and the NN model versus the experimental scour profiles measured by Adduce (2004) for the tests A2, A4, A5 and A8, respectively. As a general view from the figures, it can be said that the neural networks model predicted the scour profiles with perfect agreement (R^2=0.996, *MSE*=0.0007). Based on Figures 5.38-5.41, it can be stated that the predictions of the present hybrid model get closer to the measured ones as the discharge increases. The proposed hybrid model suffers from over-prediction of dune sections for small discharges (tests A2, A4, A5) (see Figures 5.38-5.40). Compared to Adduce (2004), we solved this problem, to some extent, by solving the non-conservative form of the scour profile equation (Eqn.(3.72). However, small discrepancies are still observed between the predictions of the present hybrid model and the measured ones (R^2=0.964, *MSE*=0.0001). The reason for this has already been stated that the present model assumes a two-dimensional scouring process, while in experimental conditions it was observed by Adduce (2004) that the scouring process is quasi-two dimensional for big discharges (tets A6-A9) and no more quasi-two-dimensional for small discharges (tets A1-A5).
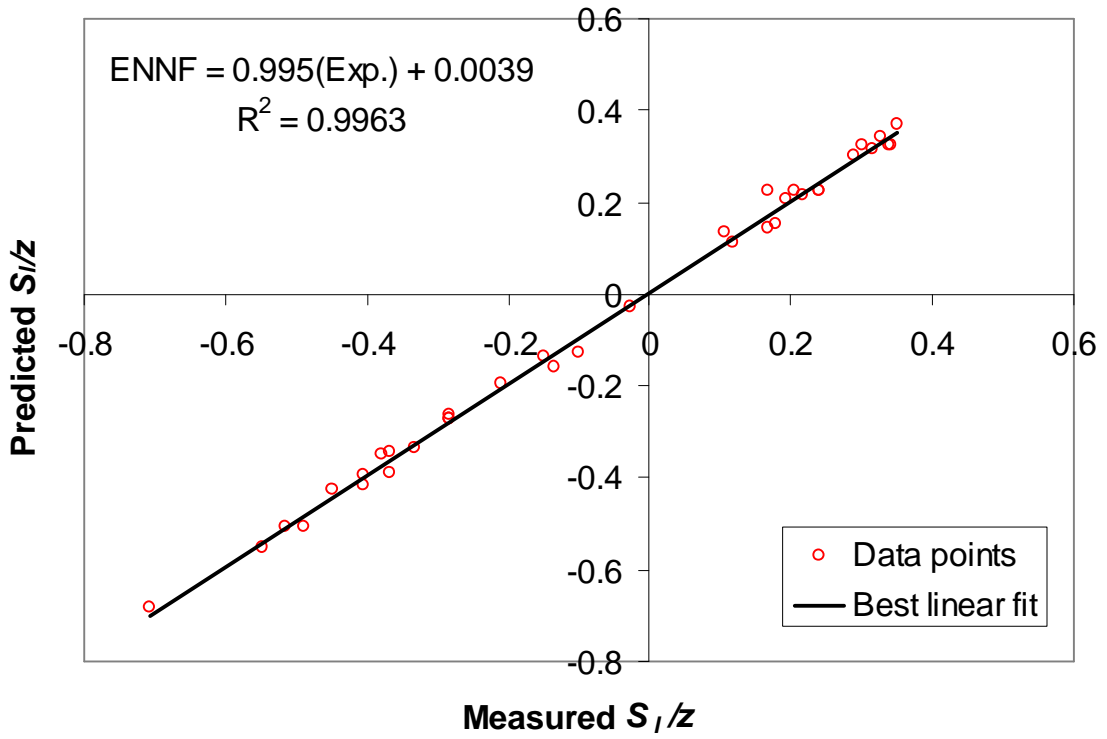
Figure 5.36 Predicted and measured S_l/z for training set
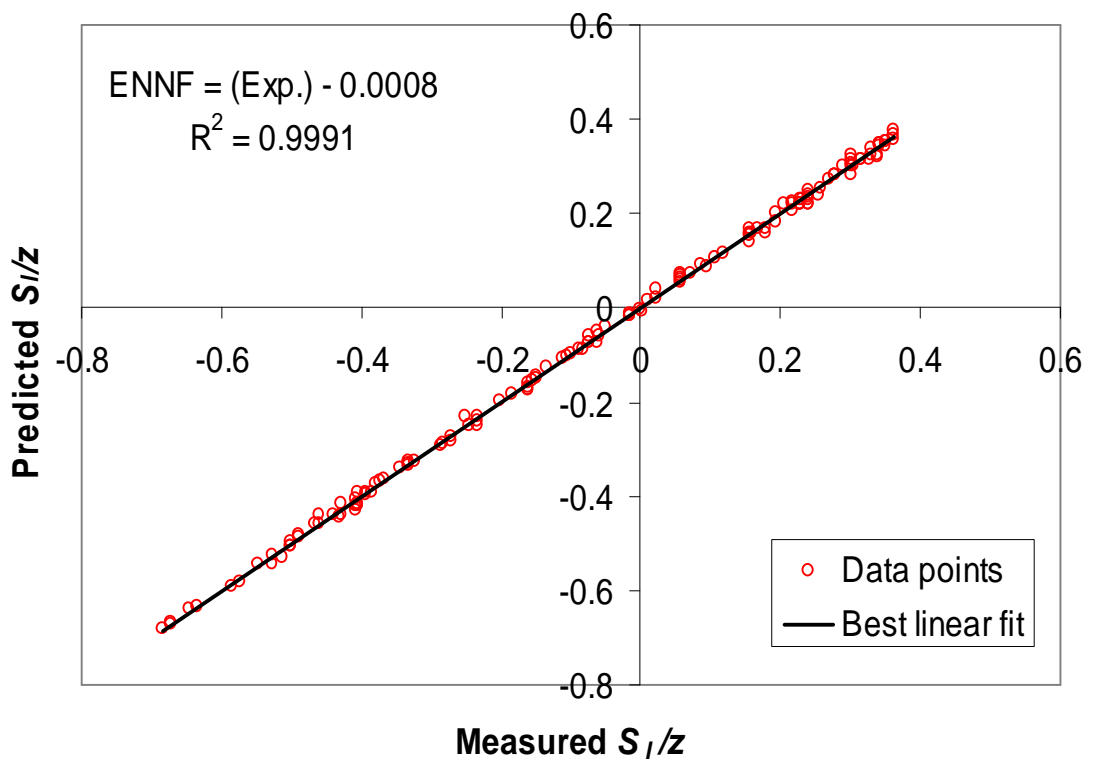
Figure 5.37 Predicted and measured S_l/z for testing set
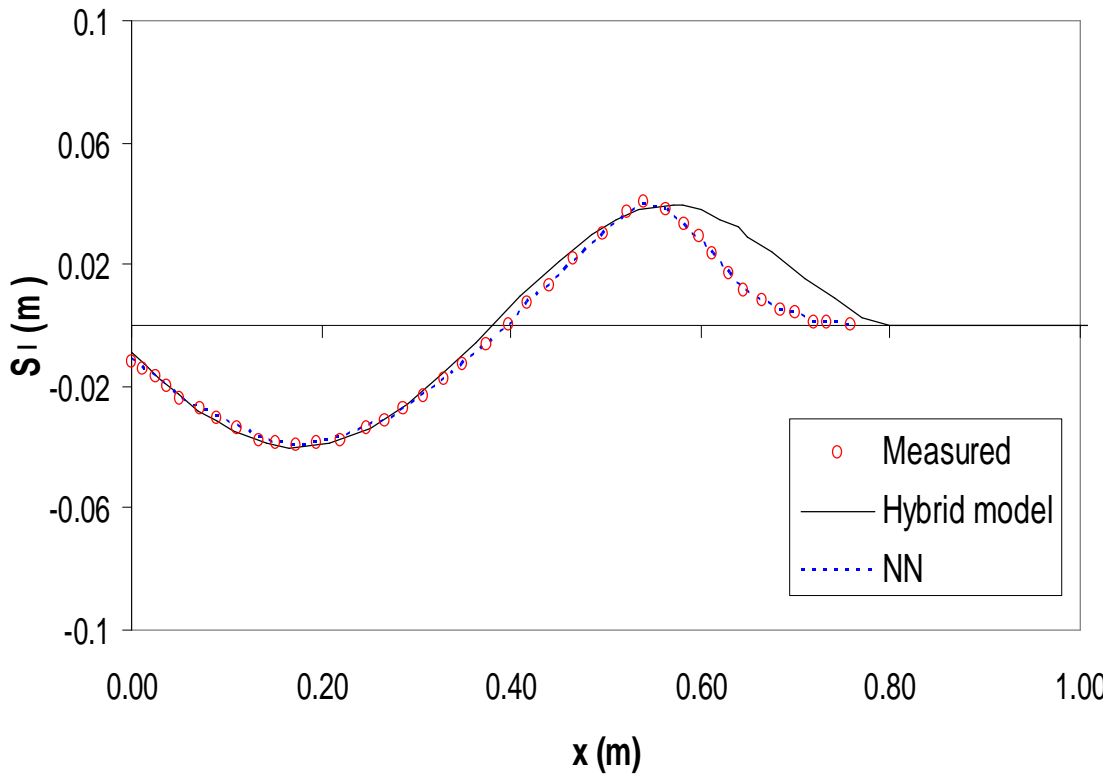
Figure 5.38 Predicted and measured scour profiles for test A2
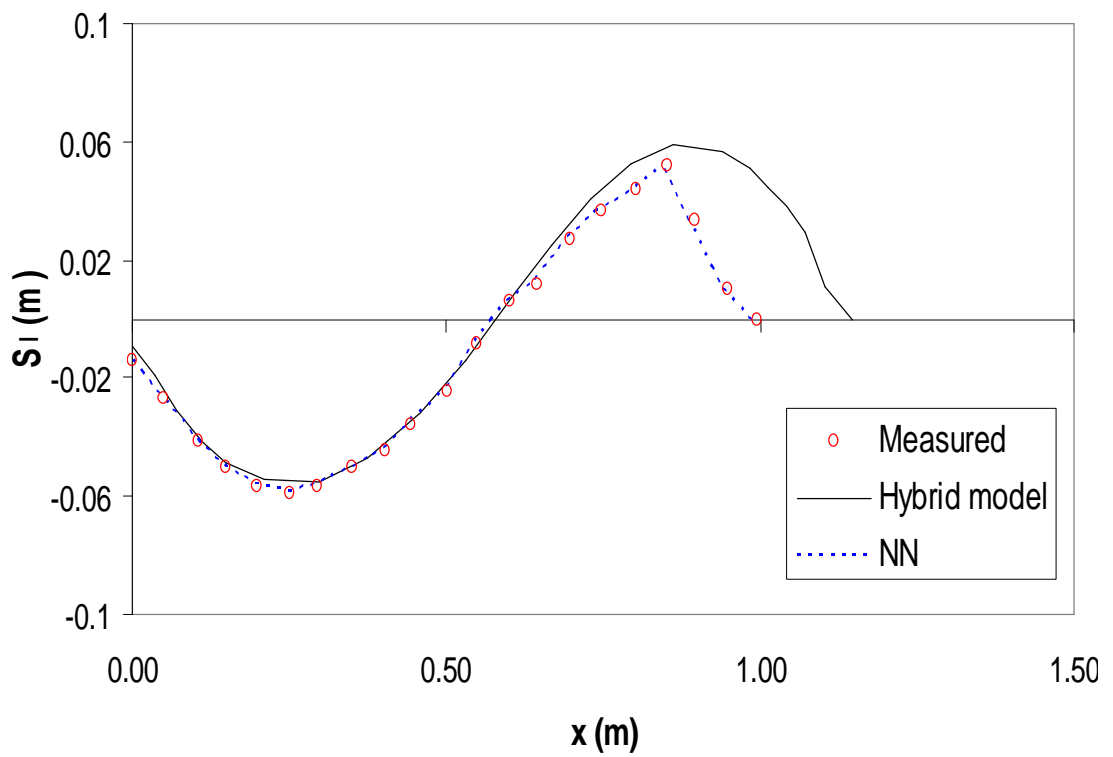
Figure 5.39 Predicted and measured scour profiles for test A4
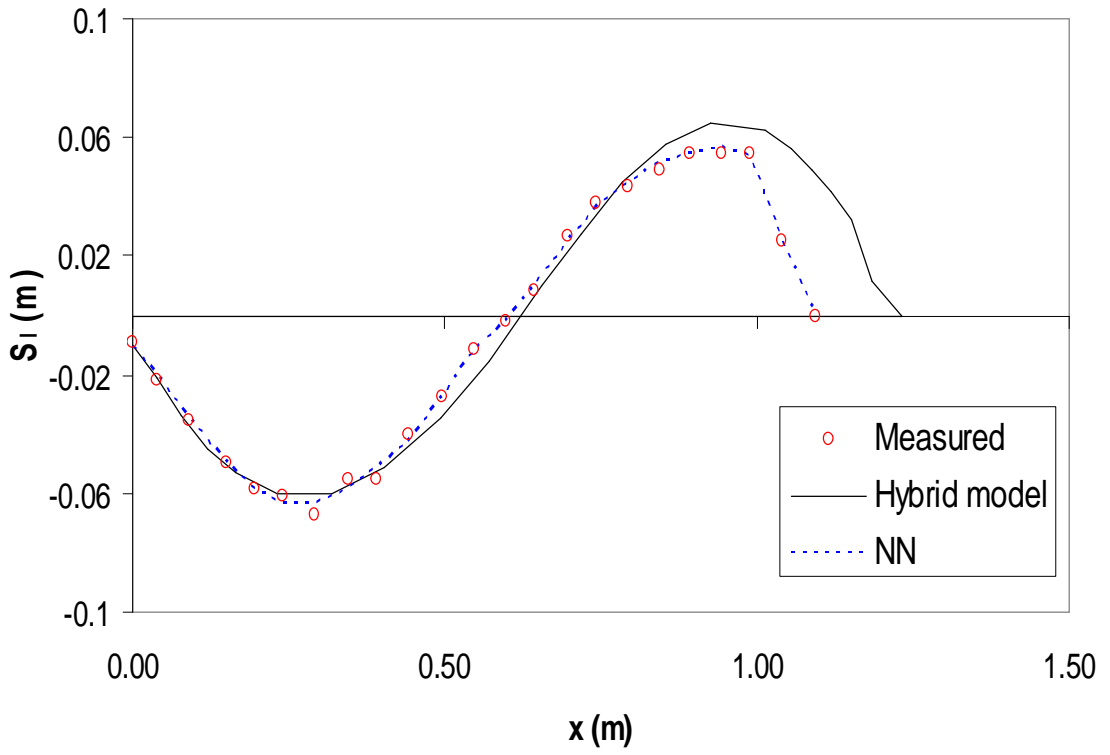
Figure 5.40 Predicted and measured scour profiles for test A5
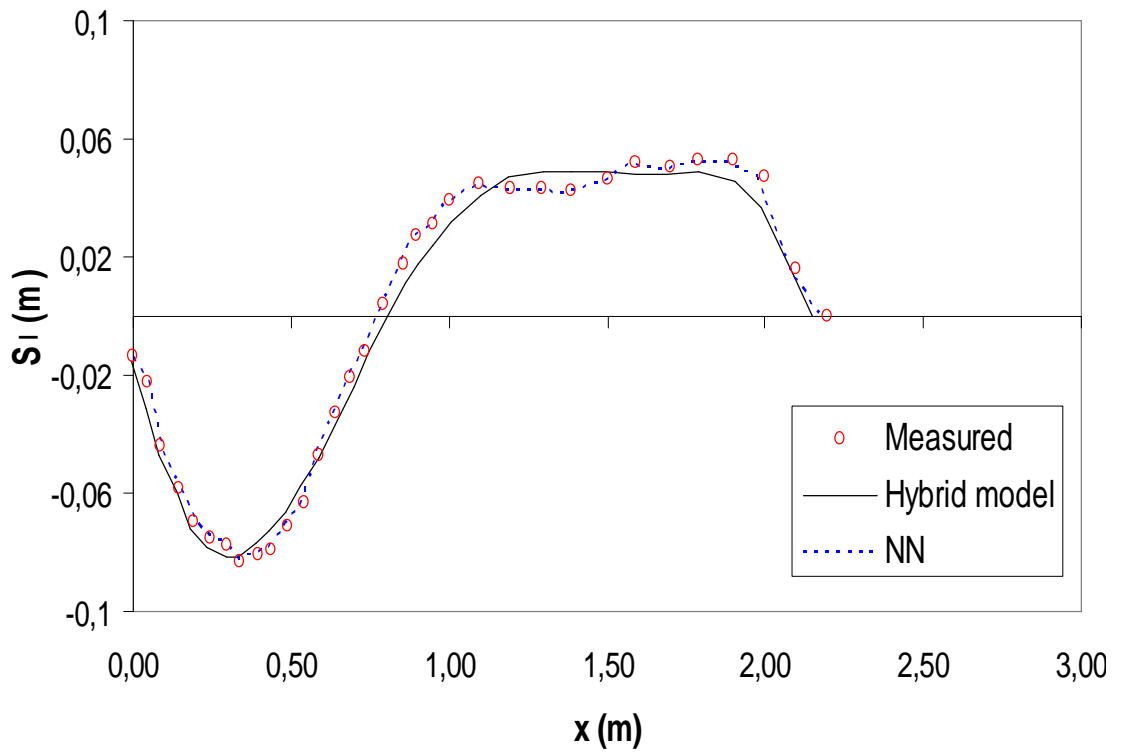
Figure 5.41 Predicted and measured scour profiles for test A8

CHAPTER 6

CONCLUSIONS AND SUGGESTIONS FOR FURTHER RESEARCH

6.1 Conclusions

The conclusions of the chapters of this thesis are as follows:

Chapter 2

Numerous researches on local scour due to turbulent jets have been carried out. Most of these studies deal with characterizing the scour process with the profile of equilibrium scour profile, maximum depth of scour and its location.

Understanding the scour process still remains a major problem in many cases. Further complexity in the flow field arises in the transition zone of the apron and the erodible bed due to the subtle change in the flow characteristics.

The literature review study revealed that the flow characteristics simulated in the laboratory differs considerably from that in the prototype due to the large-scale distortion of the model.

All the above mentioned factors act as a barrier towards a clear understanding of the local scour problems. Thus, more studies, especially large-scale model studies, are required to get answers of the problems and a comprehensive understanding the scour process.

Chapter 3

In this chapter, a literature review on numerical and analytical models of local scour downstream of hydraulic structures was performed in detail. These studies can be classified as the numerical works dealing with only the flow patterns in rigid scoured bed (Karim and Ali 2000, Gunal and Guven 2006), the numerical studies that simulate the temporal development of scour profile using k-ε turbulence modeling by relating the shape of mobile bed to a sediment-conservation model (Devantier and Larock 1986, Toro et al. 1989, Çelik and Rodi 1991, Ushijima et al. 1992, Olsen and Melaaen 1993, Olsen and Kjellesvig 1998, Garcia-Martinez, et al. 1999, Neyshabouri et al. 2001, 2004, Barron and Neyshabouri 2003), and lastly, the analytical models that analyzes directly the external forces acting on a soil particle and models the continuity equation for solid discharge (Guohou and Peisheng 1988, Hoffmans 1998, Adduce 2004, 2006, Hogg et al. 1997).

This study differs from the other studies in the literature in that our proposed hybrid model utilizes the standard k-ε turbulence modeling and an analytical model in co-operating in order to analyze the time-dependent variations in flow patterns in temporally variant mobile scour profiles. The two models can work independently for different purposes as well as they work in co-operation in harmony.

The validation of both models, separately, revealed very good agreements with the measured ones driven from the experimental studies from the literature. This proved the efficiency in modeling such complex hydraulic problems, and they promised to work well when used in co-operation. The performance of the hybrid model that contains these two models is discussed in Chapter 5.

Chapter 4

Recent developments in soft computing techniques (artificial neural networks, genetic programming, fuzzy logic, etc.) have produced high potential in simulating physical processes, based on measured data. Literature review on soft computing applications in hydraulic engineering revealed that the early studies only goes back

to a decade ago, pioneered by Karunanithi and co-workers in 1994 in predicting the river flow (Karunanithi et al. 1994).

In this chapter, two branches of soft computing technique, namely artificial neural networks and genetic programming, were proposed as new approaches to prediction of depth and location of maximum scour depth, as alternative to more conventional regression based analysis. The calibration and the validation of the proposed models were carried out using experimental and field data taken from other researches. Also the explicit formulations of the proposed models are presented in order to give opportunity to the interested researchers to use these formulations in preliminary design of hydraulic structures, in which the maximum scour depth is not considered as a design parameter.

The proposed explicit formulations were compared with regression based empirical equation of others and the results exhibited that explicit neural networks formulation (ENNF) predicted the local scour parameters with the highest accuracy and the lowest error. Gene-expression programming (GEP) based formulations did also show quite better results compared to other equations but relatively worse than (ENNF), however, the GEP formulations are shorter and more practical than those of ENNF.

Comparison of ENNF, GEP and the other equations in predicting the field data revealed that predictions of ENNF are quite better than to other formulations while considering the correlation coefficient (R=0.94, MAPE=9.76), whereas the GEP formulation predicted the field data with the lowest error (R=0.93, MAPE=8.66). In general view, the proposed formulations showed quite dominant performance against the equations of others (R=0.73, MAPE =10.13 for Eqn.(4.11) and R=0.48, MAPE=21.3 for Eqn.(4.18)).

Chapter 5

This chapter presents the validation results of the proposed hybrid numerical-analytical model with experimental data of others, and also numerical predictions of other researchers.

In this study, the calibration and evaluation of the proposed hybrid model was carried out using a huge amount of experimental data taken from most recent two Ph.D. works (Kurniawan, 2003 and Adduce, 2004) and a number of experimental researches. The details on these experimental studies are presented in this chapter. This experimental data contains temporal evolution of local scour process and also the flow patterns in scoured zone, in asymptotic state.

The proposed hybrid model was run for 9 tests of Adduce (2004), 8 tests for Kurniawan (2003) and the experimental conditions of Ali and Lim (1986). Although the physical domain for each test is different from each other, the solution domain is observed to be always rectangular and uniform, in which a boundary-fitted coordinate system is used (see Figures 51-5.3).

The models were run for the experimentally observed asymptotic state durations. The decay of the error of the present vs. iteration number showed a fluctuation during the early iterations and then a gradually variation for the rest of the total iteration number. As a general trend of the error decays presented in Figure 5.4, the error lines decline with increasing iteration number.

The temporal evolution of scour profile predictions of the present model revealed that, initially flat bed surface starts to be eroded very fast during initial time (t<1/2 T). During this stage, the scour profile develops very fast in vertical state, and much faster than the dune section, which is also experimentally observed by Adduce (2004) and Kurniawan (2003). Towards the equilibrium state, the rate of scour diminishes and approaches zero ($dS_{max}/dt \cong o$). Especially for small discharges, the present model over-predicted the dune sections, compared to the measured ones. This event is also observed by the corresponding experimental researchers, and can be explained by the fact that the present hybrid model assumes a 2-dimensional scouring process, while in nature, it is quasi-2-dimensional for big discharges and not quasi-2-dimesional for small discharges. However, as a generalization, the present hybrid model predicted the scour profiles with quite good agreement with the measured ones and much better than the predictions of Adduce (2004) (see Figures 5.8-5.12).

The present model's predictions of maximum scour depth and length of maximum scour for experimental conditions of Kurniawan (2003), given in Table 5.2, were observed to be dominantly better than the predictions of the others, and in strictly good agreement with the measured ones (see Table 5.4).

The predicted dimensionless velocity distribution over the scoured zone for $XS<x<L_s$, for the test conditions of Adduce (2004) showed a classical "wall jet" distribution, when the velocities and the vertical distances are properly non-dimensionalized. Also, The predicted dimensionless velocity distributions over $XS<x<L_s$ were close to the theoretical curve offered by Rajaratnam (1976) (see Figures 5.15-5.17).

The predicted velocity vector field for the tests A2, A4, A5, and A9 are illustrated in Figures 5.18-5.21. Although it is not clearly seen, the formation of reverse flow and vortice in maximum scour depth region and also, reverse flow near free surface profile for 0<x<0.3 m are observed.

The predicted velocity distribution over the rigid apron and the scoured zone, for the tests A2 and A5 by Adduce (2004) are in strictly good agreement with the measured ones. As a general view form the Figures 5.22-5.25, the u-velocities were observed to be higher than the v-velocities. The predicted velocity distributions for $0<x<XS$ showed a free-jet like behavior, while for $XS<x<L_s$ and -0.4<x<0, the predicted velocity distribution confirmed with the classical wall-jet distribution, as also experimentally observed by Adduce (2004). In maximum scour depth negative velocities were observed near to the bed surface, although it is not clearly seen from the Figures 5.22 and 5.24. This proves that the flow entering the scour profile impinges on the bed in maximum scour depth region and the flow separates in opposite directions, and a reverse-flow occurs towards upstream. This event has been experimentally observed by several researches (Chatterjee and Ghosh 1980, Ali and Lim 1986, Kurniawan 2003, Dey and Westrich 2003, Adduce 2004, Hill and Younkin 2006).

The predicted Reynolds stress distributions over the rigid apron and the scoured zone were in strictly good agreement with the measured ones (see Figures 5.26-5.29).

The predicted $\sqrt{u'^2}$ values were observed to be nearly two times the $\sqrt{v'^2}$ ones ($\sqrt{u'^2} = 1.6\sqrt{v'^2}$), which prove that turbulent flow is the non-isotropic.

The numerical predictions of present model and FLUENT commercial software to the measured ones by Ali and Lim (1986) showed that the both predictions are in quite good agreement with the measured ones (see Figures 5.30-5.34). The predictions of the present model to the measured temporal scour profiles proved again the well-performance of the model with relatively very small errors, especially in maximum scour depth and maximum scour length regions. One interesting and a promising result was observed that the experimental bed shear stress distribution of Ali and Lim (1986) fell between the predictions of present model and those of FLUENT RNG model. However, the present model suffered from under-prediction of bed shear stress, for negative values. The predicted dimensionless velocity profiles for XS<x<Ls were observed to be in good agreement with those of FLUENT, and both predictions were very close to the theoretical curve (see Figure 5.32).

A neural networks model was developed, which simulates the asymptotic scour profiles for the tests given in Table 5.1. The training and validation results of the proposed NNs model showed perfect agreement between the predictions of NNs and the measured ones (see Figures 5.32-5.33). Also, the explicit form of the proposed NNs model (ENNF) was offered in order for the interested researchers to use in preliminary local scour estimations. The predictions of the proposed NNs and those of present hybrid model showed that NNs predicted the scour profiles relatively better that the hybrid model, especially in dune sections. In fact, the good performance of NNs in prediction of hydraulic data is not surprising, but the use of NNs and its explicit form, ENNF is very promising in complex hydraulic problems such as scouring, in which conventional regression analysis and other analytic methods are observed to be almost useless.

The above-mentioned results of this chapter prove the efficiency of the proposed hybrid numerical-analytical and the NNs model in simulation of complex scouring process, and promise the use of these techniques in very complex hydraulic engineering problems such as turbulence modeling, sediment transportation and wall shear stress distribution, etc.

6.2 Suggestions for Further Research

A possible future development of the proposed hybrid model may be considering the suspended sediment and bed load together and improvement of the analytical model part according to this perspective.

Another one is to carry out the experimental measurements of bed-shear stress distribution in scoured zone and carry out experimental study and observe the effect of vortices on sediment transport near bed surface. A numerical model may be developed, which simulates the bed shear stress distribution under combined effect of vortices and the turbulence near bed.

In this thesis, we presented the use of a hybrid model, which is a combination of an analytic model and an implicit numerical model and a new approach, so-called soft computing. A further development of this study may be integrating the numerical modeling and the soft computing techniques, especially where the numerical models suffer from the use of some empirical models (equations), which are developed based on conventional regression analysis.

REFERENCES

Ade, F. and Rajaratnam, N. (1998). Generalized study of erosion by circular horizontal turbulent jets. *J. Hydraulic Research*, **36**(4), 613-635.

Aderibigbe, O. and Rajaratnam, N. (1996). Erosion of loose beds by submerged circular impinging vertical turbulent jets. *J. Hydraulic Research*, **34**(1), 19-33

Aderibigbe, O. and Rajaratnam, N. (1998). Effect of sediment gradation on erosion by plane turbulent wall jets. *J. Hydraulic Engineering*, ASCE, **124**(10), 1034-1042.

Adduce, C. (2004). Local scour downstream of a turbulent jet. PhD thesis, Department of Civil Engineering, University of Roma Tre, Italy.

Adduce, C. and Sciortino, G., (2006). Scour due to a horizontal jet: Nuemrical and experimental investigation. *Journal of Hydraulic Res*earch, **44**(5), 663-673.

Akaike, H. (1973). Information theory and an extension of the maximum likelihood principle. In B. N. Petrov and F. Csaki (Editors.), *Second International Symposium on Information Theory*, Academiai Kiado, Budapest, 267-281.

Akashi, N. and Saito, T. (1984). Estimation of equilibrium scour depth from submerged impinged jet. *Proceedings of 15th IAHR Cong*ress, Thailand, pp. 167-181.

Ali, K. H. M. and Lim, S. Y. (1986). Local scour caused by submerged wall jets. *Proceedings of Institution of Civil Engineers*, **81**(2), 607-645.

Ali, K. H. M. and Neyshaboury, A. A. S. (1991). Localized scour downstream of a deeply submerged horizontal jet. *Proceedings of Institution of Civil Engineers*, **91**(2), 1-18.

Altinbilek, H. D. and Okyay, S. (1973). Localized scour in a horizontal sand bed under vertical jets. *Proceedings of 15th IAHR Cong*ress, Istanbul, Vol. 1, 99-106.

Azinfar, H., Kells, J.A. and Elshorbagy, A. (2004). Use of artificial neural networks in prediction of local scour. *Proc. 32nd Annual General Conference of the Canadian Society for Civil Engineers*, GC-350, 1-10.

Azmatullah, H. MD., Deo, M.C., and Deolalikar, P.B. (2005). Neural networks for estimation of scour downstream of a Ski-Jump Bucket. *J. Hydraul. Eng.*, **131**(10), 898-908.

Azmatullah, H. MD., Deo, M.C., and Deolalikar, P.B. (2006). Estimation of scour below spillways using neural networks. *J. Hydraul. Res.*, **44**(1), 61-69.

Babovic, V., Keijzer, M., Aguilera, D. R., and Harrington, J. (2001a). An evolutionary approach to knowledge induction: Genetic programming in hydraulic engineering. *Proc., World Water & Environmental Resources Congres*s, Orlando, FL, USA, May 21–24.

Babovic, V. M. Keijzer, D. R. Aguilera, and Harrington, J. (2001b). Automatic Discovery of Settling Velocity Equations. *D2K Technical Report*, D2K-0201-1.

Balachandar, R. and Kells, J. A. (1997). Local channel scour in uniformly graded sediments: the time-scale problem. *Canadian Journal of Civil Engineering*, **24**(5), 799-807.

Balachandar, R. and Kells, J. A. (1998). Instantaneous water surface and bed scour profiles using video image analysis. *Canadian Journal of Civil Engineering*, **25**(4), 662-667.

Balachandar, R., Kells, J. A. and Thiessen, R. J. (2000). The effect of tailwater depth on the dynamics of local scour. *Canadian Journal of Civil Engineering*, **27**(1), 138-150.

Barron, R.M and Salehi Neyshabouri, A.A. (2003). Numerical Simulation of Scour by a Wall Jet Downstream of a Solid Apron. *International Conference on Computational Fluid Dynamics*, May 28 – 30, Vancouver, BC.

Bateni, S.M., Borghei, S.M. and Jeng, D.-S. (2007). Neural network and neuro-fuzzy assessments for scour depth around bridge piers. *Engineering Applications of Artificial Intelligence*, **20**, 401–414.

Baxter C.W., Zhang, Q. S., Stanley, J. R., Shariff, R., Tupas, R.T., and Stark, H.L. 2001. Drinking water quality and treatment: the use of artificial neural networks. Can. J. of Civ. Eng., **28**(S1): 26-35.

Baykasoğlu, A., Güllü, H., Çanakçı, H., and Özbakır, L. (2007). Prediction of compressive and tensile strength of limestone via genetic programming. *Expert Systems with Applications* (In Press).

Beltaos, S. (1972). Normal impingement of plane turbulent jets on smooth walls. MS thesis, Univ. of Alberta, Edmonton, Alberta, Canada.

Beltaos, S. (1974). Turbulent impinging jets. PhD thesis, University of Alberta, Edmonton, Alberta, Canada.

Beltaos, S. (1976a). Oblique impingement of plane turbulent jets. *J. Hydr. Div.*, ASCE, **102**(HY9), 1177-1192.

Beltaos, S. (1976b). Oblique impingement of circular turbulent jets. *J. Hydraulic Research*, **14**(1), 17-36.

Beltaos, S. and Rajaratnam, N. (1973). Plane turbulent impinging jets. *J. Hydraulic Research*, **11**(1), 29-59.

Beltaos, S. and Rajaratnam, N. (1974). Impinging circular turbulent jets. *J. Hydaulic Division*, ASCE, **100**, (HY10), 1313-1328.

Beltaos, S. and Rajaratnam, N. (1977). Impingement of axisymmetric developing jets. *J. Hydraulic Research*, **15**(4), 311-325.

Benim, A.C.and Zinser, W. (1985). Investigation into the Finite Element Analysis of Confined Turbulent Flows using a k-e Model of Turbulence. *Computer Methods in Applied Mechanics and Engineering*, **51**, 507-523.

Blaisdell, F. W. and Anderson, C. L. (1991). Pipe plunge pool energy dissipator. *J. Hydraulic Engineering*, ASCE, **117**(3), 303-323.

Blaisdell, F. W., Anderson, C. L. and Hebaus, G. G. (1981). Ultimate dimensions of local scour. *J. Hydaulic Div*ision, ASCE, **107**(3), 327-337.

Bormann, N. E. and Julien, P. Y. (1991). Scour downstream of grade-control structures. *J. Hydraulic Engineering*, ASCE, **117**(5), 579-594.

Breusers, H. N. C. (1965). Conformity and time scale in two-dimensional local scour. *Publ. 40, Delft Hydraulics Lab*oratory, Delft, The Netherlands.

Breusers, H. N. C. (1966). Conformity and time scale in two-dimensional local scour. *Proceedings of Symposium on Model Prototype Conformity*, Poona, India, pp. 1-8.

Breusers, H. N. C. (1991). *Scour by jets*. Hydraulic Structures Design Manuual, No. 2, Balkema, Rotterdam.

Breusers, H. N. C. and Raudkivi, A. J. (1991). *Scour*. IAHR Hydraulic Structures Handbook, Vol. 2, Taylor&Francis Group, London.

Carstens, M. R. (1966). Similarity laws for localized scour. *J. Hydraulic Div*ision, ASCE, **92**(HY3), 13-36.

Chatterjee, S. and Ghosh, S. (1980). Submerged horizontal jet over erodible bed. *Journal of Hydraulic Division*, **11**, 1765–1782.

Chatterjee, S. S., Ghosh, S. N. and Chatterjee, M. (1994). Local scour due to submerged horizontal jet. *J. Hydraulic Engineering*, ASCE, **120**(8), 973-992.

Chee, S. P. and Yuen, E. M. (1985). Erosion of unconsolidated gravel beds. *Canadian Journal of Civil Engineering*, **12**, 559-566.

Chatterjee, S. S., Ghosh, S. N. and Chatterjee, M. (1994). Local scour due to submerged horizontal jet. *J. Hydraulic Engineering*, ASCE, **120**, 973–992.

Chen, Y.S. and Kim, S.W. (1987). Computation of turbulent flows using an extended k–ϵ turbulence closure model. *NASA* (CR-179204).

Chian, M. W. (1973). Scour at downstream end of dams in Taiwan. *Proceedings of IAHR Symposium on River Mechanics*, Bangkok, Vol. 1, pp. 137-142.

Clarke, F. R. W. (1962). The action of submerged jets on moveable material. PhD thesis, Imperial College, London.

Cola, R. (1965). Energy dissipation of a high velocity vertical jet entering a basin. *Proc. 11th IAHR* Congress, Leningrad, Vol. 1, paper 1.52.

Çelik, I. and Rodi, W. 1991. Suspended sediment-transport capacity for open channel fow, *J. Hydraulic Enineering.*, **117**, 191-204.

D'Agostino, V. (1994). Indagina sullo scavo a valle di opera trasversali mediante modello fisico o fondo mobile. *Energ. Elettr.*, **7**1(2), 37-51 (In Italian)

D'Agostino, V. and Ferro, V. (2004). Scour on alluvial bed downstream of grade-control structures. *J. Hydraulic Engineering*, **130**(1), 24-36.

Damle, P. M., Venkatraman, C. P. and Desai, S. C. (1966). Evaluation of scour below ski-jump buckets of spillways. *Golden Jubilee Symp*osium, Poona, India, pp. 154-163.

Dargahi, B. (2003). Scour development downstream of a spillway. *J. Hydraulic Research*, **41**(4), 417-426.

Dey, S. and Westrich, B. (2003). Hydraulics of submerged jet subject to change in cohesive bed geometry. *J. Hydraulic Engineering*, ASCE, **129**(1), 44-53.

Dietz, J. W. (1969). Kolkbildung im feinem oder leichter sohlmaterialen bei stromenden abfluss. Mitt. Theoder Rehbock Flussbaulab, Karlsruhe, Heft. 155, pp. 1-119.

Devantier, B. A., and LaRock, B. E. (1986). Modeling a recirculation density driven turbulent flow. *International Journal for Numerical Methods in Fluids*, **6**(4), 241-253.

Doddiah, D., Albertson, M. L. and Thomas, R. (1953). Scour from jets. *Proceedings of 5th IAHR Cong.*, Minneapolis, pp. 161-169.

Dolling, O. R., and Varas, E. A. (2002). Artificial neural networks for streamflow prediction. *J. Hydraulic Research*, **40**(5), 547-554.

Dorado, J., Rabunal, J.R., Pazos, A., Rivero D., Santos, A., and Puertas, J. (2003). Prediction and Modelling of the Rainfall-Runoff Transformation of a Typical Urban Basin Using ANN and GP. *Applied Artificial Intelligence*, **17**, 329-343.

Eggenberger, W. and Mueller, R. (1944). Experimentelle und theoretische untersuchungen ueber das kolkproblem, Mitteil, Versuchsanstalt f. Wasserbau, Zurich, CH, No. 5.

Fahlbusch, F. E. (1994). Scour in rock riverbeds downstream of large dams. *Hydropower and Dams,* **1**(4), 30-32.

Farhoudi, J. and Smith, K. V. H. (1982). Time scale for scour downstream of hydraulic jump. *J. Hydralic Division*, ASCE, **108**(HY10), 1147-1162.

Farhoudi, J. and Smith, K. V. H. (1985). Local scour profiles downstream of hydraulic jump. *J. Hydraulic Research*, **23**(4), 343-358.

Ferreira C. (2001a). Gene expression programming in problem solving. *Proc., 6th Online World conference on Soft Computing in Industrial Applications* (invited tutorial).

Ferreira C. (2001b). Gene expression programming: A new adaptive algorithm for solving problems. *Complex Systems*, **13**(2), 87–129.

Ferreira C. (2002). *Gene expression programming: Mathematical modeling by an artificial intelligence*. 2nd Edition, Springer-Verlag, Germany

Flood, I. (1989). A Neural Network approach to the sequencing of construction tasks. *Proceedings of 6th Conference of SARC*, San Francisco, USA.

FLUENT USER's Guide, (1993). Fluent Incorporated, Lebanon, New Hampshire, U.S.A.

Fuchs, M., (1998). Crossover versus mutation: An empirical and theoretical case study", *Proceedings of the 3rd Annual Conference on Genetic Programming*, Morgan-Kauffman.

Garcia, R. and Kahawita, R.A. (1995). Numerical solution of the St. Venant equations with the Mac-Cormack finite difference scheme. *International journal for numerical methods in fluids*, **6**, 259-274.

Garcia-Martinez, R., I. Saavedra, B. F. De Power and Valera E. (1999). A two-dimensional computational model to simulate suspended sediment transport and bed changes. *Journal of Hydraulic Research*, **37,** 327-344.

Glauert M. B. 1956. The wall jet. *Journal of Fluid Mechanics*. **1**.

Graf, W. H. (1998). *Fluival Hydraulics*. John Wiley and Sons Ltd., England.

Giustolisi, O. (2004). Using genetic programming to determine Chezy resistance coefficient in corrugated channels. *J. Hydroinformatics*, 157-173.

Grubert, J. P. (1995). Application of Neural Networks in Stratified Flow Stability Analysis. J. Hydraulic Engineering, **121**(7), 523-532.

Gunal, M. and Guven, A. (2006). Prediction of flow patterns in scoured zone. *Canadian Journal of Civil Engineering*, **33**(1), 41-48.

Gunal, M., (1996). Numerical and Experimental Investigations of Hydraulic Jumps. Ph.D. Thesis, University of Manchester, Institute of Science and Technology.

Gunal, M., and Narayanan, R. (1998). k-ε turbulence modeling of submerged hydraulic jump using boundary-fitted coordinates. *Proceedings of the Institution of Civil Engineers Water, Maritime and Energy*, **130**, 104-114.

Guohou, J, and Peisheng G. (1988). Mathematical model of river bed scouring downstream of stilling basin. *J. Hydraulic Engineering,* **114**(4), 9-16.

Guven, A. (2003). "Local scour beneath turbulent jets". M.Sc. Thesis, Department of Civil Engineering, University of Gaziantep.

Hanjalic, K. (1970). Two Dimensional Asymmetrical Turbulent Flow in Ducts. Ph.D. Dissertation, University of London, London, U.K.

Hanjalic, K., and Launder, B.E. (1972). A Reynolds Stress model of turbulence and its application to this shear flows. *J. Fluid Mechanics*, **52**, 609-616.

Harlow, F.H., and Nakayama, P.I. (1968). Transport of turbulence energy decay rate. LA-3854, Los Alamos Science Lab., U. California, USA.

Hartung, W. (1957). Die Gesetzmassigkeit der kolkbildung hinter uberstromten wehren. Thesis, Technical University of Braunschweig.

Hartung, F. and Hausler, E. (1973). Scours, stilling basins and downstream protection under free overfall jets at dams. *Proceedings of 11th International Congress on Large Dams*, Madrid, Vol. 2, pp 39-56.

Hassan, N. M. K. N. and Narayanan, R. (1985). Local scour downstream of an apron. *J. Hydraulic Engineering*, ASCE, **111**(11), 1371-1385.

Haykin, S. (2000). *Neural Networks- A Comprehensive Foundation*. Macmillan College Publications Cooperation.

Hebb, D.O. (1949). *The Organization of Behaviour*. Wiley, New York.

Hecht-Nielsen R. (1990). *Neurocomputing. Reading*. (MA): Addison-Wesley.

Hill, D.F. and Younkin, B.D. (2006). PIV measurements of flow in and around scour hole. Experiments in Fluids, **41**, 295-307

Hoffmans, G. J. C. M. and Verheij (1997). *Scour manual*. A. A. Balkema, Rotterdam.

Hoffmans, G.J.C.M. (1998). Jet scour in equilibrium phase. *Journal of Hydraulic Engineering*, **124**(4), 430-437.

Hoffmans, G.J.C.M. and Booij, R. (1993). Two dimensional mathematical modeling of local scour holes. *J. Hydraulic Research*, **31**(5), 615-634.

Hogg, A. J., Huppert, H. E. and Dade, W. B. (1997). Erosion by planar turbulent wall jets. *J. Fluid Mech*anic, **338**, 317-340.

Hopfield, J. (1982). Neural networks and physical systems with emergent collective computational abilities. *Proceedings of the National Academy of Sciences of the USA*, 9 (2554).

Hun, D. and Changha H. (2004). A brief introduction to soft computing. *Proceedings of the Autumn Conference*, Korean Statistical Society, pp. 65–66.

Jaeger, C. (1939). Uber die ahnlichkeit bei flussbaulichen modellversuchen. *Wasserwirtschaft und Wassertecknik*, **34**(32/27), pp. 269.

Jaw, S. Y. (1991). Development of an Anisotropic Turbulence Model for Prediction of Complex Flows. Ph.D. Dissertation, Department of Mechanical Engineering, The University of Iowa, Iowa City, IA, U.S.A.

Jia, Y., Kitamura, T. and Wang. S. S. Y. (2001). Simulation of scour process in plunging pool of loose bed-material. *Journal of Hydraulic Engineering*, **127**(3), 219-229.

Johnston, A. J. (1990). Scourhole developments in shallow tailwater. *J. Hydraulic Research*, **28**(3), 341-354.

Kalogirou, S. (1999). Applications of Artificial Neural Networks in Energy Systems: A Review. *Energy Conversion and Management*, **40**(3), 1073-1087.

Karim, O.A. (1996). Prediction of two and three dimensional turbulent flows. Ph.D.Thesis, University of Liverpool.

Karim, O.A. and Ali, K.H.M. (2000). Prediction of flow patterns in local scour caused by turbulent water jets. *J. Hydraulic Res*earch, **38**(4), 279-287.

Karunanuthi, N., Grenney, W.J., Whitley, D., and Bovee, K. 1994. Neural Networks for river flows prediction. J. *Computing in Civil Engineering*, ASCE, **8**(2): 201-219.

Keijzer, M. and Babovic, V. (2002). Declarative and preferential bias in GP-based scientific discovery. *Genetic Programming and Evolvable Machines*, **3**(1), 41-79.

Kells, J. A., Balachandar, R. and Hagel, K. P. (2001). Effect of grain size on local channel scour below a sluice gate. *Canadian Journal of Civil Engineering*, **28**(3), 440-451.

Kobus, H., Leister, P. and Westrich, B. (1979). Flow field and scouring effects of steady and pulsating jets impinging on a movable bed. *J. Hydraulic Research*, **17**(3), 175-192.

Koivo H. (2000). *Soft computing in dynamical systems*. Helsinki.

Koza J.R. 1992. *Genetic programming: On the programming of computers by means of natural selection*. MIT Press, Cambridge, MA.

Kotoulas, D. (1967). Das kolkproblem in rahmen der wildbachverbauung mitteil. Schweizer Anstalt f. Forstliches Versuchswesen, Vol. 43(1).

Kurniawan, A. (2001). Flow pattern of an eroding jet. *29th IAHR Biennial Congress International Association for Hydraulic Research*, Beijing, China.

Kurniawan, A. (2003). Experimental study of local scour by a plane jet issuing from a sluice gate. PhD thesis, Environmental Hydraulics Laboratory, Technical University of Lausanne.

Lam, C.K.G. and Bremhorst, K.A. (1981). Modified form of k–ε model for predicting wall turbulence. *Journal of Fluids Engineering*, ASME, **103**, 456–460.

Lane, E. W. and Kalinske, A.A. (1941). Engineering calculations of suspended sediment. *Trans. Am. Geophys. Union*, **2**, 603-607.

Launder, B. E., A. Morse, W. Rodi, and D. B. Spalding (1972). A comparison of performance of six turbulence models. *Proceedings of NASA Conference on Free Shear Flows*, Langley, VA, U.S.A.

Launder, B.E., and Spalding, D.B. (1974). The numerical computation of turbulent flows. *Computational Methods in Applied Mechanics and Engineering*, **3**, 269-289.

Laursen, E.M. (1952). Observations on the nature of scour. *Proc. 5th Hydr. Conf. Studies in Engineering*, Bull. 34, University of Iowa, Iowa City, Iowa, pp 179-197.

Lenzi, M.A. and Comiti, F. (2003). Local scouring and morphological adjustments in steep channels with check-dam sequences. *Geomorphology*, 55, 97–109.

Levitt, R.E., Kartam, N.A., Kunz, J.C. (1988). Artificial intelligence techniques for generating construction project plans. J. *Construction Eng. and Management*, ASCE, **114**(3), 329-343.

Lim, S.Y. (1985). Scour and particle diffusion caused by water jets", Ph.D. Thesis, University of Liverpool, U.K.

Lim, S. Y. and Chin, C. O. (1992). Scour by circular wall jets with nonuniform sediments. *Advances in. Hydroscience Engineering*, **1**, 1989-1994.

Liriano, S.L. and Day, R.A. (2002). Prediction of scour depth at culvert outlets using neural networks. *J. Hydroinformatics*, **3**(4), 231-238.

Liu, W., and James, C.S. (2000). Estimation of discharge capacity in meandering compound channels using neural networks. *Canadian Journal of Civil Engineering*, **27**, 297-308.

Long, D., Steffler, P.M. and Rajaratnam, N., (1991). A numerical study of submerged hydraulic jumps. *IAHR, J. Hydraulic Research*, **29**(3), 293-308.

Lopes, H.S. and Weinert, W.R. (2004). A gene expression programming system for time series modeling. *Proceedings of XXV Iberian Latin American Congress on Computational Methods in Engineering*, Recife, Brazil (CD-Rom)

Luke, S., and L. Spector. (1998). A revised comparison of crossover and mutation in Genetic Programming. *Proceedings of the 3rd Annual Conference on Genetic Programming*, Madison, WI: Morgan-Kauffman.

Maier, H.R. and Dandy, G.C. (2000). Neural networks for forecasting of water resources variables; a review of modeling issues and applications. *Environmental Modeling and Softwatre*, **15**, 101-124.

Marion, A., Lenzi, M.A., and Comiti, F. (2004). Effect of sediment size grading and sill spacing on scouring at grade-control structures. *Earth Surface Processes and Landforms*, **29**(8), 983–993.

Martins, R. (1973). Contribution to the knowledge on the scour action of free jets on rocky river beds. *Proc. 11th Int. Cong. Large Dams*, Madrid, Spain, Vol. 2, pp 799-814.

Martins, R. (1975). Scouring of rocky river beds by free jet spillways. *International Water Power Dam Constr*uction, **27**(4), 152-153.

Mason, P. J. and Arumugam, K. (1985). Free jet scour below dams and flip buckets. *J. Hydraulic Engineering*, ASCE, **111**(2), 220-235.

Mazurek, K. A. (2001). Scour of clay by jets. PhD thesis, University of Alberta, Edmonton, Alberta, Canada.

Mazurek, K. A., Rajaratnam, N. and Sego, D. C. (2001). Scour of cohesive soil by submerged circular turbulent impinging jets. *J. Hydraulic Engineering*, ASCE, **127**(7), 1-9.

Mazurek, K. A., Rajaratnam, N. and Sego, D. C. (2003). Scour of a cohesive soil by submerged plane turbulent wall jets. *J. Hydraulic Research*, **41**(2), 195-206.

Mason, P.J., and Arumugam, K. (1985). Free jet scour below dams and flip buckets. *J. Hydraulic Engineering*, **111**(2), 220-235.

McCulloch, W. and Pitts, W. (1943). A logical calculus of the ideas immanent in nervous activity. *Bulletin of Mathematical Biophysics*, **7**, 115-133.

Meville, B.W. and Raudkivi, A.J. (1977). Flow characteristics in local scour at bridge piers. *J. Hydraulic Research*, **15**(4), 373–380.

Mih, W. C. and Kabir, J. (1983). Impingement of water jets on nonuniform streambed. *J. Hydraulic Engineering*, ASCE, **109**(4), 536-548.

Minsky, M., and Pappert, S. (1969). *Perceptrons*. MIT Press, Cam-bridge, MA.

Montana, D.J., 1995, Strongly Typed Genetic Programming. *Evolutionary Computation,* **3**(2), 199–200.

Mossa, M. (1998). Experimental study on the scour downstream of grade-control structures. *Proceedings of 26th Convegno di Idraulica e Costruzioni Idrauliche*, Catanja, September, Vol.3, 581-594.

Nagy, H.M., Watanabe, K. and Hirano, M. (2002). Prediction of sediment load concentration in rivers using artificial neural network model. *J. Hydraulic Enginnering*, **128**(6), 588-595.

Negm, A.M., Shouman, M.A., and Abdel-Gawad, A.F. (2004). Performance evaluation of Artificial Neural Networks softwares in prediction of hydraulic data. *Proc. 6th Int. Conf. on Hydroinformatics*, Liong, Phoon&Babovic (eds), World Scientific Publishing Company, ISBN 981-238-787-0.

Novak, P. (1956). Study of stilling basins with special regard to their end sill. *Proceedings of 6th IAHR Cong*ress, Hague, Vol. 3, pp. C 15.

Novak, P. (1961). Influence of bed load passage on scour and turbulence downstream of a stilling basin. *Proceedings of 9th IAHR Cong*., Dubrovnik, pp 66-75.

Philips, B. C. (1984). Spatial and temporal lag effects in bed load sediment transport. PhD thesis, University of Canterbury, New Zealand.

Olsen, N.R.B. and Melaaen, M.C. (1993). Three-dimensional calculation of scour around a cylinder. *J. Hydraulic Engineering*, **119**(9), 1048-1053.

Olsen, N.R.B., and Kjellesvig, H.M. (1998). Three-dimensional numerical flow modelling for estimation of maximum local scour depth. *J. Hydraulic. Research*, **36**(4), 579-590.

Patankar, S.V. (1980). *Numerical Heat Transfer and Fluid Flow.* McGrawhill Book Company.

Patankar, S.V. ve Spalding, D.B. (1972). A calculation procedure for heat, mass and momentum transfer in three dimensional parabolic flows. *International Journal Heat and Mass Transfer*, **15**, 1787-1816.

Poreh, M. and Hefez, E. (1967). Initial scour and sediment motion due to an impinging jet. *Proceedings of 12th IAHR Cong.*, Fort Collins, Vol. 3, pp 8.

Rabunal, J.R., Puertas, J., Suarez J., and Rivero D. (2006). Determination of the unit hydrograph of a typical urban basin using genetic programming and artificial neural networks, *Hydrological Process* (In press).

Rajaratnam. N. (1976). *Turbulent jets.* Elsevier Scientific Publishing Company, Amsterdam.

Rajaratnam, N. (1981a). Erosion by plane turbulent jets. *J. Hydraulic Research*, **19**(4), 339-358.

Rajaratnam, N. (1981b). Erosion of loose polystyrene bed by obliquely impinging circular turbulent air jets. *Rep. WRE 81-2, Deptartment of Civil Engineering*, University of Alberta, Canada.

Rajaratnam, N. (1982). Erosion by submerged circular jets. *J. Hydaulic Division*, ASCE, **108**(HY2), 262-267.

Rajaratnam, N. and Berry, S. (1977). Erosion by circular turbulent wall jets. *J. Hydraulic. Research*, **15**(3), 277-289.

Rajaratnam, N. and MacDougall, R. K. (1983). Erosion by plane wall jets with minimum tailwater. *J. Hydraulic Division*, ASCE, **109**(7), 1061-1064.

Rajaratnam, N. and Mazurek, K. A. (2002). Erosion of a polystyrene bed by obliquely impinging circular turbulent air jets. *J. Hydraulic Research*, **40**(6), 709-716.

Raju, S.K .and Kumar, N.D. (2004). Irrigation Planning using Genetic Algorithms, *Water Resources Management* , **18**, 163-176.

Rao, S.S. (1996). *Engineering optimization*. Third Edition, John Wiley & Sons, Inc., pp 806-823.

Raudkivi, A. J. (1998). *Loose boundary hydraulics*. A. A. Balkema, Rotterdam.

Rodi, W. (1980). Turbulence models and their applications in hydraulics-A state of the art review. *IAHR*, 104 pages.

Rissanen, J. (1978). Modeling by shortest data description. *Automatica*, **14**, 465-471.

Rosenblatt, F.(1957). The perceptron: A perceiving and recognizing automaton (project PARA). Technical Report 85-460-1, Cornell Aeronautical Laboratory.

Rouse, H. (1939). Criteria for similarity in transportation of sediment. *Proceedings of 1st Hydraulic Conference*, Iowa City, Iowa, pp. 33-49.

Rumelhart, D.E., Hinton, G.E., and Williams, R.J. (1986). Learning internal representation by error propagation Parallel Distributed Processing: Exploration in the Microstructure of Cognition. Vol. 1, Chapter 8, MIT Press, Cambridge, MA.

Runchal, A.K. (1972). Convergence and accuracy of three different schemes for a two-dimensional conduction and convection problem. *International Journal for Numerical Methods in Engineering*, **4**, 541–550.

Salehi-Neyshaboury, A. A. (1988). Impingement of offset jets on rigid and movable beds. PhD thesis, University of Liverpool, Liverpool, UK.

Salehi Neyshabouri, A.A., Barron, R.M. and Ferreira Da Silva, A.M. (2001). Numerical simulation of scour by a wall jet. *Water Engineering Research*, **2**(3), 179-185.

Salehi-Neyshaboury, A. A. S., Da Silva, A. M. F. and Barron, R. (2003). Numerical simulation of scour by a free falling jet. *J. Hydraulic Res*earch, **41**(5), 533-539.

Salehi Neyshabouri, A.A., Ferreira Da Silva, A.M., and Barron, R.M. (2004). Numerical simulation of scour by a free falling jet. *J. Hydraulic Research,* **41**(5), 533-539.

Sarghini, F., de Felice, G., and Santini, S. (2003). Neural Networks based subgrid scale modelling in large eddy simulations. J. *Computers and Fluids*, **32**(1), 97-108.

Sarkar, A. and Dey, S. (2004). Review on local scour due to jets. *International Journal of Sediment Research,* **19**(3), 210-239.

Savic A.D., Walters A.G., and Davidson J.W. (1999). A Genetic Programming Approach to Rainfall-Runoff Modeling, *Water Resources Management* , **13**, 219-231.

Schoklitsch, A. (1932). Kolkbildung unter uberfallstrahlen. *Die Wasserwirtschaft*, pp. 341.

Schoklitsch, A. (1935). *Stauraumverlandung und kolkabwehr*. Sprimger-Verlag, Wien.

Shalash, M. S. E. (1959). Die kolkbildung beim ausfluss unter schutzen. Dissertation, TH Munchen.

Schwarz W. H. and Cosart W. P. (1961). The two-dimensional wall-jet. *Journal of Fluid Mechanics*, **10**, 481-495.

Shy, W., Tong, S.S. and Correa, S.M. (1985). Numerical recirculation flow calculation using a body-fitted coordinate system. *Numerical Heat Transfer*, **8**, 99-113.

Simons, D. B. and Senturk, F. (1992). *Sediment transport technology, water and sediment dynamics*, Water Resources Publications.

Stein, O. R., Julien, P. Y. and Alonso, C. V. (1993). Mechanics of jet scour downstream of a headcut. *J. Hydraulic Res*earch, **31**(6), 723–738.

Takemitsu, N. (1990). An analytic study of the standard $\tilde{k}$ model. *J. of Fluid Engineering*, **112**, 192-198.

Tarapore, Z.S. (1956). Scour below a submerged sluice gate. M.Sc. Thesis, University of Minnesota, Minneapolis.

The ASCE Task Committee (2000). The ASCE Task Committee on application of Artificial Neural Networks in hydrology. *J. Hydraulic Engineering*, **5**(2), 115-137.

Toro B, Francisco M., Meijer, K., and Van Rijn, L. (1989). Quasi-3D and fully -3D modelling of suspended sediment transport. *Sediment Transportation Model Proceedings of International Symposium*, pp 45-51.

Ushijima B., Shimitzu, T., Sakasi, A. and Takizawa, Y. (1992). Prediction method for local scour by warmed cooling water jets. *J. Hydraulic Engineering*, ASCE*, **118**(8), 1164-1183.

Ushijima, S. (1996). Arbitrary Lagrangian-Eulerian numerical prediction for local scour caused by turbulent flows. *Journal of Computational Physics*, **125**, 71-82.

Uyumaz, A. (1988). Scour downstream of vertical gate. *J. Hydraulic Engineering*, ASCE, **114**(7), 811–816.

Veronese, A. (1937). Erosion de fond en avel d'dune decharge. *IAHR Meeting on* Hydraulic Structures, Berlin.

Versteeg HK, Malalasekera W. (1995). *An Introduction to Computational Fluid Dynamics*. Longman: Harlow, UK, pp 103–134, 134–155.

Westrich, B. and Kobus, H. (1973). Erosion of a uniform sand bed by continuous and pulsating jets. *Proceedings of 15th IAHR* Congress, Istanbul, Vol. 1, pp 91-98.

Whigham, P.A., and Crapper P.F. (1999). Time series modeling using Genetic Programming: An application to rainfall-runoff models. In Advances in Genetic Programming, eds. L. Spector et al., 89–104. The MIT Press, Cambridge, MA.

Whigham, P. A., and Crapper P. F. (2001). Modeling Rainfall-Runoff using Genetic Programming, *Mathematical and Computer Modeling*, **33**, 707-721.

Whittaker, J. C. and Schleiss, A. (1984). Scour related to energy dissipators for high head structures. ETH Versuchsaanstalt fur Wasserbau, Mih. Nr. 73, Zurich.

Widrow, B. and Hoff, Jr. M.E. (1960). Adaptive switching circuits. IRE WESCON Conv. Rec., Part 4, pp. 96-104.

Wilcox, D.C. 1998. *Turbulence Modeling for CFD.* (2nd edition). DCW Industries. Canada, CA, pp 49–217.

Wygnanski, I., Katz, Y. and Horev, E. (1992). On the applicability of various scaling laws to the turbulent wall jet. *J. Fluid Mech*anics, **234**, 669–690.

Yakhot V, Orszag SA. (1986). Renormalization group analysis of turbulence. I. Basic theory. *Journal of Scientific Computing*, **1**(1), 1–51.

Yap, C. (1987). Turbulent heat and momentum transfer in recirculating and impinging flows. PhD thesis, Faculty of Technology, University of Manchester.

Yoshizawa, A. (1987). Statistical modeling of a transport equation for the kinetic energy dissipation rate. *Physics of Fluid*, **3**, 628-631.

Zadeh L.A. (1994). Soft computing and fuzzy logic. *IEEE Software*, **11**(6), 48–56.

Zaghloul, N. A. and McCorquodale, J. A. (1975). Stable numerical model for local scour. *Journal of Hydraulic Research*, **13**(4), 425-444.

CURRICULUM VITAE

PERSONAL INFORMATION

Surname, Name: GÜVEN, Aytaç
Nationality: Turkish (TC)
Date and Place of Birth: 24 November 1977, Ağrı
Marital Status: Married
Phone: +90 3172429
Fax: +90 3601107
email: aguven@gantep.edu.tr, aytacguven@hotmail.com

EDUCATION

Degree	Institution	Year of Graduation
MS	Gaziantep University	2003
BS	Gaziantep University	2000
High School	Ağrı Anatolian High School	1995

WORK EXPERIENCE

Year	Place	Enrollment
2001- Present	Gaziantep University	Research Assistant

FOREIGN LANGUAGES

Turkish (Native Language), English, German

PUBLICATIONS

1. **Aytaç Güven** and Mustafa Günal (2008). Genetic Programming Approach for Prediction of Local Scour Downstream Hydraulic Structures. *Journal of Irrigation and Drainage Engineering*, 134(2), 241-249.

2. **Aytaç Güven,** Ali Aytek, M. İshak Yüce, and Hafzullah Aksoy (2008). Genetic programming-based empirical model for daily reference evapotranspiration estimation. Clean Soil Air Water (Accepted for publication)

3. **Aytaç Güven** and Mustafa Günal (2008). Prediction of local scour downstream of grade-control structures using neural networks. *Journal of Hydraulic Engineering*. (Accepted for publication)

4. **Aytaç Güven** and Mustafa Günal (2008). Assessment of large-scale local scour using neurocomputing techniques. *International Congress on Fluvial Hydraulics*, September 3-5, 2008, Çeşme-İzmir, Turkey.

5. Mustafa Günal and **Aytaç Güven** (2008). A unified explicit model for local scour downstream of grade-control structures. *International Congress on Fluvial Hydraulics*, September 3-5, 2008, Çeşme-İzmir, Turkey.

6. Mustafa Günal and **Aytaç Güven** (2008). Numerical Simulation of Flow Patterns in Scour Hole Beneath Turbulent Jets. *8th International Congress on Advances in Civil Engineering*, September 15-17, 2008, Famagusta, North Cyprus.

7. **Aytaç Güven** and Mustafa Günal (2008). Assessment of pressure fluctuations beneath hydraulic jump using neural computing techniques. *8th International Congress on Advances in Civil Engineering*, September 15-17, 2008, Famagusta, North Cyprus.

8. Hafzullah Aksoy, Aytac Guven, Ali Aytek, M. Ishak Yuce, N. Erdem Unal (2008). Comment on "Evapotranspiration modelling from climatic data using neural network computing technique". *Hydrological Sciences* (In Press)

9. Hafzullah Aksoy, **Aytaç Güven**, Ali Aytek, M. İ. Yüce and N.E. Ünal (2007). Discussion on "Generalized regression neural networks for evapotranspiration modelling" by O. Kisi. *Hydrological Sciences*, 52(4), 825-831.

10. Mustafa Günal and **Aytaç Güven** (2006). Prediction of flow patterns in scoured zone. *Canadian Journal of Civil Engineering*, 33(1), 41-48.

11. **Aytaç Güven**, Mustafa Günal and Abdulkadir Çevik (2006). Prediction of pressure fluctuations on stilling basins. *Canadian Journal of Civil Engineering*, 33(11), 1379-1388.

12. **Aytaç Güven** and Mustafa Günal (2006). Modeling Hydraulic Jump Using Neural Networks. *7th international Congrees of Hydroinformatics*, IAHR, Nice, France, CD Version.

13. **Aytaç Güven**, Mustafa Günal and Ahmet Öztaş (2006). A Knowledge Based Expert System for Decision of Water Supply Pipeline under Uncertainty. *7th Int. Cong. on Advances in Civil Engineering*, October 11-13, İstanbul, Turkey

14. **Aytaç Güven** ve Mustafa Günal (2004). Batık Yatay Jetlerin Nümerik Simülasyonu. İnşaat Mühendisleri Odası 17. Teknik Kongre, Ankara, Türkiye.

HOBBIES

Reading, Cinema, Football, Computer, Softwares.